

Doctorial Dissertation (Censored)

博士論文（要約）

**Iron-Catalyzed C–H/C–H Coupling for Synthesis of
Functional Small Molecules and Polymers**

（鉄触媒 C-H/C-H カップリングによる
機能性低分子及び高分子の合成）

**A Dissertation Submitted for the Degree of Doctor of Philosophy
December 2021**

令和 3 年 12 月博士（理学）申請

**Department of Chemistry, Graduate School of Science,
The University of Tokyo**
東京大学大学院理学系研究科化学専攻

Takahiro Doba

道場 貴大

Preface

On September 27, 1994, I was born in Komatsu, Ishikawa, a countryside where we can see a land covered with rice fields as far as the eye can see. From that time, I was thinking, "what is the origin of nature?" Soon after I entered elementary school, I learned that everything on earth is made of elements. I was surprised by the fact that a combination of only less than 100 kinds of elements can make such a wide range of things on earth. This experience triggered me to become a chemist.

Once I entered Department of Chemistry, The University of Tokyo, I got interested in Prof. Eiichi Nakamura's work on iron catalyzed C–H activation. I was attracted to this project because the concept was so universal. Iron is the most abundant transition metal on earth because it is the final product of stellar nucleosynthesis and C–H bond is also one of the most widely seen bonds in nature. This thesis studies focus on the development of iron-catalyzed C–H/C–H coupling for synthesis of functional small molecules and polymers that have potentials to solve energy problems and hence contribute to the sustainability of human beings.

All the research presented in this thesis was carried out under the supervision of Prof. Eiichi Nakamura at the Department of Chemistry, School of Science, The University of Tokyo during April 2016 to December 2021. I should not forget to mention that it includes a special period of a pandemic caused by COVID-19. All the experiments were conducted on the 7th floor of Molecular and Life Innovation Building, which is located irregularly within the grounds of The University of Tokyo Hospital. I will never forget the enjoyable (and sometimes trying) time in this group.

I wish anyone who read this book gets interested in chemistry and becomes a great scientist in the future.

Abstract

Transition-metal-catalyzed C(sp²)-H/C(sp²)-H coupling has attracted much attention as one of the most straightforward methods to construct C(sp²)-C(sp²) bonds. However, the application of this ideal transformation to the synthesis of redox-sensitive π -materials was hindered by the requirement of a strong oxidant for catalyst turnover. The purpose of this thesis is to demonstrate that iron is suitable for realizing transition-metal-catalyzed C-H/C-H coupling that is applicable to the synthesis of redox-sensitive functional small molecules and polymers. Thiophene compounds were chosen as substrates of interest because of the wide application found in materials science.

Chapter 1 describes the adequacy of using iron as a catalyst for the realization of transition-metal-catalyzed C-H/C-H coupling that operates under mildly oxidative conditions. Being aware that redox potential of catalyst is the limiting factor of the mildness of oxidant, the author focused on the low redox potential of Fe(III)/Fe(I) which has been partially proved by the use of dihaloalkanes as a mild oxidant in iron-catalyzed C-H activation reactions reported by Nakamura and co-workers.

Chapter 2 describes the development of iron-catalyzed regioselective thienyl C-H/C-H homocoupling using tridentate phosphine as a ligand, AlMe₃ as a base, and oxalate as a mild oxidant. Oxalate in combination with oxophilic AlMe₃ served as an effective but mild oxidant to oxidize Fe(I) species to regenerate Fe(III) catalyst. The electronic bias of the thienyl group helped to achieve regioselective C-H activation by a σ -bond metathesis mechanism.

Chapter 3 describes a modular synthesis of tridentate phosphine ligands by sequential addition of organolithium reagents to triphenyl phosphite. This method gave access to tridentate phosphine ligands having different substituents and accelerated further exploration of iron catalysis.

Chapter 4 describes the development of iron-catalyzed regioselective thienyl C-H/C-H polycondensation by improvement of iron-catalyzed regioselective thienyl C-H/C-H homocoupling introduced in chapter 2. New tridentate phosphine ligands possessing a heteroaryl group were designed to suppress catalyst deactivation and employed as effective ligands for polycondensation. One of the obtained polymers was used as a hole transporting material for perovskite solar cells.

(第 5 章については, 5 年以内に雑誌等で刊行予定のため, 非公開.)

Finally, chapter 6 summarizes the present studies and gives further perspectives.

Table of Contents

Chapter 1.

General Introduction	1
1-1. Transition-metal-catalyzed C–H/C–H coupling	2
1-2. Requirement of strong oxidant in transition-metal-catalyzed C–H/C–H coupling ...	4
1-3. Iron-catalyzed directed C–H activation	5
1-4. Iron-catalyzed regioselective thienyl C–H activation.....	7
1-5. Objective and outline of this thesis	9
1-6. References and notes.....	11

Chapter 2.

Iron-Catalyzed Regioselective Thienyl C–H/C–H Homocoupling.....	15
2-1. Introduction.....	16
2-2. Initial discovery	18
2-3. Catalyst poisoning by alkene	20
2-4. Diketone as a mild oxidant	21
2-5. Effect of reaction parameters	23
2-6. Substrate scope.....	25
2-7. Unsuccessful substrates	27
2-8. Addition of radical scavenger	29
2-9. The role of AlMe ₃ as a base	29
2-10. Stoichiometric experiments	30
2-11. Kinetic isotope effect experiments.....	32
2-12. Conclusion	33
2-13. Experimental	34
2-14. References and notes.....	55

Chapter 3.

Development of a Synthetic Method for Tridentate Phosphine Ligands.....	59
3-1. Introduction.....	60
3-2. Selective formation of phenoxydiarylphosphine	61
3-3. Synthesis of tridentate phosphine ligands.....	64

3-4. Modulation of all of the aryl groups	67
3-5. Conclusion	68
3-6. Experimental	69
3-7. References and notes.....	81

Chapter 4.

Iron-Catalyzed Regioselective Thienyl C–H/C–H Polycondensation.....	83
4-1. Introduction.....	84
4-2. Initial trial.....	87
4-3. Investigation of iron source	88
4-4. Determination of catalyst deactivation pathway.....	89
4-5. Ligand design.....	91
4-6. Effect of heteroaryl-TP on the efficiency of polycondensation.....	91
4-7. Substrate scope.....	93
4-8. Control experiments.....	97
4-9. Mechanism of polycondensation	97
4-10. Removal of residual catalyst from polymer.....	99
4-11. Application to perovskite solar cell	100
4-12. Conclusion	103
4-13. Experimental	104
4-14. References and notes.....	160

Chapter 5.

本章については, 5 年以内に雑誌等で刊行予定のため, 非公開.

Chapter 6.

Conclusions and Perspectives.....	209
--	------------

List of Publications	213
-----------------------------------	------------

Acknowledgements	214
-------------------------------	------------

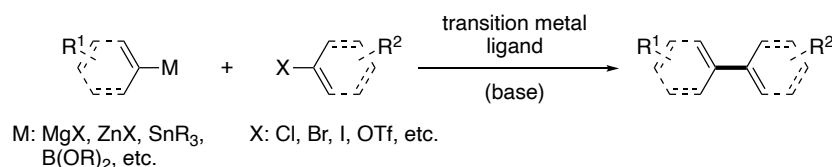
Chapter 1.

General Introduction

1-1. Transition-metal-catalyzed C–H/C–H coupling

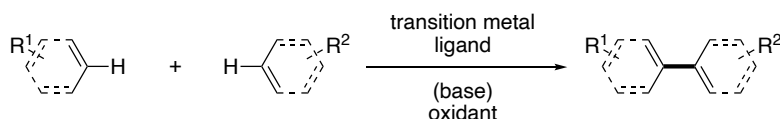
Conjugated compounds containing C(sp²)–C(sp²) linkages are one of the most important classes of compounds because of the interaction of their *p*-orbitals with electrons and photons.¹ Therefore, development of C(sp²)–C(sp²) bond-forming reactions is an important subject in organic chemistry. One of the most widely used methods is transition-metal-catalyzed cross-coupling which has been investigated extensively since 1970s² and for which the Nobel Prize in Chemistry 2010³ was awarded. Although this methodology is applicable to a broad range of substrates, it has an inevitable limitation that prefunctionalization of both substrates is required, rendering multiple steps for the synthesis of starting materials and special care in handling unstable substrates, especially heteroaryl organometallic reagents and halides.⁴

Scheme 1. Transition-metal-catalyzed cross-coupling



To overcome these problems, transition-metal-catalyzed C–H/C–H coupling which merges two C–H bonds to form a C–C bond, has attracted considerable attention as an alternative method.⁵ However, there are many hurdles to be overcome to realize this ideal transformation. First, C–H bond is more inert than C–M and C–X bonds in terms of bond dissociation energy.⁶ In addition, distinguishing multiple C–H bonds present in the molecules is challenging, which directly affects the regioselectivity and chemoselectivity.

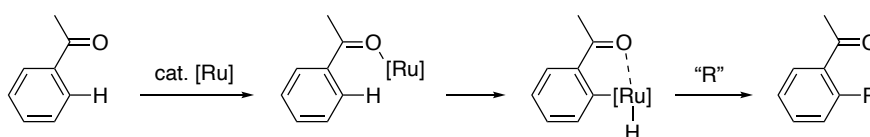
Scheme 2. Transition-metal-catalyzed C–H/C–H coupling



Currently, these issues are solved by choosing an appropriate combination of substrates and the modes of the C–H activation processes. Regarding the choice of substrates, the utilization of electronic bias or steric effect has been a classical solution.

In 1993, a groundbreaking discovery was done by Murai and co-workers⁷ in which they introduced a paradigm called "directing group strategy." A coordinating group enhances the reaction efficiency and selectivity by assisting catalyst to approach the proximal C–H bond to form a metallacycle intermediate.

Scheme 3. A directing group strategy introduced by Murai and co-workers with ruthenium



Regarding the choice of the modes of the C–H activation processes, electrophilic aromatic substitution (S_EAr),⁸ concerted-metalation-deprotonation (CMD),⁹ σ -bond metathesis,¹⁰ and oxidative addition¹¹ have been proposed as general modes. Control of the C–H activation modes by careful selection of a catalytic system allows us to achieve efficient and selective transition-metal-catalyzed C–H/C–H coupling. For example, an S_EAr pathway takes place at the most nucleophilic position, while CMD and σ -bond metathesis pathways take place mainly at the most acidic C–H bond. An oxidative addition pathway is often incompatible with the C–H/C–H coupling catalytic cycle because the oxidation state of catalyst changes before and after the C–H activation event.

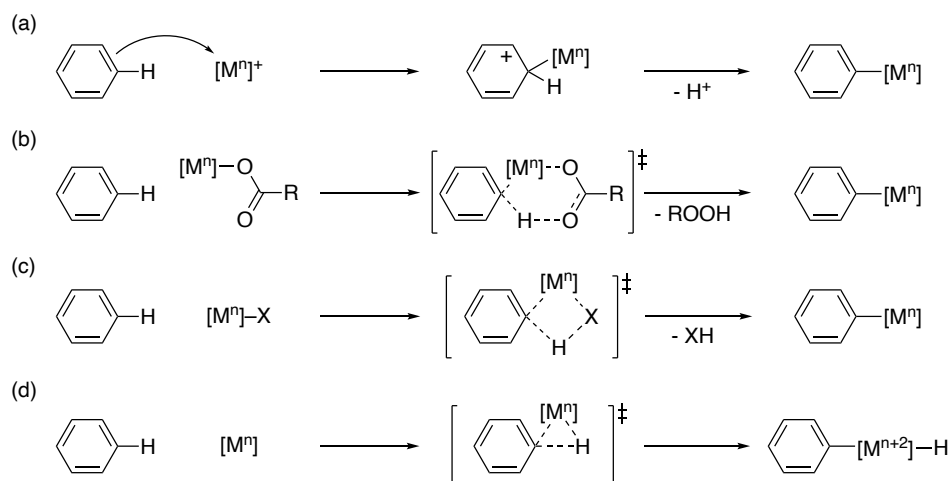
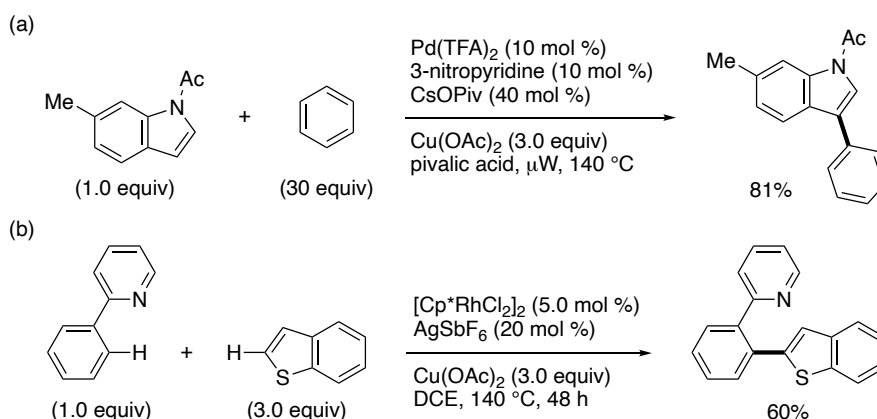


Figure 1. General modes for transition-metal-catalyzed C–H activation processes. (a) electrophilic aromatic substitution (S_EAr) (b) concerted-metalation-deprotonation (CMD) (c) σ -bond metathesis (d) oxidative addition

Currently, transition-metal-catalyzed C–H/C–H coupling reactions heavily rely on the reactivity of palladium and rhodium. Since Fagnou and co-workers reported a pioneering work using palladium as a catalyst, many researchers have investigated this reaction system to broaden the scope.¹² It has been reported that rhodium catalysis is especially effective for the reaction of heteroarenes.¹³

Scheme 4. Examples of transition-metal-catalyzed C–H/C–H coupling



1-2. Requirement of strong oxidant in transition-metal-catalyzed C–H/C–H coupling

Because transition-metal-catalyzed C–H/C–H coupling is a coupling of two nucleophiles, transition-metal-catalyzed C–H/C–H coupling requires the addition of an external oxidant for the catalyst turnover.⁵ Figure 2 shows the catalytic cycle of transition-metal-catalyzed C–H/C–H coupling. First, transition metal catalyst **I** activates the C(sp²)–H bond twice without changing its oxidation state to give intermediate **III** bearing two coupling fragments. Then **III** undergoes reductive elimination to afford the C–H/C–H coupling product and a transition metal catalyst whose oxidation state is reduced by two (**IV**). To oxidize the low-valent metal species **IV** to high-valent metal species **I**, addition of a stoichiometric oxidant is necessary.

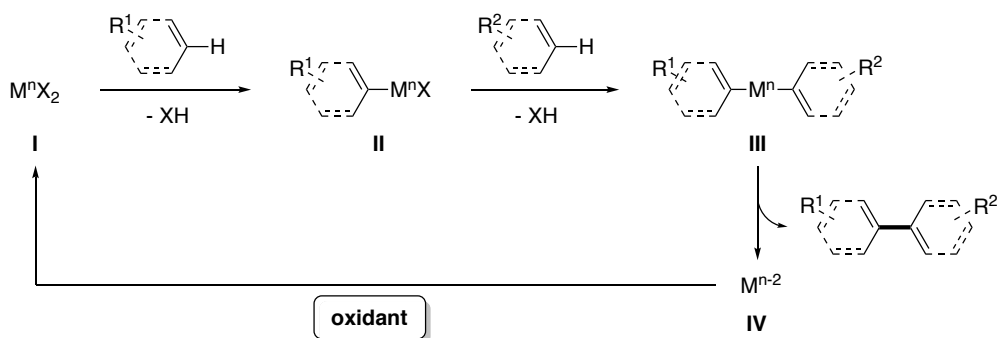


Figure 2. Requirement of oxidant in transition-metal-catalyzed C–H/C–H coupling

Currently, transition-metal-catalyzed C–H/C–H coupling requires the use of strong oxidants such as Ag(I), Cu(II), *p*-benzoquinone (BQ), and oxygen.⁵ The use of strong oxidant in transition-metal-catalyzed C–H/C–H coupling is problematic because the oxidant may oxidize not only the low-valent transition metal catalyst (IV) but also the starting material or the product, causing decomposition or unwanted side reactions.¹⁴ This situation makes it difficult to apply this attractive transformation, transition-metal-catalyzed C–H/C–H coupling, to the synthesis of redox-sensitive π -materials of importance in materials science.

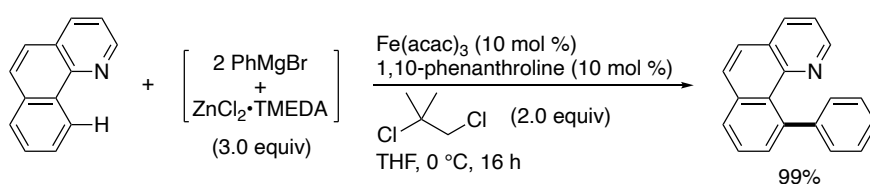
The rationale for the requirement of a strong oxidant is the high redox potential of the transition metal catalyst. For example, the redox potential of Pd(II)/Pd(0) is 0.915 V vs NHE,¹⁵ which limits the weakness of the oxidant. Therefore, if a transition metal that has a lower redox potential can successfully activate the C–H bond twice (from I to IV in Figure 2), there is a high chance of developing a versatile transition-metal-catalyzed C–H/C–H coupling that operates under mildly oxidative conditions and enables the synthesis of redox-sensitive π -materials of importance in materials science. Aiming for this ultimate goal, I envisioned to utilize the reactivity of iron.

1-3. Iron-catalyzed directed C–H activation

Iron is the final product of stellar nucleosynthesis and therefore is the most abundant transition metal on earth.¹⁶ Nakamura and co-workers have reported iron-catalyzed C–H activation taking advantage of its high abundance, low cost, and low toxicity.¹⁷ However, iron can take various oxidation states and spin states, making it difficult to express a desired reactivity.¹⁸ In 2008, Yoshikai and co-workers reported that a bipyridine ligand in combination with a pyridyl directing group can effectively control the reactivity of iron

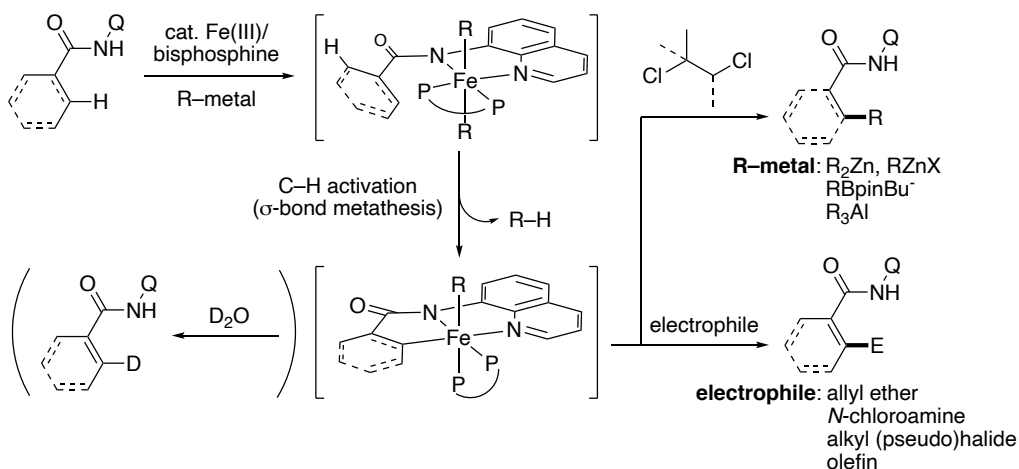
to catalyze C–H arylation with arylzinc reagents.¹⁹ Arylzinc reagents served not only as a coupling partner but also as a base for C–H activation through σ -bond metathesis and dihaloalkane was determined as an optimal oxidant. The reaction was conducted at low temperature (as low as 0 °C) to prevent the degradation of unstable organoiron intermediates.

Scheme 5. The first example of iron-catalyzed C–H activation reaction reported by Yoshikai and co-workers in 2008



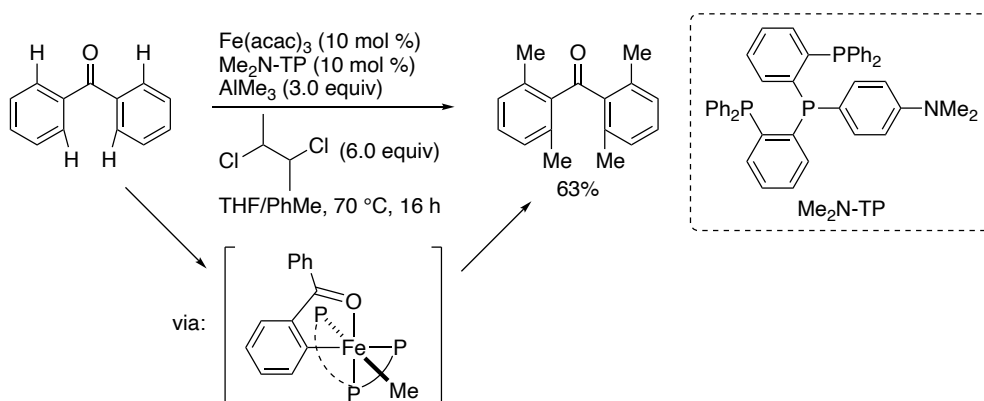
In 2013, Nakamura and co-workers reported that a combination of a bidentate phosphine ligand and a bidentate directing group²⁰ is beneficial for efficient C–H activation and stabilization of the resulting iron metallacycle intermediate, which can react with various kinds of organometallic nucleophiles²¹ and electrophiles such as allyl ether,²² *N*-chloroamine,²³ alkyl (pseudo)halide,²⁴ and olefins.²⁵ The existence of an iron metallacycle intermediate was confirmed by deuterium quenching experiments and more recently by direct isolation of the intermediate.²⁶

Scheme 6. Iron-catalyzed C–H activation reaction using a bidentate phosphine ligand and a bidentate directing group



In 2016, Nakamura and co-workers further reported that a combination of a tridentate phosphine ligand and a monodentate carbonyl directing group is also suitable for iron-catalyzed C–H activation.²⁷ Methylation of weakly coordinating aromatic ketones proceeded smoothly using AlMe_3 as a methyl source and dihaloalkane as a mild oxidant.

Scheme 7. Iron-catalyzed C–H activation reaction using a tridentate phosphine ligand and a monodentate carbonyl directing group



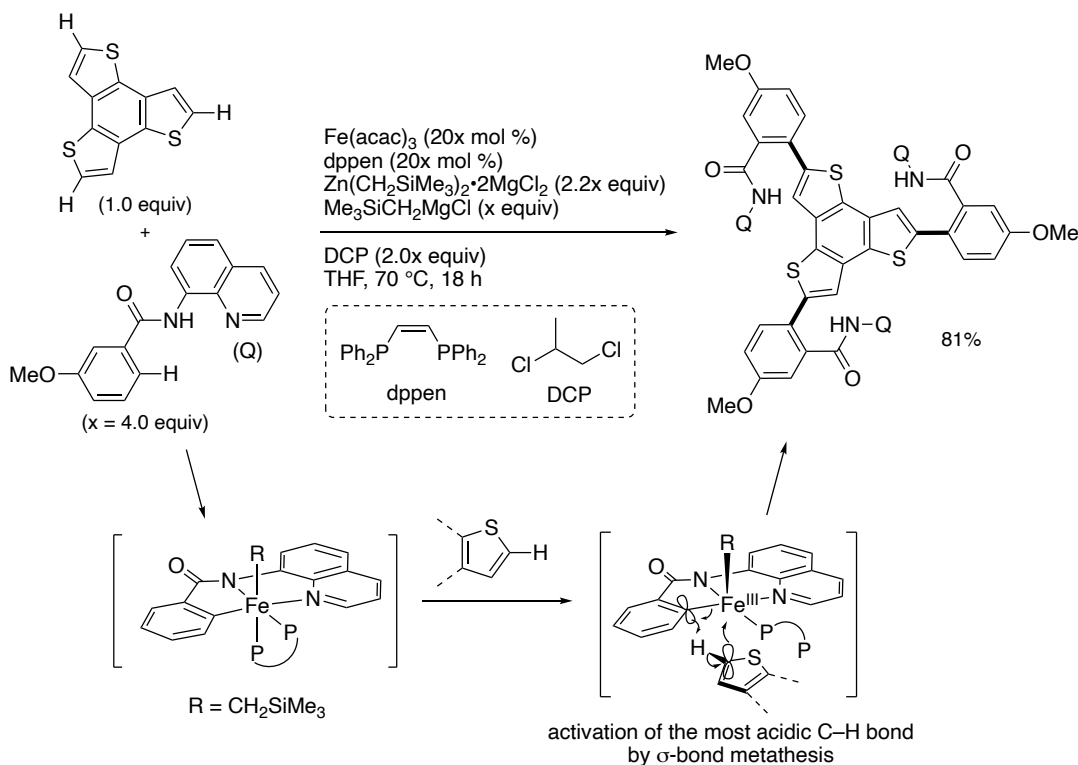
Putting together all of the iron-catalyzed C–H activation reactions described above, dihaloalkanes can be used as a mild oxidant in all cases. This is because the redox potential of Fe(III)/Fe(I) is low and Fe(I) can be easily oxidized to Fe(III) by a mild oxidant to regenerate the catalyst. The redox potential of Fe(III)/Fe(I) is estimated to be lower than 0.55 V vs NHE which is lower than that of a conventional Pd(II)/Pd(0) (0.915 V vs NHE) cycle.¹⁵ Therefore, an Fe(III)/Fe(I) catalytic cycle with a low redox potential is suitable for achieving C–H/C–H coupling that operates with a mild oxidant and enables the synthesis of redox-sensitive π -materials.

1-4. Iron-catalyzed regioselective thienyl C–H activation

As seen in the reactions described above, iron-catalyzed C–H activation reactions were limited to the synthesis of *ortho*-disubstituted arenes possessing a coordinating group for the sake of a directing group strategy. The obtained products are not always appreciated as a useful compound for practical applications and in many cases removal of a preinstalled directing group is required.²⁸

In my master course studies, I obtained a foothold for achieving iron-catalyzed C–H activation reactions that do not rely on a preinstalled directing group. In 2019, Nakamura and co-workers (including myself) reported homocoupling-free iron-catalyzed C–H/C–H cross-coupling of carboxamides with thiophenes (Scheme 8).²⁹ In this reaction, I found that the most acidic C–H bond of thiophene compounds that do not possess an extraneous directing group can be activated regioselectively by a stable organoiron species (as shown in Scheme 6) through a σ -bond metathesis mechanism. The mechanisms of iron-catalyzed thienyl C–H activation was experimentally supported by deuterium exchange between two substrates. This reaction mechanism was the key to completely suppress the formation of homocoupling products. Although a preinstalled bidentate directing group was necessary for one of the substrates, the reaction was applicable to various kinds of thiophene cores commonly found in real optoelectronic materials.³⁰

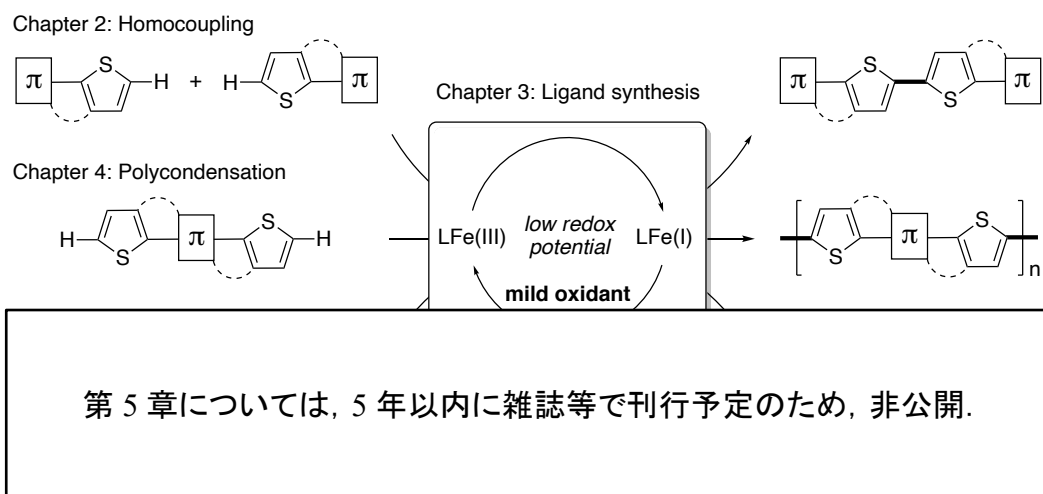
Scheme 8. Homocoupling-free iron-catalyzed C–H/C–H cross-coupling of carboxamides with thiophenes



1-5. Objective and outline of this thesis

The application of transition-metal-catalyzed C–H/C–H coupling, an ideal coupling method for the construction of a C(sp²)–C(sp²) bond, to the synthesis of redox-sensitive π -materials was hindered by the requirement of a strong oxidant to turn over the catalyst. To overcome this problem, my Ph.D. studies focused on the low redox potential of Fe(III)/Fe(I), enabling C–H/C–H coupling under mildly oxidative conditions. Thiophene compounds were chosen as substrates because of the wide application found in materials science. As revealed by my master course studies, the electronic bias created by a sulfur atom helps to make the adjacent C–H bond acidic enough for iron-catalyzed C–H activation through a σ -bond metathesis mechanism. The reactions described in this thesis do not require a preinstalled directing group, enabling direct application of the obtained products as organic materials.

To this end, I first investigated the iron catalytic system that catalyzes regioselective C–H/C–H homocoupling of thiophene compounds and determined that oxalate serves as a mild oxidant in combination with AlMe₃ base and a tridentate phosphine ligand. Then, a modular synthetic method of a tridentate phosphine ligand was developed to further accelerate the exploration of this reaction system. To expand the applicability of iron-catalyzed regioselective thienyl C–H/C–H coupling to the synthesis of polymeric compounds, iron-catalyzed regioselective thienyl C–H/C–H polycondensation was developed by suppressing catalyst deactivation by ligand design. The obtained polymer was applied as a hole transporting material for perovskite solar cells to demonstrate the practicability of this method. (第 5 章については、5 年以内に雑誌等で刊行予定のため、非公開。) The reactions described herein highlight the potential of iron, the most abundant transition metal on earth, for the direct synthesis of functional small molecules and polymers of importance in materials science.



• Regioselective • Redox-sensitive motifs tolerated • Direct synthesis of functional materials

Figure 3. Iron-catalyzed regioselective thienyl C–H/C–H coupling for synthesis of functional small molecules and polymers

1-6. References and notes

- ¹ (a) Cornil, J.; Beljonne, D.; Calbert, J.-P.; Brédas, J.-L. *Adv. Mater.* **2001**, *13*, 1053–1067. (b) Wu, W.; Liu, Y.; Zhu, D. *Chem. Soc. Rev.* **2010**, *39*, 1489–1502. (c) Wang, C.; Dong, H.; Hu, W.; Liu, Y.; Zhu, D. *Chem. Rev.* **2012**, *112*, 2208–2267. (d) Gierschner, J.; Cornil, J.; Egelhaaf, H.-J. *Adv. Mater.* **2007**, *19*, 173–191. (e) Hughes, G.; Bryce, M. R. *J. Mater. Chem.* **2005**, *15*, 94–107. (f) Tour, J. M. *Chem. Rev.* **1996**, *96*, 537–554. (g) Adachi, C. *Jpn. J. Appl. Phys.* **2014**, *53*, 060101. (h) Kanis, D. R.; Ratner, M. A.; Marks, T. J. *Chem. Rev.* **1994**, *94*, 195–242. (i) Cai, J.; Ruffieux, P.; Jaafar, R.; Bieri, M.; Braun, T.; Blankenburg, S.; Muoth, M.; Seitsonen, A. P.; Saleh, M.; Feng, X.; Müllen, K.; Fasel, R. *Nature* **2010**, *466*, 470–473. (j) Ruffieux, P.; Wang, S.; Yang, B.; Sánchez-Sánchez, C.; Liu, J.; Dienel, T.; Talirz, L.; Shinde, P.; Pignedoli, C. A.; Passerone, D.; Dumszlaff, T.; Feng, X.; Müllen, K.; Fasel, R. *Nature* **2016**, *531*, 489–492.
- ² (a) Tamura, M.; Kochi, J. K. *J. Am. Chem. Soc.* **1971**, *93*, 1487–1489. (b) Tamao, K.; Sumitani, K.; Kumada, M. *J. Am. Chem. Soc.* **1972**, *94*, 4374–4376. (c) Corriu, R. J. P.; Masse, J. P. *J. Chem. Soc., Chem. Commun.* **1972**, No. 3, 144. (d) Mizoroki, T.; Mori, K.; Ozaki, A. *Bull. Chem. Soc. Jpn.* **1971**, *44*, 581–581. (e) Heck, R. F.; Nolley, J. P. *J. Org. Chem.* **1972**, *37*, 2320–2322. (f) Yamamura, M.; Moritani, I.; Murahashi, S.-I. *J. Organometal. Chem.* **1975**, *91*, C39–C42. (g) Sonogashira, K.; Tohda, Y.; Hagihara, N. *Tetrahedron Lett.* **1975**, *16*, 4467–4470. (h) King, A. O.; Okukado, N.; Negishi, E. *J. Chem. Soc., Chem. Commun.* **1977**, No. 19, 683–684. (i) Kosugi, M.; Sasazawa, K.; Shimizu, Y.; Migita, T. *Chem. Lett.* **1977**, *6*, 301–302. (j) Milstein, D.; Stille, J. K. *J. Am. Chem. Soc.* **1978**, *100*, 3636–3638. (k) Miyaura, N.; Suzuki, A. *J. Chem. Soc., Chem. Commun.* **1979**, No. 19, 866–867. (l) Hatanaka, Y.; Hiyama, T. *J. Org. Chem.* **1988**, *53*, 918–920.
- ³ Palladium-Catalyzed Cross-Coupling in Organic Synthesis. <https://www.nobelprize.org/uploads/2018/06/advanced-chemistryprize2010-1.pdf>
- ⁴ Kinzel, T.; Zhang, Y.; Buchwald, S. L. *J. Am. Chem. Soc.* **2010**, *132*, 14073–14075.
- ⁵ Yang, Y.; Lan, J.; You, J. *Chem. Rev.* **2017**, *117*, 8787–8863.
- ⁶ McMillen, D. F.; Golden, D. M. *Annu. Rev. Phys. Chem.* **1982**, *33*, 493–532.
- ⁷ Murai, S.; Kakiuchi, F.; Sekine, S.; Tanaka, Y.; Kamatani, A.; Sonoda, M.; Chatani, N. *Nature* **1993**, *366*, 529–531.

- ⁸ (a) Pivsa-Art, S.; Satoh, T.; Kawamura, Y.; Miura, M.; Nomura, M. *Bull. Chem. Soc. Jpn.* **1998**, *71*, 467–473. (b) Lane, B. S.; Brown, M. A.; Sames, D. *J. Am. Chem. Soc.* **2005**, *127*, 8050–8057.
- ⁹ (a) García-Cuadrado, D.; de Mendoza, P.; Braga, A. A. C.; Maseras, F.; Echavarren, A. *M. J. Am. Chem. Soc.* **2007**, *129*, 6880–6886. (b) Gorelsky, S. I.; Lapointe, D.; Fagnou, K. *J. Am. Chem. Soc.* **2008**, *130*, 10848–10849. (c) Gorelsky, S. I.; Lapointe, D.; Fagnou, K. *J. Org. Chem.* **2012**, *77*, 658–668.
- ¹⁰ (a) Thompson, M. E.; Baxter, S. M.; Bulls, A. R.; Burger, B. J.; Nolan, M. C.; Santarsiero, B. D.; Schaefer, W. P.; Bercaw, J. E. *J. Am. Chem. Soc.* **1987**, *109*, 203–219. (b) Hennessy, E. J.; Buchwald, S. L. *J. Am. Chem. Soc.* **2003**, *125*, 12084–12085.
- ¹¹ (a) Janowicz, A. H.; Bergman, R. G. *J. Am. Chem. Soc.* **1982**, *104*, 352–354. (b) Chen, H.; Schlecht, S.; Semple, T. C.; Hartwig, J. F. *Science* **2000**, *287*, 1995–1997. (c) Cho, J.-Y.; Tse, M. K.; Holmes, D.; Maleczka, R. E.; Smith, M. R. *Science* **2002**, *295*, 305–308. (d) Ishiyama, T.; Takagi, J.; Ishida, K.; Miyaura, N.; Anastasi, N. R.; Hartwig, J. F. *J. Am. Chem. Soc.* **2002**, *124*, 390–391.
- ¹² Stuart, D. R.; Fagnou, K. *Science* **2007**, *316*, 1172–1175.
- ¹³ Dong, J.; Long, Z.; Song, F.; Wu, N.; Guo, Q.; Lan, J.; You, J. *Angew. Chem. Int. Ed.* **2013**, *52*, 580–584.
- ¹⁴ Grzybowski, M.; Skonieczny, K.; Butenschön, H.; Gryko, D. T. *Angew. Chem. Int. Ed.* **2013**, *52*, 9900–9930.
- ¹⁵ Shriver, D.; Atkins, P.; Overton, T.; Rourke, J.; Weller, M.; Armstrong, F. *Shriver & Atkins Inorganic Chemistry*. Oxford, Oxford University Press, 2006.
- ¹⁶ (a) Hoyle, F. *Monthly Notices of the Royal Astronomical Society* **1946**, *106*, 343–383. (b) Burbidge, E. M.; Burbidge, G. R.; Fowler, W. A.; Hoyle, F. *Rev. Mod. Phys.* **1957**, *29*, 547–650.
- ¹⁷ (a) Nakamura, E.; Sato, K. *Nature Mater* **2011**, *10*, 158–161. (b) Shang, R.; Ilies, L.; Nakamura, E. *Chem. Rev.* **2017**, *117*, 9086–9139.
- ¹⁸ Sun, Y.; Tang, H.; Chen, K.; Hu, L.; Yao, J.; Shaik, S.; Chen, H. *J. Am. Chem. Soc.* **2016**, *138*, 3715–3730.
- ¹⁹ Norinder, J.; Matsumoto, A.; Yoshikai, N.; Nakamura, E. *J. Am. Chem. Soc.* **2008**, *130*, 5858–5859.

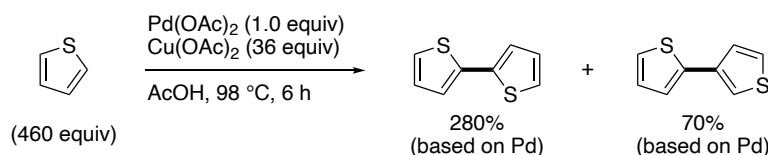
- ²⁰ Zaitsev, V. G.; Shabashov, D.; Daugulis, O. *J. Am. Chem. Soc.* **2005**, *127*, 13154–13155.
- ²¹ (a) Shang, R.; Ilies, L.; Matsumoto, A.; Nakamura, E. *J. Am. Chem. Soc.* **2013**, *135*, 6030–6032. (b) Shang, R.; Ilies, L.; Asako, S.; Nakamura, E. *J. Am. Chem. Soc.* **2014**, *136*, 14349–14352. (c) Shang, R.; Ilies, L.; Nakamura, E. *J. Am. Chem. Soc.* **2015**, *137*, 7660–7663. (d) Ilies, L.; Ichikawa, S.; Asako, S.; Matsubara, T.; Nakamura, E. *Adv. Synth. Catal.* **2015**, *357*, 2175–2179. (e) Ilies, L.; Itabashi, Y.; Shang, R.; Nakamura, E. *ACS Catal.* **2017**, *7*, 89–92.
- ²² Asako, S.; Ilies, L.; Nakamura, E. *J. Am. Chem. Soc.* **2013**, *135*, 17755–17757.
- ²³ Matsubara, T.; Asako, S.; Ilies, L.; Nakamura, E. *J. Am. Chem. Soc.* **2014**, *136*, 646–649.
- ²⁴ Ilies, L.; Matsubara, T.; Ichikawa, S.; Asako, S.; Nakamura, E. *J. Am. Chem. Soc.* **2014**, *136*, 13126–13129.
- ²⁵ (a) Matsubara, T.; Ilies, L.; Nakamura, E. *Chem. Asian J.* **2016**, *11*, 380–384. (b) Ilies, L.; Zhou, Y.; Yang, H.; Matsubara, T.; Shang, R.; Nakamura, E. *ACS Catal.* **2018**, *8*, 11478–11482. (c) Ilies, L.; Arslanoglu, Y.; Matsubara, T.; Nakamura, E. *Asian J. Org. Chem.* **2018**, *7*, 1327–1329.
- ²⁶ Boddie, T. E.; Carpenter, S. H.; Baker, T. M.; DeMuth, J. C.; Cera, G.; Brennessel, W. W.; Ackermann, L.; Neidig, M. L. *J. Am. Chem. Soc.* **2019**, *141*, 12338–12345.
- ²⁷ Shang, R.; Ilies, L.; Nakamura, E. *J. Am. Chem. Soc.* **2016**, *138*, 10132–10135.
- ²⁸ Kuhl, N.; Hopkinson, M. N.; Wencel-Delord, J.; Glorius, F. *Angew. Chem. Int. Ed.* **2012**, *51*, 10236–10254.
- ²⁹ Doba, T.; Matsubara, T.; Ilies, L.; Shang, R.; Nakamura, E. *Nat. Catal.* **2019**, *2*, 400–406.
- ³⁰ (a) Shirota, Y.; Kageyama, H. *Chem. Rev.* **2007**, *107*, 953–1010. (b) Wang, C.; Dong, H.; Hu, W.; Liu, Y.; Zhu, D. *Chem. Rev.* **2012**, *112*, 2208–2267. (c) Sirringhaus, H. *Adv. Mater.* **2014**, *26*, 1319–1335. (d) Facchetti, A. *Materials Today* **2007**, *10*, 28–37. (e) Wu, W.; Liu, Y.; Zhu, D. *Chem. Soc. Rev.* **2010**, *39*, 1489–1502. (f) O'Neill, M.; Kelly, S. M. *Adv. Mater.* **2011**, *23*, 566–584. (g) Murphy, A. R.; Fréchet, J. M. J. *Chem. Rev.* **2007**, *107*, 1066–1096. (h) Zhang, F.; Wu, D.; Xu, Y.; Feng, X. *J. Mater. Chem.* **2011**, *21*, 17590. (i) Ameri, T.; Khoram, P.; Min, J.; Brabec, C. *Adv. Mater.* **2013**, *25*, 4245–4266.

Chapter 2.
Iron-Catalyzed Regioselective Thienyl C–H/C–H Homocoupling

2-1. Introduction

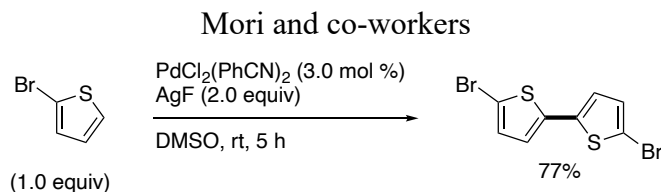
Bithiophene compounds have wide application in the field of organic electronics such as organic field-effect transistors (OFETs), organic light-emitting diodes (OLEDs), and organic solar cells (OSCs).¹ Aiming for the direct synthesis of bithiophene compounds, transition-metal-catalyzed thienyl C–H/C–H homocoupling have attracted much attention as one of the most straightforward methods to synthesize those compounds from simple thiophene substrates. The first example of transition-metal-catalyzed thienyl C–H/C–H homocoupling was reported by Kozhevnikov in 1976 using $\text{Pd}(\text{OAc})_2$ as a catalyst and $\text{Cu}(\text{OAc})_2$ as an oxidant (Scheme 1).² This reaction gave a mixture of 2,2'-bithiophene and 2,3'-bithiophene.

Scheme 1. The first example of transition-metal-catalyzed thienyl C–H/C–H homocoupling



Despite the synthetic significance of transition-metal-catalyzed thienyl C–H/C–H homocoupling, it is only recently that a synthetically useful versions have been investigated seriously. In 2004, Mori and co-workers succeeded in reducing the amount of thiophene starting materials to 1 equiv in palladium-catalyzed thienyl C–H/C–H homocoupling (Scheme 2).³ The key was the use of AgF both as an oxidant and an effective promoter to generate an active catalytic intermediate.

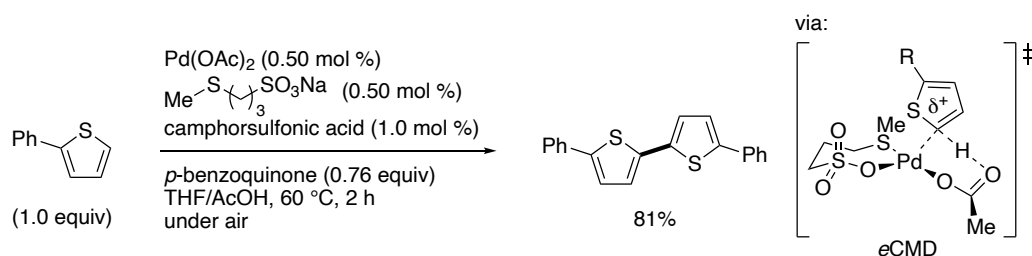
Scheme 2. Palladium-catalyzed thienyl C–H/C–H homocoupling reported by



After this report, several other palladium catalytic systems were reported. In 2019, Carrow and co-workers reported that a thioether ligand facilitates the palladium-catalyzed

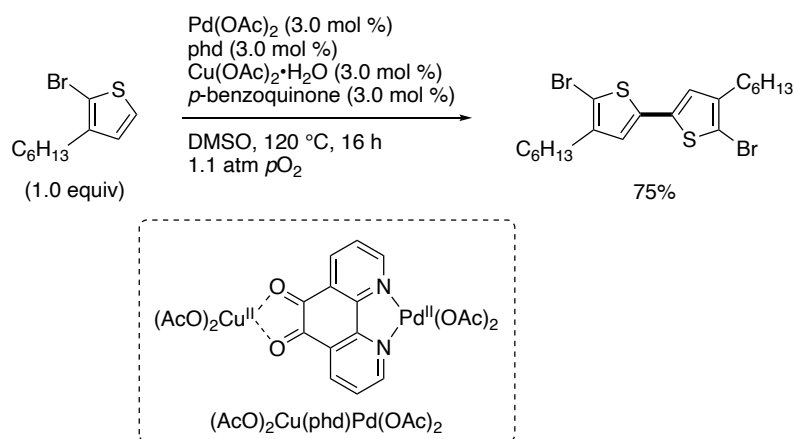
thienyl C–H/C–H homocoupling by *electrophilic* concerted metalation-deprotonation (*eCMD*) mechanism where positive charge buildup is observed on the substrate.⁴

Scheme 3. Palladium-catalyzed thienyl C–H/C–H homocoupling through *eCMD* process



Stahl and co-workers also reported the palladium-catalyzed aerobic thienyl C–H/C–H homocoupling using phenanthroline dione (phd) as an ancillary ligand and $\text{Cu}(\text{OAc})_2$ as a cocatalyst.⁵ They ascribed the superior performance of the phd ligand to the formation of a phd-bridged bimetallic species, $(\text{AcO})_2\text{Cu}(\text{phd})\text{Pd}(\text{OAc})_2$.

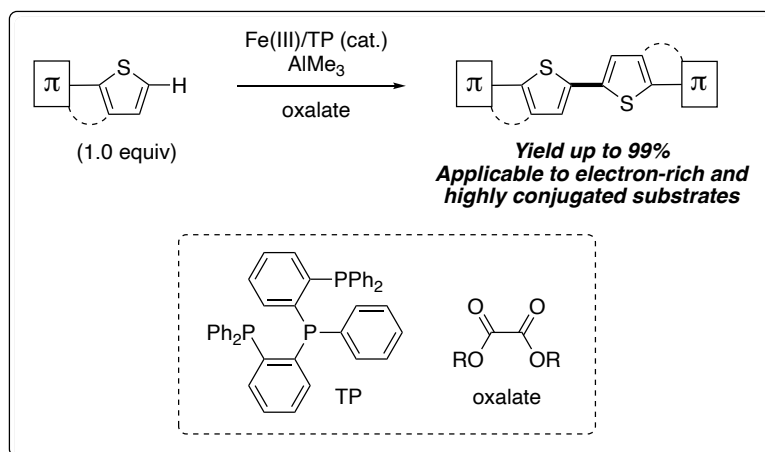
Scheme 4. Palladium-catalyzed aerobic thienyl C–H/C–H homocoupling



As explained above, a modern palladium-catalyzed C–H activation has broadened the scope, realizing a simple synthetic route to dimeric thiophene compounds. However, these reactions require strongly oxidizing conditions to turn over the $\text{Pd}(\text{II})/\text{Pd}(0)$ cycle with a large redox potential [$E^\circ(\text{Pd}^{\text{II}}/\text{Pd}^0) = +0.915 \text{ V vs NHE}$], which limits substrate versatility and reaction selectivity, especially in the synthesis of electron-rich and highly conjugated molecules. In this chapter I report iron-catalyzed regioselective thienyl C–

H/C–H homocoupling using conjugated tridentate phosphine as a ligand, AlMe_3 as a base, and diethyl oxalate as a mild oxidant, enabling the synthesis of π -conjugated dimeric and oligomeric thiophene compounds of importance in materials science.

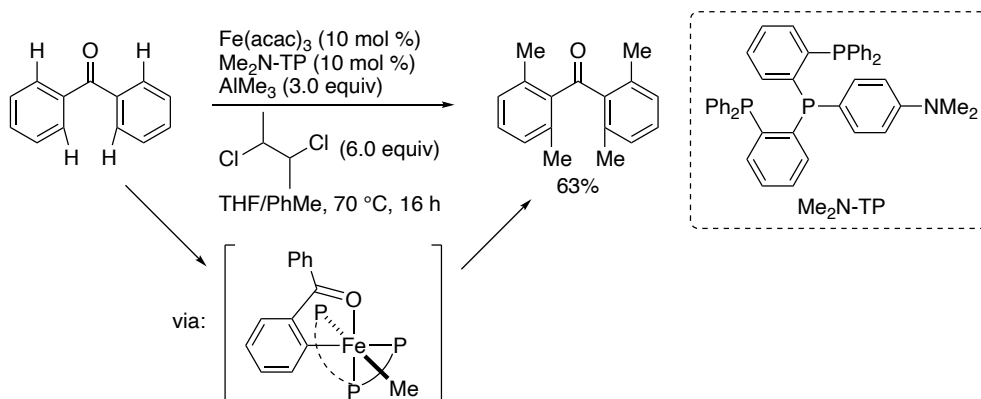
Scheme 5. Iron-catalyzed regioselective thienyl C–H/C–H homocoupling



2-2. Initial discovery

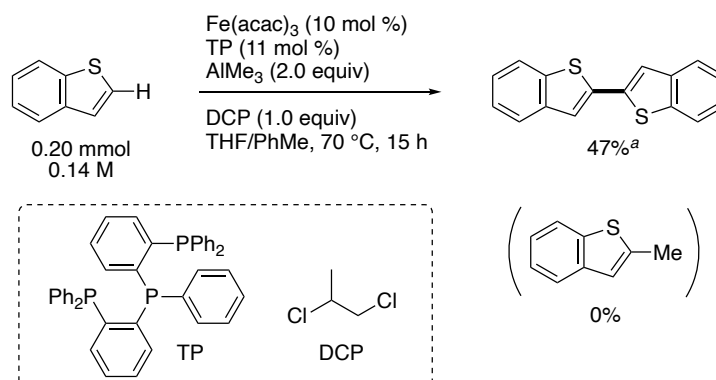
The starting point of the investigation was the iron-catalyzed *ortho* C–H methylation of aromatics bearing a simple carbonyl group as a directing group reported by Nakamura and co-workers in 2016 (Scheme 6).⁶ The key to the success was to use tridentate phosphine as a ligand and AlMe_3 as a mild base and a methyl donor to generate organoiron species stable enough to activate the C–H bond of weakly coordinating substrates. As seen in the crystal structure of Fe(II)/TP complexes,⁷ three phosphine groups are suitable for tridentate coordination. AlMe_3 was solely effective and other organometallic reagents such as AlEt_3 , AlPh_3 , ZnMe_2 , MeMgBr were all ineffective.

Scheme 6. Iron-catalyzed *ortho* C–H methylation of aromatics bearing a simple carbonyl group as a directing group



Based on these results, I expected that this reaction system is also applicable to the C–H activation of thiophene compounds that do not possess a directing group, which is also weakly coordinating through the sulfur atom or the π orbitals.⁸ To my delight, using benzo[*b*]thiophene as a substrate, the desired homocoupling product was obtained in moderate yield by regioselective C–H activations at the most acidic C–H bond next to the sulfur atom (Scheme 7).⁹ Notably, no methylation product was detected probably because of the slow reductive elimination with the methyl group.¹⁰ However, even after rigorous investigation of the reaction parameters, the yield reached no higher than 50%.

Scheme 7. Initial discovery of iron-catalyzed regioselective thienyl C–H/C–H homocoupling

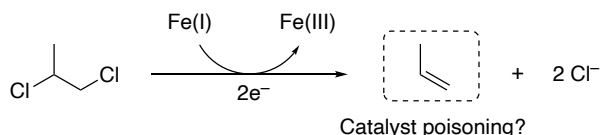


^a The yield was determined by ^1H NMR using 1,1,2,2-tetrachloroethane as an internal standard.

2-3. Catalyst poisoning by alkene

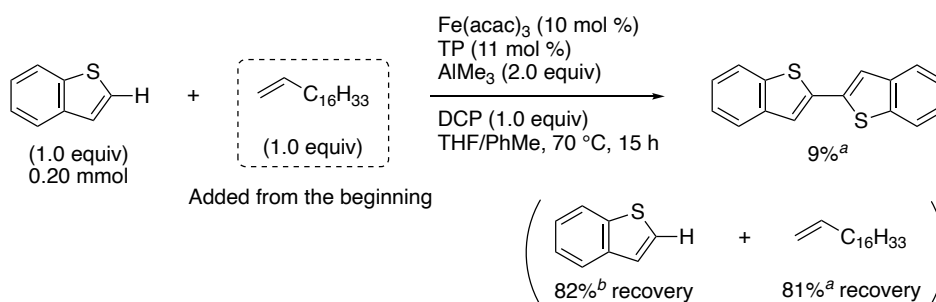
Taking into account that the yield of the homocoupling product always stopped at around 50%, I speculated that propene generated by reduction of DCP is inhibiting the reaction by catalyst poisoning.

Scheme 8. Generation of propene by reduction of DCP



To investigate the inhibition effect of alkene, 1-octadecene was added from the beginning of the reaction (Scheme 9). As expected, the catalyst failed to turnover, giving only 9% of the homocoupling product with recovery of benzo[*b*]thiophene and 1-octadecene in 82% and 81%, respectively. This result clearly shows that the reaction is inhibited by the coordination of alkene to the catalyst when DCP is used as an oxidant. This is in stark contrast with iron-catalyzed directed C–H activation,¹¹ where substrates have a stronger coordinating ability than alkenes so that the efficiency of the reactions are not affected by a growing amount of alkene. Therefore, in order to further improve the efficiency of the homocoupling reaction, investigation of other oxidants that do not generate alkenes after its reduction is necessary.

Scheme 9. Inhibition effect of alkene



^a Yields were determined by ¹H NMR using 1,1,2,2-tetrachloroethane as an internal standard.

^b The yield was determined by GC using tridecane as an internal standard.

2-4. Diketone as a mild oxidant

By knowing that a carbonyl group can coordinate to iron and accept electron in the iron-catalyzed *ortho* C–H methylation reaction, I came up with the idea of using diketone as a mild oxidant in the iron-catalyzed thienyl C–H/C–H homocoupling reaction. The working hypothesis is shown in Figure 1. First, Fe(III)-Me₂ species (**I**) activates the most acidic C–H bond of a thiophene twice through σ -bond metathesis mechanism to afford the Fe(III)-Ar₂ species (**II**). After reductive elimination, the homocoupling product and Fe(I) species is generated. This low-valent species is oxidized by diketone in combination with AlMe₃ via inner-sphere electron transfer (**III**) to form an aluminum enediolate (**IV**) to close the catalytic cycle. The strong oxophilicity of Al(III) contributes as the driving force for effective catalyst turnover.

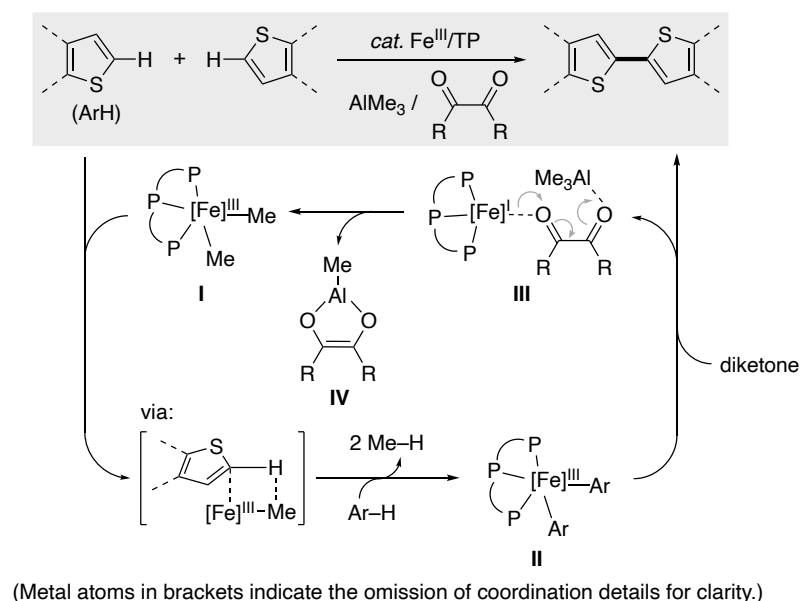
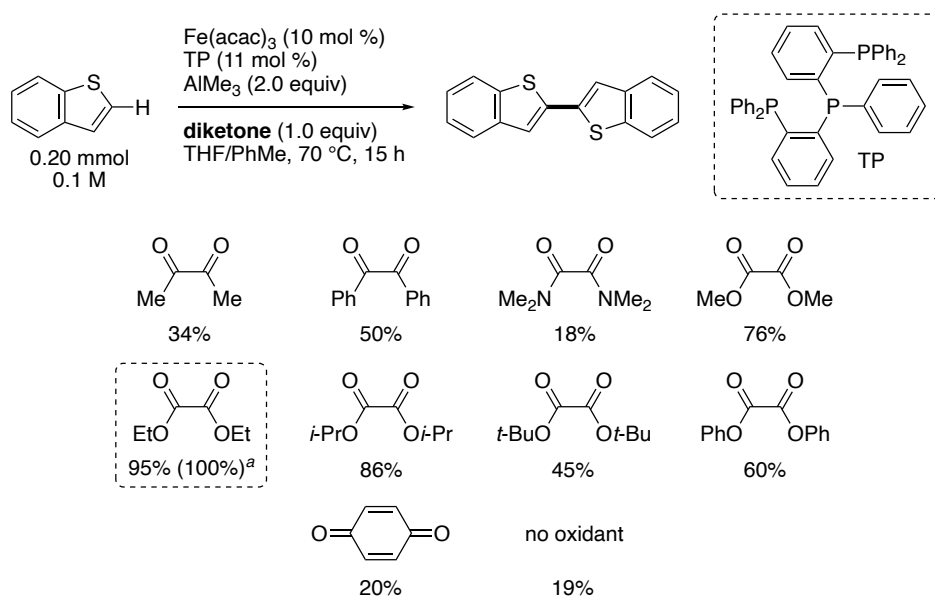


Figure 1. The idea of using diketone as an oxidant

Based on this concept, various kinds of diketones were tested as an oxidant (Table 1). Among diacetyl, dibenzoyl (benzil), diamide, and diester (oxalate), diester gave the highest conversion of the starting material. No methylation of benzo[*b*]thiophene was observed in any cases. After determining oxalate as a suitable oxidant, the effect of substituents on oxalates was examined. Generally speaking, oxalates with lower LUMO energy gave higher conversion because of higher ability to accept electron, but dimethyl oxalate was inferior to diethyl oxalate. This phenomena can be ascribed to the instability

of dimethyl oxalate under the reaction conditions (Scheme 10). Diphenyl oxalate also gave lower conversion possibly due to the same reason. By increasing the concentration to 0.7 M, 1.0 equiv of AlMe_3 and 0.50 equiv of diethyl oxalate were enough to achieve a full conversion of the starting material. *p*-Benzoquinone often used in palladium-catalyzed C–H activation¹² were ineffective for this reaction. It is a great advantage of using diethyl oxalate as an oxidant because of its mildness, natural abundance, and low cost compared to metal oxidants (e.g. Ag(I) , Cu(II)).

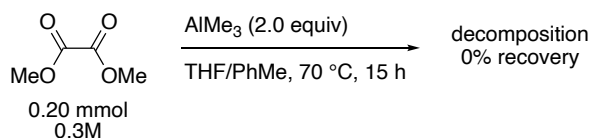
Table 1. Investigation of diketone as a mild oxidant



Conversion yields were determined by GC using tridecane as an internal standard.

^a The reaction was performed with 1.0 equiv of AlMe_3 and 0.50 equiv of $(\text{COOEt})_2$ in 0.7 M.

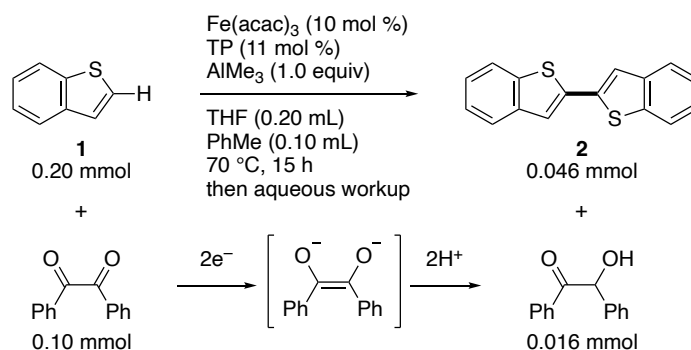
Scheme 10. Instability of dimethyl oxalate



Attempts to detect ethyl glyoxalate after hydrolysis or enediolate **IV** *in situ* have failed so far probably because of the aggregation and high oxophilicity of Al(III) species. However, the reaction using benzil in place of diethyl oxalate produced the homocoupling product in moderate yield and benzoin, providing evidence for the formation of **IV**, and

the role of diethyl oxalate as a two-electron acceptor from the iron catalytic cycle. Moreover, two-electron reduction of diethyl oxalate with alkali metal has been reported.¹³

Scheme 11. Detection of benzoin

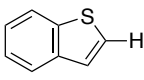
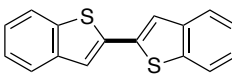


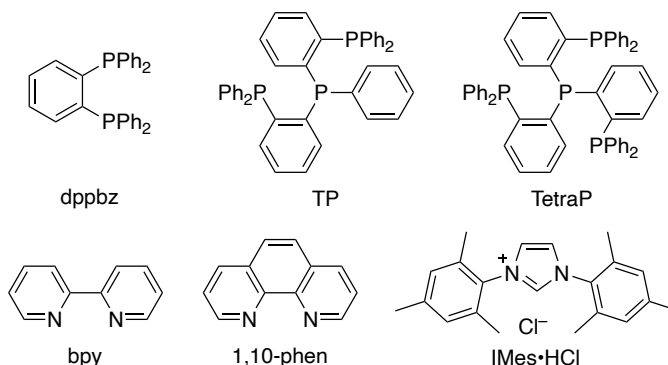
2-5. Effect of reaction parameters

With optimal oxidant in hand, I investigated the effect of other reaction parameters on the product yield. Notably, in all cases, no methylation of the starting material was observed and the recovery of the starting material accounted for the mass balance. Under the standard conditions using 10 mol % of $\text{Fe}(\text{acac})_3$ as a catalyst, 11 mol % of TP as a ligand, 1.0 equiv of AlMe_3 as a base, and 0.50 equiv of diethyl oxalate as an oxidant in a mixed solvent of THF and toluene at 70 °C for 15 h, the reaction proceeded in quantitative yield (Table 2, entry 1). A commercially available toluene solution of AlMe_3 (2 M) instead of a neat AlMe_3 was used to safely operate the organometallic reagent. Control experiments proved that all of the components including THF are necessary (entry 2–6). Etheral solvent may help to stabilize organoiron species by coordination to the vacant site. The use of Fe(II) instead of Fe(III) significantly decreased the yield, suggesting that the reaction proceeds through a Fe(III)/Fe(I) cycle rather than a Fe(II)/Fe(0) cycle (entry 7). Interestingly, the use of monodentate or bidentate phosphine ligands failed to give the product and iron black was observed, indicating that the stabilization of iron from over-reduction by organometallic base is not sufficient (entry 8 and 9). A tetradentate phosphine ligand, TetraP, also failed to give the product possibly because of the steric hindrance of an additional diphenylphosphino group (entry 10). Other common ligands such as bipyridine, phenanthroline, and *N*-heterocyclic carbene ligands were all ineffective (entry 11–13). Ineffectiveness of AlEt_3 was ascribed to the formation of an inactive iron-hydride species after β -hydride elimination of the ethyl group (entry 14).⁶

MeLi, MeMgBr, and MeZnBr were also ineffective because of their strong nucleophilicity incompatible with oxalate and high reducing ability (entry 15).¹⁴ Reaction with less catalyst loading and reaction at lower temperature resulted in incomplete conversions (entry 16 and 17).

Table 2. Effect of reaction parameters

<div style="display: flex; align-items: center; justify-content: space-around;"> <div style="text-align: center;">  <p>1 0.20 mmol</p> </div> <div style="text-align: center;"> <p>Fe(acac)₃ (10 mol %) TP (11 mol %) AlMe₃ (1.0 equiv) (COOEt)₂ (0.50 equiv) THF (0.20 mL) PhMe (0.10 mL) 70 °C, 15 h</p> </div> <div style="text-align: center;">  <p>2</p> </div> </div>		
entry	variation from standard condition	yield (%) ^a
1	none	100
2	without Fe(acac) ₃	0
3	without TP	0
4	without AlMe ₃	0
5	without (COOEt) ₂	7
6	without THF	34
7	Fe(acac) ₂ instead of Fe(acac) ₃	47
8	PPh ₃ (33 mol %) instead of TP	0
9	dppbz instead of TP	0
10	TetraP instead of TP	0
11	bpy instead of TP	0
12	1,10-phen instead of TP	0
13	IMes•HCl instead of TP	0
14	AlEt ₃ instead of AlMe ₃	0
15	MeLi, MeMgBr, or MeZnBr instead of AlMe ₃	0
16	Fe(acac) ₃ (1.0 mol %), TP (1.1 mol %)	40
17	50 °C instead of 70 °C	35



No methylation of **1** was detected by GC.

^a Yields were determined by ¹H NMR using 1,3,5-trimethoxybenzene as an internal standard.

2-6. Substrate scope

Table 3 illustrates the scope of iron-catalyzed regioselective thienyl C–H/C–H homocoupling. The reaction cleanly produced the desired product, which was easily isolated either by silica gel chromatography or by filtration and reprecipitation. The reaction took place exclusively at the C–H bond next to the sulfur atom on thiophenes. These results clearly demonstrate that iron-catalyzed C–H activation through σ -bond metathesis mechanism, which favors the most acidic C–H bond, is beneficial to control the regioselectivity of the reaction. C–H methylation instead of C–H/C–H homocoupling barely took place (detected for **15**, **16**, and **17** in <1% yield). Dimers of benzo[*b*]thiophene (**2**), 2-phenylthiophene (**3**), and 2,3-disubstituted thiophenes (**4**, **5**) were obtained in high to excellent yields. On the other hand, a hexyl substituent next to the potentially active C–H bond inhibits the C–H activation, producing head-to-head coupled tetrathiophene (**6**) as an exclusive product. π -Motifs commonly found in optoelectronic materials, such as benzofuran (**7**), benzo[1,2-*b*:4,5-*b'*]dithiophene (**8**), vinylene (**9**), fluorene (**13**), carbazoles (**16**, **17**), and electron-rich triarylaminines (**18**, **19**), were well tolerated under mildly oxidative conditions. The reaction tolerates triisopropylsilyl (**8–10**), tributyltin (**11**), and pinacoboronate (**12**) on arenes, which are useful for transition-metal-catalyzed cross-coupling reactions for further functionalization. An oligo-thienylenevinylene product (**9**), which is susceptible to electron-transfer side reactions, was obtained in high yield without isomerization of the double bond. Since 1-octadecene heavily suppressed the reaction (Scheme 9), this contrast suggests that the Fe(III)/TP coordination site is sensitive to steric effects of the incoming π -substrates. Electron-rich oligothiophenes with silicon and tin protection at the terminal position were obtained in high yields (**10**, **11**). The nonoxidative conditions created by a mild oxalate oxidant keeps intact the multi-aromatic array in **14**, which is potentially susceptible to the conventional oxidative aromatic coupling under strongly oxidizing conditions.¹⁵ Electron-rich 3,4-ethylenedioxythiophene (EDOT)¹⁶ reacted in moderate yield due to steric hindrance by the 3,4-substituents (**15**). Because of the mildness of oxalate as an oxidant for iron, a hole-transporting material for perovskite solar cells (**19**),¹⁷ which is susceptible to direct oxidation by strong oxidant, was synthesized in excellent yield. Reactions under Mori's conditions (PdCl₂(PhCN)₂ (3.0 mol %), AgF (2.0 equiv), DMSO, 60 °C, 5 h) only gave the homocoupling products in moderate yields (**2**, **16**), demonstrating the usefulness of the iron homocoupling method.

Table 3. Substrate scope

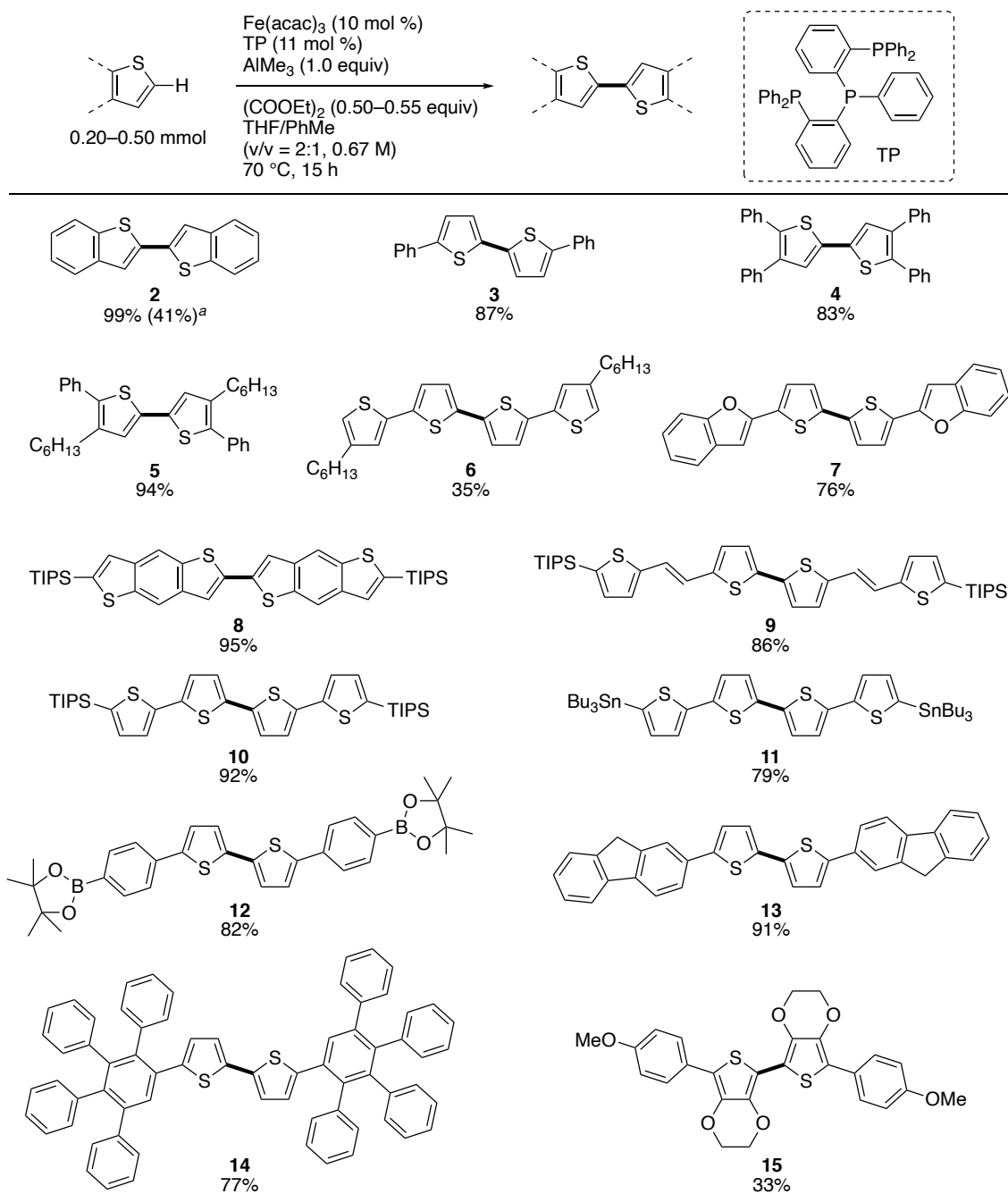
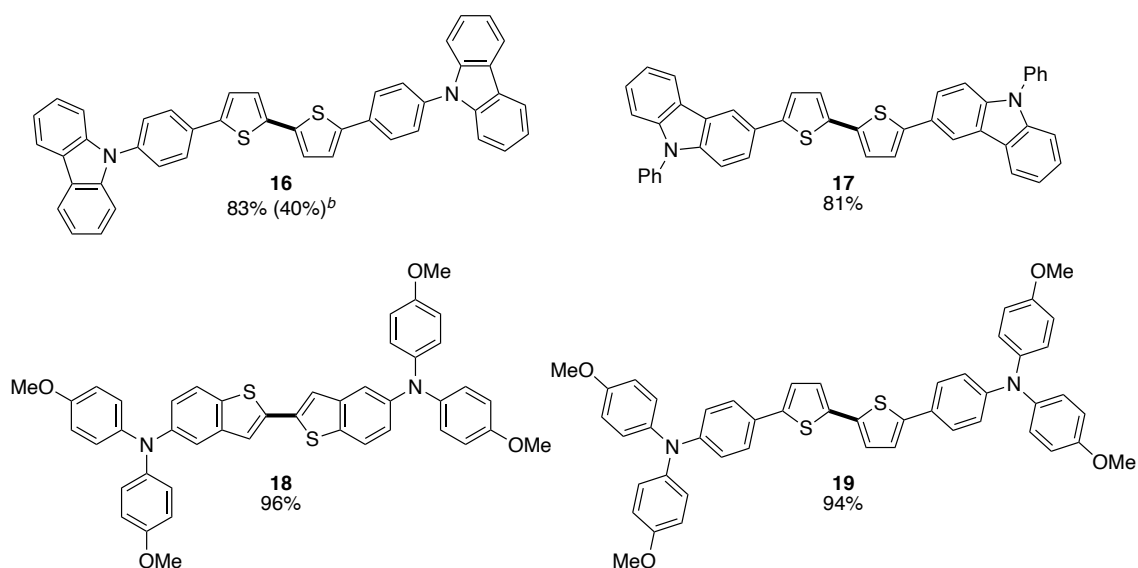


Table 3. (continued)



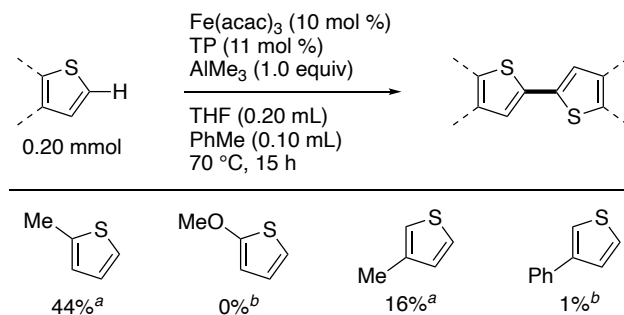
All yields are isolated yields unless otherwise noted.

^a Reported isolate yield under Mori's conditions: PdCl₂(PhCN)₂ (3.0 mol %), AgF (2.0 equiv), DMSO, 60 °C, 5 h.

^b ¹H NMR yield under Mori's conditions.

2-7. Unsuccessful substrates

Table 4 illustrates the examples of unsuccessful substrates. Notably, the efficiency of this iron-catalyzed thienyl C–H/C–H homocoupling significantly drops with thiophene substrates that do not have an extended π conjugation. NICS(1) values¹⁸ calculated at the B3LYP/6-31G(d) level of theory clearly showed that substrates with lower aromaticity are more reactive and substrates with higher aromaticity are less reactive (Figure 2a). As reported in other transition-metal-catalyzed reactions,¹⁹ this phenomena can be ascribed to the partial loss of aromaticity in the transition state of C–H activation. With non- π -extended substrates, or substrates with higher aromaticity, the activation energy of C–H activation would be too high because of large dearomatization energy of the thienyl group (Figure 2b).

Table 4. Unsuccessful substrates

^a Yields were determined by ¹H NMR using 1,1,2,2-tetrachloroethane as an internal standard.

^b The yield was estimated by GC using tridecane as an internal standard.

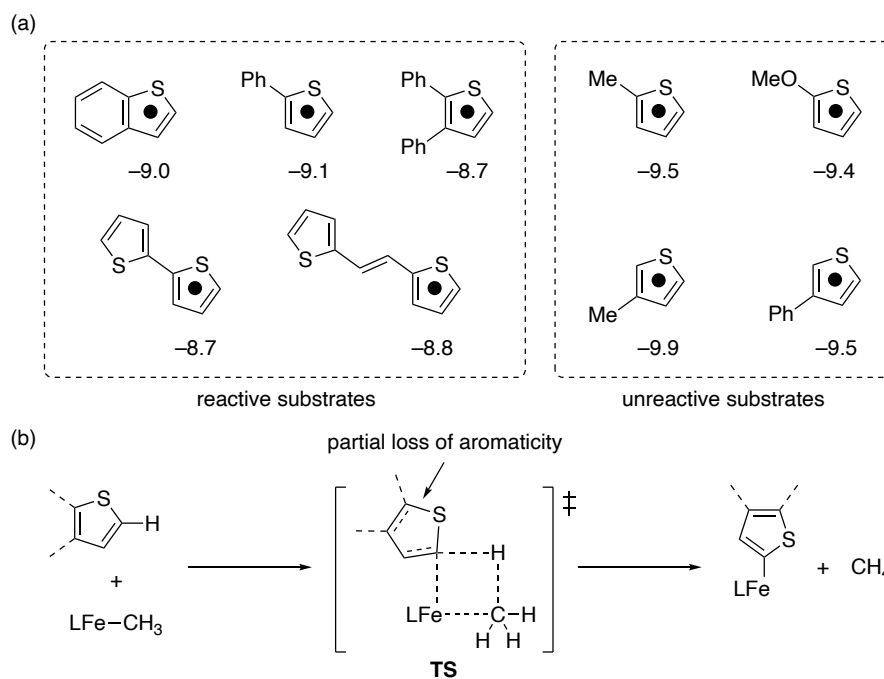


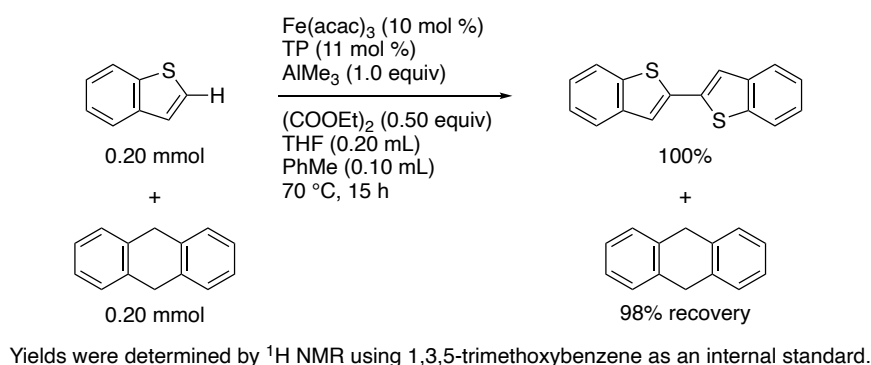
Figure 2. Reactivity of π -extended and non- π -extended thiophenes. (a) NICS(1) values.

(b) Partial loss of aromaticity in the transition state.

2-8. Addition of radical scavenger

To see if any radical process is taking place, iron-catalyzed regioselective thienyl C–H/C–H homocoupling was conducted in the presence of a radical scavenger, 9,10-dihydroanthracene. As shown in Scheme 12, the homocoupling product was obtained in quantitative yield even in the presence of a radical scavenger and the radical scavenger was fully recovered. These results rule out the possibility of C–H activation through a radical process and indicate that the reaction proceeds through a two-electron process.

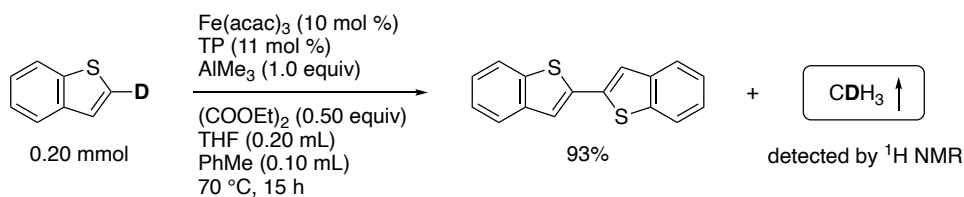
Scheme 12. Iron-catalyzed regioselective thienyl C–H/C–H homocoupling in the presence of a radical scavenger



2-9. The role of AlMe_3 as a base

To confirm the role of AlMe_3 as a base in iron-catalyzed thienyl C–H activation through a two-electron process, detection of CDH_3 was attempted using benzo[*b*]thiophene-2-*d* as a substrate. The reaction was conducted in a sealed Schlenk tube and the gas was collected by the water displacement method and analyzed by ^1H NMR. A triplet peak of CDH_3 was observed, which provides evidence that the methyl group coming from AlMe_3 abstracts proton from the thiophene substrate.

Scheme 13. Detection of CDH_3



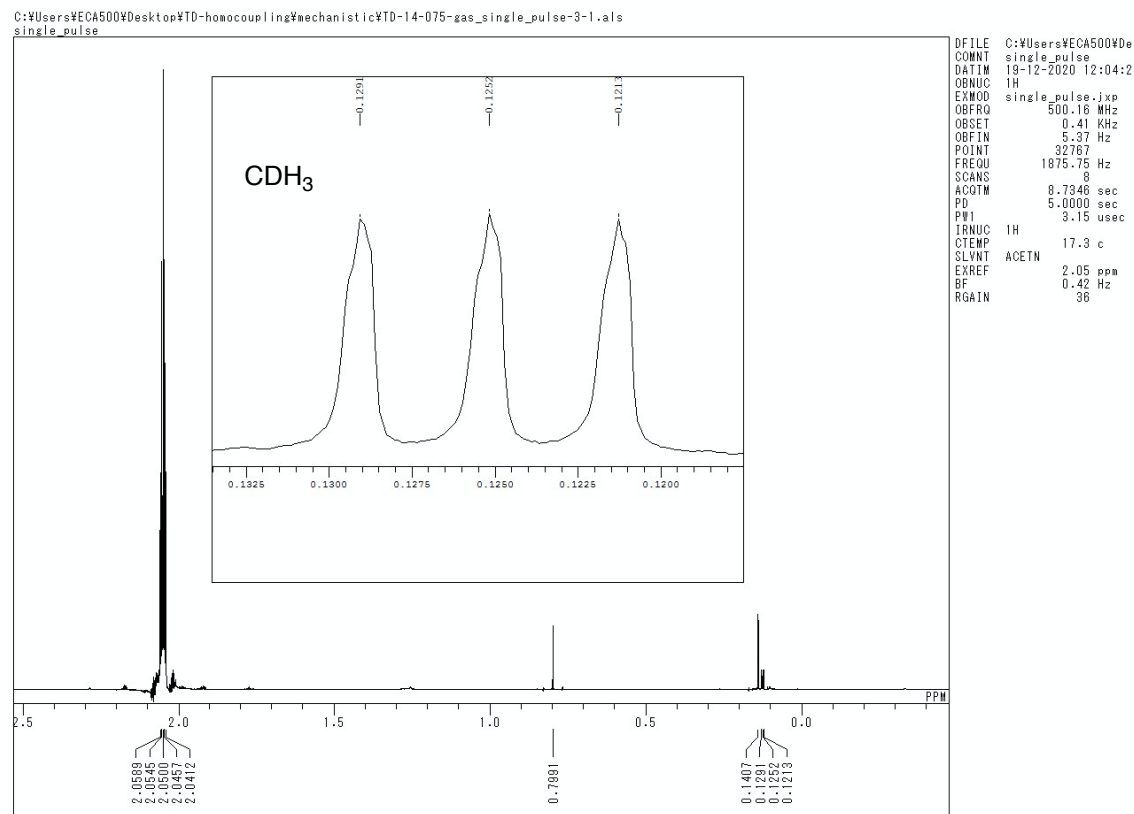
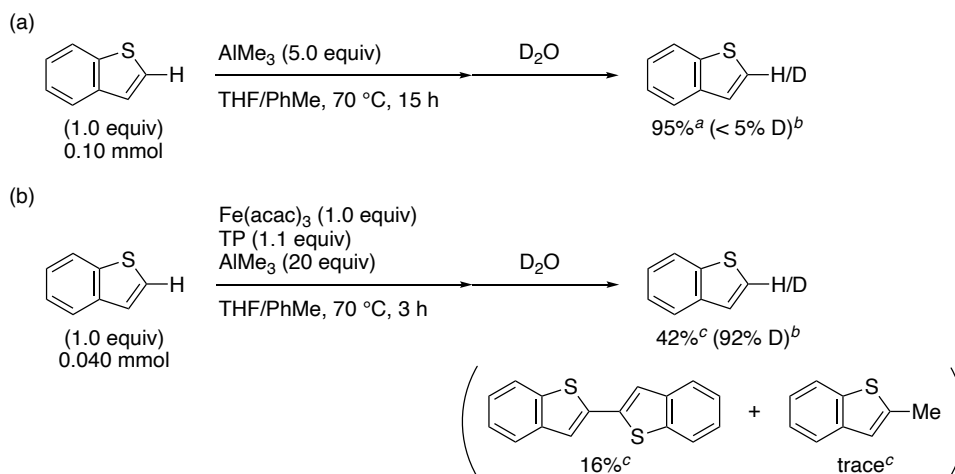


Figure 3. ^1H NMR spectrum of CDH_3

2-10. Stoichiometric experiments

To obtain direct evidence that the C–H bond is activated by iron catalyst, stoichiometric experiments were conducted. When 1.0 equiv of benzo[*b*]thiophene was treated with 1.0 equiv of AlMe_3 without iron catalyst at 70 °C for 15 h and quenched with D_2O , no deuterium incorporation was observed (Scheme 14a). This indicates that there is no alunimation to form a C–Al bond by deprotonation of a C–H bond by AlMe_3 . On the other hand, when a similar experiment was performed in the presence of a stoichiometric amount of $\text{Fe}(\text{acac})_3/\text{TP}$, 92% of deuterium incorporation on the starting material was observed, accompanying the formation of a small amount of the homocoupling product and a trace amount of the methylation product (Scheme 14b). These results strongly suggest that Fe-thiophene species is involved in the C–H activation steps.

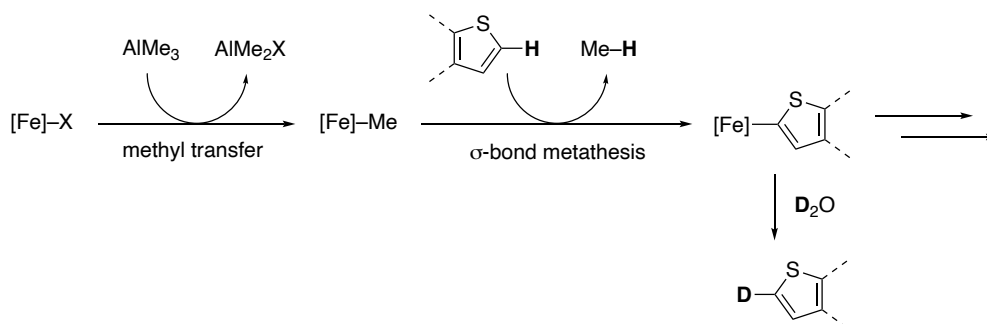
Scheme 14. Stoichiometric experiments

^a The yield was determined by GC using tridecane as an internal standard.

^b The deuterium incorporation ratio was determined by ^1H NMR.

^c Yields were determined by ^1H NMR using 1,1,2,2-tetrachloroethane as an internal standard.

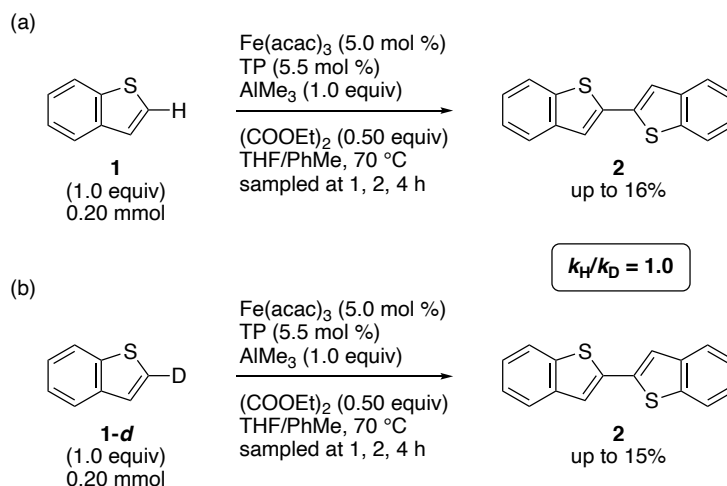
These mechanistic studies altogether support the mechanism in which the methyl group of AlMe_3 transfers to iron catalyst to form an Fe-Me species, which activates the C–H bond of a thiophene through σ -bond metathesis to generate an Fe -thiophene species by releasing methane (Scheme 15). Subsequent second C–H activation and reductive elimination steps will give the observed homocoupling product.

Scheme 15. A proposed mechanism of C–H activation

2-11. Kinetic isotope effect experiments

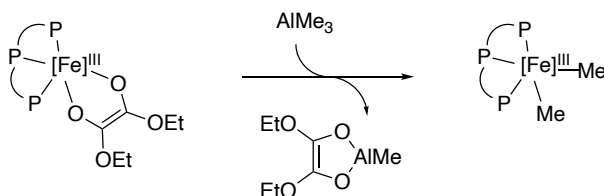
To examine if either of the C–H activation steps is the turnover-limiting step, kinetic isotope effect experiments were conducted for two parallel reactions (Scheme 16). The initial reaction rates of benzo[*b*]thiophene and benzo[*b*]thiophene-2-*d* in a separate reaction vessels were measured by tracing the yields of the homocoupling product up to 16%. As a result, no difference of reaction rates was observed between two reactions. This suggests that neither of the C–H activation steps is the turnover-limiting step and the catalyst regeneration is the turnover-limiting step.²⁰ This is in line with the assumed catalyst regeneration mechanism where strongly binding bidentate enediolate has to undergo ligand exchange from Fe(III) to Al(III).

Scheme 16. Kinetic isotope effect experiments for two parallel reactions



Yields were determined by ¹H NMR using 1,3,5-trimethoxybenzene as an internal standard.

Scheme 17. Slow catalyst regeneration step



2-12. Conclusion

In conclusion, iron-catalyzed regioselective thienyl C–H/C–H homocoupling was developed using tridentate phosphine as a ligand, AlMe_3 as a base, and oxalate as a mild oxidant. Tridentate phosphine ligand was uniquely effective for this transformation and oxalate in combination with oxophilic AlMe_3 served as an effective but mild oxidant to oxidize Fe(I) species to regenerate Fe(III) catalyst. This reaction takes place exclusively at the C–H bond next to the sulfur atom of thienyl group and tolerates various kinds of redox-sensitive π motifs widely used in optoelectronic materials due to the mildness of the iron catalytic cycle created by the combination of low redox potential of Fe(III)/Fe(I) and mild oxalate oxidant. This work highlights the benefits of iron catalysis for the synthesis of π -conjugated dimeric and oligomeric compounds of importance in energy device applications. Further development of this homocoupling reaction to polymerization reaction will be discussed in the next chapter.

2-13. Experimental

Materials and methods

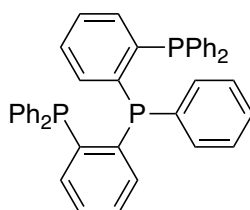
All air or moisture sensitive reactions were performed in a dry reaction vessel under argon atmosphere. Air or moisture sensitive liquids and solutions were transferred with syringe or Teflon cannula. The water content of solvents was confirmed to be less than 30 ppm by Karl-Fischer titration performed with MKC-210 (Kyoto Electronics Manufacturing Co., Ltd.). Analytical thin-layer chromatography (TLC) was performed with a glass plate coated with 0.25mm 230-400 mesh silica gel containing a fluorescent indicator. Organic solutions were evacuated with a diaphragm pump through a rotary evaporator. Flash column chromatography was performed as described by Still *et al.*²¹ Preparative recycling gel permeation chromatography (GPC) was performed with LC-92XX II NEXT instrument (Japan Analytical Industry Co., Ltd.) equipped with JAIGEL-2HR polystyrene columns using chloroform as an eluent at the flow rate of 7.5 mL/min.

Gas chromatography (GC) was performed with GC-2014 instrument (Shimadzu Co.) equipped with an ULBON HR-1 (0.25 mm I.D. x 25 m, 0.25 μ m, Shinwa Chemical Industries, Ltd.) capillary column. Mass spectra (GC-MS) were taken with Parvum 2 instrument (Shimadzu Co.). High-resolution mass spectra (HRMS) were taken with LCMS-IT-TOF (Shimadzu Co.) using reserpine (MW 608.2734) as an internal standard. Melting points of solid compounds were measured on a Mel-Temp capillary melting-point apparatus and were uncorrected. Nuclear magnetic resonance (NMR) spectra were taken with ECZ-500 (JEOL, Ltd.) at room temperature unless otherwise noted and reported in parts per million (ppm). ¹H NMR spectra were internally referenced to tetramethylsilane (0.00 ppm), CHCl₃ (7.26 ppm), CHDCl₂ (5.32 ppm), C₂HDCl₄ (5.97 ppm), or (CHD₂)(CD₃)SO (2.50 ppm). ¹³C NMR spectra were internally referenced to tetramethylsilane (0.0 ppm), CDCl₃ (77.0 ppm), CD₂Cl₂ (53.8 ppm), C₂D₂Cl₄ (73.8 ppm), or (CD₃)₂SO (39.5 ppm). ¹⁹F NMR spectra were internally referenced to C₆F₆ (−164.9 ppm). ³¹P NMR spectra were internally referenced to (CH₃O)₃PO (2.1 ppm). ICP analysis was performed on Shimadzu ICPS-7510 equipment.

Unless otherwise noted, reagents were purchased from Tokyo Chemical Industry Co., Ltd., Sigma-Aldrich Co., LCC, FUJIFILM Wako Pure Chemical Co., and other commercial suppliers and were used as received. Anhydrous tetrahydrofuran and diethyl ether were purchased from KANTO Chemical Co., Inc. and purified prior to use by a solvent purification system (GlassContour) equipped with columns of activated alumina

and supported copper catalyst.²² $\text{Fe}(\text{acac})_3$ (99.9% trace metal basis) was purchased from Sigma-Aldrich Co., LCC and used as received. Diethyl oxalate was purchased from Tokyo Chemical Industry Co., degassed by Freeze-Pump-Thaw cycling for three times, dried with molecular sieves 4A and kept in a storage flask. Starting materials were synthesized according to the literature.²³

Preparation of ((Phenylphosphanediy)bis(2,1-phenylene))bis(diphenylphosphane) (TP):



A hexane solution of BuLi (1.59 mol/L, 3.87 mL, 6.15 mmol) was added dropwise to a solution of (2-bromophenyl)diphenylphosphane (2.05 g, 6.00 mmol) in THF (12 mL) at $-78\text{ }^{\circ}\text{C}$. After stirring for 1 h, dichloro(phenyl)phosphane (0.41 mL, 3.0 mmol) was added in one portion and the reaction mixture was gradually warmed to room temperature. The reaction mixture was stirred for 16 h and quenched with water (50 mL). The aqueous layer was extracted with dichloromethane (500 mL), and the combined organic layers were washed with brine and dried over Na_2SO_4 . Most of the solvent was removed under reduced pressure and methanol (100 mL) was added under sonication. The white precipitate was collected by filtration and washed with methanol to afford the product as white solid (1.7 g, 91%). The compound data was in good agreement with the literature.⁶

A representative procedure for the investigation of key reaction parameters of homocoupling (Table 2)

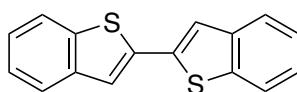
In an oven-dried Schlenk tube was added benzo[*b*]thiophene (27 mg, 0.20 mmol), TP (14 mg, 0.022 mmol), and a THF solution of $\text{Fe}(\text{acac})_3$ (0.10 mol/L, 0.20 mL, 0.020 mmol). Then, a toluene solution of AlMe_3 (2.0 mol/L, 0.10 mL, 0.20 mmol) was added dropwise at room temperature and the reaction mixture was stirred for 5 min to give a clear dark reddish brown solution. Diethyl oxalate (14 μL , 0.10 mmol) was added and the reaction mixture was stirred at $70\text{ }^{\circ}\text{C}$ for 15 h. The reaction mixture was cooled to rt, diluted with ethyl acetate (2 mL), and quenched carefully with methanol (0.1 mL). A saturated

aqueous solution of potassium sodium tartrate (1 mL) was added and the mixture was stirred vigorously until clear phase separation was observed. Tridecane (30 μ L) was added as an internal standard and a portion of the organic layer was passed through a pad of Florisil and analyzed by GC. For ^1H NMR analysis, the crude mixture was extracted with chloroform and 1,3,5-trimethoxybenzene was added as an internal standard. A portion of the organic layer was passed through a pad of Florisil and the solvent was removed under reduced pressure and the crude mixture was analyzed by ^1H NMR.

A general procedure for iron-catalyzed thienyl C–H/C–H homocoupling (Table 3)

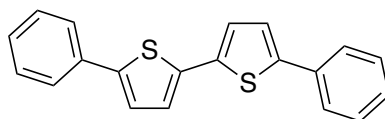
In an oven-dried Schlenk tube was added a thiophene (0.40 mmol), TP (28 mg, 0.044 mmol), and a THF solution of $\text{Fe}(\text{acac})_3$ (0.10 mol/L, 0.40 mL, 0.040 mmol). Then, a toluene solution of AlMe_3 (2.0 mol/L, 0.20 mL, 0.40 mmol) was added dropwise at rt and the reaction mixture was stirred for 5 min to give a clear dark reddish brown solution. Diethyl oxalate (27 μ L, 0.20 mmol) was added and the reaction mixture was stirred at 70 $^\circ\text{C}$ for 15 h. The reaction mixture was cooled to rt, diluted with ethyl acetate (4 mL), and quenched carefully with methanol (0.2 mL). A saturated aqueous solution of potassium sodium tartrate (2 mL) was added and the mixture was stirred vigorously until clear phase separation was observed. The aqueous layer was extracted with dichloromethane, and the combined organic layers were washed with brine and dried over Na_2SO_4 . The solvent was removed under reduced pressure and the crude product was purified by the indicated method below to afford the homocoupling product.

2,2'-Bibenzo[*b*]thiophene (2):



The title compound was obtained as white solid in 99% yield. The reaction was performed on a 0.40 mmol scale and the crude product was purified by silica gel chromatography (dichloromethane only). The compound data was in good agreement with the literature.²⁴ ^1H NMR (500 MHz, CDCl_3): δ 7.82 (d, J = 7.7 Hz, 2H), 7.77 (d, J = 7.7 Hz, 2H), 7.52 (s, 2H), 7.38–7.32 (m, 4H).

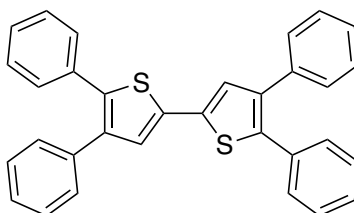
^{13}C NMR (125 MHz, CDCl_3): δ 140.2, 139.4, 137.2, 124.9, 124.8, 123.7, 122.2, 121.4.

5,5'-Diphenyl-2,2'-bithiophene (3):

The title compound was obtained as yellow solid in 87% yield. The reaction was performed on a 0.40 mmol scale and the crude product was purified by silica gel chromatography (dichloromethane only). The compound data was in good agreement with the literature.⁴

¹H NMR (500 MHz, CDCl₃): δ 7.62–7.60 (m, 4H), 7.41–7.39 (m, 4H), 7.31–7.28 (m, 2H), 7.25 (d, *J* = 3.9 Hz, 2H), 7.18 (d, *J* = 3.9 Hz, 2H).

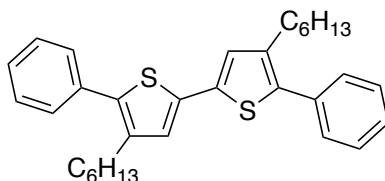
¹³C NMR (125 MHz, CDCl₃): δ 143.1, 136.7, 134.0, 129.0, 127.6, 125.6, 124.5, 123.8.

4,4',5,5'-Tetraphenyl-2,2'-bithiophene (4):

The title compound was obtained as yellow solid in 83% yield. The reaction was performed on a 0.20 mmol scale and the crude product was purified by silica gel chromatography (hexane: dichloromethane = 19/1 to 9/1). The compound data was in good agreement with the literature.²⁵

¹H NMR (500 MHz, CD₂Cl₂): δ 7.34–7.27 (m, 22H).

¹³C NMR (125 MHz, CD₂Cl₂): δ 139.3, 137.9, 136.6, 135.7, 134.2, 129.5, 129.4, 128.9, 128.8, 128.0, 128.0, 127.5, 127.5, 127.4, 127.3. (Multiple signals were observed because of slow rotation of bonds.)

4,4'-Diethyl-5,5'-diphenyl-2,2'-bithiophene (5):

The title compound was obtained as yellow solid in 94% yield. The reaction was performed on a 0.40 mmol scale and the crude product was purified by silica gel chromatography (dichloromethane only).

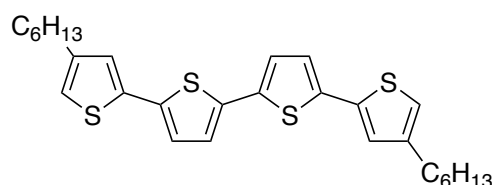
Melting point: 65–66 °C (dichloromethane)

¹H NMR (500 MHz, CDCl₃): δ 7.46–7.39 (m, 8H), 7.34–7.31 (m, 2H), 7.05 (s, 2H), 2.63 (t, *J* = 7.8 Hz, 4H), 1.64–1.61 (m, 4H), 1.34–1.25 (m, 12H), 0.86 (t, *J* = 6.9 Hz, 6H).

¹³C NMR (125 MHz, CDCl₃): δ 139.5, 136.6, 135.5, 134.4, 129.2, 128.5, 127.3, 125.9, 31.6, 30.9, 29.2, 28.8, 22.6, 14.1.

HRMS (APCI+): *m/z* calcd for C₃₂H₃₈S₂ [M+H⁺] 487.2488; found: 487.2498.

4,4'''-Dihexyl-2,2':5',2'':5'',2'''-quaterthiophene (6):



The title compound was obtained as orange solid in 35% yield. The reaction was performed on a 0.40 mmol scale and the crude product was purified by silica gel chromatography (hexane only).

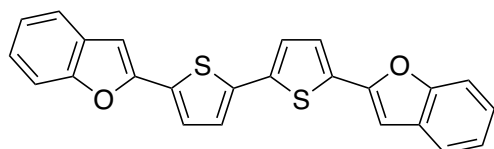
Melting point: 109–110 °C (dichloromethane)

¹H NMR (500 MHz, CDCl₃): δ 7.05–7.04 (m, 4H), 7.01 (d, *J* = 1.3 Hz, 2H), 6.81 (d, *J* = 1.3 Hz, 2H), 2.58 (t, *J* = 7.8 Hz, 4H), 1.64–1.55 (m, 4H), 1.37–1.30 (m, 12H), 0.90 (t, *J* = 7.2 Hz, 6H).

¹³C NMR (125 MHz, CDCl₃): δ 144.2, 136.6, 136.6, 135.6, 125.1, 124.1, 124.0, 119.2, 31.7, 30.5, 30.4, 29.0, 22.6, 14.1.

HRMS (APCI+): *m/z* calcd for C₂₈H₃₄S₄ [M+H⁺] 499.1616; found: 499.1630.

5,5'-Di(benzofuran-2-yl)-2,2'-bithiophene (7):



The title compound was obtained as orange solid in 76% yield. The reaction was performed on a 0.50 mmol scale using 0.55 equiv of diethyl oxalate and the pure product

was obtained by filtration of the crude reaction mixture and by washing the solid with minimal amounts of THF, an aqueous solution of HCl (1 M), and acetone.

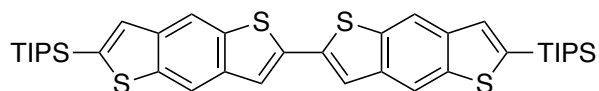
Melting point: 267–268 °C (THF/toluene)

^1H NMR (500 MHz, CDCl_3): δ 7.57 (d, J = 7.8 Hz, 2H), 7.51 (d, J = 8.1 Hz, 2H), 7.42 (d, J = 3.7 Hz, 2H), 7.31–7.28 (m, 2H), 7.25–7.22 (m, 4H), 6.90 (s, 2H).

^{13}C NMR (125 MHz, CDCl_3): δ 154.6, 150.6, 137.1, 132.2, 129.0, 125.4, 124.7, 124.5, 123.2, 120.8, 111.1, 101.5.

HRMS (APCI+): m/z calcd for $\text{C}_{24}\text{H}_{14}\text{O}_2\text{S}_2$ [$\text{M}+\text{H}^+$] 399.0508; found: 399.0503.

6,6'-Bis(triisopropylsilyl)-2,2'-bibenzo[1,2-*b*:4,5-*b'*]dithiophene (8):



The title compound was obtained as yellow solid in 95% yield. The reaction was performed on a 0.20 mmol scale and the crude product was purified by silica gel chromatography (hexane: chloroform = 5:1).

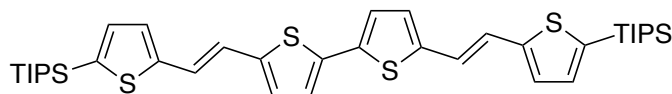
Melting point: 239–241 °C (chloroform)

^1H NMR (500 MHz, CDCl_3): δ 8.24 (s, 2H), 8.23 (s, 2H), 7.55 (s, 2H), 7.51 (s, 2H), 1.44 (sep, J = 7.6 Hz, 6H), 7.6 (d, J = 7.6 Hz, 36H).

^{13}C NMR (125 MHz, CDCl_3): δ 141.3, 139.4, 138.6, 137.9, 137.8, 136.5, 131.5, 120.7, 116.3, 116.1, 18.6, 11.8.

HRMS (APCI+): m/z calcd for $\text{C}_{38}\text{H}_{50}\text{O}_4\text{Si}_2$ [$\text{M}+\text{H}^+$] 691.2407; found: 691.2392.

5,5'-Bis((*E*)-2-(5-(triisopropylsilyl)thiophen-2-yl)vinyl)-2,2'-bithiophene (9):



The title compound was obtained as orange solid in 86% yield. The reaction was performed on a 0.20 mmol scale and the crude product was purified by silica gel chromatography (hexane: chloroform = 5:1).

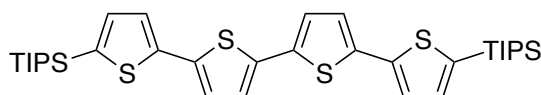
Melting point: 161–162 °C (chloroform)

^1H NMR (500 MHz, CDCl_3): δ 7.15 (d, J = 3.5 Hz, 2H), 7.12 (d, J = 3.5, 2H), 7.07–7.00 (m, 6H), 6.92 (d, J = 3.7 Hz, 2H), 1.34 (sep, J = 7.5 Hz, 6H), 1.12 (d, J = 7.5 Hz, 36H).

^{13}C NMR (125 MHz, CDCl_3): δ 147.2, 141.7, 136.4, 136.0, 134.4, 127.3, 127.1, 124.2, 121.5, 121.3, 18.6, 11.8.

HRMS (APCI+): m/z calcd for $C_{38}H_{54}S_4Si_2$ $[M+H]^+$ 695.2720; found: 695.2733.

5,5'''-Bis(triisopropylsilyl)-2,2':5',2'':5'',2'''-quaterthiophene (10):

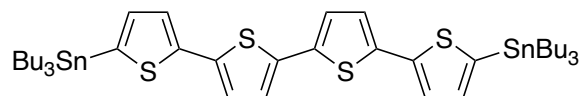


The title compound was obtained as yellow solid in 92% yield. The reaction was performed on a 0.20 mmol scale and the crude product was purified by silica gel chromatography (hexane: chloroform = 5:1). The compound data was in good agreement with the literature.²⁶

1H NMR (500 MHz, C_6D_6): δ 6.80 (d, J = 3.4 Hz, 2H), 6.64 (d, J = 3.4 Hz, 2H), 6.52 (d, J = 3.7 Hz, 2H), 6.43 (d, J = 3.7 Hz, 2H), 0.87 (sep, J = 7.4 Hz, 6H), 0.73 (d, J = 7.4 Hz, 36H).

^{13}C NMR (125 MHz, C_6D_6): δ 142.7, 137.0, 136.7, 136.4, 133.9, 125.3, 125.0, 124.7, 18.7, 12.1.

5,5'''-Bis(tributylstannyl)-2,2':5',2'':5'',2'''-quaterthiophene (11):



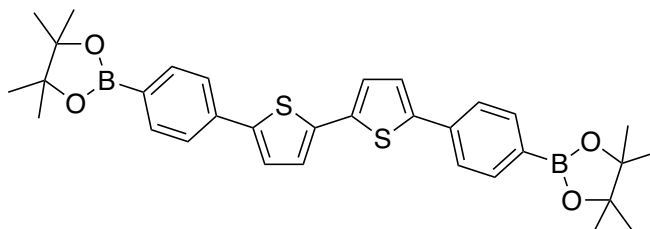
The title compound was obtained as orange oil in 79% yield. The reaction was performed on a 0.20 mmol scale and the crude product was passed through a pad of Florisil and purified by gel permeation chromatography (toluene). Purification by silica gel chromatography failed because of the destannylation of the product.

1H NMR (500 MHz, C_6D_6): δ 6.91 (d, J = 3.3 Hz, 2H), 6.69 (d, J = 3.3 Hz, 2H), 6.53 (d, J = 3.7 Hz, 2H), 6.42 (d, J = 3.7 Hz, 2H), 1.26–1.20 (m, 12H), 1.00–0.93 (m, 12H), 0.74–0.71 (m, 12H), 0.52 (t, J = 7.2 Hz, 18H).

^{13}C NMR (125 MHz, $CDCl_3$): δ 142.4, 137.1, 136.4, 136.2, 135.6, 124.9, 124.1 (two signals overlapped), 28.9, 27.3, 13.7, 10.9.

HRMS (APCI+): m/z calcd for $C_{40}H_{62}S_4Sn_2$ $[M+H]^+$ 909.1853; found: 909.1840.

5,5'-Bis(4-(4,4,5,5-tetramethyl-1,3,2-dioxaborolan-2-yl)phenyl)-2,2'-bithiophene (12):

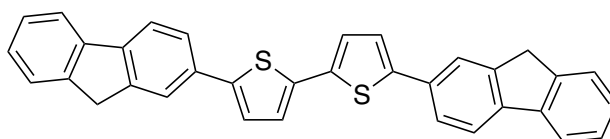


The title compound was obtained as yellow solid in 82% yield. The reaction was performed on a 0.20 mmol scale using 0.55 equiv of diethyl oxalate and the pure product was obtained by filtration of the crude reaction mixture and by washing the solid with minimal amounts of THF, an aqueous solution of HCl (1 M), and acetone. The filtrate was collected and further purified by silica gel chromatography (dichloromethane only). The compound data was in good agreement with the literature.²⁷

¹H NMR (500 MHz, CDCl₃): δ 7.83–7.81 (m, 4H), 7.62–7.60 (m, 4H), 7.31 (d, J = 3.9 Hz, 2H), 7.19 (d, J = 3.9 Hz, 2H), 1.36 (s, 24H).

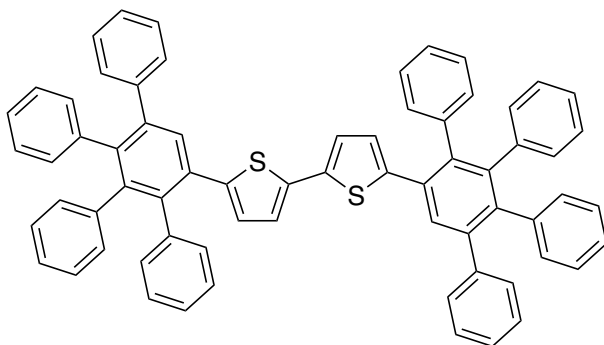
¹³C NMR (125 MHz, CDCl₃): δ 143.0, 137.1, 136.4, 135.4, 128.3 (determined by HMBC), 124.6, 124.6, 124.4, 83.9, 24.9.

5,5'-Di(9H-fluoren-2-yl)-2,2'-bithiophene (13):



The title compound was obtained as yellow solid in 91% yield. The reaction was performed on a 0.50 mmol scale using 0.55 equiv of diethyl oxalate and the pure product was obtained by filtration of the crude reaction mixture and by washing the solid with minimal amounts of THF, an aqueous solution of HCl (1 M), and acetone. The compound data was in good agreement with the literature.⁴

¹H NMR (500 MHz, C₂D₂Cl₄, 125 °C): δ 7.85–7.78 (br, 6H), 7.71–7.65 (br, 2H), 7.61–7.55 (br, 2H), 7.44–7.22 (br, 8H), 3.98 (br s, 4H).

5,5'-Bis(3',6'-diphenyl-[1,1':2',1''-terphenyl]-4'-yl)-2,2'-bithiophene (14):

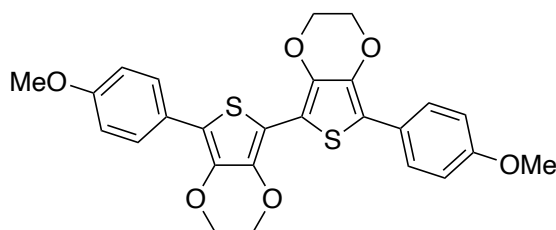
The title compound was obtained as yellow solid in 77% yield. The reaction was performed on a 0.20 mmol scale and the crude product was purified by silica gel chromatography (hexane: dichloromethane = 4:1 to 2:1).

Melting point: 363–365 °C (dichloromethane)

^1H NMR (500 MHz, CDCl_3): δ 7.70 (s, 2H), 7.18–7.15 (m, 10H), 7.07–7.05 (m, 6H), 7.00–6.98 (m, 4H), 6.92–6.90 (m, 6H), 6.86–6.80 (m, 10H), 6.78–6.75 (m, 6H), 6.44 (d, J = 3.8 Hz, 2H).

^{13}C NMR (125 MHz, CDCl_3): δ 142.3, 142.0, 141.3, 141.0, 140.0, 139.7, 139.7, 139.6, 138.9, 137.4, 132.8, 131.3, 131.2, 131.1, 130.7, 129.9, 127.9, 127.6, 127.5, 126.9, 126.6, 126.4, 126.4, 125.7, 125.4, 123.2.

HRMS (APCI+): m/z calcd for $\text{C}_{68}\text{H}_{46}\text{S}_2$ [$\text{M}+\text{H}^+$] 927.3114; found: 927.3106.

7,7'-Bis(4-methoxyphenyl)-2,2',3,3'-tetrahydro-5,5'-bithieno[3,4-*b*][1,4]dioxine (15):

The title compound was obtained as yellow solid in 33% yield. The reaction was performed on a 0.40 mmol scale and the pure product was obtained by filtration of the crude reaction mixture and by washing the solid with minimal amounts of THF, an aqueous solution of HCl (1 M), and acetone.

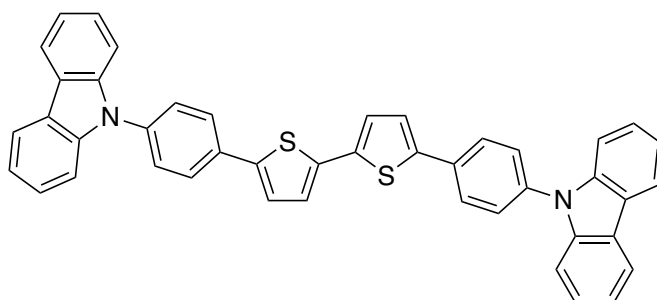
Melting point: 310 °C, decomp.

^1H NMR (500 MHz, $(\text{CD}_3)_2\text{SO}$): δ 7.54–7.51 (m, 4H), 6.92–6.89 (m, 4H), 4.35–4.30 (m, 8H), 3.71 (s, 6H).

^{13}C NMR (125 MHz, $(\text{CD}_3)_2\text{SO}$): δ 157.9, 137.4, 137.0, 126.6, 125.1, 114.3, 113.5, 105.9, 64.9, 64.6, 55.1.

HRMS (APCI+): m/z calcd for $\text{C}_{26}\text{H}_{22}\text{O}_6\text{S}_2$ $[\text{M}+\text{H}^+]$ 495.0931; found: 495.0924.

5,5'-Bis(4-(9H-carbazol-9-yl)phenyl)-2,2'-bithiophene (16):

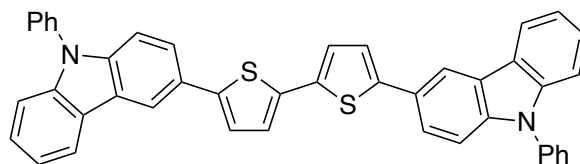


The title compound was obtained as yellow solid in 83% yield. The reaction was performed on a 0.50 mmol scale using 0.55 equiv of diethyl oxalate and the pure product was obtained by filtration of the crude reaction mixture and by washing the solid with minimal amounts of THF, an aqueous solution of HCl (1 M), and acetone. This compound is known.²⁸

^1H NMR (500 MHz, CDCl_3): δ 8.17 (d, $J = 7.7$ Hz, 4H), 7.87–7.85 (m, 4H), 7.63–7.62 (m, 4H), 7.49–7.43 (m, 8H), 7.38 (d, $J = 4.0$ Hz, 2H), 7.33–7.28 (m, 6H).

^{13}C NMR (125 MHz, CDCl_3): δ 142.3, 140.7, 137.1, 137.0, 133.0, 127.5, 126.9, 126.0, 124.9, 124.4, 123.5, 120.4, 120.1, 109.8.

5,5'-Bis(9-phenyl-9H-carbazol-3-yl)-2,2'-bithiophene (17):



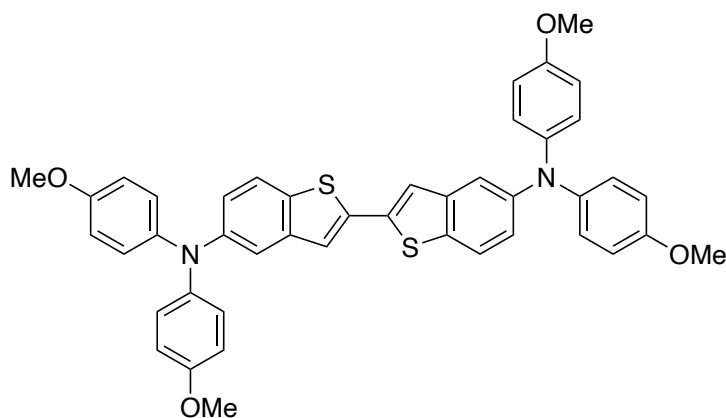
The title compound was obtained as yellow solid in 81% yield. The reaction was performed on a 0.50 mmol scale using 0.55 equiv of diethyl oxalate and the pure product was obtained by filtration of the crude reaction mixture and by washing the solid with minimal amounts of THF, an aqueous solution of HCl (1 M), and acetone. The filtrate

was collected and further purified by silica gel chromatography (dichloromethane only). The compound data was in good agreement with the literature.²⁹

¹H NMR (500 MHz, CDCl₃): δ 8.38 (d, J = 1.5 Hz, 2H), 8.20 (d, J = 7.7 Hz, 2H), 7.69 (dd, J = 8.6, 1.7 Hz, 2H), 7.65–7.58 (m, 8H), 7.51–7.41 (m, 8H), 7.34–7.30 (m, 4H), 7.24 (d, J = 3.7 Hz, 2H).

¹³C NMR (125 MHz, CDCl₃): δ 144.1, 141.4, 140.4, 137.4, 136.0, 130.0, 127.6, 127.0, 126.4, 126.3, 124.3, 124.2, 123.9, 123.2, 122.9, 120.5, 120.2, 117.4, 110.2, 110.0.

***N*5,*N*5,*N*5',*N*5'-tetrakis(4-methoxyphenyl)-[2,2'-bibenzo[*b*]thiophene]-5,5'-diamine (18):**



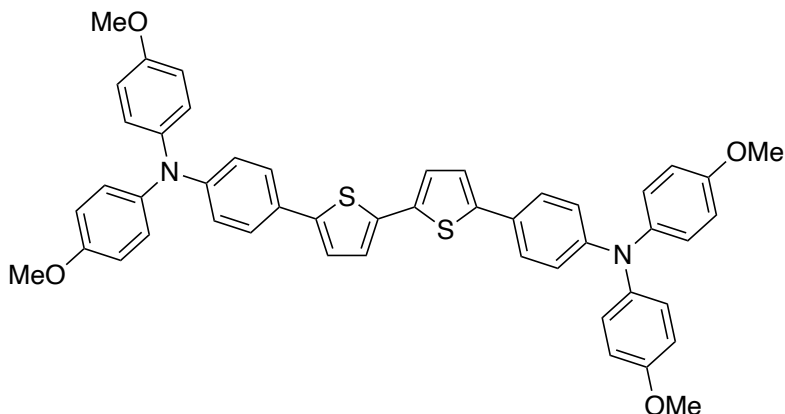
The title compound was obtained as yellow solid in 96% yield. The reaction was performed on a 0.20 mmol scale using 0.55 equiv of diethyl oxalate and the crude product was purified by silica gel chromatography (dichloromethane only).

Melting point: 221–223 °C (dichloromethane)

¹H NMR (500 MHz, CD₂Cl₂): δ 7.58 (d, J = 8.9 Hz, 2H), 7.28 (s, 2H), 7.25 (d, J = 2.3 Hz, 2H), 7.05–7.03 (m, 8H), 7.01 (dd, J = 8.9, 2.3 Hz, 2H), 6.84–6.82 (m, 8H), 3.78 (s, 12H).

¹³C NMR (125 MHz, CD₂Cl₂): δ 156.1, 147.1, 141.7, 141.6, 138.2, 132.4, 126.5, 122.7, 121.2, 121.2, 115.8, 115.0, 55.8.

HRMS (APCI⁺): m/z calcd for C₄₄H₃₆N₂O₄S₂ [M+H⁺] 721.2189; found: 721.2190.

4,4'-([2,2'-Bithiophene]-5,5'-diyl)bis(*N,N*-bis(4-methoxyphenyl)aniline) (19):

The title compound was obtained as orange solid in 94% yield. The reaction was performed on a 0.20 mmol scale and the crude product was purified by silica gel chromatography (hexane: dichloromethane = 1:1). The compound data was in good agreement with the literature.³⁰

¹H NMR (500 MHz, CD₂Cl₂): δ 7.33–7.30 (m, 4H), 7.03–7.02 (m, 4H), 7.00–6.97 (m, 8H), 6.81–6.75 (m, 12H), 3.71 (s, 12H).

¹³C NMR (125 MHz, CD₂Cl₂): δ 156.6, 148.8, 143.4, 140.8, 135.7, 127.2, 126.4, 126.1, 124.5, 122.6, 120.4, 115.0, 55.8.

Procedure for control experiment (Table 3, compound 16)

Mori's condition^{3a} was used for the synthesis of compound **16**. In an oven-dried Schlenk tube was added PdCl₂(PhCN)₂ (2.3 mg, 0.0060 mmol), DMSO (1.2 mL), and 9-(4-(thiophen-2-yl)phenyl)-9*H*-carbazole (65 mg, 0.20 mmol). To the resulting reaction mixture silver(I) fluoride (51 mg, 0.40 mmol) was added and heated at 60 °C for 5 h. Then, the mixture was cooled to rt, diluted with chloroform (50 mL), and washed with water. 1,3,5-trimethoxybenzene was added as an internal standard and a portion of the organic phase was passed through a pad for Florisil. The solvent was removed under reduced pressure and the crude product was analyzed by ¹H NMR. The yield of **16** was determined to be 40%.

Procedure for detection of CDH₃ (Scheme 13)

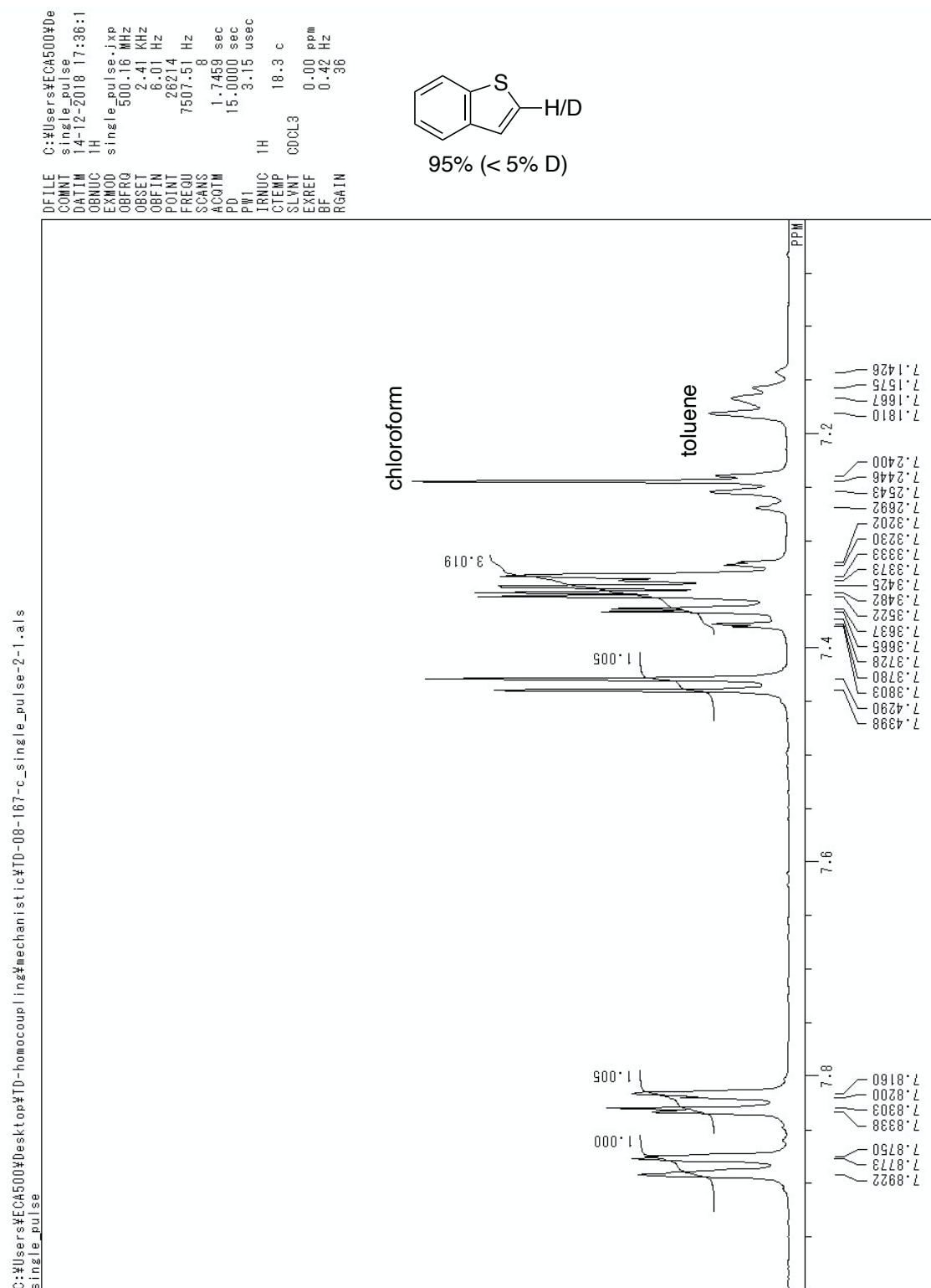
In an oven-dried Schlenk tube was added benzo[*b*]thiophene-2-*d* (27 mg, 0.20 mmol), TP (14 mg, 0.022 mmol), and a THF solution of Fe(acac)₃ (0.10 mol/L, 0.20 mL, 0.020 mmol). Then, a toluene solution of AlMe₃ (2.0 mol/L, 0.10 mL, 0.20 mmol) was added

dropwise at rt and the reaction mixture was stirred for 5 min to give a clear dark reddish brown solution. Diethyl oxalate (14 μ L, 0.10 mmol) was added and the reaction mixture was stirred at 70 °C for 15 h. After cooling to rt, the Schlenk tube was connected with a needle and the gas was collected by the water displacement method by carefully opening the J. Young cap. 3 mL of the collected gas was taken by a gas tight syringe and was transferred to an NMR tube fitted with a septum and a short needle by the upward displacement method. The gas tight syringe and the short needle were removed quickly and acetone-*d*₆ was injected without releasing the pressure. The NMR tube was shaken vigorously for 30 seconds and the obtained sample was analyzed by ¹H NMR within 5 minutes. The triplet peak of CDH₃ was observed. The spectroscopic data was in good agreement with the literature.³¹ The reaction mixture was diluted with ethyl acetate (2 mL), and quenched carefully with methanol (0.1 mL). A saturated aqueous solution of potassium sodium tartrate (1 mL) was added and the mixture was stirred vigorously until clear phase separation was observed. The crude mixture was extracted with chloroform and 1,3,5-trimethoxybenzene was added as an internal standard. A portion of the organic layer was passed through a pad of Florisil and the solvent was removed under reduced pressure and the crude mixture was analyzed by ¹H NMR. The yield of **2** was determined to be 93%.

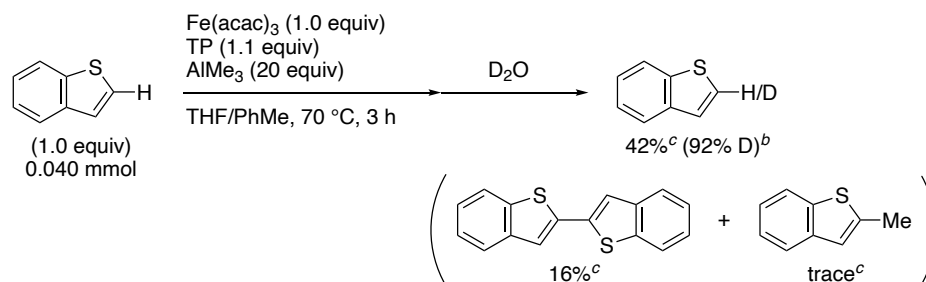
Reaction of benzo[*b*]thiophene with AlMe₃ (Scheme 14a)

A mixture of benzo[*b*]thiophene (13 mg, 0.10 mmol) and AlMe₃ (2.0 mol/L, 0.25 mL, 0.50 mmol) in THF (0.25 mL) was stirred at 70 °C for 15 h. The reaction mixture was quenched carefully with D₂O (1.0 mL) and stirred at 70 °C for another 1 h. The reaction mixture was cooled to room temperature and a saturated aqueous solution of potassium sodium tartrate (2.5 mL) was added. The mixture was stirred vigorously until clear phase separation was observed. The aqueous layer was extracted with diethyl ether (2 mL x 3) and the combined organic layers were passed through a pad of Florisil. The yield of recovered benzo[*b*]thiophene was determined by GC using tridecane as an internal standard and the deuterium incorporation ratio was determined by ¹H NMR.

Chapter 2



Procedure for stoichiometric experiment (Scheme 14b)

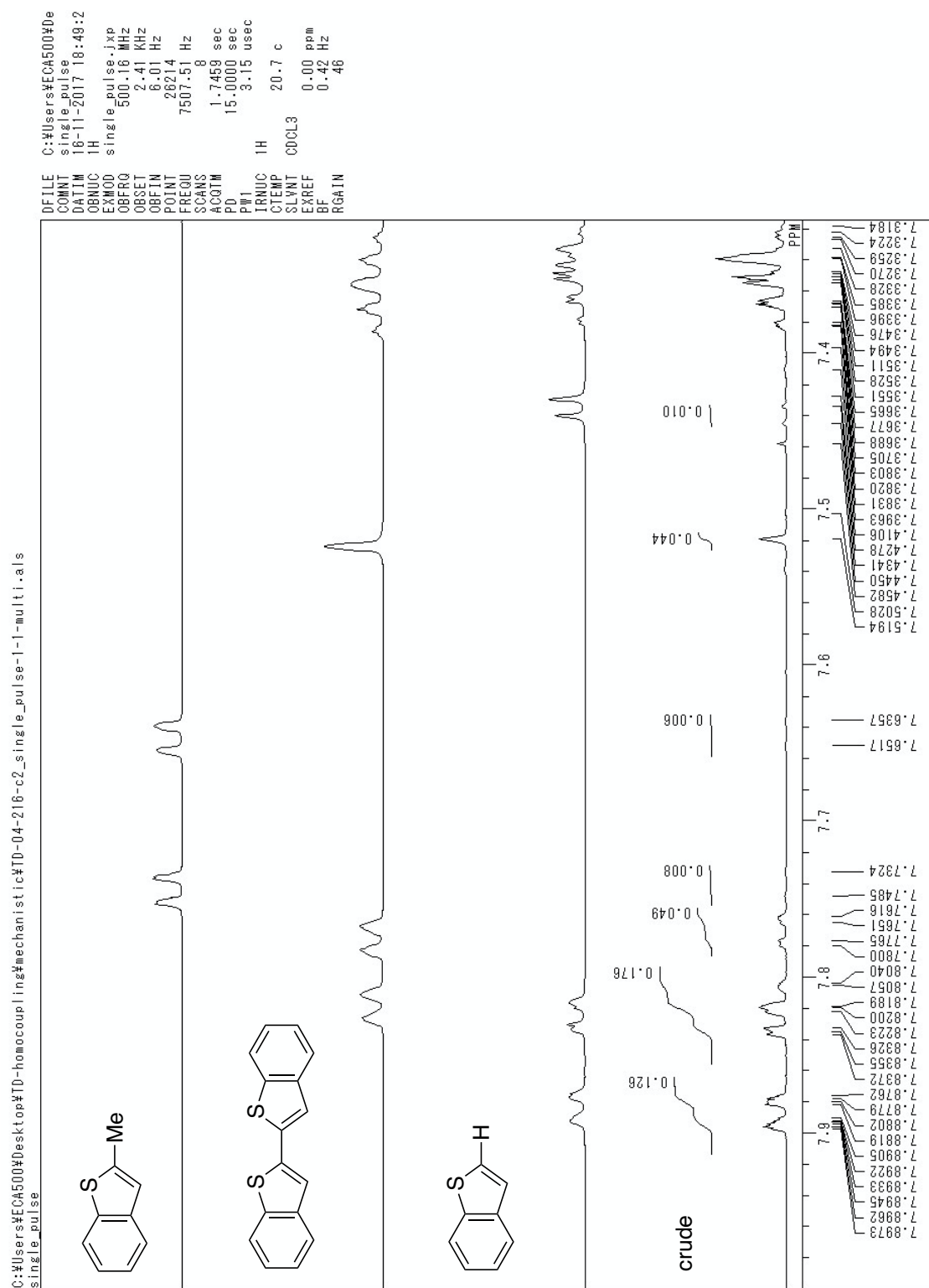


^a The yield was determined by GC using tridecane as an internal standard.

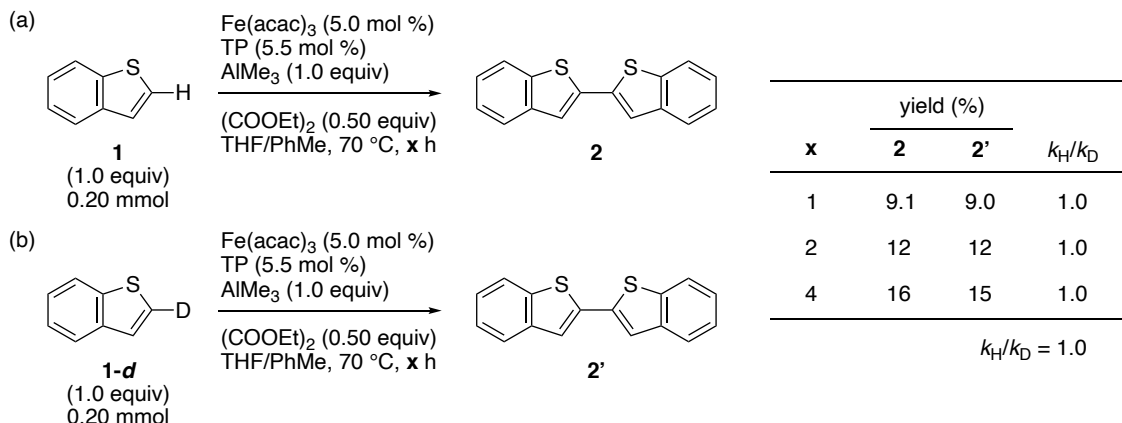
^b The deuterium incorporation ratio was determined by ¹H NMR.

^c Yields were determined by ¹H NMR using 1,1,2,2-tetrachloroethane as an internal standard.

In an oven-dried Schlenk tube was added benzo[*b*]thiophene (5.4 mg, 0.040 mmol), TP (28 mg, 0.044 mmol), and a THF solution of Fe(acac)₃ (0.10 mol/L, 0.40 mL, 0.040 mmol). Then, a toluene solution of AlMe₃ (2.0 mol/L, 0.40 mL, 0.80 mmol) was added dropwise at room temperature and the reaction mixture was stirred for 5 min to give a clear dark reddish brown solution. The reaction mixture was stirred at 70 °C for 3 h, cooled to room temperature, and quenched carefully with D₂O (1.0 mL). After stirring for 1 h, a saturated aqueous solution of potassium sodium tartrate (1.0 mL) was added and the mixture was stirred vigorously until clear phase separation was observed. The aqueous layer was extracted with dichloromethane (20 mL x 3) and the combined organic layers were passed through a pad of Florisil. The solvent was removed under reduced pressure and the crude mixture was analyzed by ¹H NMR using 1,1,2,2-tetrachloroethane as an internal standard. The deuterium incorporation ratio was also determined by ¹H NMR.



Kinetic isotope effect experiments for two parallel reactions (Scheme 16)



Yields were determined by ^1H NMR using 1,3,5-trimethoxybenzene as an internal standard.

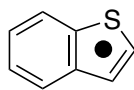
In an oven-dried Schlenk tube was added benzo[*b*]thiophene (27 mg, 0.20 mmol), TP (6.9 mg, 0.011 mmol), a THF solution of $\text{Fe}(\text{acac})_3$ and 1,3,5-trimethoxybenzene (0.10 mol/L, 0.10 mL, 0.010 mmol each), and THF (1.0 mL). Then, a toluene solution of AlMe_3 (2.0 mol/L, 0.10 mL, 0.20 mmol) was added dropwise at room temperature and the reaction mixture was stirred for 5 min to give a clear dark reddish brown solution. Diethyl oxalate (14 μL , 0.20 mmol) was added and the reaction mixture was stirred at 70 °C and sampled after 1, 2, and 4 h. Exactly the same experiment using the same solutions of reagents and the same oil bath was conducted at the same time for benzo[*b*]thiophene-2-*d* (27 mg, 0.20 mmol). Each sample was quenched with a saturated aqueous solution of potassium sodium tartrate (0.5 mL), and the aqueous layer was extracted with dichloromethane (0.5 mL x 3). The combined organic layers were passed through a pad of Florisil and the solvent was removed under reduced pressure. All the samples were analyzed by ^1H NMR using the singlet aromatic peak of 1,3,5-trimethoxybenzene as an internal standard.

Calculation of NICS(1) values (Figure 2a)

Theoretical calculations were performed using Gaussian 09 software package.³² Geometry optimizations of all compounds were performed at the B3LYP/6-31G(d) level of theory. Nucleus independent chemical shifts (NICS)¹⁸ were calculated using the gauge invariant atomic orbital (GIAO) approach at the B3LYP/6-31G(d) level of theory.

Chapter 2

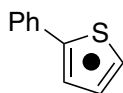
Cartesian coordinates of the optimized structures (Bq stands for ghost atom):



0 1

C 0.06190302 -0.55391131 0.00006416
 C -0.11104371 0.85304021 -0.00009849
 C -1.41877907 1.37381417 -0.00004243
 C -2.50296922 0.50771631 0.00016906
 C -2.31026701 -0.88622326 0.00032832
 C -1.02975939 -1.42816272 0.00027740
 C 2.21876023 0.71253789 -0.00029684
 C 1.15035227 1.54993073 -0.00030447
 H -1.57109706 2.45015525 -0.00016475
 H -3.51296258 0.90804916 0.00021306
 H -3.17165461 -1.54833655 0.00049310
 H -0.88198825 -2.50430519 0.00040046
 H 3.26789901 0.97813098 -0.00042800
 H 1.23737946 2.63139938 -0.00044990
 S 1.76770258 -0.98047157 -0.00004026

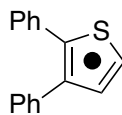
Bq 1.01762789 0.31635213 0.99986481
 Bq 1.01744195 0.31609816 -1.00013517



0 1

C 0.76651871 0.41436306 0.63157807
 C 1.53714219 1.52099222 0.35527483
 C 2.93930284 1.27632616 0.42311061
 C 3.23635370 -0.01740036 0.75227275
 S 1.79958845 -0.95823459 0.99177924
 H 1.10934609 2.47908972 0.08046195
 H 3.69310690 2.03112377 0.22603547

H 4.20921484 -0.47519278 0.87128385
 C -0.69801957 0.30267107 0.65691638
 C -1.35082302 -0.91104394 0.37678352
 C -1.48791069 1.42690967 0.96121234
 C -2.74133596 -0.99689908 0.39968430
 H -0.76370567 -1.78875764 0.12003675
 C -2.87799191 1.34151909 0.97131093
 H -1.00361726 2.36622397 1.21160972
 C -3.51273434 0.12902266 0.69286716
 H -3.22312811 -1.94546758 0.17789291
 H -3.46719099 2.22298164 1.21043935
 H -4.59707272 0.06210603 0.70726601
 Bq 2.05000036 0.69696076 1.59909581
 Bq 2.06156197 0.19745791 -0.33748963

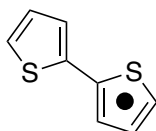
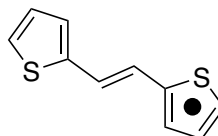


0 1

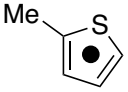
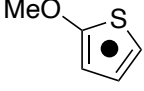
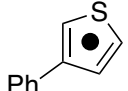
C 0.73706656 0.97996510 0.00165661
 C -0.63081686 1.20215749 -0.01956266
 C -0.95103481 2.60246205 -0.01576747
 C 0.14229522 3.41785602 -0.00200335
 S 1.61012763 2.50131490 0.02138406
 H -1.97065487 2.96986902 -0.06117543
 H 0.17223716 4.49910022 -0.01795697
 C 1.50335542 -0.27844922 0.08052480
 C 2.66195552 -0.46623014 -0.69386032
 C 1.11366749 -1.30532721 0.95950261
 C 3.40431506 -1.64251802 -0.59595503
 H 2.97184076 0.31162656 -1.38656617

Chapter 2

C	1.85268531	-2.48269486	1.04894478	C	0.09760225	-0.71865042	-0.00004095
H	0.23287012	-1.16924400	1.57835349	C	1.27480548	-1.43579409	-0.00035151
C	3.00134749	-2.65716314	0.27324440	S	-1.27480548	-1.81591009	0.00026553
H	4.29515410	-1.76736938	-1.20584363	C	1.08472778	-2.84665890	-0.00018393
H	1.53536790	-3.26301926	1.73569923	H	2.25144112	-0.96303686	-0.00063194
H	3.57806027	-3.57506314	0.34832539	C	-0.23439018	-3.20590623	0.00001528
C	-1.68802392	0.16361267	-0.09341828	H	1.89875383	-3.56347984	-0.00032920
C	-2.83483027	0.26754631	0.71183680	H	-0.66347608	-4.19872485	0.00007936
C	-1.60005735	-0.91330805	-0.99173285	Bq	-0.18980993	2.00458220	0.99994086
C	-3.85667965	-0.67830818	0.62866677	Bq	-0.18936605	2.00458569	-1.00005909
H	-2.91604322	1.08958569	1.41824592				
C	-2.62081846	-1.85862798	-1.07353796				
H	-0.72995203	-0.99935332	-1.63496620				
C	-3.75349249	-1.74615318	-0.26397335				
H	-4.73265941	-0.58123927	1.26488302	0 1			
H	-2.53450149	-2.68172421	-1.77813761	C	1.89320844	0.36485723	0.00006824
H	-4.54936694	-2.48312518	-0.33039900	C	2.81450445	1.39361605	0.00051131
Bq	0.16551314	2.13697603	0.99700607	C	4.16768934	0.95452498	0.00041514
Bq	0.19754195	2.14452619	-1.00272320	C	4.28093371	-0.40878819	0.00042714
				S	2.72634390	-1.18387637	-0.00004569
				H	2.51642170	2.43713404	0.00069505
				H	5.02086097	1.62429146	0.00056937
				H	5.18088998	-1.00895955	0.00053115
				C	0.45550961	0.50047139	-0.00014270
				H	0.10832770	1.53367607	-0.00006538
				C	-0.45545049	-0.50040359	-0.00022792
				H	-0.10822720	-1.53359636	-0.00016875
				C	-1.89318652	-0.36482672	-0.00018646
				C	-2.81446421	-1.39360686	0.00009213
				S	-2.72639294	1.18386638	-0.00033118
				C	-4.16767088	-0.95455941	-0.00014646
				H	-2.51634819	-2.43711387	0.00026053



Chapter 2

C	-4.28096882	0.40874695	-0.00007859	H	0.55199303	2.47244364	-0.00705389
H	-5.02082205	-1.62435162	-0.00012905	H	2.93296275	1.31751964	0.00675161
H	-5.18094616	1.00888875	-0.00005391	H	2.74597975	-1.31315408	0.01200121
Bq	3.17635599	0.22389635	1.00027519	O	-1.62079466	0.82324519	-0.01328979
Bq	3.17671595	0.22423713	-0.99972474	C	-2.57147871	-0.23415578	-0.01598924
				H	-3.55300704	0.24228143	-0.02165158
				H	-2.46316722	-0.86188205	-0.91019131
				H	-2.47192475	-0.85858051	0.88153632
				Bq	0.94724276	0.17172235	0.99971894
				Bq	0.93080183	0.17937720	-0.99999483
0 1							
C	-0.78653977	0.22277281	0.01562729				
C	-0.02024184	1.35747410	0.03125821				
C	1.38721030	1.10352170	0.00787782				
C	1.68258474	-0.22883647	-0.02569882				
S	0.23800164	-1.19630286	-0.02907268				
H	-0.45226552	2.35311725	0.05898925				
H	2.14163072	1.88314112	0.01583049				
H	2.65398976	-0.70414739	-0.04858649				
C	-2.28198706	0.10505907	0.03186779				
H	-2.66394123	-0.40840029	-0.85910062				
H	-2.64168112	-0.44820016	0.90815304				
H	-2.73074795	1.10311378	0.05998745				
Bq	0.51284820	0.22936647	0.99966839				
Bq	0.48755780	0.27408525	-0.99967166				
							
0 1							
C	-0.30951680	0.49708801	-0.00651577				
C	0.71776974	1.40191208	-0.00378877				
C	1.99759550	0.76769164	0.00366488				
C	1.93784367	-0.59524873	0.00649825				
S	0.28692589	-1.16303781	0.00009928				
							
0 1							

Chapter 2

C	-1.47804901	-0.97217753	-0.31575376
C	-0.65635426	0.07604464	0.02908482
C	-1.42138519	1.23685061	0.40060074
C	-2.77015212	1.04349372	0.33234463
S	-3.15653726	-0.56428952	-0.19480900
H	-0.97161983	2.16539835	0.73468869
H	-3.55999166	1.74157552	0.57482036
H	-1.18671801	-1.95077943	-0.67212826
C	0.82094523	0.02172472	0.01646607
C	1.57940925	1.16593782	-0.28395047
C	1.50605063	-1.17213863	0.30019795
C	2.97251177	1.11692280	-0.30431603
H	1.07196666	2.09572727	-0.52576422
C	2.89831972	-1.22274202	0.27379166
H	0.93991099	-2.06033112	0.56706064
C	3.63901601	-0.07792620	-0.02764407
H	3.53796718	2.01373719	-0.54394175
H	3.40637691	-2.15647109	0.50066321
H	4.72483201	-0.11616388	-0.04338388
Bq	-1.90301026	-0.14483836	1.00139079
Bq	-1.88998090	0.47280714	-0.90080381

2-14. References and notes

- ¹ (a) Shirota, Y.; Kageyama, H. *Chem. Rev.* **2007**, *107*, 953–1010. (b) Wang, C.; Dong, H.; Hu, W.; Liu, Y.; Zhu, D. *Chem. Rev.* **2012**, *112*, 2208–2267. (c) Sirringhaus, H. *Adv. Mater.* **2014**, *26*, 1319–1335. (d) Facchetti, A. *Materials Today* **2007**, *10*, 28–37. (e) Wu, W.; Liu, Y.; Zhu, D. *Chem. Soc. Rev.* **2010**, *39*, 1489–1502. (f) O'Neill, M.; Kelly, S. M. *Adv. Mater.* **2011**, *23*, 566–584. (g) Murphy, A. R.; Fréchet, J. M. J. *Chem. Rev.* **2007**, *107*, 1066–1096. (h) Zhang, F.; Wu, D.; Xu, Y.; Feng, X. *J. Mater. Chem.* **2011**, *21*, 17590. (i) Ameri, T.; Khoram, P.; Min, J.; Brabec, C. J. *Adv. Mater.* **2013**, *25*, 4245–4266.
- ² (a) Kozhevnikov, I. V. *React. Kinet. Catal. Lett.* **1976**, *4*, 451–458. (b) Kozhevnikov, I. V. *React. Kinet. Catal. Lett.* **1977**, *6*, 401–408.
- ³ (a) Masui, K.; Ikegami, H.; Mori, A. *J. Am. Chem. Soc.* **2004**, *126*, 5074–5075. (b) Takahashi, M.; Masui, K.; Sekiguchi, H.; Kobayashi, N.; Mori, A.; Funahashi, M.; Tamaoki, N. *J. Am. Chem. Soc.* **2006**, *128*, 10930–10933. (c) Kobayashi, K.; Sugie, A.; Takahashi, M.; Masui, K.; Mori, A. *Org. Lett.* **2005**, *7*, 5083–5085.
- ⁴ Wang, L.; Carrow, B. P. *ACS Catal.* **2019**, *9*, 6821–6836.
- ⁵ Tereniak, S. J.; Bruns, D. L.; Stahl, S. S. *J. Am. Chem. Soc.* **2020**, *142*, 20318–20323.
- ⁶ Shang, R.; Ilies, L.; Nakamura, E. *J. Am. Chem. Soc.* **2016**, *138*, 10132–10135.
- ⁷ Li, P.; de Bruin, B.; Reek, J. N. H.; Dzik, W. I. *Organometallics* **2015**, *34*, 5009–5014.
- ⁸ (a) Ohki, Y.; Hatanaka, T.; Tatsumi, K. *J. Am. Chem. Soc.* **2008**, *130*, 17174–17186. (b) Hatanaka, T.; Ohki, Y.; Tatsumi, K. *Chem. Asian J.* **2010**, *5*, 1657–1666.
- ⁹ Shen, K.; Fu, Y.; Li, J.-N.; Liu, L.; Guo, Q.-X. *Tetrahedron* **2007**, *63*, 1568–1576.
- ¹⁰ Mann, G.; Baranano, D.; Hartwig, J. F.; Rheingold, A. L.; Guzei, I. A. *J. Am. Chem. Soc.* **1998**, *120*, 9205–9219.
- ¹¹ Shang, R.; Ilies, L.; Nakamura, E. *Chem. Rev.* **2017**, *117*, 9086–9139.
- ¹² (a) Hull, K. L.; Sanford, M. S. *J. Am. Chem. Soc.* **2007**, *129*, 11904–11905. (b) Bruns, D. L.; Musaev, D. G.; Stahl, S. S. *J. Am. Chem. Soc.* **2020**, *142*, 19678–19688. (c) Salazar, C. A.; Flesch, K. N.; Haines, B. E.; Zhou, P. S.; Musaev, D. G.; Stahl, S. S. *Science* **2020**, *370*, 1454–1460.
- ¹³ Kuo, Y.-N.; Chen, F.; Ainsworth, C.; Bloomfield, J. J. *J. Chem. Soc. D* **1971**, 136–137.
- ¹⁴ Shang, R.; Ilies, L.; Nakamura, E. *J. Am. Chem. Soc.* **2015**, *137*, 7660–7663.

- ¹⁵ (a) Grzybowski, M.; Skonieczny, K.; Butenschön, H.; Gryko, D. T. *Angew. Chem. Int. Ed.* **2013**, *52*, 9900–9930. (b) Watson, M. D.; Fechtenkötter, A.; Müllen, K. *Chem. Rev.* **2001**, *101*, 1267–1300.
- ¹⁶ Roncali, J.; Blanchard, P.; Frère, P. *J. Mater. Chem.* **2005**, *15*, 1589–1610.
- ¹⁷ Wu, Y.; Wang, Z.; Liang, M.; Cheng, H.; Li, M.; Liu, L.; Wang, B.; Wu, J.; Prasad Ghimire, R.; Wang, X.; Sun, Z.; Xue, S.; Qiao, Q. *ACS Appl. Mater. Interfaces* **2018**, *10*, 17883–17895.
- ¹⁸ (a) Schleyer, P. von R.; Maerker, C.; Dransfeld, A.; Jiao, H.; van Eikema Hommes, N. J. R. *J. Am. Chem. Soc.* **1996**, *118*, 6317–6318. (b) Schleyer, P. von R.; Manoharan, M.; Wang, Z.-X.; Kiran, B.; Jiao, H.; Puchta, R.; van Eikema Hommes, N. J. R. *Org. Lett.* **2001**, *3*, 2465–2468.
- ¹⁹ (a) Xu, J.; Bercher, O. P.; Watson, M. P. *J. Am. Chem. Soc.* **2021**, *143*, 8608–8613. (b) Tobisu, M.; Shimasaki, T.; Chatani, N. *Angew. Chem. Int. Ed.* **2008**, *47*, 4866–4869. (c) Yu, D.-G.; Shi, Z.-J. *Angew. Chem. Int. Ed.* **2011**, *50*, 7097–7100. (d) Guo, L.; Liu, X.; Baumann, C.; Rueping, M. *Angew. Chem. Int. Ed.* **2016**, *55*, 15415–15419. (e) Koch, E.; Takise, R.; Studer, A.; Yamaguchi, J.; Itami, K. *Chem. Commun.* **2015**, *51*, 855–857. (f) Wang, T.-H.; Ambre, R.; Wang, Q.; Lee, W.-C.; Wang, P.-C.; Liu, Y.; Zhao, L.; Ong, T.-G. *ACS Catal.* **2018**, *8*, 11368–11376.
- ²⁰ Simmons, E. M.; Hartwig, J. F. *Angew. Chem. Int. Ed.* **2012**, *51*, 3066–3072.
- ²¹ Still, W. C.; Kahn, M.; Mitra, A. *J. Org. Chem.* **1978**, *43*, 2923–2925.
- ²² Pangborn, A. B.; Giardello, M. A.; Grubbs, R. H.; Rosen, R. K.; Timmers, F. J. *Organometallics* **1996**, *15*, 1518–1520.
- ²³ Doba, T.; Ilies, L.; Sato, W.; Shang, R.; Nakamura, E. *Nat. Catal.* **2021**, *4*, 631–638.
- ²⁴ Truong, T.; Alvarado, J.; Tran, L. D.; Daugulis, O. *Org. Lett.* **2010**, *12*, 1200–1203.
- ²⁵ Schroth, W.; Hintzsche, E.; Jordan, H.; Jende, T.; Spitzner, R.; Thondorf, I. *Tetrahedron* **1997**, *53*, 7509–7528.
- ²⁶ Yassar, A.; Garnier, F.; Deloffre, F.; Horowitz, G.; Ricard, L. *Adv. Mater.* **1994**, *6*, 660–663.
- ²⁷ Ball, M.; Zhong, Y.; Fowler, B.; Zhang, B.; Li, P.; Etkin, G.; Paley, D. W.; Decatur, J.; Dalsania, A. K.; Li, H.; Xiao, S.; Ng, F.; Steigerwald, M. L.; Nuckolls, C. *J. Am. Chem. Soc.* **2016**, *138*, 12861–12867.

- ²⁸ Holzer, B.; Bintinger, J.; Lumpi, D.; Choi, C.; Kim, Y.; Stöger, B.; Hametner, C.; Marchetti-Deschmann, M.; Plasser, F.; Horkel, E.; Kymissis, I.; Fröhlich, J. *ChemPhysChem* **2017**, *18*, 549–563.
- ²⁹ Song, J.; Wei, F.; Sun, W.; Cao, X.; Liu, C.; Xie, L.; Huang, W. *Org. Chem. Front.* **2014**, *1*, 817–820.
- ³⁰ Wu, Y.; Wang, Z.; Liang, M.; Cheng, H.; Li, M.; Liu, L.; Wang, B.; Wu, J.; Prasad Ghimire, R.; Wang, X.; Sun, Z.; Xue, S.; Qiao, Q. *ACS Appl. Mater. Interfaces* **2018**, *10*, 17883–17895.
- ³¹ Skakovskii, E. D.; Stankevich, A. I.; Tychinskaya, L. Yu.; Shirokii, O. V.; Choban, Yu. P.; Murashko, V. L.; Rykov, S. V. *Zh. Obshch. Khim.* **2004**, *74*, 1719–1725.
- ³² Gaussian 09, Revision B.01, Frisch, M. J.; Trucks, G. W.; Schlegel, H. B.; G. E. Scuseria, ; Robb, M. A.; Cheeseman, J. R.; Scalmani, G.; Barone, V.; Mennucci, B.; Petersson, G. A.; Nakatsuji, H.; Caricato, M.; Li, X.; Hratchian, H. P.; Izmaylov, A. F.; Bloino, J.; Zheng, G.; Sonnenberg, J. L.; Hada, M.; Ehara, M.; Toyota, K.; Fukuda, R.; Hasegawa, J.; Ishida, M.; Nakajima, T.; Honda, Y.; Kitao, O.; Nakai, H.; Vreven, T.; Montgomery Jr. J. A.; , Peralta, J. E.; Ogliaro, F.; Bearpark, M.; Heyd, J. J.; Brothers, E.; Kudin, K. N.; Staroverov, V. N.; Keith, T.; Kobayashi, R.; Normand, J.; Raghavachari, K.; Rendell, A.; Burant, J. C.; Iyengar, S. S.; Tomasi, J.; Cossi, M.; Rega, N.; Millam, J. M.; Klene, M.; Knox, J. E.; Cross, J. B.; Bakken, V.; Adamo, C.; Jaramillo, J.; Gomperts, R.; Stratmann, R. E.; Yazyev, O.; Austin, A. J.; Cammi, R.; Pomelli, C.; Ochterski, J. W.; Martin, R. L.; Morokuma, K.; Zakrzewski, V. G.; Voth, G. A.; Salvador, P.; Dan nenberg, J. J.; Dapprich, S.; Daniels, A. D.; Farkas, O.; Foresman, J. B.; Ortiz, J. V.; Cioslowski, J.; Fox, D. J. Gaussian, Inc., Wallingford CT, 2010.

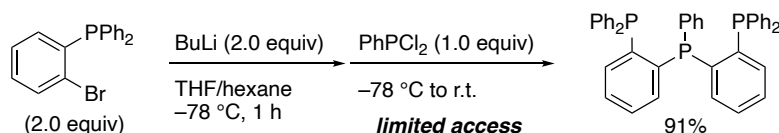
Chapter 3.

Development of a Synthetic Method for Tridentate Phosphine Ligands

3-1. Introduction

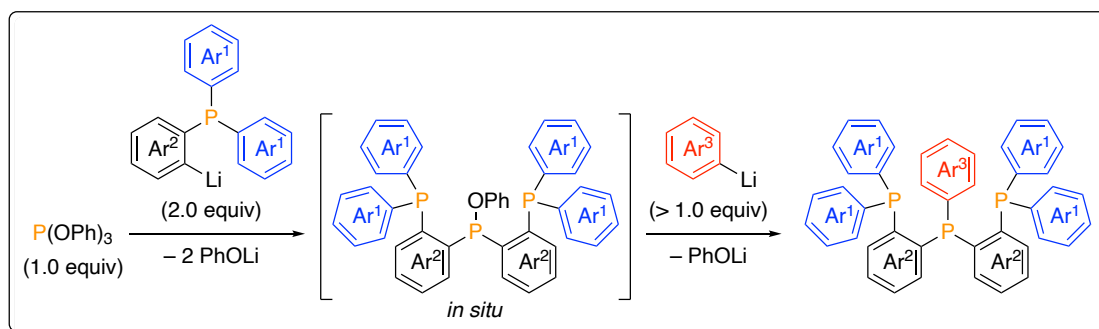
Tridentate phosphine compounds have been reported to be an effective ligand for various kinds of transition-metal-catalyzed reactions such as iron-catalyzed C–H activation,¹ iron-catalyzed nitrogen reduction,² cobalt-catalyzed addition to alkynes,³ cobalt-catalyzed hydrogenation of carboxylic acids,⁴ ruthenium-catalyzed hydrogenation,⁵ and molybdenum-catalyzed nitrogen reduction.⁶ In addition to transition metal catalysis, their copper complexes have been reported to be useful for OLEDs.⁷ Currently, the synthetic methods for conjugated tridentate phosphine ligands rely on the use of phosphine chlorides that are toxic, difficult to handle, and limited in access (Scheme 1).

Scheme 1. Synthesis of a conjugated tridentate phosphine ligand



To accelerate the research in which tridentate phosphine ligands are used, a modular and practical method to synthesize tridentate phosphine ligands is desirable. In this work, I developed a simple and scalable method to synthesize tridentate phosphine ligands by sequential addition of organolithium reagents to $P(O\text{Ph})_3$ (Scheme 2). The use of phosphine chlorides was eliminated and all of the aryl groups on three phosphines were introduced in a controlled manner by lithium-halogen exchange or lithiation of the corresponding starting materials.

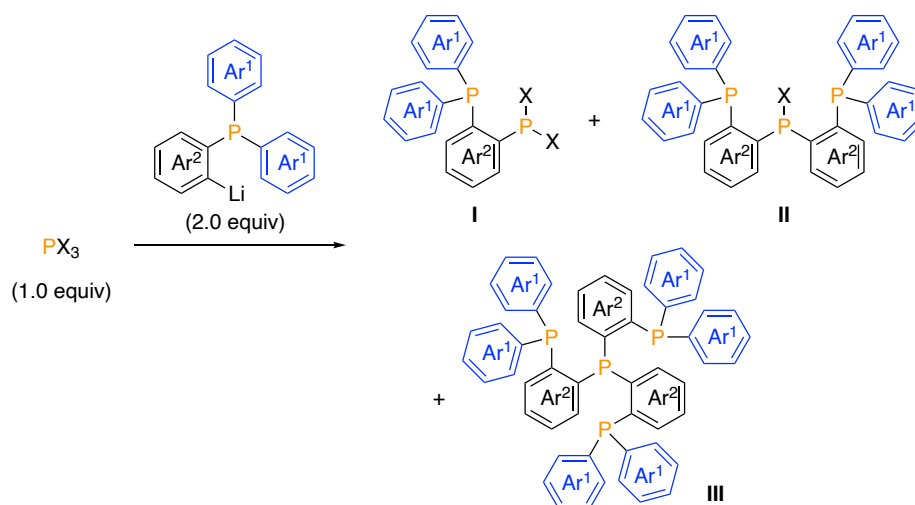
Scheme 2. Synthesis of tridentate phosphine ligands by sequential addition of organolithium reagents to $P(O\text{Ph})_3$



3-2. Selective formation of phenoxydiarylphosphine

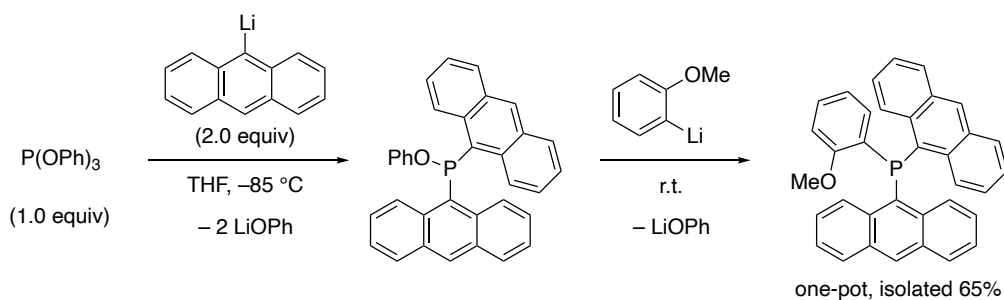
To achieve clean formation of the desired tridentate phosphine ligand by sequential addition of organolithium reagents to an electrophilic phosphine reagent (PX_3), the first reaction of an organolithium reagent with an electrophilic phosphine reagent needs to selectively generate a tridentate phosphine precursor (**II**) out of bidentate (**I**) and tetradentate (**III**) ones (Scheme 3).

Scheme 3. Selectivity issue in the addition of the first organolithium reagent



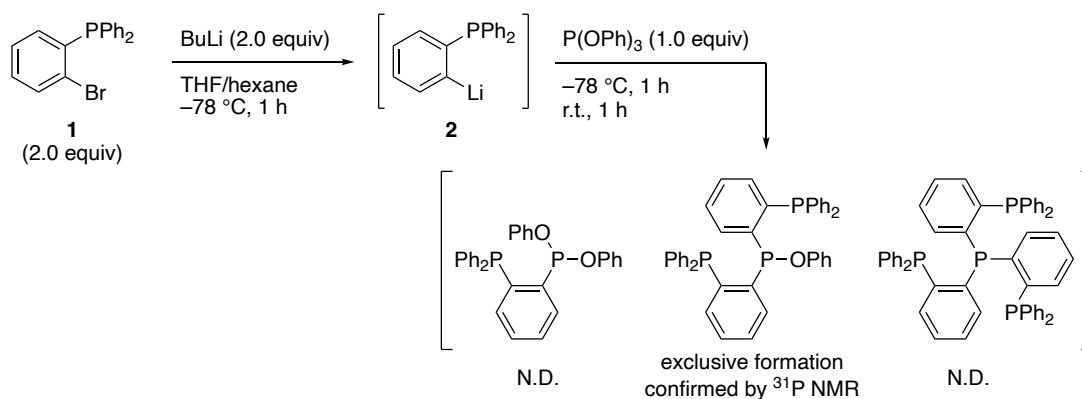
Knowing this potential difficulty in this strategy, I thought that $\text{P}(\text{OPh})_3$ can be used as the electrophilic phosphine to selectively form **II** based on the report by Straub and co-workers that $\text{P}(\text{OPh})_3$ can undergo selective stepwise nucleophilic substitution in one-pot (Scheme 4).⁸

Scheme 4. One-pot synthesis of sterically shielded phosphorus ligands by selective stepwise nucleophilic substitution at $\text{P}(\text{OPh})_3$



Following their procedure, 2.0 equiv of (2-bromophenyl)diphenylphosphane (**1**) was treated with 2.0 equiv of BuLi for lithium-halogen exchange and the generated (2-(diphenylphosphaneyl)phenyl)lithium (**2**) was reacted with 1.0 equiv of P(OPh)₃ at –78 °C. After gradually warming to room temperature, the crude reaction mixture was analyzed by ³¹P NMR. The NMR spectrum supported the exclusive formation of the tridentate phosphine precursor and absence of the bidentate and tetradentate ones (Scheme 5, Figure 1). This indicates that subsequent reaction of the crude reaction mixture with another organolithium reagent will cleanly afford the tridentate phosphine ligand.

Scheme 5. Synthesis of a tridentate phosphine ligand precursor by treatment of P(OPh)₃ with (2-(diphenylphosphaneyl)phenyl)lithium



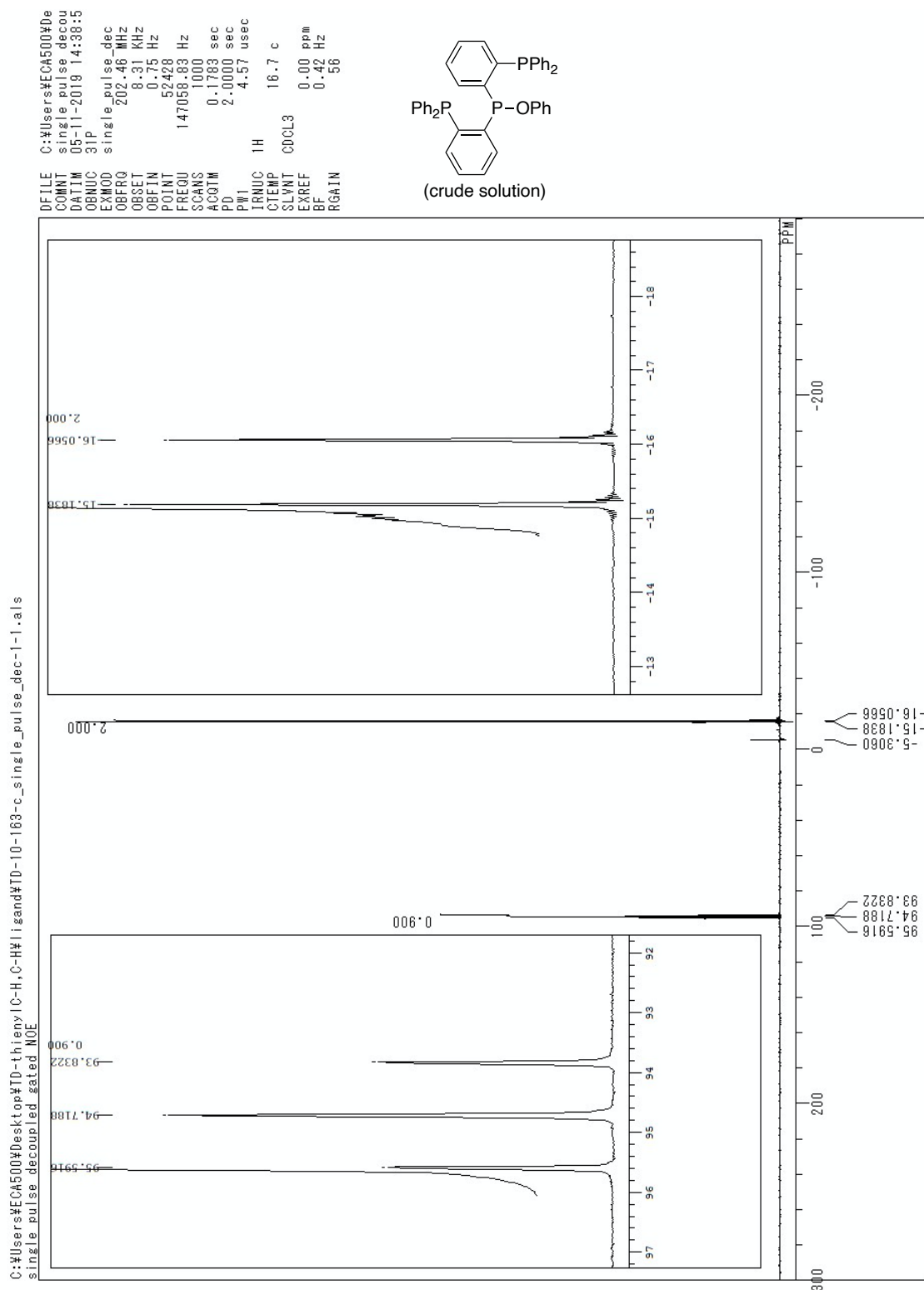
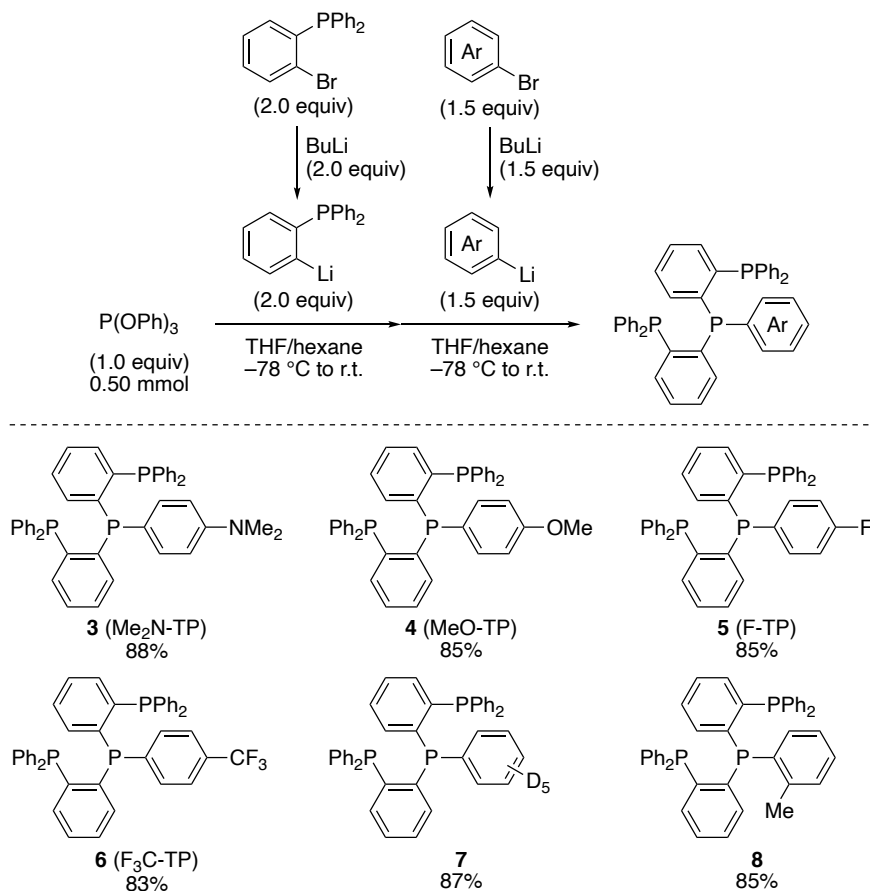


Figure 1. ^{31}P NMR spectrum of the crude reaction mixture after the first organolithium addition to $\text{P}(\text{O}^i\text{Pr})_3$

3-3. Synthesis of tridentate phosphine ligands

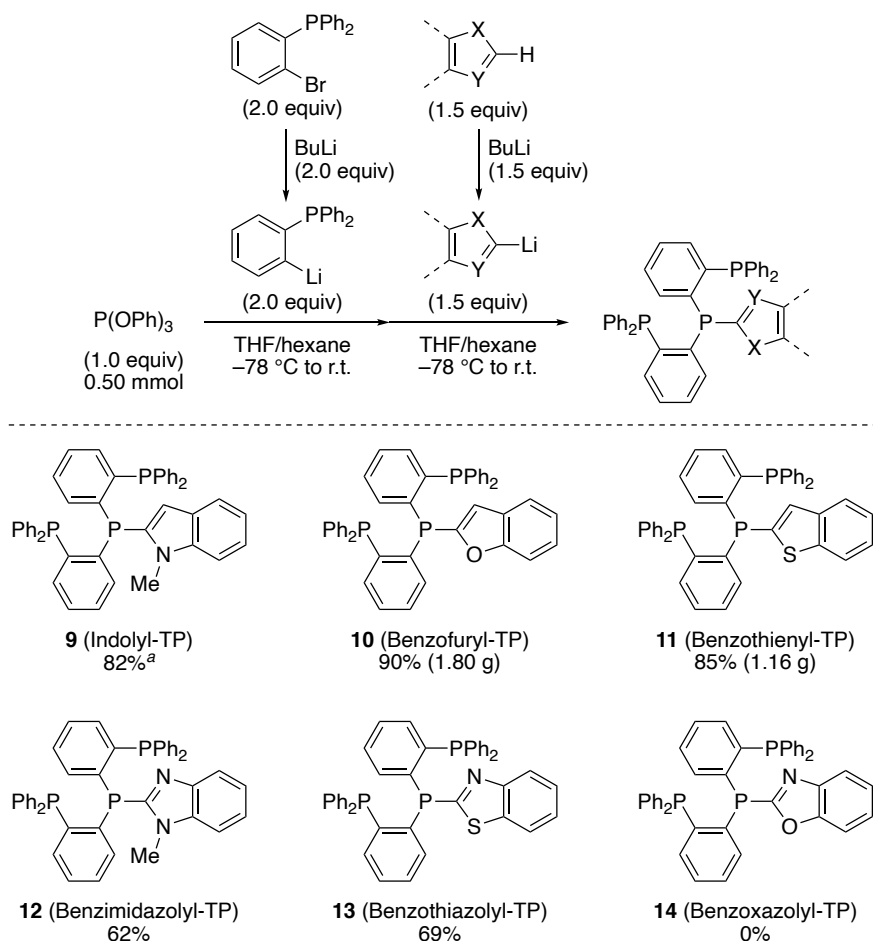
With the tridentate phosphine ligand precursor in hand, a subsequent reaction of the precursor with various kinds of organolithium reagents was attempted to synthesize tridentate phosphine ligands as a final product. As shown in Table 1, the tridentate phosphine ligand precursor was treated with 1.5 equiv of aryl lithium reagents generated by lithium-halogen exchange of the corresponding aryl bromides with BuLi. The pure tridentate phosphine ligands were obtained in high yields by recrystallization from dichloromethane/alcohol. This method is applicable to various kinds of aryl groups ranging from electron rich to deficient ones (**3–6**). This method is also useful for the synthesis of a deuterium-labeled tridentate phosphine ligand which is difficult to be synthesized by any other synthetic methods (**7**). Notably, an *ortho*-substituted organolithium reagent was reactive (**8**), opening up the possibility of using this method even for the synthesis of tetradentate ligands.

Table 1. Synthesis of aryl-TPs



Furthermore, the synthesis of heteroaryl-TP was attempted by reacting the tridentate phosphine ligand precursor with 1.5 equiv of heteroaryl lithium reagents generated by lithiation of the corresponding heteroarenes with BuLi. Also in this case, the pure products were obtained in high yields by simple recrystallization. TMEDA was added as an additive for the lithiation of 1-methylindole to afford indolyl-TP (**9**). This method was widely effective for the synthesis of benzofuryl-TP (**10**), benzothieryl-TP (**11**), benzimidazolyl-TP (**12**), and benzothiazolyl-TP (**13**). However, the synthesis of benzoxazolyl-TP (**14**) failed possibly because of the ring opening of benzoxazolyl lithium reagent.⁹ Gram-scale syntheses were achieved with **10** and **11** without silica gel chromatography, which demonstrates the practicality of this method.

Table 2. Synthesis of heteroaryl-TPs



^a BuLi (1.5 equiv)/TMEDA (1.5 equiv) in Et_2O at r.t. for the deprotonation of 1-methylindole.

Slow diffusion of hexane into an ethyl acetate solution of benzofuryl-TP (**10**) gave a single crystal suitable for X-ray crystallographic analysis. The X-ray crystal data confirmed the structure of a tridentate phosphine ligand having a benzofuryl group as a central aryl group. The distance from the central phosphorus atom to the closest hydrogen atom of the central aryl group was determined to be 3.14 Å, which is longer than in the case of Me₂N-TP (**3**) (2.80 Å). This feature may help to create less sterically hindered catalytic center and facilitate transition-metal catalysis.

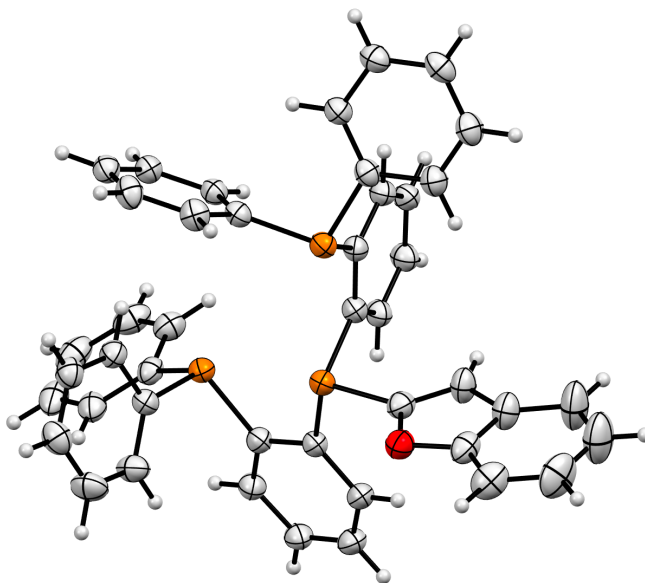
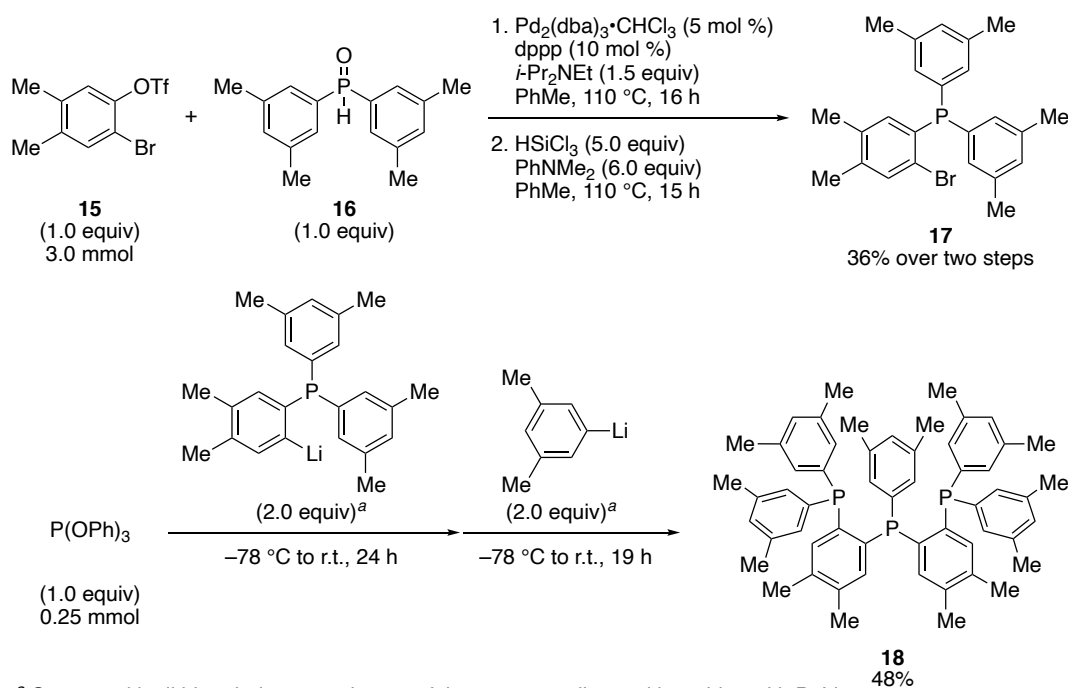


Figure 2. ORTEP drawing of benzofuryl-TP (**10**). Thermal ellipsoids are shown at 30% probability.

3-4. Modulation of all of the aryl groups

Finally, to demonstrate the flexibility of this method, modulation of all of the aryl groups on the tridentate phosphine ligand was attempted. A fully *meta*-substituted TP was chosen as a target. First, *ortho*-bromo triarylphosphine was synthesized by following the reported two-step procedure: Palladium-catalyzed C–P bond formation between aryl triflate (**15**) and diarylphosphine oxide (**16**), and subsequent reduction of triarylphosphine oxide to triarylphosphine (**17**).¹⁰ Aryl triflate (**15**) and diarylphosphine oxide (**16**) starting materials were synthesized from the corresponding Grignard reagent and phenol, respectively. Thus, this two-step procedure allows us to introduce various kinds of substituents to the *ortho*-bromo triarylphosphines starting from readily available aryl bromides and phenols. Finally, sequential addition of two organolithium reagents generated from the *ortho*-bromo triarylphosphine and an aryl bromide to P(OPh)₃ afforded the fully *meta*-substituted TP as a pure product.

Scheme 6. Synthesis of a fully *meta*-substituted TP



3-5. Conclusion

In conclusion, various kinds of conjugated tridentate phosphine ligands were synthesized by sequential addition of two different organolithium reagents to P(OPh)_3 . The use of P(OPh)_3 as a electrophilic phosphine source was the key to selectively synthesize tridentate phosphine ligand out of bidentate or tetradentate ones. This method was applicable to the synthesis of aryl-TPs and heteroaryl-TPs and the pure products were obtained on a gram scale by simple recrystallization from common organic solvents. This method helps to accelerate the investigation of catalytic reactions and functional complexes using tridentate phosphine ligands. The use of heteroaryl-TPs for iron-catalyzed regioselective thienyl C–H/C–H polycondensation will be discussed in the next chapter.

3-6. Experimental

Materials and methods

All air or moisture sensitive reactions were performed in a dry reaction vessel under argon atmosphere. Air or moisture sensitive liquids and solutions were transferred with syringe or Teflon cannula. The water content of solvents was confirmed to be less than 30 ppm by Karl-Fischer titration performed with MKC-210 (Kyoto Electronics Manufacturing Co., Ltd.). Analytical thin-layer chromatography (TLC) was performed with a glass plate coated with 0.25mm 230-400 mesh silica gel containing a fluorescent indicator. Organic solutions were evacuated with a diaphragm pump through a rotary evaporator. Flash column chromatography was performed as described by Still *et al.*¹¹ Preparative recycling gel permeation chromatography (GPC) was performed with LC-92XX II NEXT instrument (Japan Analytical Industry Co., Ltd.) equipped with JAIGEL-2HR polystyrene columns using chloroform as an eluent at the flow rate of 7.5 mL/min.

Gas chromatography (GC) was performed with GC-2014 instrument (Shimadzu Co.) equipped with an ULBON HR-1 (0.25 mm I.D. x 25 m, 0.25 μ m, Shinwa Chemical Industries, Ltd.) capillary column. Mass spectra (GC-MS) were taken with Parvum 2 instrument (Shimadzu Co.). High-resolution mass spectra (HRMS) were taken with LCMS-IT-TOF (Shimadzu Co.) using reserpine (MW 608.2734) as an internal standard. Melting points of solid compounds were measured on a Mel-Temp capillary melting-point apparatus and were uncorrected. Nuclear magnetic resonance (NMR) spectra were taken with ECZ-500 (JEOL, Ltd.) at room temperature unless otherwise noted and reported in parts per million (ppm). ^1H NMR spectra were internally referenced to tetramethylsilane (0.00 ppm), CHCl_3 (7.26 ppm), CHDCl_2 (5.32 ppm), C_2HDCl_4 (5.97 ppm), or $(\text{CHD}_2)(\text{CD}_3)\text{SO}$ (2.50 ppm). ^{13}C NMR spectra were internally referenced to tetramethylsilane (0.0 ppm), CDCl_3 (77.0 ppm), CD_2Cl_2 (53.8 ppm), $\text{C}_2\text{D}_2\text{Cl}_4$ (73.8 ppm), or $(\text{CD}_3)_2\text{SO}$ (39.5 ppm). ^{19}F NMR spectra were internally referenced to C_6F_6 (−164.9 ppm). ^{31}P NMR spectra were internally referenced to $(\text{CH}_3\text{O})_3\text{PO}$ (2.1 ppm). ICP analysis was performed on Shimadzu ICPS-7510 equipment.

Unless otherwise noted, reagents were purchased from Tokyo Chemical Industry Co., Ltd., Sigma-Aldrich Co., LCC, FUJIFILM Wako Pure Chemical Co., and other commercial suppliers and were used as received. Anhydrous tetrahydrofuran and diethyl ether were purchased from KANTO Chemical Co., Inc. and purified prior to use by a solvent purification system (GlassContour) equipped with columns of activated alumina

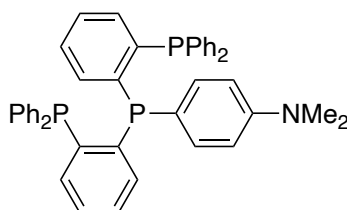
and supported copper catalyst.¹² (2-bromophenyl)diphenylphosphane was purchased from Tokyo Chemical Industry Co., Ltd. and used as received. A tetrahydrofuran solution of butyllithium was purchased from Tokyo Chemical Industry Co., Ltd and titrated prior to use.

Preparation of the crude solution of ((phenoxyphosphanediyl)bis(2,1-phenylene))bis(diphenylphosphane) (Scheme 5)

A hexane solution of BuLi (1.60 mol/L, 3.75 mL, 6.00 mmol) was added dropwise to a solution of (2-bromophenyl)diphenylphosphane (2.05 g, 6.00 mmol) in THF (12 mL) at $-78\text{ }^{\circ}\text{C}$. After stirring for 1 h, $\text{P}(\text{OPh})_3$ (0.78 mL, 3.0 mmol) dissolved in THF (6.0 mL) was added dropwise and the reaction mixture was stirred at $-78\text{ }^{\circ}\text{C}$ for 1 h and then at rt for 1 h. ^{31}P NMR analysis of the crude mixture showed a clean formation of ((phenoxyphosphanediyl)bis(2,1-phenylene))bis(diphenylphosphane). The obtained solution was used as a 0.133 mol/L (= 3.00 mmol/22.5 mL) solution of ((phenoxyphosphanediyl)bis(2,1-phenylene))bis(diphenylphosphane) in the next step. The solution can be stored at rt under argon over one week.

A general synthetic procedure for aryl-TPs (Table 1, compound 3–8)

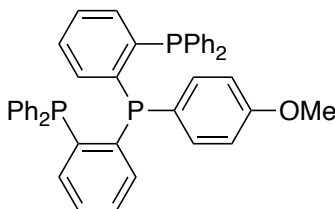
A hexane solution of BuLi (1.53 mol/L, 0.49 mL, 0.75 mmol) was added dropwise to a solution of an aryl bromide (0.75 mmol) in THF (1.5 mL) at $-78\text{ }^{\circ}\text{C}$. After stirring for 1 h, the crude solution of ((phenoxyphosphanediyl)bis(2,1-phenylene))bis(diphenylphosphane) (0.132 mol/L, 3.8 mL, 0.50 mmol) was added dropwise and the reaction mixture was stirred at rt for 18 h. The reaction mixture was quenched by addition of water and the aqueous layer was extracted with dichloromethane. The combined organic layers were dried over Na_2SO_4 and passed through a pad of Florisil. The solvent was removed under reduced pressure and the pure product was obtained by recrystallization.

4-(Bis(2-(diphenylphosphaneyl)phenyl)phosphaneyl)-*N,N*-dimethylaniline (3):

The title compound was obtained as white solid in 88% yield on a 0.5 mmol scale using 4-bromo-*N,N*-dimethylaniline as the aryl bromide. Dichloromethane/methanol was used for recrystallization. The compound data was in good agreement with the literature.¹

¹H NMR (500 MHz, CDCl₃): δ 7.26–6.97 (m, 28H), 6.90–6.87 (m, 2H), 6.50–6.49 (m, 2H), 2.92 (s, 6H).

³¹P NMR (202 MHz, CDCl₃): δ –15.7 (AB₂m, J = 151 Hz, 2P), –20.4 (AB₂m, J = 151 Hz, 1P).

((4-Methoxyphenyl)phosphanedyl)bis(2,1-phenylene))bis(diphenylphosphane) (4):

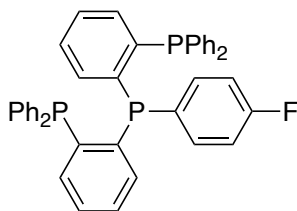
The title compound was obtained as white solid in 85% yield on a 0.5 mmol scale using 1-bromo-4-methoxybenzene as the aryl bromide. Dichloromethane/methanol was used for recrystallization.

Melting point: 231–232 °C (methanol)

¹H NMR (500 MHz, CDCl₃): δ 7.26–7.02 (m, 28H), 6.86–6.82 (m, 2H), 6.68–6.67 (m, 2H), 3.76 (s, 3H).

³¹P NMR (202 MHz, CDCl₃): δ –15.5 (AB₂m, J = 153 Hz, 2P), –20.6 (AB₂m, J = 153 Hz, 1P).

HRMS (APCI+): m/z calcd for C₄₃H₃₅OP₃ [M+H⁺] 661.1974; found: 661.1949.

((4-Fluorophenyl)phosphanediyl)bis(2,1-phenylene))bis(diphenylphosphane) (5):

The title compound was obtained as white solid in 85% yield on a 0.5 mmol scale using 1-bromo-4-fluorobenzene as the aryl bromide. Dichloromethane/methanol was used for recrystallization.

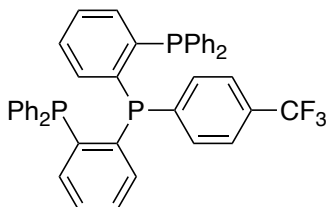
Melting point: 215–217 °C (methanol)

^1H NMR (500 MHz, CDCl_3): δ 7.26–7.03 (m, 28H), 6.83–6.79 (m, 4H).

^{31}P NMR (202 MHz, CDCl_3): δ –15.4 (AB₂m, J = 155 Hz, 2P), –20.9 (AB₂m, J = 155 Hz, 1P).

^{19}F NMR (471 MHz, CDCl_3): δ –116.7.

HRMS (APCI+): m/z calcd for $\text{C}_{42}\text{H}_{32}\text{FP}_3$ [$\text{M}+\text{H}^+$] 649.1774; found: 649.1778.

((4-(Trifluoromethyl)phenyl)phosphanediyl)bis(2,1-phenylene))bis(diphenylphosphane) (6):

The title compound was obtained as pale orange solid in 83% yield on a 0.5 mmol scale using 1-bromo-4-(trifluoromethyl)benzene as the aryl bromide. Dichloromethane/ethanol was used for recrystallization.

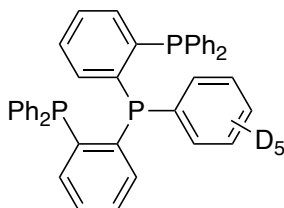
Melting point: 240–241 °C (ethanol)

^1H NMR (500 MHz, CDCl_3): δ 7.30–7.29 (m, 2H), 7.26–7.07 (m, 28H), 6.81–6.80 (m, 2H).

^{31}P NMR (202 MHz, CDCl_3): δ –15.2 (AB₂m, J = 155 Hz, 2P), –20.2 (AB₂m, J = 155 Hz, 1P).

^{19}F NMR (471 MHz, CDCl_3): δ –65.9.

HRMS (APCI+): m/z calcd for $\text{C}_{43}\text{H}_{32}\text{F}_3\text{P}_3$ [$\text{M}+\text{H}^+$] 699.1742; found: 699.1755.

((Phenyl-*d*5)phosphanediyl)bis(2,1-phenylene))bis(diphenylphosphane) (7):

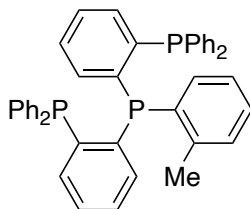
The title compound was obtained as white solid in 87% yield on a 0.5 mmol scale using 1-bromobenzene-2,3,4,5,6-*d*5 as the aryl bromide. Dichloromethane/methanol was used for recrystallization.

Melting point: 217–218 °C (methanol)

¹H NMR (500 MHz, CDCl₃): δ 7.26–7.06 (m, 26H), 6.84–6.83 (m, 2H).

³¹P NMR (202 MHz, CDCl₃): δ –15.3 (AB₂m, *J* = 155 Hz, 2P), –19.2 (AB₂m, *J* = 155 Hz, 1P).

HRMS (APCI+): *m/z* calcd for C₄₂H₂₈D₅P₃ [M+H⁺] 636.2182; found: 636.2183.

((*o*-Tolylphosphanediyl)bis(2,1-phenylene))bis(diphenylphosphane) (8):

The title compound was obtained as white solid in 85% yield on a 0.5 mmol scale using 1-bromo-2-methylbenzene as the aryl bromide. Dichloromethane/methanol was used for recrystallization.

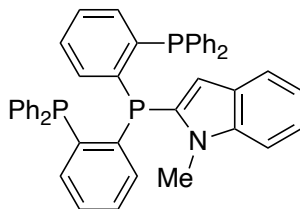
Melting point: 229–232 °C (methanol)

¹H NMR (500 MHz, CDCl₃): δ 7.26–7.04 (m, 28H), 6.91–6.85 (m, 3H), 6.66–6.64 (m, 1H), 2.09 (s, 3H).

³¹P NMR (202 MHz, CDCl₃): δ –14.3 (d, *J* = 156 Hz, 2P), –25.6 (t, *J* = 156 Hz, 1P).

HRMS (APCI+): *m/z* calcd for C₄₃H₃₅P₃ [M+H⁺] 645.2024; found: 645.2015.

2-(Bis(2-(diphenylphosphaneyl)phenyl)phosphaneyl)-1-methyl-1*H*-indole (Table 2, compound 9):



A hexane solution of BuLi (1.53 mol/L, 0.49 mL, 0.75 mmol) was added dropwise to a mixture of 1-methyl-1*H*-indole (94 μ L, 0.75 mmol) and TMEDA (112 μ L, 0.75 mmol) in diethyl ether (1.5 mL) at rt. After stirring for 4 h, the crude solution of ((phenoxyphosphanediy)bis(2,1-phenylene))bis(diphenylphosphane) (0.132 mol/L, 3.8 mL, 0.50 mmol) was added dropwise at 0 °C and the reaction mixture was stirred at rt for 10 h. The reaction mixture was quenched by addition of water (10 mL) and the aqueous layer was extracted with dichloromethane (50 mL). The combined organic layers were washed with brine, dried over Na₂SO₄, and passed through a pad of Florisil. The solvent was removed under reduced pressure and the crude product was carefully recrystallized from dichloromethane/methanol to afford the product as white solid (0.28 g, 82%).

Melting point: 239–240 °C (methanol)

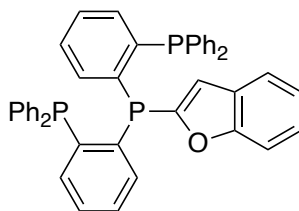
¹H NMR (500 MHz, CDCl₃): δ 7.39 (d, J = 7.7 Hz, 1H), 7.26–6.96 (m, 31H), 5.91 (s, 1H), 3.45 (s, 3H).

³¹P NMR (202 MHz, CDCl₃): δ –13.7 (d, J = 154 Hz, 2P), –42.8 (t, J = 154 Hz, 1P).

HRMS (APCI+): m/z calcd for C₄₅H₃₆NP₃ [M+H⁺] 684.2133; found: 684.2121.

A general synthetic procedure for heteroaryl-TPs (Table 2, compound 10–13)

A hexane solution of BuLi (1.53 mol/L, 1.96 mL, 3.00 mmol) was added dropwise to a solution of a heteroarene (3.00 mmol) in THF (6.0 mL) at –78 °C. After stirring for 1 h, the crude solution of ((phenoxyphosphanediy)bis(2,1-phenylene))bis(diphenylphosphane) (0.132 mol/L, 15 mL, 2.0 mmol) was added dropwise and the reaction mixture was stirred at rt for 12 h. The reaction mixture was quenched by addition of water and the aqueous layer was extracted with dichloromethane. The combined organic layers were washed with brine, dried over Na₂SO₄, and passed through a pad of Florisil. The solvent was removed under reduced pressure and the pure product was obtained by recrystallization.

((Benzofuran-2-ylphosphanediyl)bis(2,1-phenylene))bis(diphenylphosphane) (10):

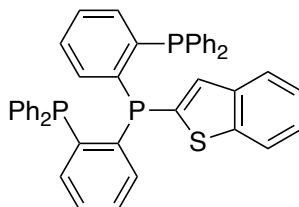
The title compound was obtained as white solid in 90% yield on a 3.0 mmol scale using 2,3-benzofuran as the heteroarene. Dichloromethane/methanol was used for recrystallization.

Melting point: 246–248 °C (methanol)

^1H NMR (500 MHz, CDCl_3): δ 7.36–7.33 (m, 2H), 7.23–7.06 (m, 30H), 6.44–6.43 (m, 1H).

^{31}P NMR (202 MHz, CDCl_3): δ –14.7 (AB_2m , $J = 154$ Hz, 2P), –37.6 (AB_2m , $J = 154$ Hz, 1P).

HRMS (APCI+): m/z calcd for $\text{C}_{44}\text{H}_{33}\text{OP}_3$ $[\text{M}+\text{H}^+]$ 671.1817; found: 671.1816.

((Benzo[*b*]thiophen-2-ylphosphanediyl)bis(2,1-phenylene))bis(diphenylphosphane) (11):

The title compound was obtained as white solid in 85% yield on a 2.0 mmol scale using benzo[*b*]thiophene as the heteroarene. Dichloromethane/methanol was used for recrystallization.

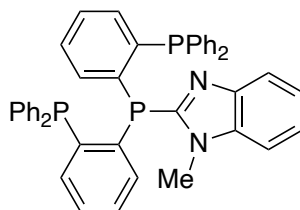
Melting point: 259–260 °C (methanol)

^1H NMR (500 MHz, CD_2Cl_2): δ 7.65–7.63 (m, 1H), 7.55–7.53 (m, 1H), 7.24–6.97 (m, 31H).

^{31}P NMR (202 MHz, CD_2Cl_2): δ –14.7 (AB_2m , $J = 154$ Hz, 2P), –30.1 (AB_2m , $J = 154$ Hz, 1P).

HRMS (APCI+): m/z calcd for $\text{C}_{44}\text{H}_{33}\text{P}_3\text{S}$ $[\text{M}+\text{H}^+]$ 687.1589; found: 687.1567.

2-(Bis(2-(diphenylphosphaneyl)phenyl)phosphaneyl)-1-methyl-1*H*-benzo[*d*]imidazole (12):



The title compound was obtained as white solid in 62% yield on a 0.5 mmol scale using 1-methylbenzimidazole as the heteroarene. The pure product was obtained by recrystallization from dichloromethane/diethyl ether twice.

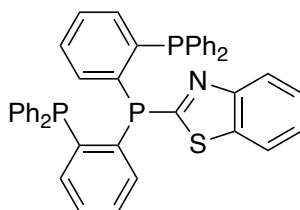
Melting point: 163–164 °C (diethyl ether)

^1H NMR (500 MHz, CDCl_3): δ 7.62 (d, J = 8.1 Hz, 1H), 7.33–7.29 (m, 2H), 7.25–6.98 (m, 29H), 3.46 (s, 3H).

^{31}P NMR (202 MHz, CDCl_3): δ –13.0 (d, J = 154 Hz, 2P), –44.6 (t, J = 154 Hz, 1P).

HRMS (APCI+): m/z calcd for $\text{C}_{44}\text{H}_{35}\text{N}_2\text{P}_3$ [$\text{M}+\text{H}^+$] 685.2086; found: 685.2090.

2-(Bis(2-(diphenylphosphaneyl)phenyl)phosphaneyl)benzo[*d*]thiazole (13):



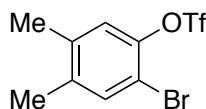
The title compound was obtained as pale yellow solid in 69% yield on a 0.5 mmol scale using benzothiazole as the heteroarene. The pure product was obtained by recrystallization from dichloromethane/methanol twice.

Melting point: 246–248 °C (methanol)

^1H NMR (500 MHz, CD_2Cl_2): δ 8.00 (d, J = 8.0 Hz, 1H), 7.82 (d, J = 8.1 Hz, 1H), 7.47–7.02 (m, 30H).

^{31}P NMR (202 MHz, CD_2Cl_2): δ –14.3 (AB₂m, J = 165 Hz, 2P), –20.7 (AB₂m, J = 165 Hz, 1P).

HRMS (APCI+): m/z calcd for $\text{C}_{43}\text{H}_{32}\text{NP}_3\text{S}$ [$\text{M}+\text{H}^+$] 688.1541; found: 688.1554.

2-Bromo-4,5-dimethylphenyl trifluoromethanesulfonate (15):

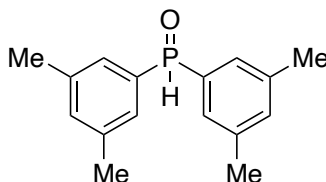
Trifluoromethanesulfonic anhydride (2.7 mL, 17 mmol) was added dropwise at 0 °C to a solution of 2-bromo-4,5-dimethylphenol¹³ (3.0 g, 15 mmol) and pyridine (1.8 mL, 23 mmol) in dichloromethane (15 mL). The reaction mixture was gradually warmed to rt and stirred for 12 h. The reaction mixture was quenched by addition of an aqueous solution of HCl (2 M, 5 mL) and the organic layer was washed with water and brine and dried over Na₂SO₄. The solvent was removed under reduced pressure and the product was used in the next step without further purification.

¹H NMR (500 MHz, CDCl₃): δ 7.42 (s, 1H), 7.09 (s, 1H), 2.26 (s, 3H), 2.25 (s, 3H).

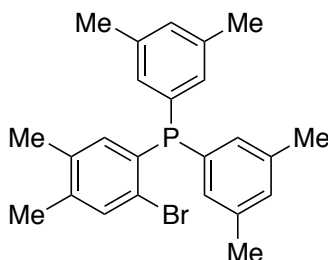
¹³C NMR (125 MHz, CDCl₃): δ 144.7, 138.8, 138.3, 134.6, 123.4, 118.6 (q, *J* = 321 Hz), 112.0, 19.6, 19.2.

¹⁹F NMR (471 MHz, CDCl₃): δ -76.6.

GC MS (EI) *m/z* (relative intensity): 334 (M⁺, 21), 332 (20), 201 (50), 199 (51), 173 (11), 171 (12), 92 (100), 91 (75).

Bis(3,5-dimethylphenyl)phosphine oxide (16):

The title compound was prepared according to the literature.¹⁴ The compound data was in good agreement with the literature.

(2-Bromo-4,5-dimethylphenyl)bis(3,5-dimethylphenyl)phosphane (17):

A mixture of 2-bromo-4,5-dimethylphenyl trifluoromethanesulfonate (1.00 g, 3.0 mmol), bis(3,5-dimethylphenyl)phosphine oxide (0.77 g, 3.0 mmol), $\text{Pd}_2(\text{dba})_3 \cdot \text{CHCl}_3$ (155 mg, 0.15 mmol), 1,3-bis(diphenylphosphino)propane (dppp, 124 mg, 0.30 mmol), and *i*- Pr_2NEt (0.77 mL, 4.5 mmol) in toluene (9.0 mL) was stirred under argon atmosphere at 110 °C for 16 h. The reaction mixture was quenched by addition of an aqueous solution of HCl (1 M, 9 mL) and the aqueous layer was extracted with ethyl acetate (5 mL x 3). The combined organic layers were washed with water and brine and dried over Na_2SO_4 . The solvent was removed under reduced pressure and the crude product was purified by silica gel chromatography (hexane: ethyl acetate = 1:1) to afford (2-bromo-4,5-dimethylphenyl)bis(3,5-dimethylphenyl)phosphine oxide containing inseparable impurities (0.75 g in total). This product was used in the next step without further purification.

A mixture of (2-bromo-4,5-dimethylphenyl)bis(3,5-dimethylphenyl)phosphine oxide (0.75 g, 1.7 mmol), trichlorosilane (0.85 mL, 8.5 mmol), and *N,N*-dimethylaniline (1.28 mL, 10 mmol) in toluene (11 mL) was stirred under argon atmosphere at 110 °C for 15 h. The reaction mixture was carefully quenched by addition of an aqueous solution of NaOH (25%, 6 mL) at 0 °C and the aqueous layer was extracted with toluene (5 mL x 3). The combined organic layers were washed with an aqueous solution of HCl (1 M), water, and brine, and dried over Na_2SO_4 . The solvent was removed under reduced pressure and the crude product was purified by silica gel chromatography (hexane: ethyl acetate = 50:1) to afford the product as pale yellow solid (0.46 g, 36% over two steps).

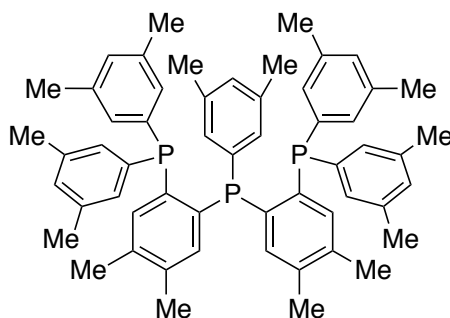
Melting point: 120–121 °C (ethyl acetate)

^1H NMR (500 MHz, CDCl_3): δ 7.37 (d, J = 3.7 Hz, 1H), 6.98 (s, 2H), 6.88 (d, J = 8.0 Hz, 4H), 6.50 (d, J = 2.9 Hz, 1H), 2.27 (s, 12H), 2.23 (s, 3H), 2.06 (s, 3H).

^{31}P NMR (202 MHz, CDCl_3): δ -6.1.

HRMS (APCI+): m/z calcd for $\text{C}_{24}\text{H}_{26}\text{BrP}$ [$\text{M}+\text{H}^+$] 427.1011; found: 427.1019.

((3,5-Dimethylphenyl)phosphanediyl)bis(4,5-dimethyl-2,1-phenylene))bis(bis(3,5-dimethylphenyl)phosphane) (18):



The title compound was obtained as white solid in 48% yield on a 0.25 mmol scale by following the general synthetic procedure for aryl-TPs using (2-Bromo-4,5-dimethylphenyl)bis(3,5-dimethylphenyl)phosphane (**17**) and 1-bromo-3,5-dimethylbenzene as the aryl bromides. The crude reaction mixture was purified by gel permeation chromatography (chloroform).

Melting point: 122–124 °C (chloroform)

^1H NMR (500 MHz, CDCl_3): δ 6.95–6.93 (m, 2H), 6.83–6.81 (m, 6H), 6.77 (s, 3H), 6.72 (d, $J = 6.6$ Hz, 6H), 6.49–6.47 (m, 2H), 2.14–2.13 (m, 30H), 2.07 (s, 6H), 1.93 (s, 6H).

^{31}P NMR (202 MHz, CDCl_3): δ –16.6 (AB₂m, $J = 151$ Hz, 2P), –20.6 (AB₂m, $J = 151$ Hz, 1P).

HRMS (APCI+): m/z calcd for $\text{C}_{56}\text{H}_{61}\text{P}_3$ [$\text{M}+\text{H}^+$] 827.4059; found: 827.4053.

Crystallographic study

The diffraction images for X-ray crystallographic analysis were collected on a Rigaku VariMax Dual equipped with a hybrid photon counting detector using $\text{Cu K}\alpha$ ($\lambda = 1.5418$ Å) radiation. A single crystal was coated with mineral oil and mounted on a loop-type mount. The structure was solved by the direct method with SHELXT¹⁵ and refined by the full-matrix least-squares method with SHELXL¹⁶ using Olex2¹⁷ interface.

Crystal data and structure refinement for benzofuryl-TP (10)

Empirical formula	C ₄₄ H ₃₃ OP ₃
Formula weight	670.61
Temperature/K	93
Crystal system	monoclinic
Space group	P2 ₁ /n
a/Å	9.8806(7)
b/Å	21.4720(15)
c/Å	16.9263(11)
α /°	90
β /°	104.235(7)
γ /°	90
Volume/Å ³	3480.8(4)
Z	4
ρ_{calc} /cm ³	1.280
μ /mm ⁻¹	1.830
F(000)	1400.0
2 Θ range for data collection/°	6.78 to 143.606
Index ranges	-11 ≤ h ≤ 12, -25 ≤ k ≤ 23, -20 ≤ l ≤ 18
Reflections collected	19808
Independent reflections	6593 [$R_{\text{int}} = 0.0747$, $R_{\text{sigma}} = 0.0740$]
Data/restraints/parameters	6593/0/433
Goodness-of-fit on F ²	1.045
Final R indexes [$I \geq 2\sigma(I)$]	$R_1 = 0.0779$, $wR_2 = 0.2120$
Final R indexes [all data]	$R_1 = 0.0924$, $wR_2 = 0.2310$
Largest diff. peak/hole / e Å ⁻³	1.12/-0.54

3-7. References and notes

- ¹ (a) Shang, R.; Ilies, L.; Nakamura, E. *J. Am. Chem. Soc.* **2016**, *138*, 10132–10135. (b) Doba, T.; Ilies, L.; Sato, W.; Shang, R.; Nakamura, E. *Nat. Catal.* **2021**, *4*, 631–638.
- ² (a) Buscagan, T. M.; Oyala, P. H.; Peters, J. C. *Angew. Chem. Int. Ed.* **2017**, *56*, 6921–6926. (b) Cavaillé, A.; Joyeux, B.; Saffon-Merceron, N.; Nebra, N.; Fustier-Boutignon, M.; Mézailles, N. Triphos–Fe *Chem. Commun.* **2018**, *54*, 11953–11956. (c) Schild, D. J.; Peters, J. C. *ACS Catal.* **2019**, *9*, 4286–4295. (d) Tanabe, Y.; Nishibayashi, Y. *Coordination Chemistry Reviews* **2019**, *389*, 73–93.
- ³ (a) Chen, J.-F.; Li, C. *Org. Lett.* **2018**, *20*, 6719–6724. (b) Chen, J.-F.; Li, C. *ACS Catal.* **2020**, *10*, 3881–3889.
- ⁴ Korstanje, T. J.; Ivar van der Vlugt, J.; Elsevier, C. J.; de Bruin, B. *Science* **2015**, *350*, 298–302.
- ⁵ (a) Adam, R.; Bheeter, C. B.; Jackstell, R.; Beller, M. *ChemCatChem* **2016**, *8*, 1329–1334. (a) Deng, L.; Kang, B.; Englert, U.; Klankermayer, J.; Palkovits, R. *ChemSusChem* **2016**, *9*, 177–180. (c) Lee, H. M.; Bianchini, C.; Jia, G.; Barbaro, P. *Organometallics* **1999**, *18*, 1961–1966.
- ⁶ Liao, Q.; Saffon-Merceron, N.; Mézailles, N. *ACS Catal.* **2015**, *5*, 6902–6906.
- ⁷ Zhang, J.; Duan, C.; Han, C.; Yang, H.; Wei, Y.; Xu, H. *Adv. Mater.* **2016**, *28*, 5975–5979.
- ⁸ Keller, J.; Schlierf, C.; Nolte, C.; Mayer, P.; Straub, B. F. *Synthesis* **2006**, No. 2, 354–365.
- ⁹ Pirrung, M. C.; Ghorai, S. *J. Am. Chem. Soc.* **2006**, *128*, 11772–11773.
- ¹⁰ Matsumura, K.; Shimizu, H.; Saito, T.; Kumobayashi, H. *Adv. Synth. Catal.* **2003**, *345*, 180–184.
- ¹¹ Still, W. C.; Kahn, M.; Mitra, A. *J. Org. Chem.* **1978**, *43*, 2923–2925.
- ¹² Pangborn, A. B.; Giardello, M. A.; Grubbs, R. H.; Rosen, R. K.; Timmers, F. J. *Organometallics* **1996**, *15*, 1518–1520.
- ¹³ Cheng, X.; Peng, Y.; Wu, J.; Deng, G.-J. *Org. Biomol. Chem.* **2016**, *14*, 2819–2823.
- ¹⁴ Jin, M.; Nakamura, M. *Chem. Lett.* **2013**, *42*, 1035–1037.
- ¹⁵ Sheldrick, G. M. *Acta Crystallogr. Sect. A* **2015**, *71*, 3–8.
- ¹⁶ Sheldrick, G. M. *Acta Crystallogr. Sect. C* **2015**, *71*, 3–8.

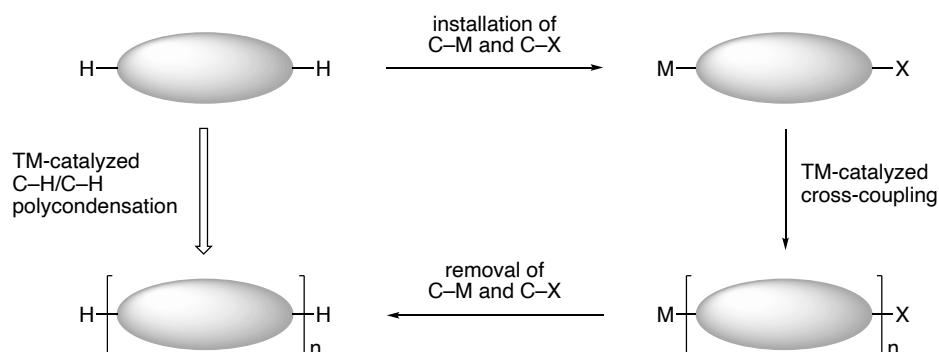
¹⁷ Dolomanov, O. V.; Bourhis, L. J.; Gildea, R. J.; Howard, J. A. K.; Puschmann, H. *J. Appl. Crystallogr.* **2009**, *42*, 339–341.

Chapter 4.
Iron-Catalyzed Regioselective Thienyl C–H/C–H Polycondensation

4-1. Introduction

π -Conjugated polymeric compounds have found a wide application in the field of organic electronics such as organic field-effect transistors (OFETs), organic light-emitting diodes (OLEDs), and organic solar cells (OSCs).¹ Currently, these polymers have been synthesized by a sequence of preinstallation of C–M (M: metal) bond and C–X (X: (pseudo)halide) bond to a hydrocarbon monomer, transition-metal-catalyzed cross-coupling,² and removal of C–M and C–X bonds by an end capping procedure.³ Taking into account the multiple synthetic steps required, transition-metal-catalyzed C–H/C–H polycondensation serves as a straightforward method to synthesize conjugated polymers from simple C–H monomers. However, extremely efficient transition-metal-catalyzed C–H/C–H coupling reaction is essential to achieve polymerization and obtain sufficiently long polymers, which is recognized as a big challenge.⁴

Scheme 1. Synthesis of polymer from hydrocarbon monomer



Although direct arylation polymerization (DArP) where the preinstallation of a C–M bond is omitted has been extensively studied since 2010s,⁵ there are only a limited number of reports on transition-metal-catalyzed C–H/C–H polycondensation. In 2013, Ogino and co-workers reported palladium-catalyzed C–H/C–H polycondensation of simple thiophene monomers to synthesize polythiophenes (Figure 1a).⁶ $\text{Cu}(\text{OAc})_2$ and O_2 were used as an oxidant and CF_3COOH was added to increase the molecular weight of the polymer. NMR analysis of the polymer revealed that there are linkage at the 4-position of thiophene and branching of the polymer chain resulting from low regioselectivity of C–H/C–H coupling (Figure 1b). Later on, it was found that thiophene substrates possessing an ester or an amide group were suitable for polymerization possibly due to the directing effect of a carbonyl group.⁷

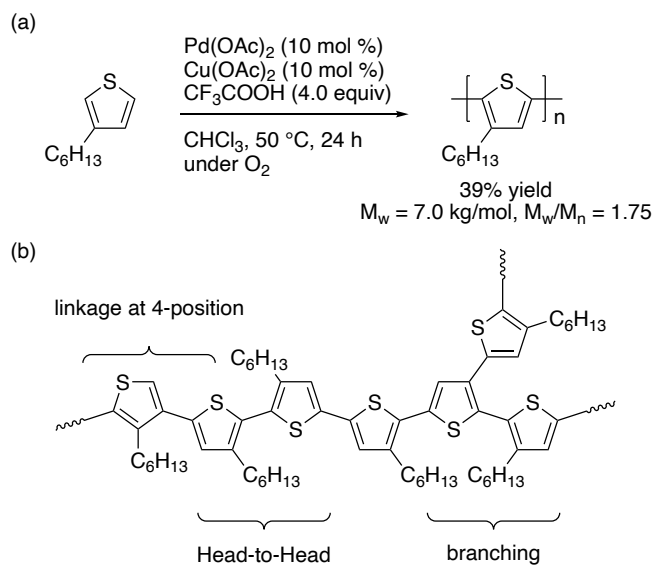
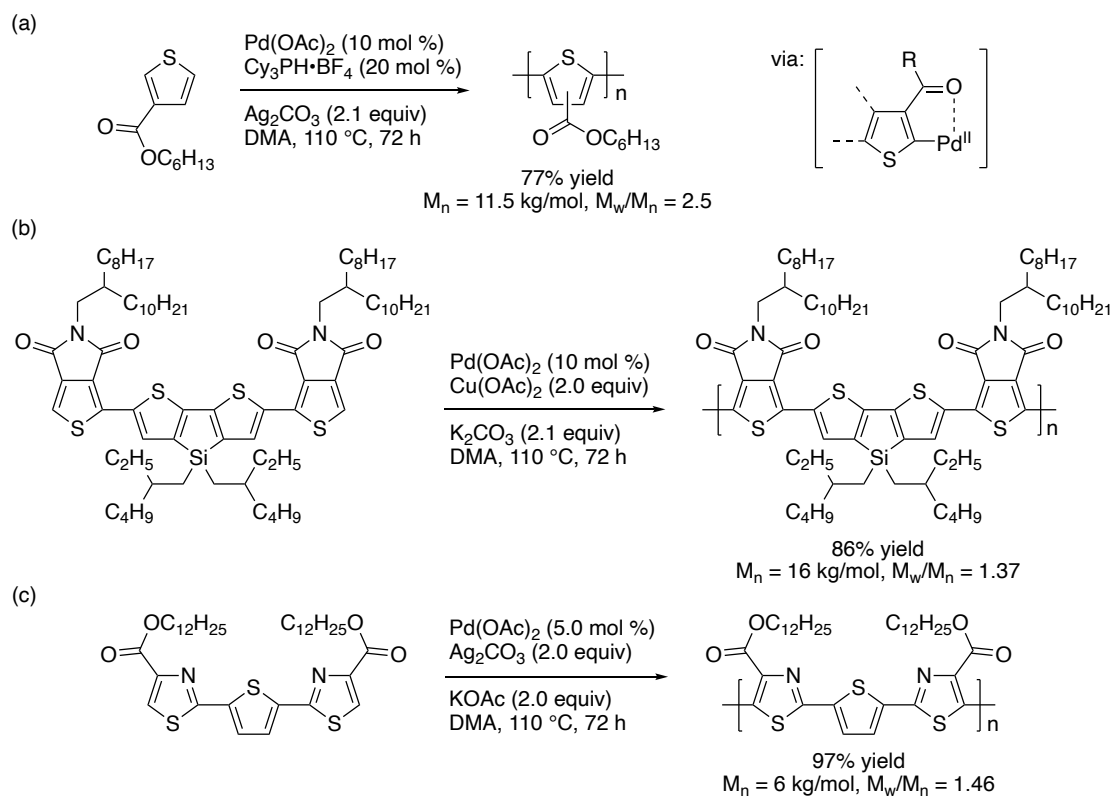


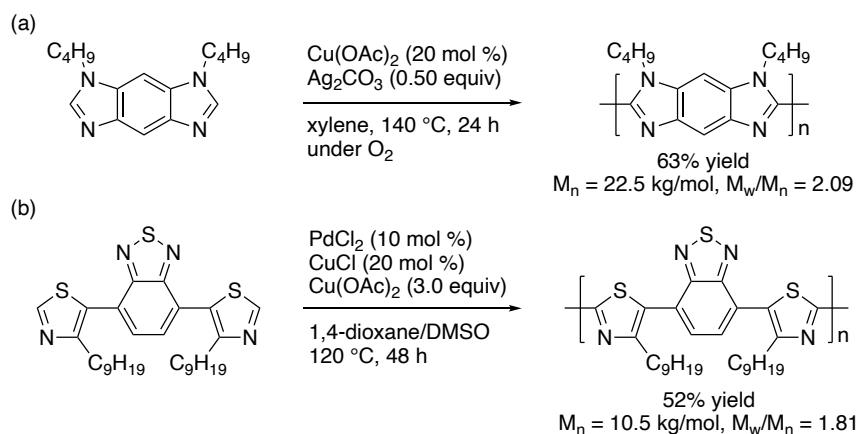
Figure 1. Pioneering work on transition-metal-catalyzed C–H/C–H polycondensation

Scheme 2. Palladium-catalyzed C–H/C–H polycondensation of carbonyl containing thiophene monomers

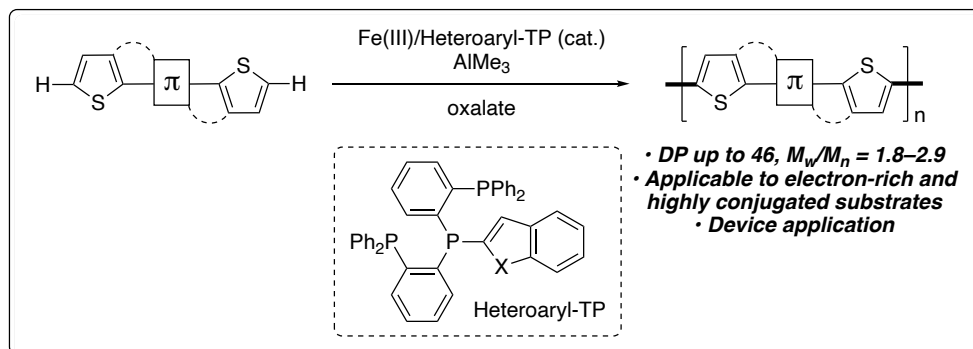


In addition to thiophenes, azoles have also been examined as a substrate for transition-metal-catalyzed C–H/C–H polycondensation. In 2014, You and co-workers reported copper-catalyzed C–H/C–H polycondensation of imidazoles.⁸ More recently, the same group reported a palladium/copper-cocatalyzed system to achieve C–H/C–H polycondensation of thiazoles.⁹

Scheme 3. Transition-metal-catalyzed C–H/C–H polycondensation of azole monomers



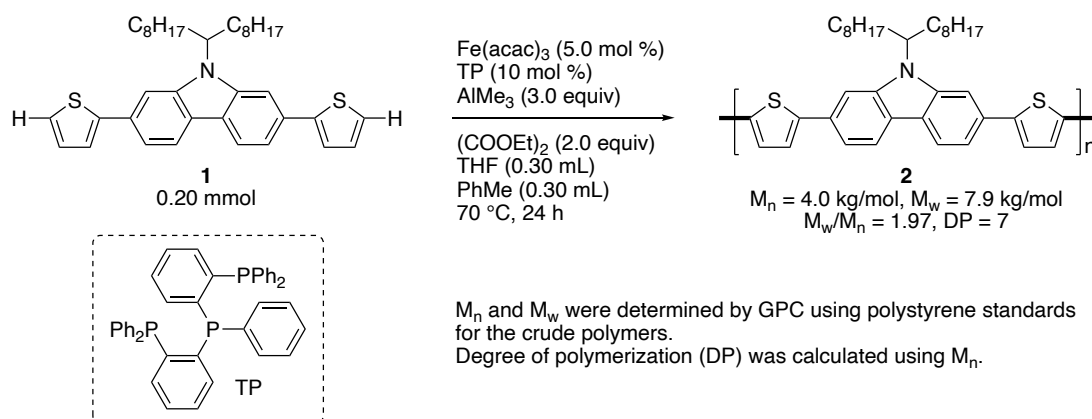
As explained above, transition-metal-catalyzed C–H/C–H polycondensation has emerged as one of the most straightforward methods to synthesize conjugated polymers. However, this methodology is still underdeveloped and the scope is limited to heteroarenes with special substitution patterns. Also, in all cases, the use of monomers containing electron-rich motifs are avoided to prevent direct oxidation of polymer by external oxidant that is added to turn over the catalyst. In this chapter I report iron-catalyzed regioselective thienyl C–H/C–H polycondensation that operates under mildly oxidative conditions and enables polymerization of a wide range of thiophene monomers containing electron-rich and highly conjugated π -motifs. This reaction was realized by improving the efficiency of iron-catalyzed regioselective thienyl C–H/C–H homocoupling by suppression of catalyst deactivation using heteroaryl-TP as a ligand (as described in the next section). This method gives direct access to thiophene polymers which are an important class of compounds for optoelectronic device applications.

Scheme 4. Iron-catalyzed regioselective thienyl C–H/C–H polycondensation

4-2. Initial trial

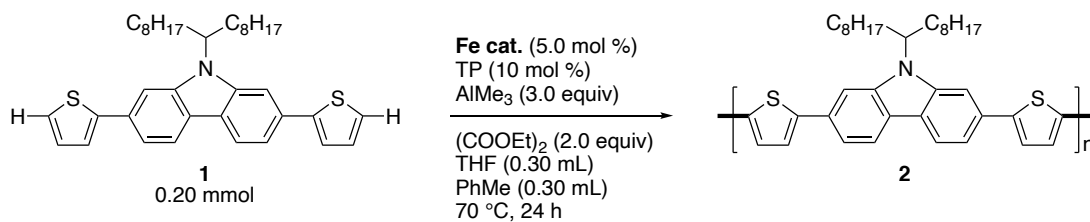
As an initial trial, polycondensation of a dithienylcarbazole monomer (**1**) to poly[(2,7-carbazole)-*alt*-bithiophene] (**2**), which has been reported as a *p*-type semiconductor in OFET,¹⁰ was attempted using the reaction conditions for iron-catalyzed regioselective thienyl C–H/C–H homocoupling described in the previous chapter. After quenching the reaction by addition of acid, the crude reaction mixture was analyzed by analytical gel permeation chromatography (GPC). The number average molecular weight (M_n) and weight average molecular weight (M_w) were determined using polystyrene standards of known molecular weights. Disappointingly, only a short oligomer containing approximately 7 monomer units was obtained. Polydispersity index (PDI, M_w/M_n) was close to the value of 2, indicating that polycondensation proceeds through a step-growth mechanism. Notably, the efficiency of step-growth polymerization is mostly affected by the reaction efficiency at the late stage of the reaction, meaning that suppression of catalyst deactivation even under low concentration of the reactive thienyl C–H bond is necessary to achieve efficient polycondensation.

Scheme 5. Initial trial of iron-catalyzed regioselective thienyl C–H/C–H polycondensation.



4-3. Investigation of iron source

Assuming that acetylacetonate (acac^-) has an inhibition effect by strong binding to iron, effect of iron source on the efficiency of polymerization was investigated. When FeCl_3 was used instead of $\text{Fe}(\text{acac})_3$, slight increase of the molecular weight was observed (Table 1, entry 2). The use of $\text{FeCl}_3 \cdot 6\text{H}_2\text{O}$, an air stable analog of FeCl_3 , further improved the reaction efficiency (entry 3). It is noteworthy that 5.0 mol % of $\text{FeCl}_3 \cdot 6\text{H}_2\text{O}$, releasing 30 mol % of H_2O , had no inhibition effect because of the oxophilicity of $\text{Al}(\text{III})$ which prevents O^{2-} binding to $\text{Fe}(\text{III})$ catalytic species (entry 2 and 4). Fluorine containing counter anions were not suitable for the reaction possibly because of the formation of a strong Fe-F bond (entry 5, 6, 8).¹¹ $\text{Fe}(\text{II})$ salts were less effective than $\text{Fe}(\text{III})$ salts, indicating that the reaction proceeds through an $\text{Fe}(\text{III})/\text{Fe}(\text{I})$ catalytic cycle (entry 7 and 8). Eventually, the DP value of the longest polymer was 9 (entry 3), which prompted me to further improve the efficiency of the iron-catalyzed regioselective thienyl C–H/C–H polycondensation reaction by suppression of catalyst deactivation.

Table 1. Effect of iron source

entry	Fe cat.	M_n (kg/mol) ^a	M_w (kg/mol) ^a	M_w/M_n ^a	DP ^b
1	Fe(acac) ₃	4.0	7.9	1.97	7
2	FeCl ₃	4.5	9.3	2.06	8
3	FeCl ₃ ·6H ₂ O	5.1	10.8	2.12	9
4 ^c	FeCl ₃ + H ₂ O (30 mol %)	4.6	9.3	2.05	8
5	FeF ₃ ·3H ₂ O	2.8	5.0	1.77	5
6	Fe(OTf) ₃	1.4	1.5	1.10	2
7	FeCl ₂ ·4H ₂ O	3.1	5.9	1.88	5
8	Fe(BF ₄) ₂ ·6H ₂ O	1.8	2.4	1.30	3

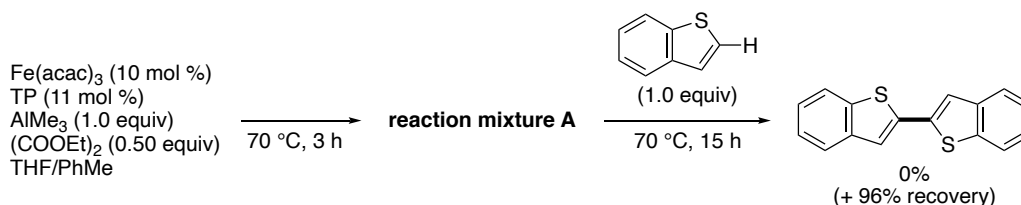
^a M_n and M_w were determined by GPC using polystyrene standards for the crude polymers.

^b Degree of polymerization was calculated using M_n .

^c H₂O (30 mol %) was premixed with AlMe₃ (3.0 equiv).

4-4. Determination of catalyst deactivation pathway

To determine the catalyst deactivation pathway at the late stage of the reaction where the concentration of the substrate is significantly low, the outcome of the reaction *without* substrate was considered as an extreme condition. First, Fe(acac)₃/TP catalyst, AlMe₃ and (COOEt)₂ were heated at 70 °C for 3 h without a thiophene substrate and then the substrate was added and heated at 70 °C for 15 h. As expected, the homocoupling product was not obtained at all and the starting material was fully recovered. This clearly demonstrates that the catalyst is totally deactivated in the reaction mixture A (Scheme 6).

Scheme 6. Catalyst deactivation under no substrate

To understand what happened to the iron catalyst after catalyst deactivation, the tridentate phosphine ligand was recovered from the reaction mixture A by treatment with EDTA. HRMS spectrum of the recovered ligand showed peaks that are heavier than the molecular weight of TP by 14 and 28 (Figure 2). This indicates that the ligand is mono- and dimethylated by the methyl group provided by AlMe_3 . Although the position of methylation could not be determined by HRMS, it is expected that methylation took place at the *ortho* position of a phenyl group of TP according to the precedent of *ortho*-metalation of 1,2-bis(diphenylphosphino)ethane (dppe) under almost identical conditions.¹² First, TP ligand undergoes directed *ortho*-C–H activation intramolecularly through a σ -bond metathesis mechanism to form four-membered cyclometalated species **II**. After reductive elimination of the metallacycle with a methyl group, the ligand is methylated (**III**). Because of the compactness of the iron catalytic center, the sterics of the methyl group at the *ortho* position kills the catalytic activity. Therefore, suppression of *ortho*-metalation of the tridentate phosphine ligand would be the key to suppress the catalyst deactivation and achieve efficient polycondensation reaction.

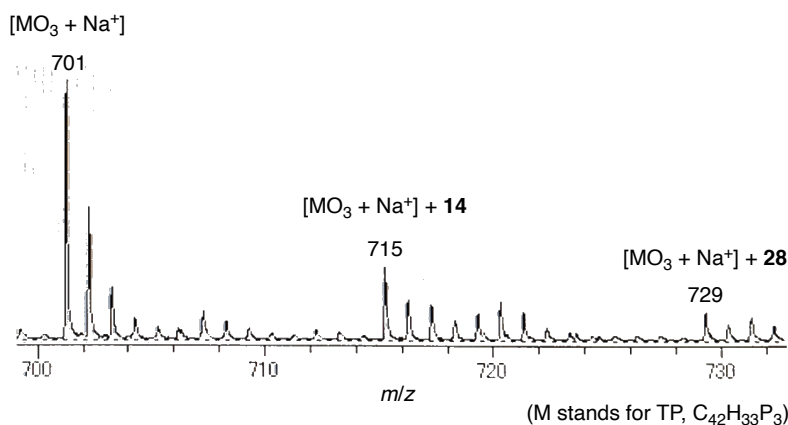


Figure 2. HRMS spectrum of the recovered ligand

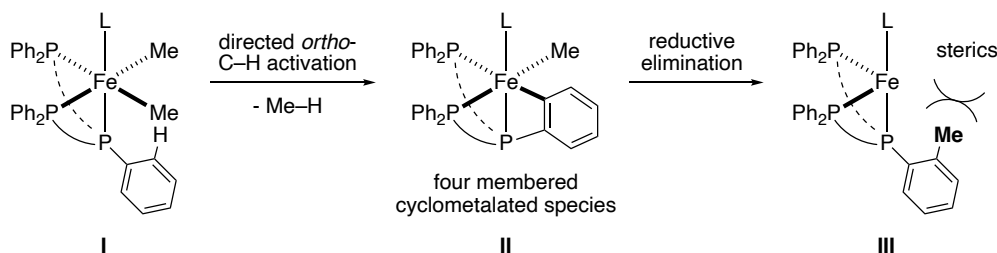


Figure 3. Methylation of TP

4-5. Ligand design

To suppress *ortho*-metalation of the tridentate phosphine ligand, I designed a new ligand, heteroaryl-TP (Figure 4). The ligand design is based on the assumption that a cyclometalated species of 4-membered ring and 5-membered ring is more strained than that of 4-membered ring and 6-membered ring because of the larger deviation from the ideal bond angles, making it more difficult to form a cyclometalated species and helping to suppress the catalyst deactivation. In other words, as described in the previous chapter, the distance from the central phosphorus atom to the closest hydrogen atom of the central heteroaryl group is over 3.00 Å, which is longer than in the case of Me₂N-TP (2.80 Å), making the directed *ortho*-C–H activation of the ligand more difficult. In addition to this merit, smaller steric hinderance of a heteroaryl group compared to that of a phenyl group may have an effect of facilitating the iron catalysis.

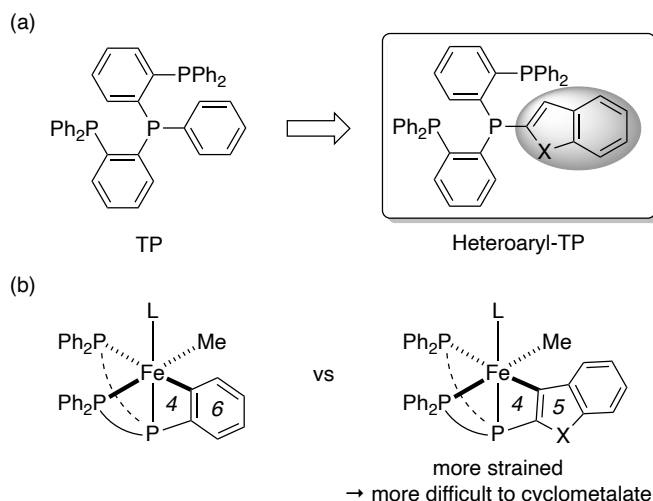


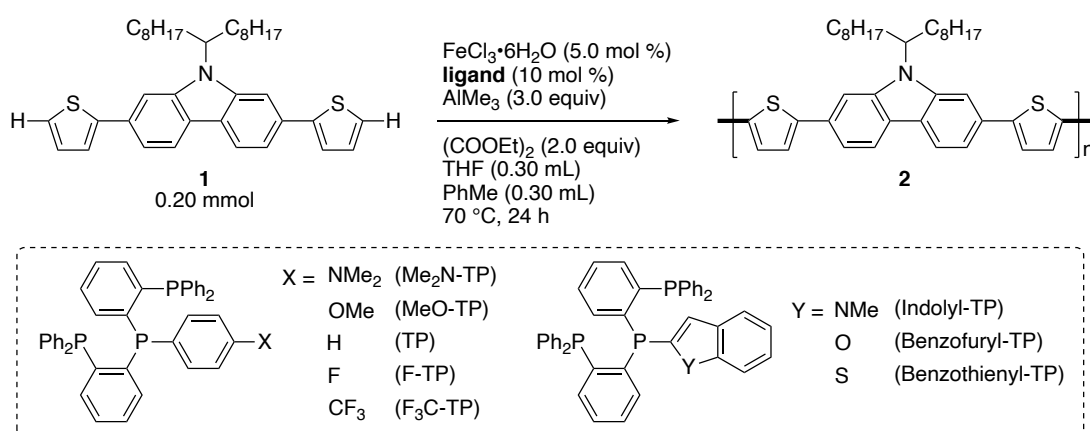
Figure 4. Design of heteroaryl-TP

4-6. Effect of heteroaryl-TP on the efficiency of polycondensation

Heteroaryl-TPs were synthesized using the method described in the previous chapter and used for the polycondensation of dithienylcarbazole monomer (**1**). First, the effect of electronic properties of aryl-TPs was investigated (Table 2, entry 1–5). Judging from the molecular weights (M_n and M_w) and the degree of polymerization (DP), installation of an electron-rich aryl group on the central phosphine atom significantly decreased the polymer length. Next, the effect of heteroaryl-TPs on the efficiency of polycondensation was examined. The poor performance of indolyl-TP can be ascribed to the electron-rich

indole group and steric hindrance of the *N*-methyl substituent. Benzofuryl- and benzothienyl-TP produced polymer **2** with DP of 23 and 21 with PDI of around 2, which were isolated in 86% and 88% yield, respectively. Notably, branched polymer was not generated as judged by the lack of a conspicuous singlet peak that would appear in the aromatic region of the ^1H NMR spectrum in case of formation of a branched product (Figure 5).

Table 2. Effect of ligand on the efficiency of polycondensation



entry	ligand	M_n (kg/mol) ^a	M_w (kg/mol) ^a	M_w/M_n ^a	DP ^b	yield (%) ^c
1	Me ₂ N-TP	1.6	2.0	1.23	3	-
2	MeO-TP	3.0	5.9	1.99	5	-
3	TP	5.1	10.8	2.12	9	-
4	F-TP	5.0	10.4	2.09	9	-
5	F ₃ C-TP	6.4	13.2	2.07	11	-
6	Indolyl-TP	1.7	2.2	1.30	3	-
7	Benzofuryl-TP	13.3	22.6	1.70	23	86
8	Benzothienyl-TP	11.9	21.0	1.76	21	88

^a M_n and M_w were determined by GPC using polystyrene standards for the crude polymers.

^b Degree of polymerization was calculated using M_n .

^c Isolated by precipitation. Yields were not determined for short oligomers.

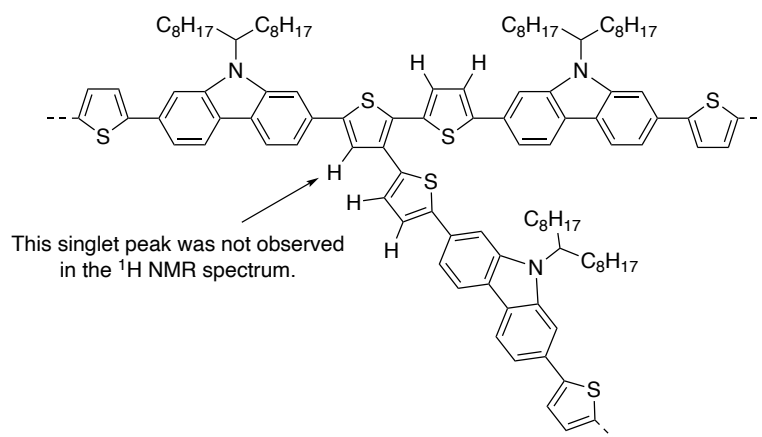


Figure 5. The absence of polymer branching

4-7. Substrate scope

Using benzofuryl-TP as the optimal ligand, the scope of iron-catalyzed regioselective thienyl C–H/C–H polycondensation was investigated. Table 3 shows the examples of straightforward conversion of monomers to the corresponding polymers inaccessible either by the conventional oxidative aromatic C–H/C–H coupling or by palladium-catalyzed C–H/C–H coupling. Homopolymers and copolymers were obtained with DP up to 46 with a unimodal distribution and PDI values of around 2 as confirmed by GPC analyses. The reaction took place exclusively at the C–H bond next to the sulfur atom of the thienyl group and no branching of the polymers were observed as judged by NMR spectra. This iron-catalyzed method afforded poly(9,9-dioctylfluorene-*alt*-bithiophene) (**3**, abbreviated as F8T2) in 91% yield with a large molecular weight ($M_n = 20.3$ kg/mol, DP = 37) reaching the length of a commercially available F8T2 (for example, $M_n = 16$ kg/mol from Ossila). F8T2 is widely used for organic light-emitting diodes, photovoltaics, and field-effect transistors.¹³ Installation of alkyl substituents on monomers for F8T2 synthesis helped to increase M_n to 33 kg/mol and DP to 42–46 (**4**, **5**) by increasing solubility. This method was applicable not only to the synthesis of donor polymers but also to the synthesis of polymers containing electron acceptor moieties such as ester or amide groups (**6**, **7**). The excellent regioselectivity of iron-catalyzed thienyl C–H/C–H coupling allowed us to synthesize a polythiophene (**8**) that contains an average of 69 thiophene units from a 3,3"-dihexyl-2,2':5',2"-terthiophene monomer bearing hexyl side chains at predetermined positions.¹⁴ The reaction of a fused thiophene monomer, 4,8-dialkoxybenzo[1,2-*b*:4,5-*b'*]dithiophene, afforded the corresponding polymer with

DP of 22 and PDI of 2.16 (**9**). The end-group signals were observed in the ^1H NMR spectra of **8** and **9** and the DP values were determined as 21 and 28, respectively. These values are in good agreement with the DP values determined by GPC analysis using polystyrene standards of known molecular weights. Copolycondensation of two and three different monomers was also successful, in which the initial reactant ratios were reflected to the ratios of the monomer units in the polymer products (**10**, **11**).

Table 3. Substrate scope

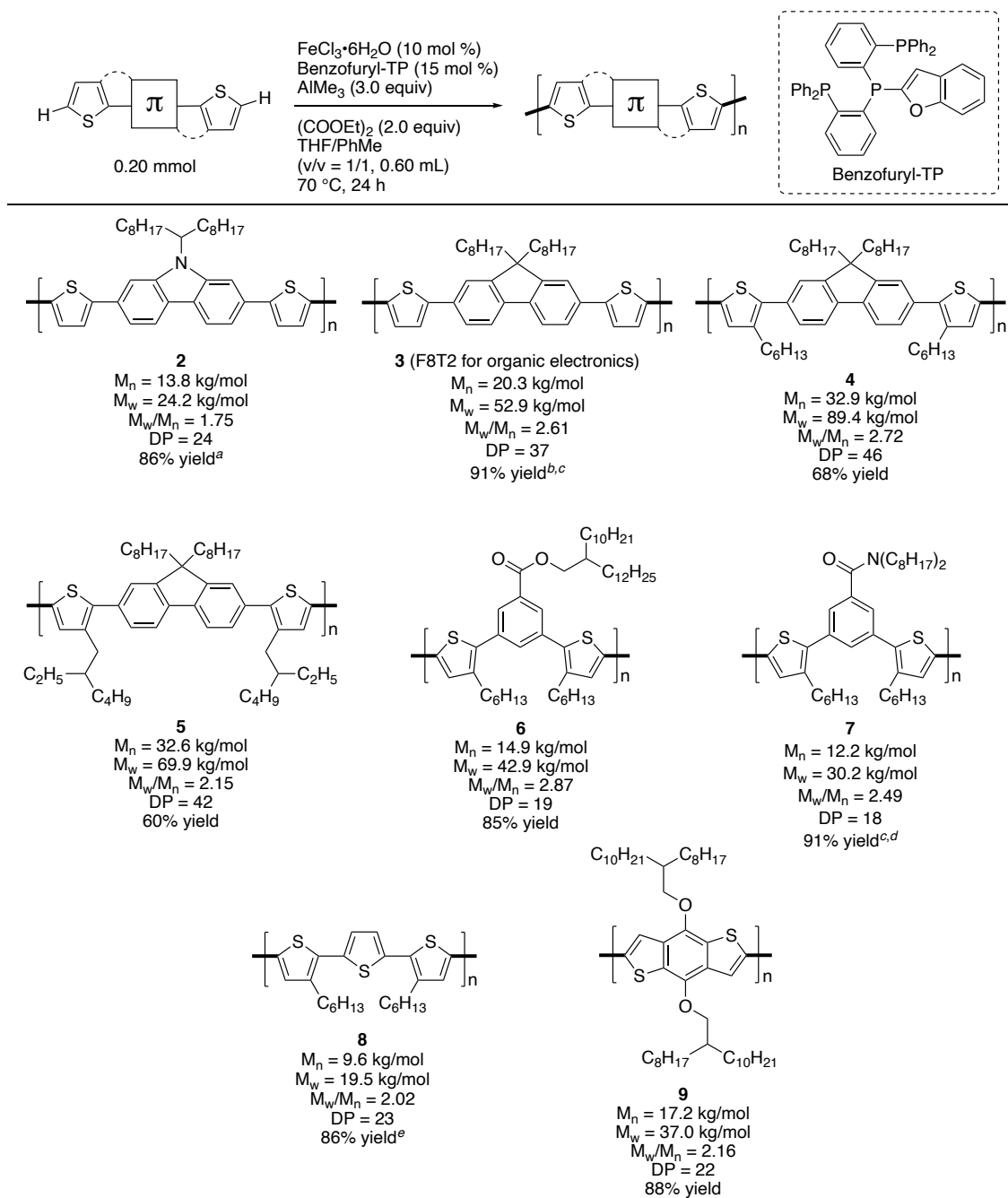
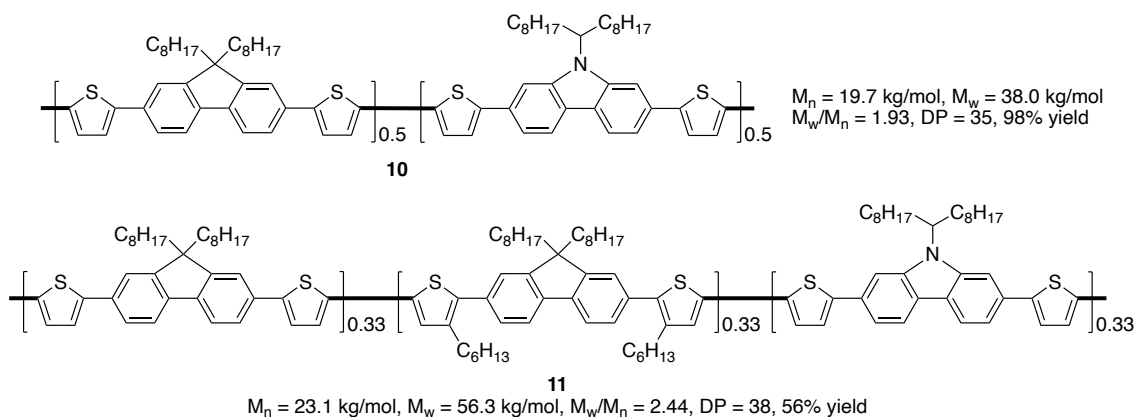


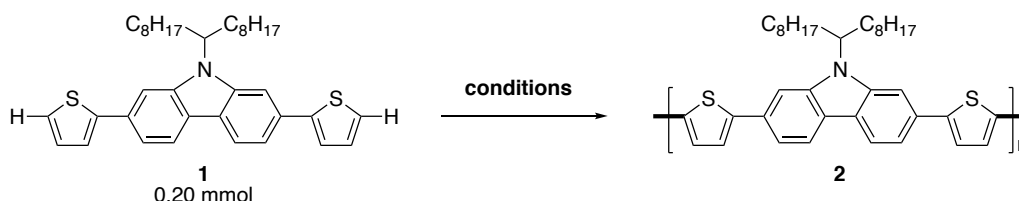
Table 3. (Continued)

All yields are isolated yields. M_n and M_w were determined by GPC using polystyrene standards for the polymers isolated either by precipitation or by GPC. Degree of polymerization was calculated using M_n . ^a With $\text{FeCl}_3 \cdot 6\text{H}_2\text{O}$ (5.0 mol %) and benzofuryl-TP (10 mol %). ^b With THF (0.15 mL). ^c For 48 h. ^d With benzofuryl-TP (20 mol %). ^e At 60 °C.

4-8. Control experiments

To prove the superiority of the iron-catalyzed regioselective thienyl C–H/C–H polycondensation to other transition-metal-catalyzed methods, control experiments were conducted. As described above, the iron catalyzed method produced polymer **2** with DP of 23. However, when palladium-catalyzed methods using either $\text{Cu}(\text{OAc})_2$ or Ag_2CO_3 as an oxidant reported by Chen and co-workers^{7b,c} were applied to monomer **1**, only short oligomers with DP of 4 or 7 were obtained, respectively. These results clearly show that the iron-catalyzed regioselective thienyl C–H/C–H polycondensation gives straightforward access to polymers inaccessible by previously reported palladium-catalyzed C–H/C–H coupling.

Table 4. Control experiments with palladium-catalyzed C–H/C–H coupling



entry	conditions	M_n (kg/mol) ^a	M_w (kg/mol) ^a	M_w/M_n ^a	DP ^b
1	$\text{FeCl}_3 \cdot 6\text{H}_2\text{O}$ (10 mol %), Benzofuryl-TP (15 mol %), AlMe_3 (3.0 equiv), $(\text{COOEt})_2$ (2.0 equiv), THF (0.30 mL), PhMe (0.30 mL), 70 °C, 24 h	13.3	22.6	1.70	23
2	$\text{Pd}(\text{OAc})_2$ (10 mol %), K_2CO_3 (2.1 equiv), $\text{Cu}(\text{OAc})_2$ (2.0 equiv), DMA (2.5 mL), 110 °C, 72 h.	2.0	3.3	1.64	4
3	$\text{Pd}(\text{OAc})_2$ (5.0 mol %), KOAc (2.0 equiv), Ag_2CO_3 (2.0 equiv), DMA (2.5 mL), 110 °C, 72 h.	3.7	9.2	2.53	7

^a M_n and M_w were determined by GPC using polystyrene standards for the crude polymers.

^b Degree of polymerization was calculated using M_n .

4-9. Mechanism of polycondensation

To gain insight into the mechanism of iron-catalyzed regioselective thienyl C–H/C–H polycondensation, reaction progress was monitored by sampling the reaction mixture after specific reaction times. Figure 6 shows the plots of M_n and M_w/M_n (PDI) as a function of monomer conversion. Late-stage increase of M_n and convergence of PDI to 2 indicated that the reaction proceeds through a step-growth mechanism.¹⁵ This can be ascribed to the weak interaction of the Fe(III) catalyst with the π -surface of the polymer chain (Figure 7a). The polycondensation mechanism of the iron-catalyzed method is in

contrast with a chain-growth mechanism where, for example, Pd(0) sticks to the polymer chain through strong interaction with the π -surface and activates the terminus intramolecularly (Figure 7b).¹⁶

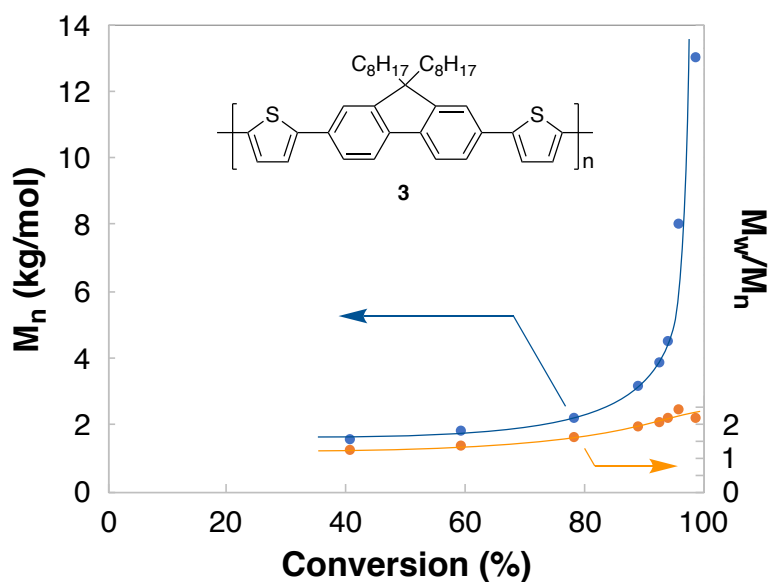


Figure 6. M_n and M_w/M_n of F8T2 as a function of monomer conversion

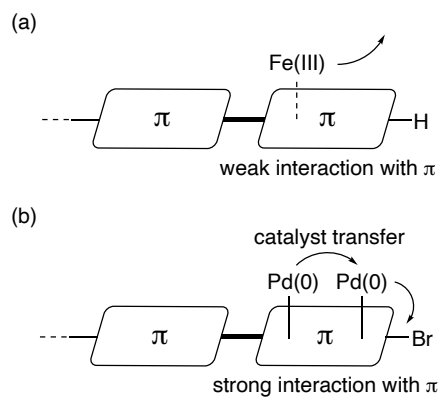


Figure 7. Step-growth polymerization and chain-growth polymerization

4-10. Removal of residual catalyst from polymer

It has been known that a residual catalyst in the polymer product may affect the device performance.¹⁷ Therefore, removal of residual catalyst from the polymer synthesized by the iron-catalyzed method was attempted considering the optoelectronic device applications of polymers. Using F8T2 as a model polymer for investigation, it was determined that a thiol-functionalized silica scavenger (purchased from Fuji Silysia Chemical Ltd.) effectively removes both residual iron and phosphorus from the polymer down to 26 ppm and 175 ppm, respectively. The amount of elements were determined by inductively coupled plasma (ICP) analysis. For comparison, the palladium content of an F8T2 polymer purchased from a commercial supplier was determined to be over 200 ppm, showing the advantage of using iron-catalyzed method for the synthesis of polymer containing less catalyst residues.

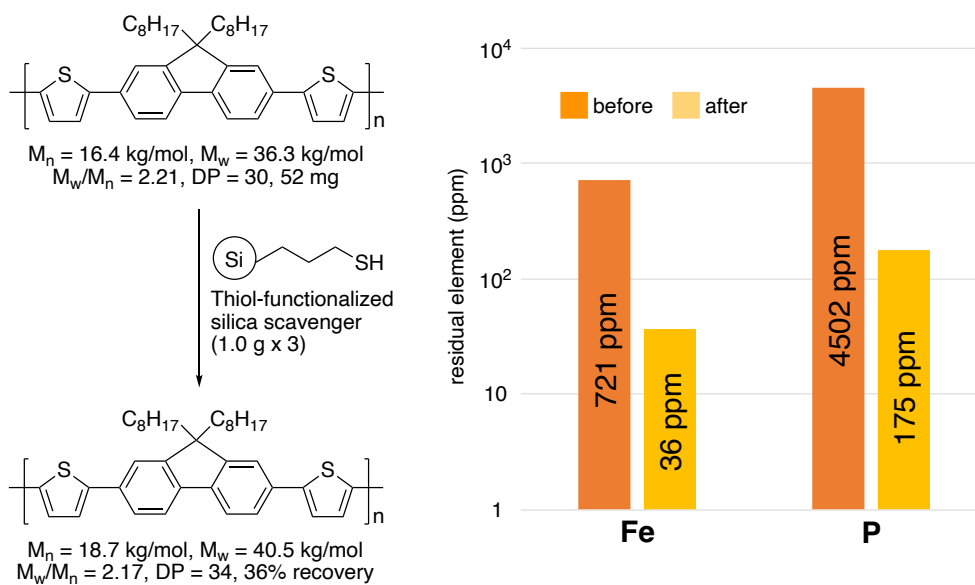


Figure 8. Removal of residual catalyst from F8T2

4-11. Application to perovskite solar cell

本章については, 5 年以内に雑誌等で刊行予定のため, 非公開.

4-12. Conclusion

In conclusion, iron-catalyzed regioselective thienyl C–H/C–H polycondensation was developed using tridentate phosphine as a ligand, AlMe_3 as a base, and diketone as a mild oxidant. Intramolecular C–H activation of the ligand was determined as a catalyst deactivation pathway and the use of heteroaryl-TP was effective to suppress the catalyst deactivation and achieve efficient polycondensation. This reaction took place exclusively at the C–H bond next to the sulfur atom of thienyl group and no branching of the polymer was observed. Monomers containing various kinds of redox-sensitive π -motifs were well tolerated due to the mildness of the iron catalytic cycle created by the combination of low redox potential of Fe(III)/Fe(I) and mild oxalate oxidant, which enabled the synthesis of a wide range of thiophene materials of interest in materials science. Because of the weak interaction of Fe(III) with the π -surface of the polymer chain, polycondensation proceeded through a step-growth mechanism and the residual catalyst was easily removed by post treatment with a thiol-functionalized silica scavenger. **(4-11. Application to perovskite solar cell** については, 5 年以内に雑誌等で刊行予定のため, 非公開.) This work highlights the benefits of iron catalysis for the synthesis of π -conjugated polymeric compounds of importance in energy device applications.

4-13. Experimental

Materials and methods

All air or moisture sensitive reactions were performed in a dry reaction vessel under argon atmosphere. Air or moisture sensitive liquids and solutions were transferred with syringe or Teflon cannula. The water content of solvents was confirmed to be less than 30 ppm by Karl-Fischer titration performed with MKC-210 (Kyoto Electronics Manufacturing Co., Ltd.). Analytical thin-layer chromatography (TLC) was performed with a glass plate coated with 0.25mm 230-400 mesh silica gel containing a fluorescent indicator. Organic solutions were evacuated with a diaphragm pump through a rotary evaporator. Flash column chromatography was performed as described by Still *et al.*¹⁸ Preparative recycling gel permeation chromatography (GPC) was performed with LC-92XX II NEXT instrument (Japan Analytical Industry Co., Ltd.) equipped with JAIGEL-2HR polystyrene columns using chloroform as an eluent at the flow rate of 7.5 mL/min. Gas chromatography (GC) was performed with GC-2014 instrument (Shimadzu Co.) equipped with an ULBON HR-1 (0.25 mm I.D. x 25 mL, 0.25 μ m, Shinwa Chemical Industries, Ltd.) capillary column. Mass spectra (GC-MS) were taken with Parvum 2 instrument (Shimadzu Co.). High-resolution mass spectra (HRMS) were taken with LCMS-IT-TOF (Shimadzu Co.) using reserpine (MW 608.2734) as an internal standard. Analytical GPC was performed with Prominence instrument (Shimadzu Co.) equipped with a KF-805L (Shodex) column at 40 °C using chloroform as an eluent at the flow rate of 1.0 mL/min. Calibration curves were obtained with ReadyCal Kit (Polymer Standards Service, GmbH) standard polystyrenes. Melting points of solid compounds were measured on a Mel-Temp capillary melting-point apparatus and were uncorrected. Nuclear magnetic resonance (NMR) spectra were taken with ECZ-500 (JEOL, Ltd.) at room temperature unless otherwise noted and reported in parts per million (ppm). ¹H NMR spectra were internally referenced to tetramethylsilane (0.00 ppm), CHCl₃ (7.26 ppm), CHDCl₂ (5.32 ppm), C₂HDCl₄ (5.97 ppm), or (CHD₂)(CD₃)SO (2.50 ppm). ¹³C NMR spectra were internally referenced to tetramethylsilane (0.0 ppm), CDCl₃ (77.0 ppm), CD₂Cl₂ (53.8 ppm), C₂D₂Cl₄ (73.8 ppm), or (CD₃)₂SO (39.5 ppm). ¹⁹F NMR spectra were internally referenced to C₆F₆ (−164.9 ppm). ³¹P NMR spectra were internally referenced to (CH₃O)₃PO (2.1 ppm). ICP analysis was performed on Shimadzu ICPS-7510 equipment.

Unless otherwise noted, reagents were purchased from Tokyo Chemical Industry Co., Ltd., Sigma-Aldrich Co., LCC, FUJIFILM Wako Pure Chemical Co., and other commercial suppliers and were used as received. Anhydrous tetrahydrofuran and diethyl ether were purchased from KANTO Chemical Co., Inc. and purified prior to use by a solvent purification system (GlassContour) equipped with columns of activated alumina and supported copper catalyst.¹⁹ $\text{Fe}(\text{acac})_3$ (99.9% trace metal basis) was purchased from Sigma-Aldrich Co., LCC and used as received. $\text{FeCl}_3 \cdot 6\text{H}_2\text{O}$ (99.0+%) was purchased from FUJIFILM Wako Pure Chemical Co. and used as received. Diethyl oxalate was purchased from Tokyo Chemical Industry Co., degassed by Freeze-Pump-Thaw cycling for three times, dried with molecular sieves 4A and kept in a storage flask. Concentrated sulfuric acid (for trace analysis), nitric acid 1.42 (for trace analysis), chloroform (primepure), and methanol (primepure) for ICP analysis were purchased from KANTO Chemical Co., Inc. and used as received. Stating materials were synthesized according to the literature.²⁰

A representative procedure for the investigation of key reaction parameters of polycondensation (Table 1 and Table 2)

In an oven-dried Schlenk tube was added 9-(heptadecan-9-yl)-2,7-di(thiophen-2-yl)-9*H*-carbazole (114 mg, 0.20 mmol) and benzofuryl-TP (13 mg, 0.020 mmol) and the Schlenk tube was evacuated and refilled with argon for three times. Then a THF solution of $\text{FeCl}_3 \cdot 6\text{H}_2\text{O}$ (0.033 mol/L, 0.30 mL, 0.010 mmol) was added and a toluene solution of AlMe_3 (2.0 mol/L, 0.30 mL, 0.60 mmol) was added by rinsing the wall of the Schlenk tube at rt. Finally, diethyl oxalate (54 μL , 0.40 mmol) was added and the reaction mixture was degassed by Freeze-Pump-Thaw cycling for three times. After stirring with an agitation rate of 500 rpm at 70 °C for 24 h, the reaction mixture was diluted with THF (2 mL) and quenched by addition of a dioxane solution of HCl (4 mol/L, 0.50 mL), and stirred for 1 h. ~10 mg of the resulting dark brown solution was sampled, diluted with 1 mL of chloroform and analyzed by GPC to determine the M_n , M_w , M_w/M_n values. Degree of polymerization (DP) was determined by dividing the M_n value by the molecular weight of the monomer unit. The rest of the crude solution was transferred to a 15 mL centrifuge tube and further diluted with THF up to 5 mL. Water was added up to 10 mL and the tube was shaken vigorously after which orange polymer precipitated immediately. The mixture was centrifuged (4000 rpm, 10 min) and the solution was discarded. Then

THF/water (1:1) was added up to 10 mL and the tube was shaken vigorously and centrifuged (4000 rpm, 10 min), and the solution was discarded. Finally, methanol was added up to 10 mL and the tube was shaken vigorously and the solid was filtered. The orange polymer was dried under vacuum overnight.

Note: The reaction mixture remained homogeneous over the entire course of reaction, and we observed little effects of stirring rate on the outcome of the reaction. Technically, too fast stirring is not recommended because the magnetic stirring bar cannot catch up with the stirring rate of the stirrer causing vibration or jump of the stirring bar when the reaction mixture became viscous as polymer accumulates in solution.

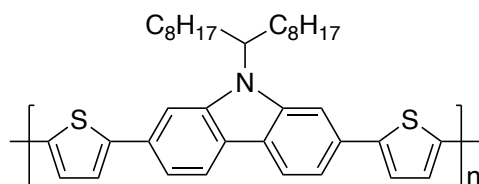
A general procedure for iron-catalyzed thienyl C–H/C–H polycondensation (Table 3)

Procedure A: In an oven-dried Schlenk tube was added a monomer (0.20 mmol) and benzofuryl-TP (20 mg, 0.030 mmol) and the Schlenk tube was evacuated and refilled with argon for three times. Then a THF solution of $\text{FeCl}_3 \cdot 6\text{H}_2\text{O}$ (0.067 mol/L, 0.30 mL, 0.020 mmol) was added and a toluene solution of AlMe_3 (2.0 mol/L, 0.30 mL, 0.60 mmol) was added by rinsing the wall of the Schlenk tube at rt. Finally, diethyl oxalate (54 μL , 0.40 mmol) was added and the reaction mixture was degassed by Freeze-Pump-Thaw cycling for three times. After stirring with an agitation rate of 500 rpm at 70 °C for 24 h, the reaction mixture was diluted with THF (2 mL) and quenched by addition of a dioxane solution of HCl (4 mol/L, 0.50 mL), and stirred for 1 h. The crude solution was transferred to a 15 mL centrifuge tube and further diluted with THF up to 5 mL. Water was added up to 10 mL and the tube was shaken vigorously after which a solid polymer precipitated immediately. The mixture was centrifuged (4000 rpm, 10 min) and the solution was discarded. Then THF/water (1:1) was added up to 10 mL and the tube was shaken vigorously and centrifuged (4000 rpm, 10 min), and the solution was discarded. Finally, methanol was added up to 10 mL and the tube was shaken vigorously. The solid was filtered and dried under vacuum overnight. A chloroform solution of the product was prepared and analyzed by GPC to determine the M_n , M_w , M_w/M_n values of the isolated polymer. Degree of polymerization (DP) was determined by dividing the M_n value by the molecular weight of the monomer unit.

Procedure B: In an oven-dried Schlenk tube was added a monomer (0.20 mmol) and benzofuryl-TP (20 mg, 0.030 mmol) and the Schlenk tube was evacuated and refilled

with argon for three times. Then a THF solution of $\text{FeCl}_3 \cdot 6\text{H}_2\text{O}$ (0.067 mol/L, 0.30 mL, 0.020 mmol) was added and a toluene solution of AlMe_3 (2.0 mol/L, 0.30 mL, 0.60 mmol) was added by rinsing the wall of the Schlenk tube at rt. Finally, diethyl oxalate (54 μL , 0.40 mmol) was added and the reaction mixture was degassed by Freeze-Pump-Thaw cycling for three times. After stirring with an agitation rate of 500 rpm at 70 °C for 24 h, the reaction mixture was diluted with THF (2 mL) and quenched by addition of a dioxane solution of HCl (4 mol/L, 0.50 mL), and stirred for 1 h. The crude solution was diluted with chloroform (10 mL) and washed with water. When emulsion occurred, the solution was filtered through a membrane filter to give a clear solution. The organic phase was dried over Na_2SO_4 and passed through a pad of Florisil. The solvent was removed under reduced pressure and the crude product was purified by gel permeation chromatography (chloroform) to afford the product. The product was dried under vacuum overnight. A chloroform solution of the product was prepared and analyzed by GPC to determine the M_n , M_w , M_w/M_n values of the isolated polymer. Degree of polymerization (DP) was determined by dividing the M_n value by the molecular weight of the monomer unit.

Polymer 2:



The title compound was obtained as orange solid in 86% yield. The reaction was performed according to Procedure A using benzofuryl-TP (13 mg, 0.020 mmol) and a THF solution of $\text{FeCl}_3 \cdot 6\text{H}_2\text{O}$ (0.033 mol/L, 0.30 mL, 0.010 mmol). This compound is known.¹⁰

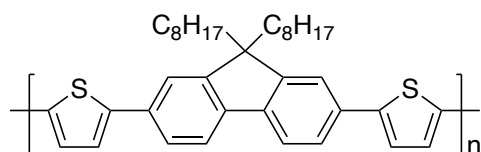
^1H NMR (500 MHz, $\text{C}_2\text{D}_2\text{Cl}_4$, 120 °C): δ 8.10 (br d, $J = 8.2$ Hz, 2H), 7.75 (br s, 2H), 7.55 (br d, $J = 8.2$ Hz, 2H), 7.38 (br d, $J = 3.1$ Hz, 2H), 7.30 (br d, $J = 3.1$ Hz, 2H), 4.75–4.60 (br, 1H), 2.48–2.38 (br, 2H), 2.20–2.05 (br, 2H), 1.38–1.25 (br, 24H), 0.88 (br t, $J = 7.2$ Hz, 6H).

^{13}C NMR (125 MHz, $\text{C}_2\text{D}_2\text{Cl}_4$, 120 °C): δ 144.8, 136.6, 131.7, 124.9, 124.5, 123.6, 122.8, 120.3, 117.5, 107.4, 56.7, 33.8, 31.5, 29.1, 29.0, 28.8, 26.7, 22.2, 13.6.

$M_n = 13.8$ kg/mol, $M_w = 24.2$ kg/mol, $M_w/M_n = 1.75$, DP = 24.

Anal. Calcd for $(C_{37}H_{45}NS_2)_n$: C, 78.26; H, 7.99; N, 2.47. Found: C, 77.62; H, 7.53; N, 2.33.

Polymer 3:



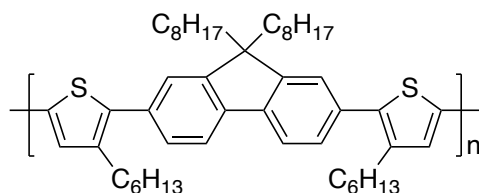
The title compound was obtained as yellow orange solid in 91% yield. The reaction was performed according to Procedure A using THF (0.15 mL) and the reaction time was 48 h. The compound data was in good agreement with that of commercially available F8T2 (Sigma-Aldrich Co., LCC).

^1H NMR (500 MHz, $\text{C}_2\text{D}_2\text{Cl}_4$, 120 °C): δ 7.46 (br d, $J = 8.1$ Hz, 2H), 7.37–7.35 (br, 4H), 7.10–7.03 (br, 2H), 7.00–6.95 (br, 2H), 1.95–1.75 (br, 4H), 0.99–0.89 (br, 20H), 0.58 (br t, $J = 7.2$ Hz, 10H).

^{13}C NMR (125 MHz, $\text{C}_2\text{D}_2\text{Cl}_4$, 120 °C): δ 151.9, 144.2, 140.3, 136.5, 132.9, 124.7, 124.5, 123.5, 120.1, 119.9, 55.3, 39.9, 31.5, 29.7, 28.9, 28.8, 23.8, 22.2, 13.6.

$M_n = 20.3$ kg/mol, $M_w = 52.9$ kg/mol, $M_w/M_n = 2.61$, DP = 37.

Polymer 4:



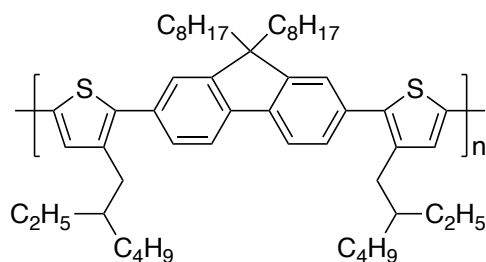
The title compound was obtained as yellow solid in 68% yield. The reaction was performed according to Procedure B.

^1H NMR (500 MHz, $\text{C}_2\text{D}_2\text{Cl}_4$, 120 °C): δ 7.65 (br d, $J = 8.1$ Hz, 2H), 7.38–7.36 (br, 4H), 7.00 (br s, 2H), 2.65–2.58 (br, 4H), 2.05–1.80 (br, 4H), 1.65–1.55 (br, 4H), 1.30–1.00 (br, 32H), 0.82–0.74 (br, 16H).

^{13}C NMR (125 MHz, $\text{C}_2\text{D}_2\text{Cl}_4$, 120 °C): δ 151.3, 139.9, 139.4, 137.5, 135.2, 133.2, 128.0, 126.1, 123.7, 119.5, 55.1, 40.0, 31.5, 31.4, 30.5, 29.8, 29.0 (two signals overlapped), 28.9, 28.8, 23.9, 22.2 (two signals overlapped), 13.6 (two signals overlapped).

$M_n = 32.9$ kg/mol, $M_w = 89.4$ kg/mol, $M_w/M_n = 2.72$, $DP = 46$.

Polymer 5:



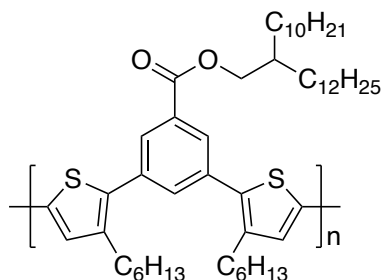
The title compound was obtained as yellow solid in 60% yield. The reaction was performed according to Procedure B.

^1H NMR (500 MHz, $\text{C}_2\text{D}_2\text{Cl}_4$, 120 °C): δ 7.64 (br d, $J = 8.3$ Hz, 2H), 7.37–7.36 (br, 4H), 6.98 (br s, 2H), 2.60–2.55 (br, 4H), 2.05–1.95 (br, 4H), 1.55–1.50 (br, 2H), 1.35–1.05 (br, 36H), 0.79–0.71 (br, 22H).

^{13}C NMR (125 MHz, $\text{C}_2\text{D}_2\text{Cl}_4$, 120 °C): δ 151.3, 140.0, 138.5, 138.1, 135.2, 133.4, 128.3, 126.4 (multiple signals were observed because of slow rotation of bonds), 126.0 (multiple signals were observed because of slow rotation of bonds), 124.0, 119.5, 55.2, 40.6 (multiple signals were observed because of slow rotation of bonds), 40.4 (multiple signals were observed because of slow rotation of bonds), 40.1, 33.3, 32.8, 31.5, 29.9, 29.0, 28.9, 28.7, 26.0, 23.9, 22.7, 22.2, 13.6 (two signals overlapped), 10.5.

$M_n = 32.6$ kg/mol, $M_w = 69.9$ kg/mol, $M_w/M_n = 2.15$, $DP = 42$.

Polymer 6:



The title compound was obtained as brown solid in 85% yield. The reaction was performed according to Procedure B. Small peaks observed in the ^1H NMR spectrum

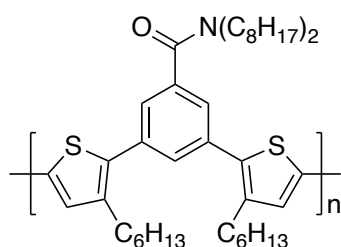
(~5% to the main peaks) were assigned to the monomer unit that underwent transesterification with ethanol of diethyl oxalate.

^1H NMR (500 MHz, $\text{C}_2\text{D}_2\text{Cl}_4$, 120 °C): δ 8.02 (br s, 2H), 7.67 (br s, 1H), 7.06 (br s, 2H), 4.25–4.15 (br, 2H), 2.70–2.60 (br, 4H), 1.75–1.70 (br, 1H), 1.70–1.60 (br, 4H), 1.40–1.10 (br, 52H), 0.80–0.75 (br, 12H).

^{13}C NMR (125 MHz, $\text{C}_2\text{D}_2\text{Cl}_4$, 120 °C): δ 166.0, 140.4, 135.7, 135.0, 134.9, 133.3, 131.2, 128.6, 126.2, 68.1, 37.3, 31.8, 31.8, 31.5 (two signals overlapped), 31.3, 30.7, 29.9, 29.6, 29.5, 29.5, 29.5, 29.2, 29.2, 29.1, 28.8, 26.7, 22.6 (two signals overlapped), 22.5, 14.1, 14.0 (two signals overlapped).

$M_n = 14.9$ kg/mol, $M_w = 42.9$ kg/mol, $M_w/M_n = 2.87$, DP = 19.

Polymer 7:

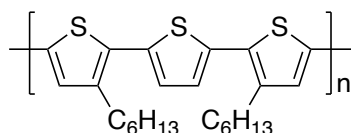


The title compound was obtained as brown solid in 91% yield. The reaction was performed according to Procedure B using benzofuryl-TP (27 mg, 0.040 mmol) and the reaction time was 48 h.

^1H NMR (500 MHz, $\text{C}_2\text{D}_2\text{Cl}_4$, 120 °C): δ 7.50 (br s, 1H), 7.31 (br s, 2H), 6.98 (br s, 2H), 3.35–3.25 (br, 4H), 2.65–2.55 (br, 4H), 1.60–1.45 (br, 8H), 1.35–1.10 (br, 32H), 0.80–0.75 (br t, $J = 7.2$ Hz, 12H).

^{13}C NMR (125 MHz, $\text{C}_2\text{D}_2\text{Cl}_4$, 120 °C): δ 170.3, 140.2, 137.9, 135.6, 135.1, 134.7, 129.9, 126.1, 125.8, 123.4, 120.2, 99.3, 49.1, 44.7, 31.7, 31.6, 31.6, 30.8, 29.3, 29.2, 29.1, 29.1, 28.9, 28.7, 27.4, 27.0, 26.5, 22.6, 22.5, 14.1, 14.1. (Multiple signals were observed because of slow rotation of bonds.)

$M_n = 12.2$ kg/mol, $M_w = 30.2$ kg/mol, $M_w/M_n = 2.49$, DP = 18.

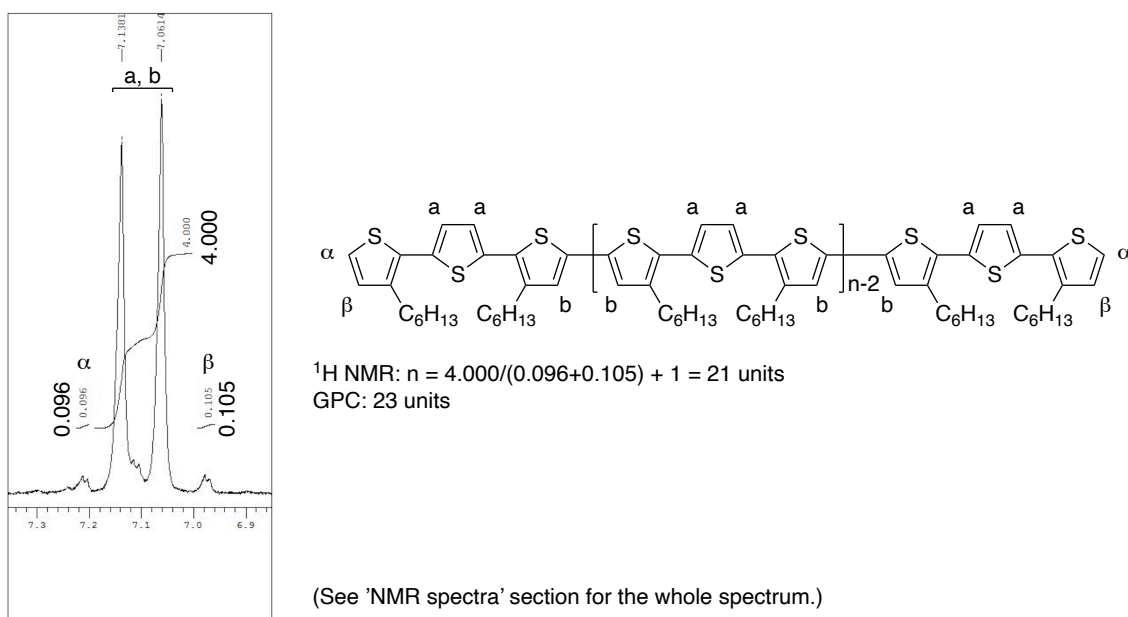
Polymer 8:

In an oven-dried Schlenk tube was added 3,3''-dihexyl-2,2':5',2''-terthiophene (83 mg, 0.20 mmol) and benzofuryl-TP (20 mg, 0.030 mmol) and the Schlenk tube was evacuated and refilled with argon for three times. Then a THF solution of $\text{FeCl}_3 \cdot 6\text{H}_2\text{O}$ (0.067 mol/L, 0.30 mL, 0.020 mmol) was added and a toluene solution of AlMe_3 (2.0 mol/L, 0.30 mL, 0.60 mmol) was added by rinsing the wall of the Schlenk tube at rt. Finally, diethyl oxalate (54 μL , 0.40 mmol) was added and the reaction mixture was degassed by Freeze-Pump-Thaw cycling for three times. After stirring with an agitation rate of 500 rpm at 60 °C for 24 h, the reaction mixture was diluted with THF (2 mL) and quenched by addition of a dioxane solution of HCl (4 mol/L, 0.50 mL), and stirred for 1 h. The crude solution was diluted with chloroform (10 mL) and the insoluble purple solid was filtered. The solid was washed with minimal amounts of chloroform, THF, an aqueous solution of HCl (1 M), and acetone to afford the product as purple solid (71 mg, 86%). This compound is known.²¹ The product was dissolved in $\text{C}_2\text{D}_2\text{Cl}_4$ at 120 °C, diluted with chloroform, and the soluble portion was analyzed by GPC to determine the M_n , M_w , M_w/M_n values. Small peaks observed in the ^1H NMR spectrum were assigned to the thiophene termini of the polymer. By integration of these peaks, DP was calculated to be $4.000/(0.096+0.105) + 1 = 21$.

^1H NMR (500 MHz, $\text{C}_2\text{D}_2\text{Cl}_4$, 120 °C): δ 7.14 (br s, 2H), 7.06 (br s, 2H), 2.90–2.85 (br, 4H), 1.80–1.75 (br, 4H), 1.55–1.35 (br, 12H), 1.00–0.95 (br, 6H).

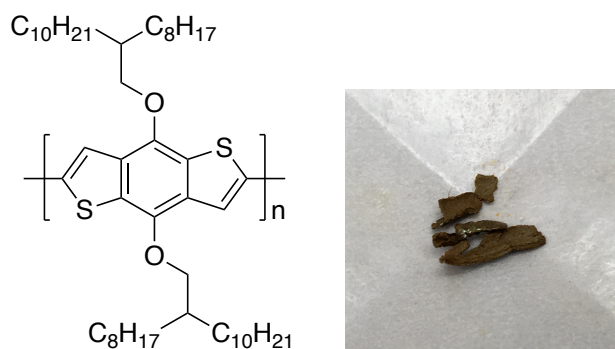
^{13}C NMR (125 MHz, $\text{C}_2\text{D}_2\text{Cl}_4$, 120 °C): δ 140.6, 135.9, 135.0, 129.6, 126.7, 126.3, 126.1, 125.8, 31.4, 30.1, 29.4, 28.9, 22.3, 13.6. (Multiple signals were observed because of slow rotation of bonds.)

$M_n = 9.6$ kg/mol, $M_w = 19.5$ kg/mol, $M_w/M_n = 2.02$, DP = 23.



Supplementary Figure 1. Determination of DP of polymer **8** by $^1\text{H NMR}$

Polymer 9:

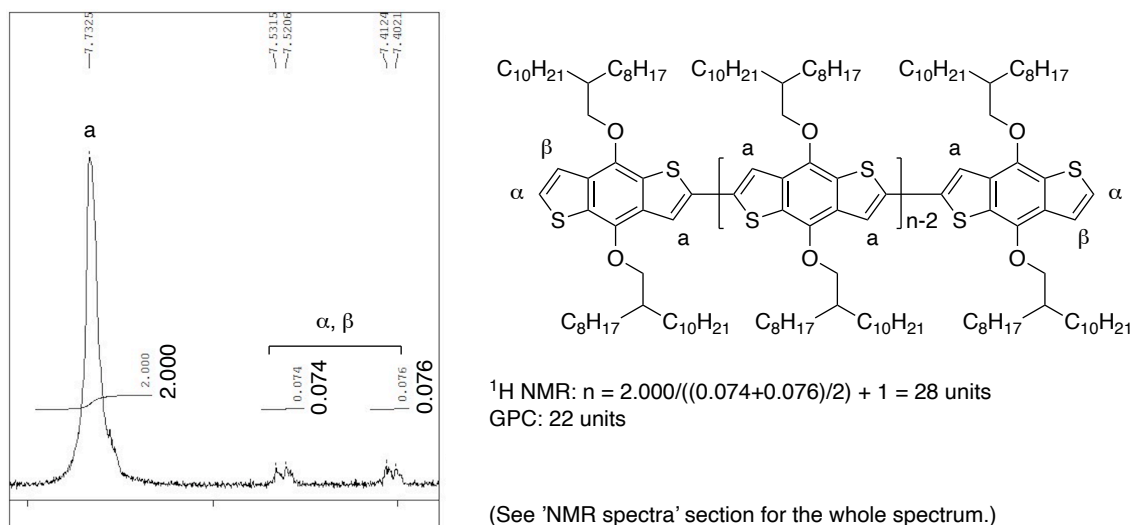


The title compound was obtained as dark red solid in 88% yield. The reaction was performed according to Procedure B. Small peaks observed in the $^1\text{H NMR}$ spectrum were assigned to the termini of the polymer. By integration of these peaks, DP was calculated to be $2.000/((0.074+0.076)/2) + 1 = 28$.

$^1\text{H NMR}$ (500 MHz, $\text{C}_2\text{D}_2\text{Cl}_4$, 120 $^\circ\text{C}$): δ 7.73 (br s, 2H), 4.45–4.30 (br, 4H), 2.05–2.00 (br, 2H), 1.75–1.25 (br, 64H), 0.97–0.87 (br, 12H).

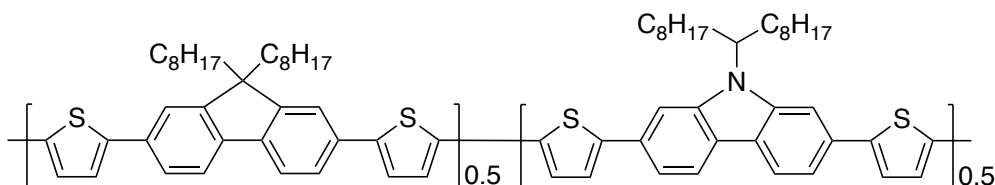
$^{13}\text{C NMR}$ (125 MHz, $\text{C}_2\text{D}_2\text{Cl}_4$, 120 $^\circ\text{C}$): δ 144.4, 136.7, 132.4, 129.3, 118.3, 76.8, 39.4, 31.6 (two signals overlapped), 31.5 (two signals overlapped), 29.9 (two signals overlapped), 29.4 (four signals overlapped), 29.0 (two signals overlapped), 26.9 (two signals overlapped), 22.3 (two signals overlapped), 13.6 (two signals overlapped).

$M_n = 17.2 \text{ kg/mol}$, $M_w = 37.0 \text{ kg/mol}$, $M_w/M_n = 2.16$, DP = 22.



Supplementary Figure 2. Determination of DP of polymer **9** by $^1\text{H NMR}$

Polymer 10:



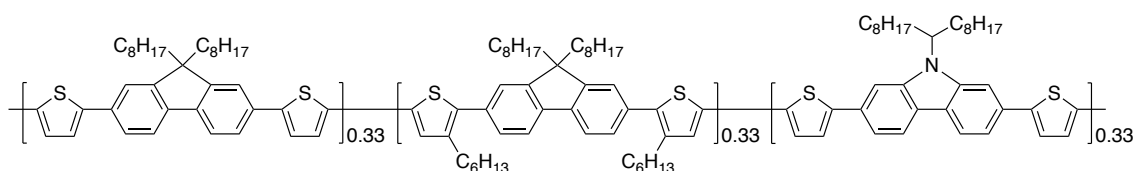
In an oven-dried Schlenk tube was added 2,2'-(9,9-dioctyl-9H-fluorene-2,7-diyl)dithiophene (55 mg, 0.10 mmol), 9-(heptadecan-9-yl)-2,7-di(thiophen-2-yl)-9H-carbazole (57 mg, 0.10 mmol) and benzofuryl-TP (20 mg, 0.030 mmol) and the Schlenk tube was evacuated and refilled with argon for three times. Then a THF solution of $\text{FeCl}_3 \cdot 6\text{H}_2\text{O}$ (0.067 mol/L, 0.30 mL, 0.020 mmol) was added and a toluene solution of AlMe_3 (2.0 mol/L, 0.30 mL, 0.60 mmol) was added by rinsing the wall of the Schlenk tube at rt. Finally, diethyl oxalate (54 μL , 0.40 mmol) was added and the reaction mixture was degassed by Freeze-Pump-Thaw cycling for three times. After stirring with an agitation rate of 500 rpm at 70 $^\circ\text{C}$ for 24 h, the reaction mixture was diluted with THF (2 mL) and quenched by addition of a dioxane solution of HCl (4 mol/L, 0.50 mL), and stirred for 1 h. The crude solution was transferred to a 15 mL centrifuge tube and further

diluted with THF up to 5 mL. Water was added up to 10 mL and the tube was shaken vigorously after which orange polymer precipitated immediately. The mixture was centrifuged (4000 rpm, 10 min) and the solution was discarded. Then THF/water (1:1) was added up to 10 mL and the tube was shaken vigorously and centrifuged (4000 rpm, 10 min), and the solution was discarded. Finally, methanol was added up to 10 mL and the tube was shaken vigorously. The solid was filtered and dried under vacuum overnight to afford the product as orange solid (110 mg, 98%). A chloroform solution of the product was prepared and analyzed by GPC to determine the M_n , M_w , M_w/M_n values of the isolated polymer. ^{13}C NMR spectrum could not be analyzed because of the weak intensity of the signals.

^1H NMR (500 MHz, $\text{C}_2\text{D}_2\text{Cl}_4$, 120 °C): δ 8.10 (br d, $J = 8.0$ Hz, 2H), 7.78–7.72 (br, 4H), 7.68–7.63 (br, 4H), 7.55 (br d, $J = 8.0$ Hz, 2H), 7.40–7.33 (br, 4H), 7.32–7.25 (br, 4H), 4.70–4.65 (br, 1H), 2.45–2.40 (br, 2H), 2.15–2.05 (br, 6H), 1.40–1.15 (br, 44H), 0.95–0.85 (br, 16H).

$M_n = 19.7$ kg/mol, $M_w = 38.0$ kg/mol, $M_w/M_n = 1.93$, DP = 35.

Polymer 11:



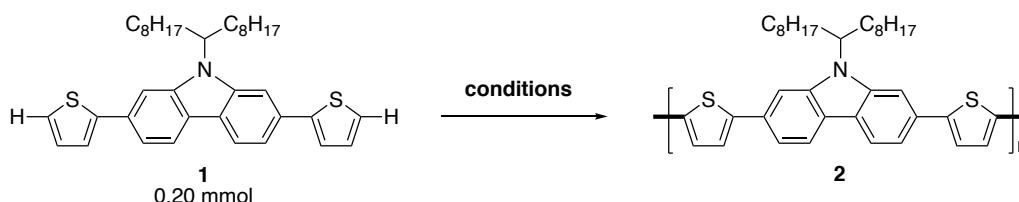
In an oven-dried Schlenk tube was added 2,2'-(9,9-dioctyl-9H-fluorene-2,7-diyl)dithiophene (37 mg, 0.067 mmol), 2,2'-(9,9-dioctyl-9H-fluorene-2,7-diyl)bis(3-hexylthiophene) (48 mg, 0.067 mmol), 9-(heptadecan-9-yl)-2,7-di(thiophen-2-yl)-9H-carbazole (38 mg, 0.10 mmol) and benzofuryl-TP (20 mg, 0.030 mmol) and the Schlenk tube was evacuated and refilled with argon for three times. Then a THF solution of $\text{FeCl}_3 \cdot 6\text{H}_2\text{O}$ (0.067 mol/L, 0.30 mL, 0.020 mmol) was added and a toluene solution of AlMe_3 (2.0 mol/L, 0.30 mL, 0.60 mmol) was added by rinsing the wall of the Schlenk

tube at rt. Finally, diethyl oxalate (54 μ L, 0.40 mmol) was added and the reaction mixture was degassed by Freeze-Pump-Thaw cycling for three times. After stirring with an agitation rate of 500 rpm at 70 °C for 24 h, the reaction mixture was diluted with THF (2 mL) and quenched by addition of a dioxane solution of HCl (4 mol/L, 0.50 mL), and stirred for 1 h. The crude solution was diluted with chloroform (10 mL) and washed with water. The solution was filtered through a membrane filter to give a clear solution. The organic phase was dried over Na₂SO₄ and passed through a pad of Florisil. The solvent was removed under reduced pressure and the crude product was purified by gel permeation chromatography (chloroform) to afford the product as yellow solid (68 mg, 56%). A chloroform solution of the product was prepared and analyzed by GPC to determine the M_n , M_w , M_w/M_n values of the isolated polymer. ¹³C NMR spectrum could not be analyzed because of the weak intensity of the signals.

¹H NMR (500 MHz, C₂D₂Cl₄, 120 °C): δ 8.12–8.06 (br, 2H), 7.81–7.72 (br, 6H), 7.68–7.61 (br, 4H), 7.58–7.48 (br, 6H), 7.39–7.32 (br, 4H), 7.31–7.22 (br, 4H), 7.20–7.13 (br, 2H), 4.70–4.65 (br, 1H), 2.80–2.75 (br, 4H), 2.40–2.35 (br, 2H), 2.15–2.05 (br, 10H), 1.75–1.70 (br, 4H), 1.45–1.10 (br, 76H), 0.95–0.85 (br, 32H).

M_n = 23.1 kg/mol, M_w = 56.3 kg/mol, M_w/M_n = 2.44, DP = 38.

Procedure for control experiments (Table 4)



entry	conditions	M_n (kg/mol) ^a	M_w (kg/mol) ^a	M_w/M_n ^a	DP ^b
1	FeCl ₃ ·6H ₂ O (10 mol %), Benzofuryl-TP (15 mol %), AlMe ₃ (3.0 equiv), (COOEt) ₂ (2.0 equiv), THF (0.30 mL), PhMe (0.30 mL), 70 °C, 24 h	13.3	22.6	1.70	23
2	Pd(OAc) ₂ (10 mol %), K ₂ CO ₃ (2.1 equiv), Cu(OAc) ₂ (2.0 equiv), DMA (2.5 mL), 110 °C, 72 h.	2.0	3.3	1.64	4
3	Pd(OAc) ₂ (5.0 mol %), KOAc (2.0 equiv), Ag ₂ CO ₃ (2.0 equiv), DMA (2.5 mL), 110 °C, 72 h.	3.7	9.2	2.53	7

^a M_n and M_w were determined by GPC using polystyrene standards for the crude polymers.

^b Degree of polymerization was calculated using M_n .

Procedure for entry 2^b: In an oven-dried Schlenk tube was added 9-(heptadecan-9-yl)-2,7-di(thiophen-2-yl)-9H-carbazole (114 mg, 0.20 mmol), Cu(OAc)₂ (73 mg, 0.40 mmol),

and K_2CO_3 (58 mg, 0.42 mmol). DMA (2.0 mL) was added and the mixture was stirred at 110 °C for 10 min, then $\text{Pd}(\text{OAc})_2$ (4.5 mg, 0.020 mmol) dissolved in 0.50 mL of DMA was added to the reaction flask and reacted for 72 h. The mixture was cooled to rt, diluted with chloroform, and analyzed by GPC to determine the M_n , M_w , M_w/M_n values. Degree of polymerization (DP) was determined by dividing the M_n value by the molecular weight of the monomer unit.

Procedure for entry 3^{7c}: In an oven-dried Schlenk tube was added a monomer (0.20 mmol), Ag_2CO_3 (110 mg, 0.40 mmol), KOAc (39 mg, 0.40 mmol) and DMA (2.0 mL). The mixture was stirred at 110 °C for 10 min, then $\text{Pd}(\text{OAc})_2$ (2.2 mg, 0.010 mmol) dissolved in 0.50 mL of DMA was added to the reaction flask and reacted for 72 h. The mixture was cooled to rt, diluted with chloroform, and analyzed by GPC to determine the M_n , M_w , M_w/M_n values. Degree of polymerization (DP) was determined by dividing the M_n value by the molecular weight of the monomer unit.

Procedure for plotting M_n and M_w/M_n values as a function of monomer conversion (Figure 6)

In an oven-dried Schlenk tube was added 2,2'-(9,9-dioctyl-9H-fluorene-2,7-diyl)dithiophene (111 mg, 0.20 mmol) and benzofuryl-TP (13 mg, 0.020 mmol) and the Schlenk tube was evacuated and refilled with argon for three times. Then a THF solution of $\text{FeCl}_3 \cdot 6\text{H}_2\text{O}$ (0.033 mol/L, 0.30 mL, 0.010 mmol) was added and a toluene solution of AlMe_3 (2.0 mol/L, 0.30 mL, 0.60 mmol) was added by rinsing the wall of the Schlenk tube. Finally, diethyl oxalate (54 μL , 0.40 mmol) was added and the reaction mixture was degassed by Freeze-Pump-Thaw cycling for three times. The reaction mixture was stirred in agitation rate of 500 rpm at 70 °C and sampled at the reaction time of 0.5, 1, 2, 4, 6, 8, 24, and 74 h. These samples were quenched by addition of a dioxane solution of HCl (4 mol/L, 0.10 mL), diluted with CHCl_3 (2 mL), sonicated for 15 min, washed with water, and analyzed by GPC using polystyrene standards.

Procedure for removal of residual catalyst from polymer (Figure 8)

	residual element (ppm ^a)	
	before treatment	after treatment
Fe	721	36
P	4502	175
Al	_ ^b	_ ^b

^a Calculated based on [amount of residual element (mg)]/[amount of polymer (kg)].

^b Determination of Al content in polymer was hindered because of the presence of Al in high concentration (~1.5 ppm) even in the blank sample. 1.5 ppm of Al in ICP sample corresponds to 1500 ppm of Al in 10 mg of polymer.

Polymer **3** (52 mg, $M_n = 16.4$ kg/mol, $M_w = 36.3$ kg/mol, $M_w/M_n = 2.21$, DP = 30) was dissolved in chloroform (20 mL) under sonication for 15 min and thiol-functionalized silica scavenger (1.0 g, Fuji Silysia Chemical Ltd.) was added. After stirring for 1 h, the solution was filtered and thiol-functionalized silica scavenger (1.0 g) was added. After stirring for another 1 h, the solution was filtered and thiol-functionalized silica scavenger (1.0 g) was added. After stirring for another 1 h, the solution was filtered and the amount of chloroform was reduced to 4 mL under reduced pressure. Methanol (20 mL) was added and the solid was filtered and dried under vacuum overnight to afford the product as yellow solid (19 mg, 36% recovery, $M_n = 18.7$ kg/mol, $M_w = 40.5$ kg/mol, $M_w/M_n = 2.17$, DP = 34).

For ICP analysis, a polymer sample (~10 mg) was heated in sulfuric acid (0.20 mL) at 200 °C and nitric acid was added intermittently until a clear colorless solution was obtained. After evaporating the remaining nitric acid at 200 °C, the solution was cooled to rt and diluted to 10 mL with pure water. ICP analysis was conducted using standard solutions of Fe, P, and Al (blank, 0.10, 0.20, 0.50, 1.0 ppm for each element) for calibration.

When the same polymer **3** (26 mg) in chloroform (10 mL) was treated only once with thiol-functionalized silica scavenger (0.50 g), the polymer was recovered in 59% and the Fe content was 43 ppm.

For comparison, ICP analysis was conducted for the commercially available F8T2 (Sigma-Aldrich Co., LCC) and the Pd content was determined to be 222 ppm.

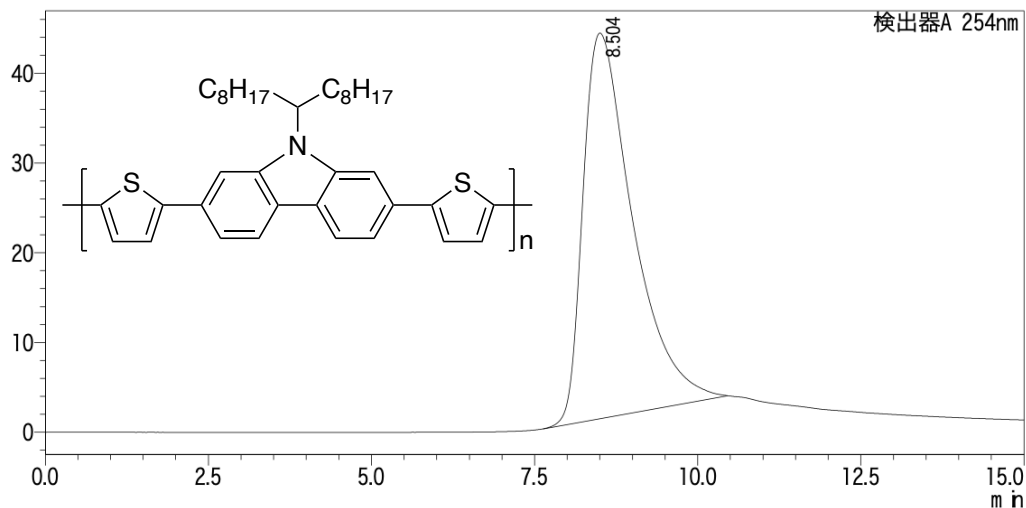
Without this post-treatment procedure, most of other polymers contained over 1000 ppm of residual iron. For device applications, this procedure is recommended to ensure reproducibility.

(4-11. Application to perovskite solar cell については, 5 年以内に雑誌等で刊行予定のため, 非公開.)

GPC chromatograms

GPC chromatogram of polymer 2

mV



検出器A 254nm

ピーク#	保持時間	面積	高さ	濃度	単位	マーク	化合物名
1	8.504	2281644	42964	0.000		M	
合計		2281644	42964				

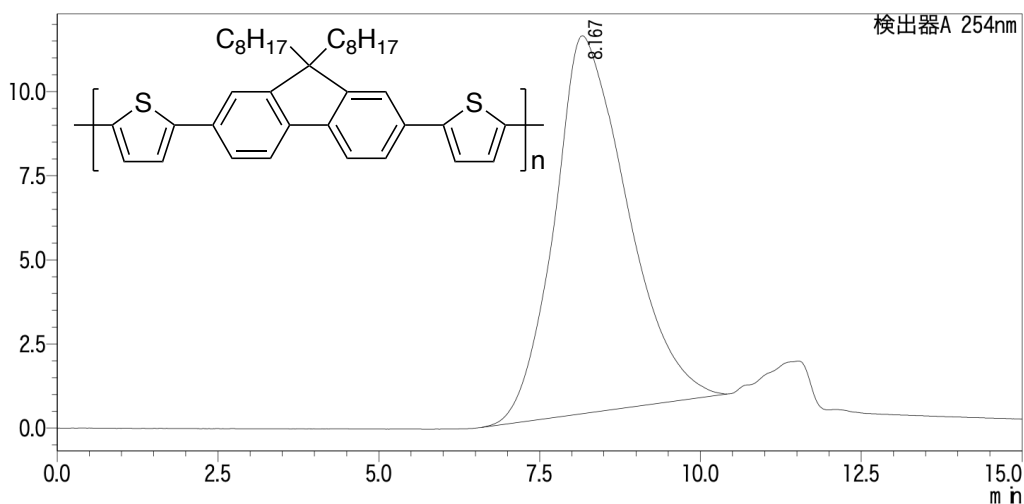
GPC 計算結果

Peak#1 (検出器A 254nm)

平均分子量
 数平均分子量 (Mn) 13802
 重量平均分子量 (Mw) 24158
 Mw/Mn 1.75042
 % 100.0

GPC chromatogram of polymer 3

mV



検出器A 254nm

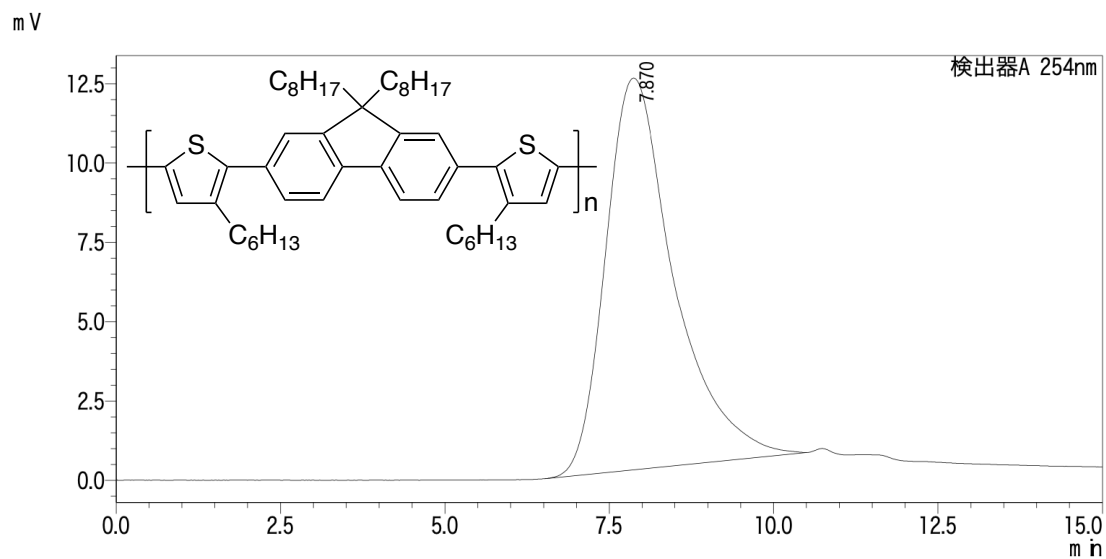
ピーク#	保持時間	面積	高さ	濃度	単位	マーク	化合物名
1	8.167	888111	11232	0.000		M	
合計		888111	11232				

GPC 計算結果

Peak#1 (検出器A 254nm)

平均分子量
 数平均分子量 (Mn) 20285
 重量平均分子量 (Mw) 52875
 Mw/Mn 2.60662
 % 100.0

GPC chromatogram of polymer 4



検出器A 254nm

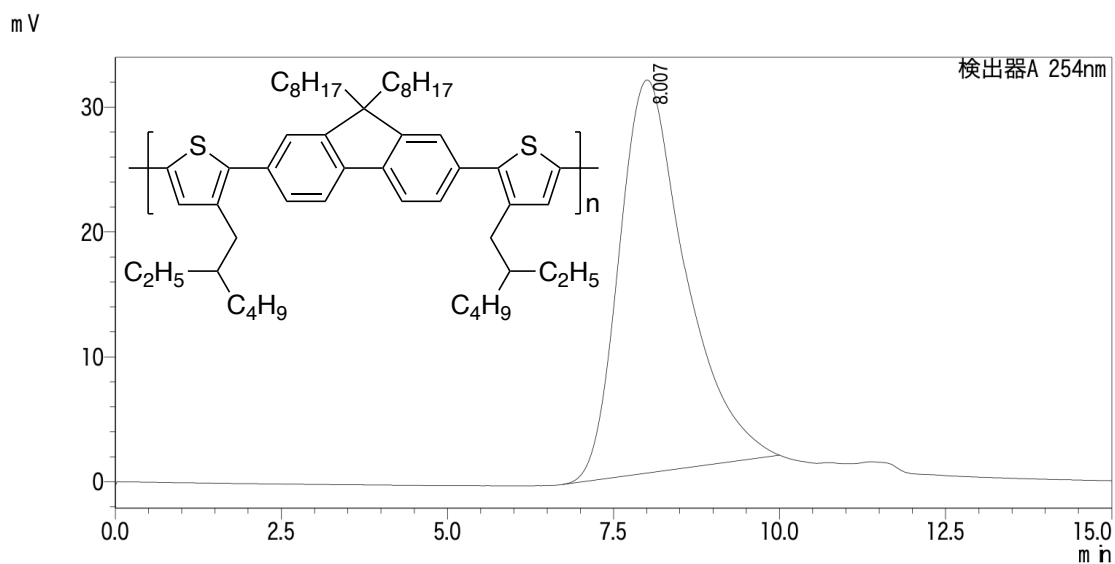
ピーク#	保持時間	面積	高さ	濃度	単位	マーク	化合物名
1	7.870	895773	12347	0.000		M	
合計		895773	12347				

GPC 計算結果

Peak#1 (検出器A 254nm)

平均分子量	
数平均分子量 (Mn)	32871
重量平均分子量 (Mw)	89355
Mw/Mn	2.71839
%	100.0

GPC chromatogram of polymer 5



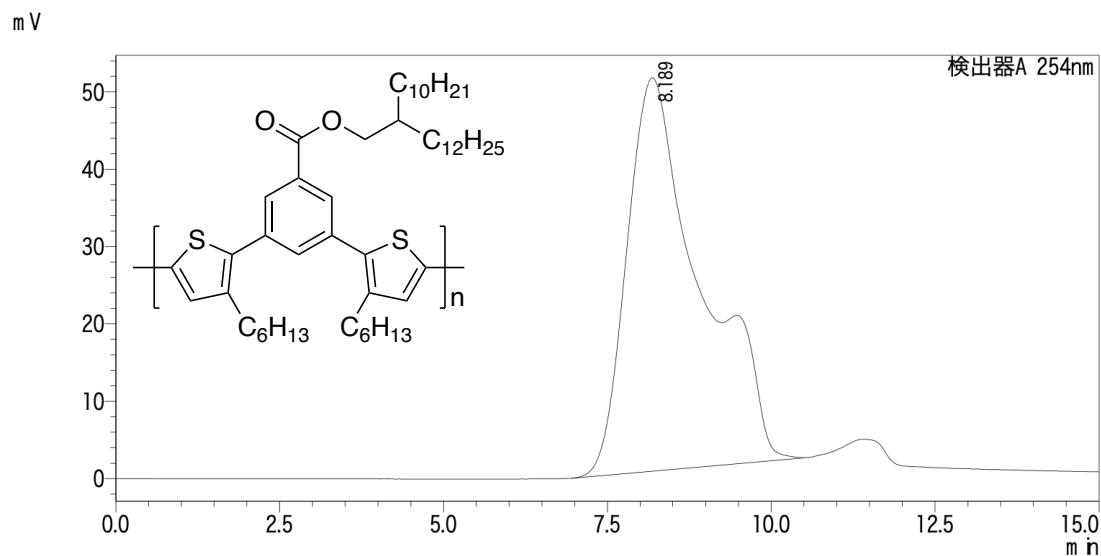
検出器A 254nm

ピーク#	保持時間	面積	高さ	濃度	単位	マーク	化合物名
1	8.007	2199323	31480	0.000		M	
合計		2199323	31480				

GPC 計算結果

Peak#1 (検出器A 254nm)

平均分子量	
数平均分子量 (Mn)	32574
重量平均分子量 (Mw)	69904
Mw/Mn	2.14605
%	100.0

GPC chromatogram of polymer **6**

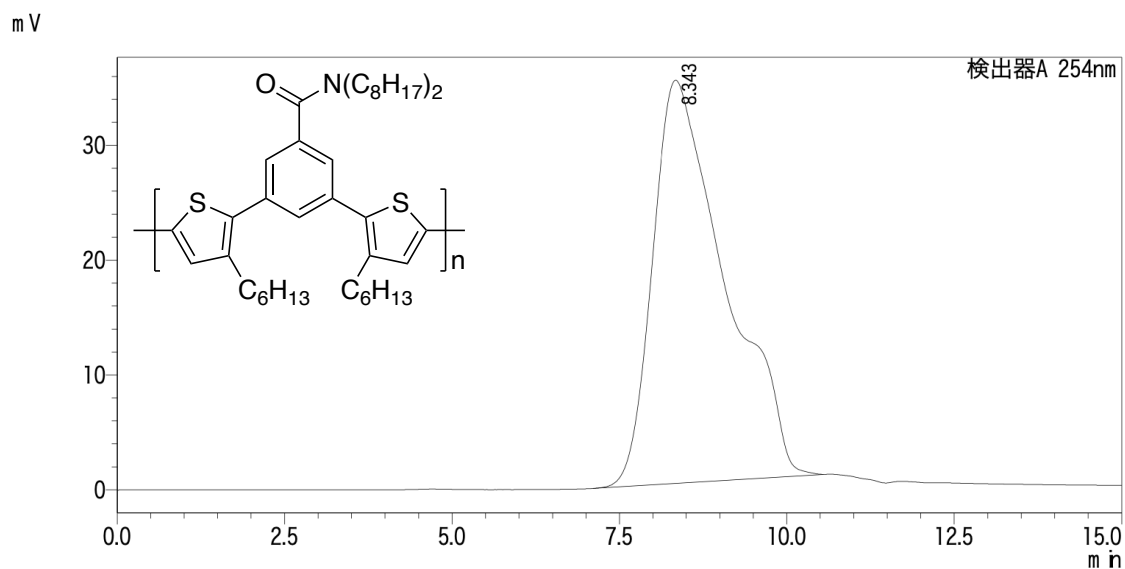
検出器A 254nm

ピーク#	保持時間	面積	高さ	濃度	単位	マーク	化合物名
1	8.189	3980729	50850	0.000		M	
合計		3980729	50850				

GPC 計算結果

Peak#1 (検出器A 254nm)

[平均分子量]
 数平均分子量 (Mn) 14936
 重量平均分子量 (Mw) 42850
 Mw/Mn 2.86890
 % 100.0

GPC chromatogram of polymer **7**

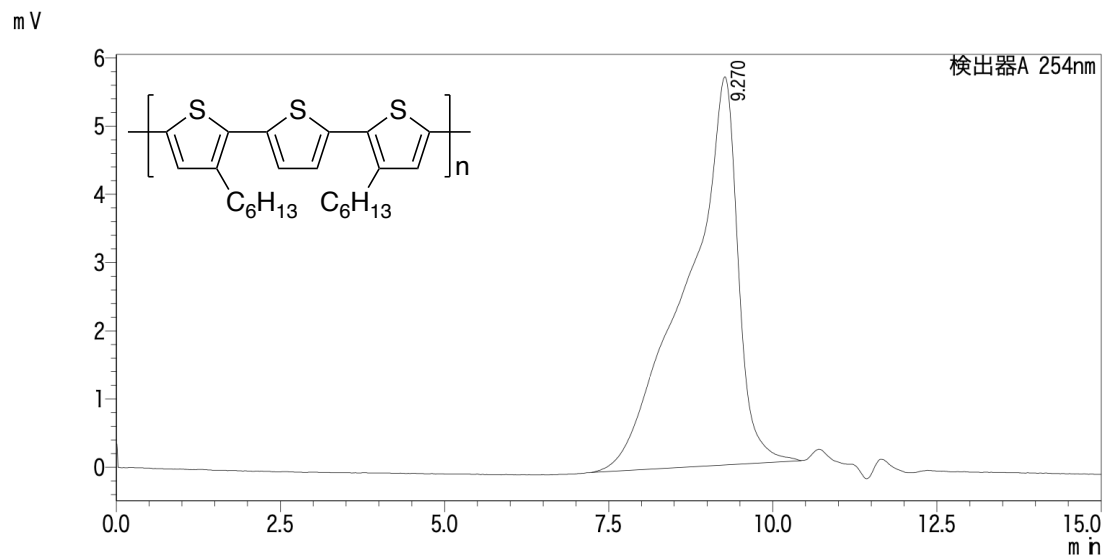
検出器A 254nm

ピーク#	保持時間	面積	高さ	濃度	単位	マーク	化合物名
1	8.343	2631822	35108	0.000		M	
合計		2631822	35108				

GPC 計算結果

Peak#1 (検出器A 254nm)

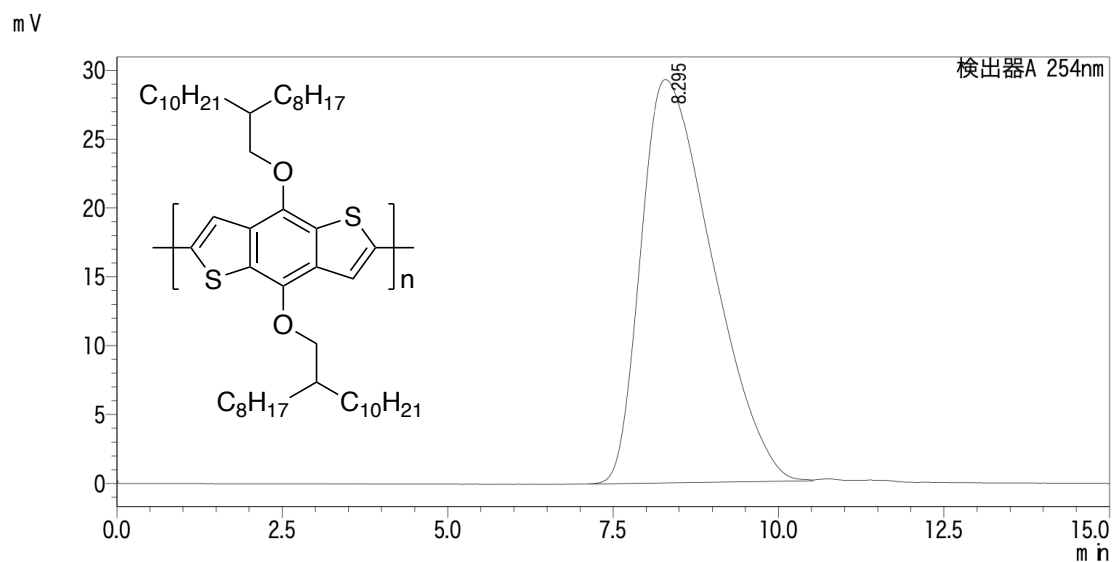
[平均分子量]
 数平均分子量 (Mn) 12155
 重量平均分子量 (Mw) 30236
 Mw/Mn 2.48763
 % 100.0

GPC chromatogram of polymer **8**

検出器A 254nm							
ピーク#	保持時間	面積	高さ	濃度	単位	マーク	化合物名
1	9.270	308636	5688	0.000		M	
合計		308636	5688				

GPC 計算結果

Peak#1 (検出器A 254nm)
 [平均分子量]
 数平均分子量 (Mn) 9645
 重量平均分子量 (Mw) 19495
 Mw/Mn 2.02126
 % 100.0

GPC chromatogram of polymer **9**

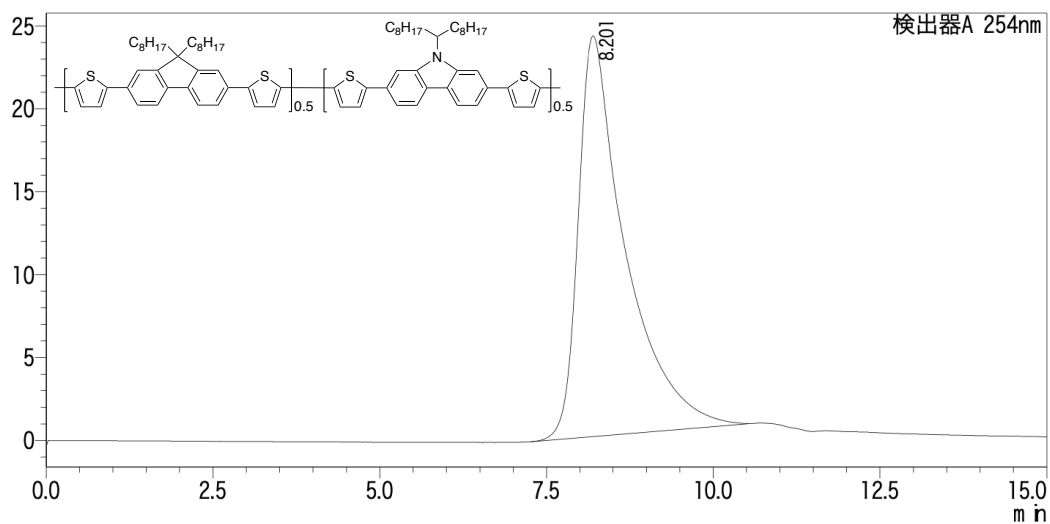
検出器A 254nm							
ピーク#	保持時間	面積	高さ	濃度	単位	マーク	化合物名
1	8.295	2202544	29298	0.000			
合計		2202544	29298				

GPC 計算結果

Peak#1 (検出器A 254nm)
 [平均分子量]
 数平均分子量 (Mn) 17158
 重量平均分子量 (Mw) 37011
 Mw/Mn 2.15708
 % 100.0

GPC chromatogram of polymer **10**

mV



検出器A 254nm

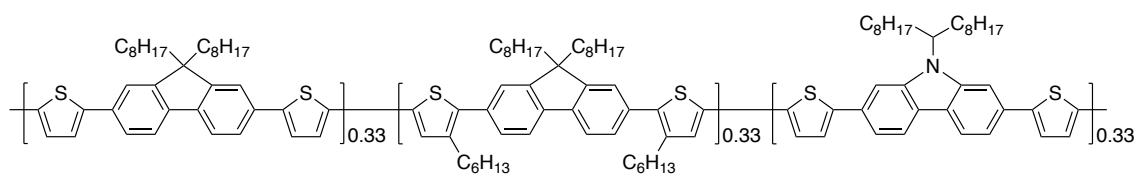
ピーク#	保持時間	面積	高さ	濃度	単位	マーク	化合物名
1	8.201	1195329	24168	0.000		M	
合計		1195329	24168				

GPC 計算結果

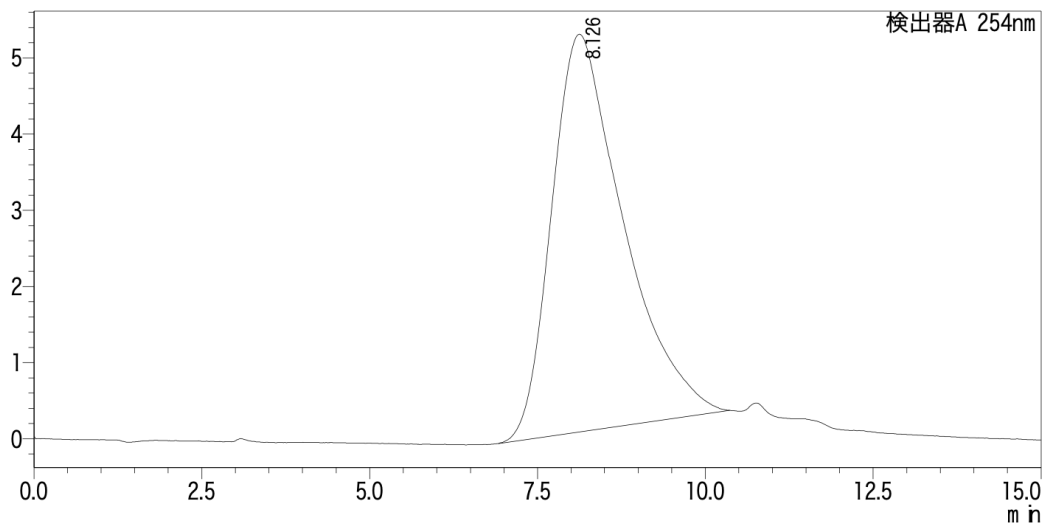
Peak# 1 (検出器A 254nm)

[平均分子量]

数平均分子量 (Mn) 19746
 重量平均分子量 (Mw) 38042
 Mw/Mn 1.92655
 % 100.0

GPC chromatogram of polymer **11**

mV



検出器A 254nm

ピーク#	保持時間	面積	高さ	濃度	単位	マーク	化合物名
1	8.126	389408	5223	0.000			
合計		389408	5223				

GPC 計算結果

Peak#:1 (検出器A 254nm)

[平均分子量]

数平均分子量 (Mn) 23067

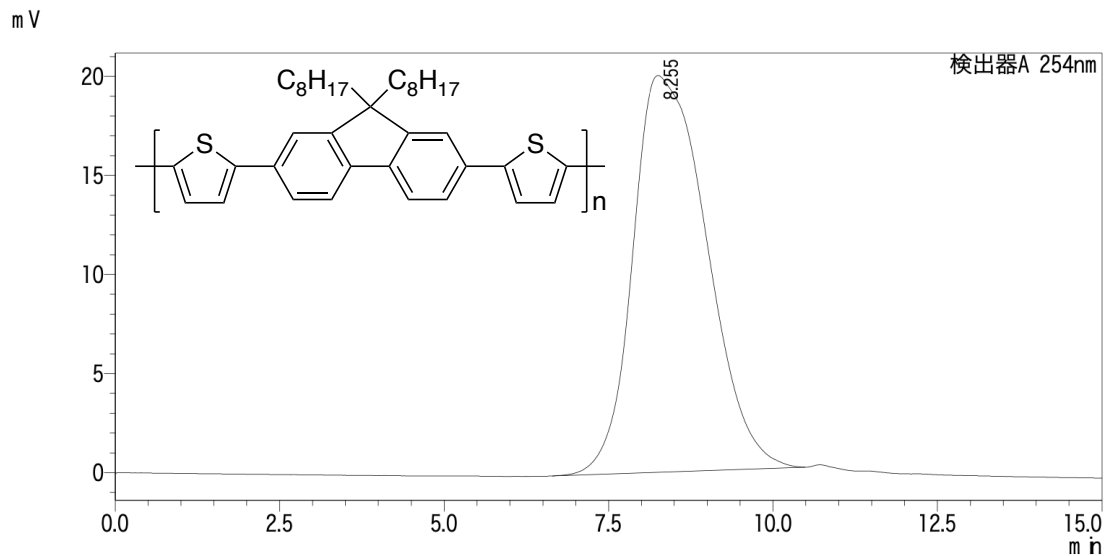
重量平均分子量 (Mw) 56328

Mw/Mn 2.44192

%

100.0

GPC chromatogram of polymer **3** after the post-treatment procedure



検出器A 254nm

ピーク#	保持時間	面積	高さ	濃度	単位	マーク	化合物名
1	8.255	1566474	20024	0.000		M	
合計		1566474	20024				

GPC 計算結果

Peak#1 (検出器A 254nm)

[平均分子量]

数平均分子量 (Mn) 18686

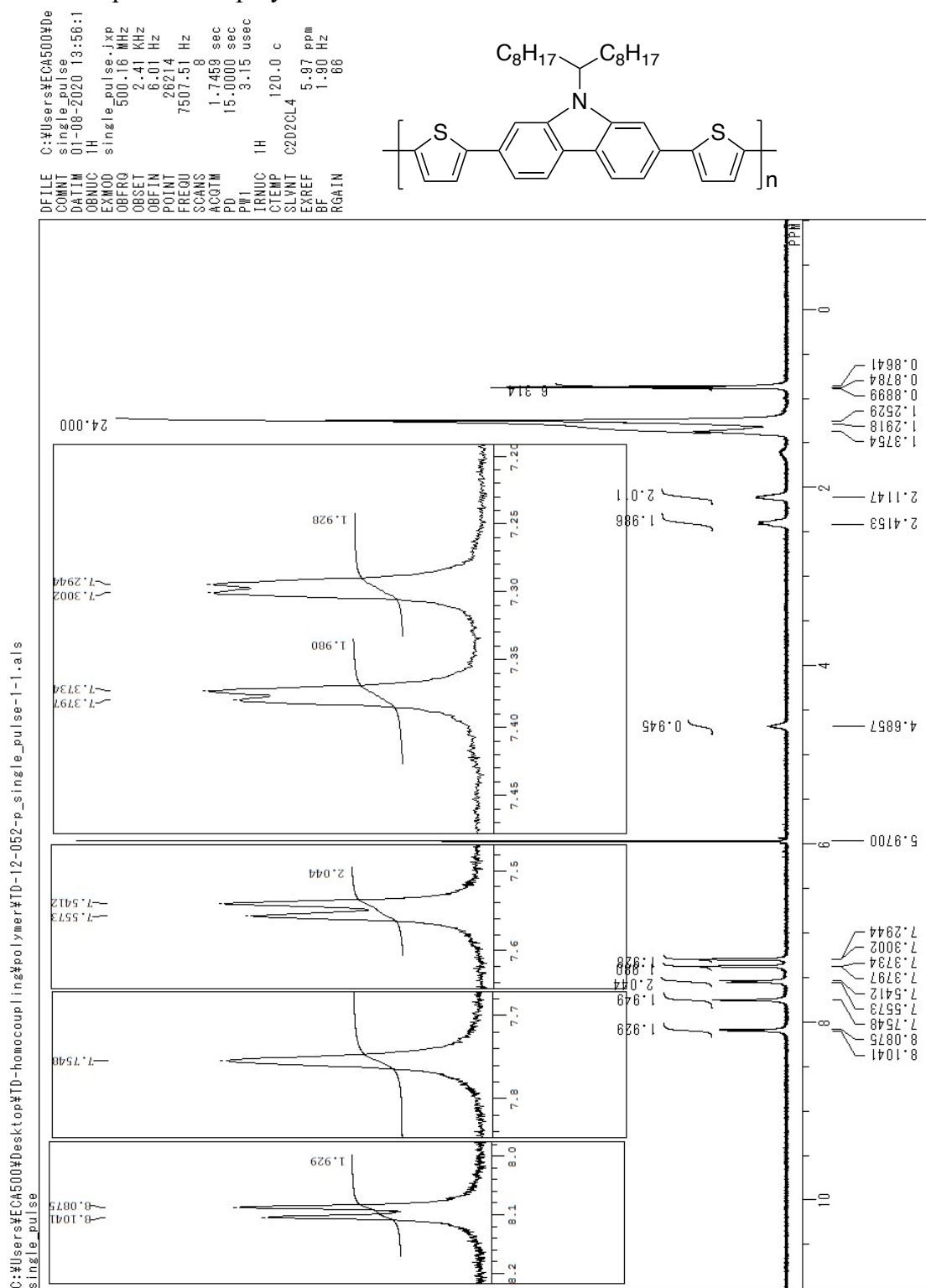
重量平均分子量 (Mw) 40506

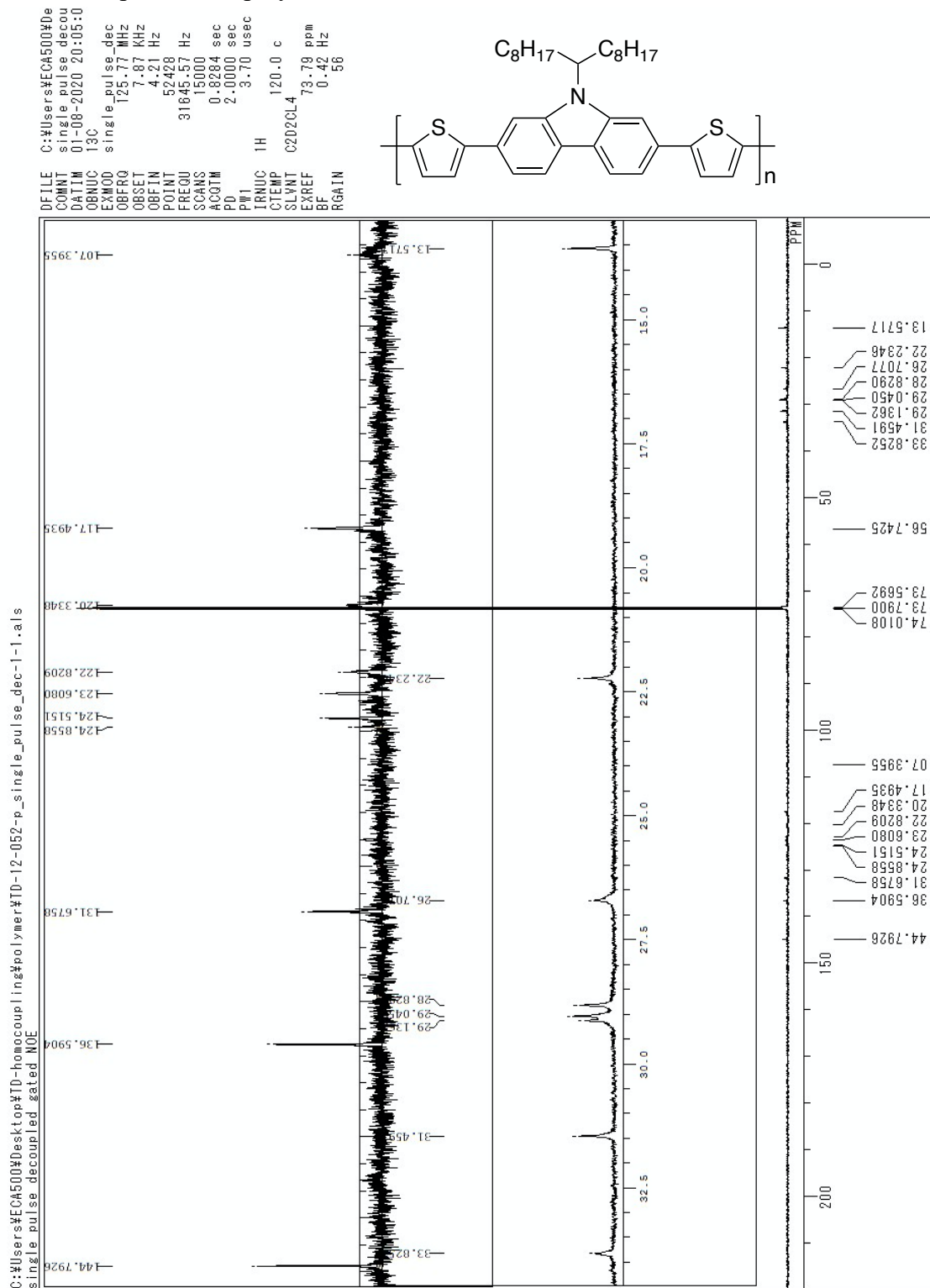
Mw/Mn 2.16772

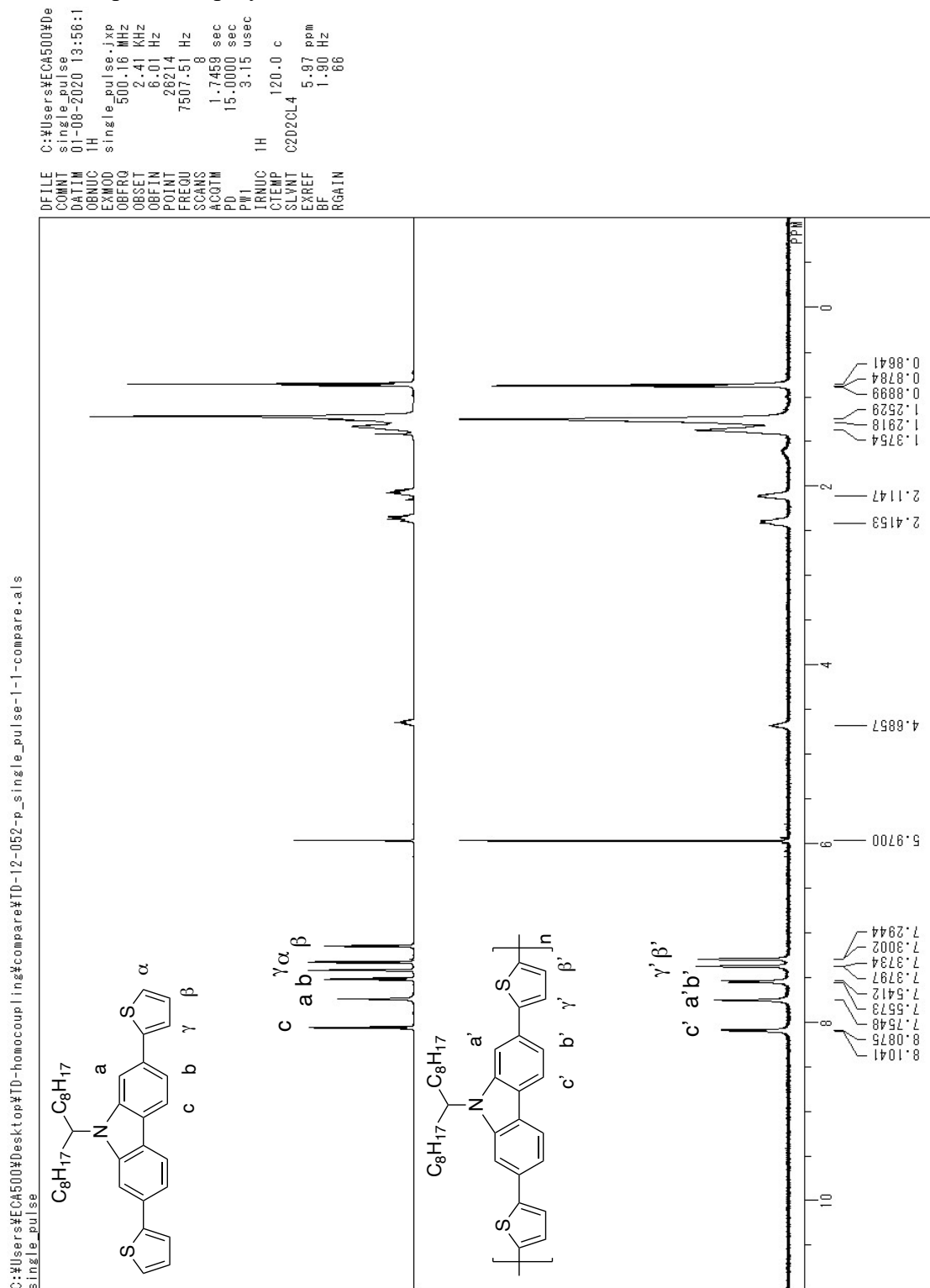
% 100.0

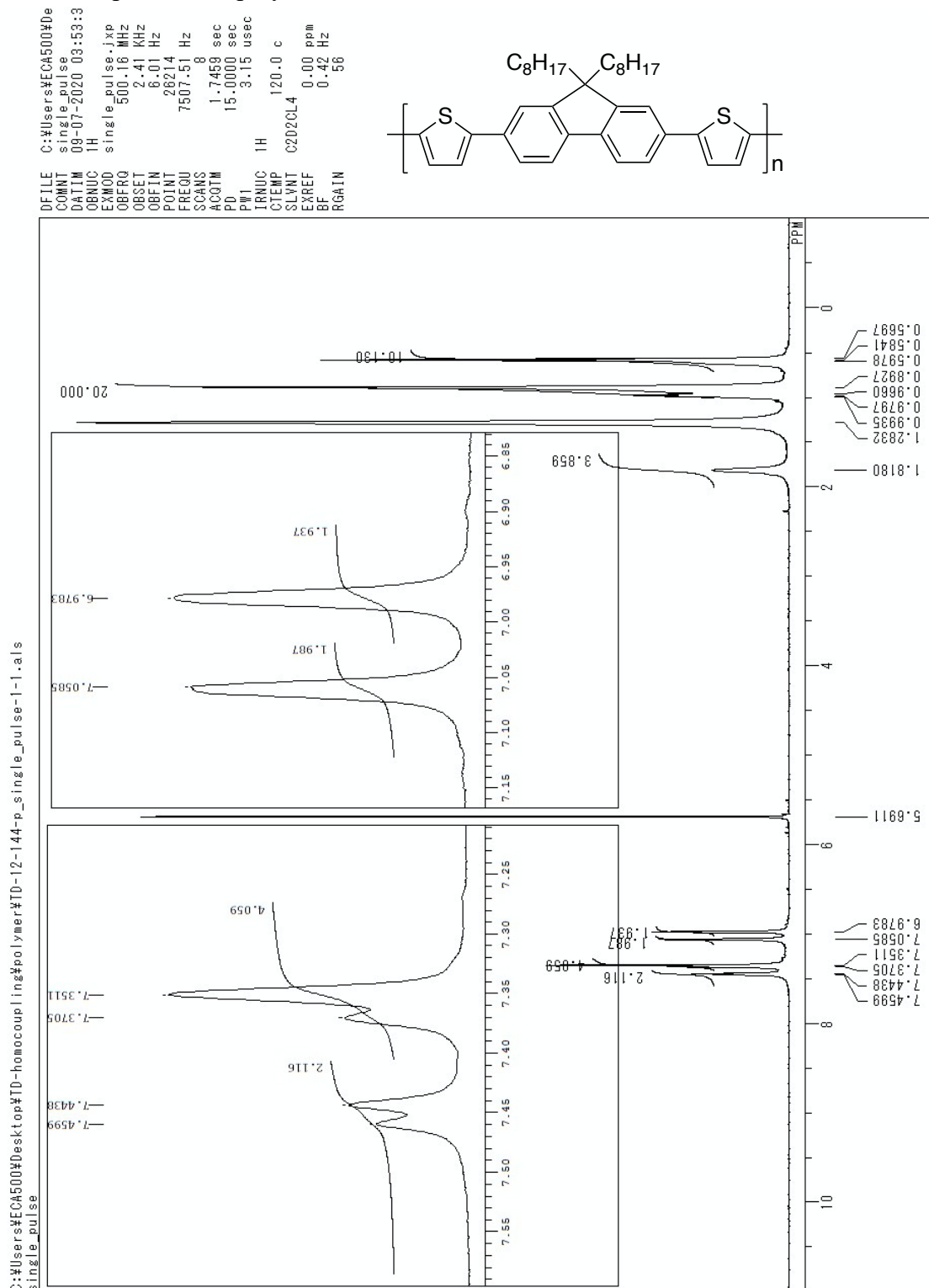
(4-11. Application to perovskite solar cell については, 5 年以内に雑誌等で刊行予定のため, 非公開.)

NMR spectra

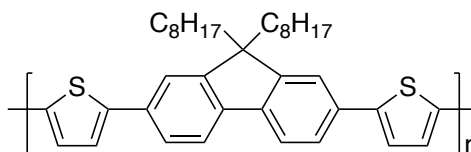
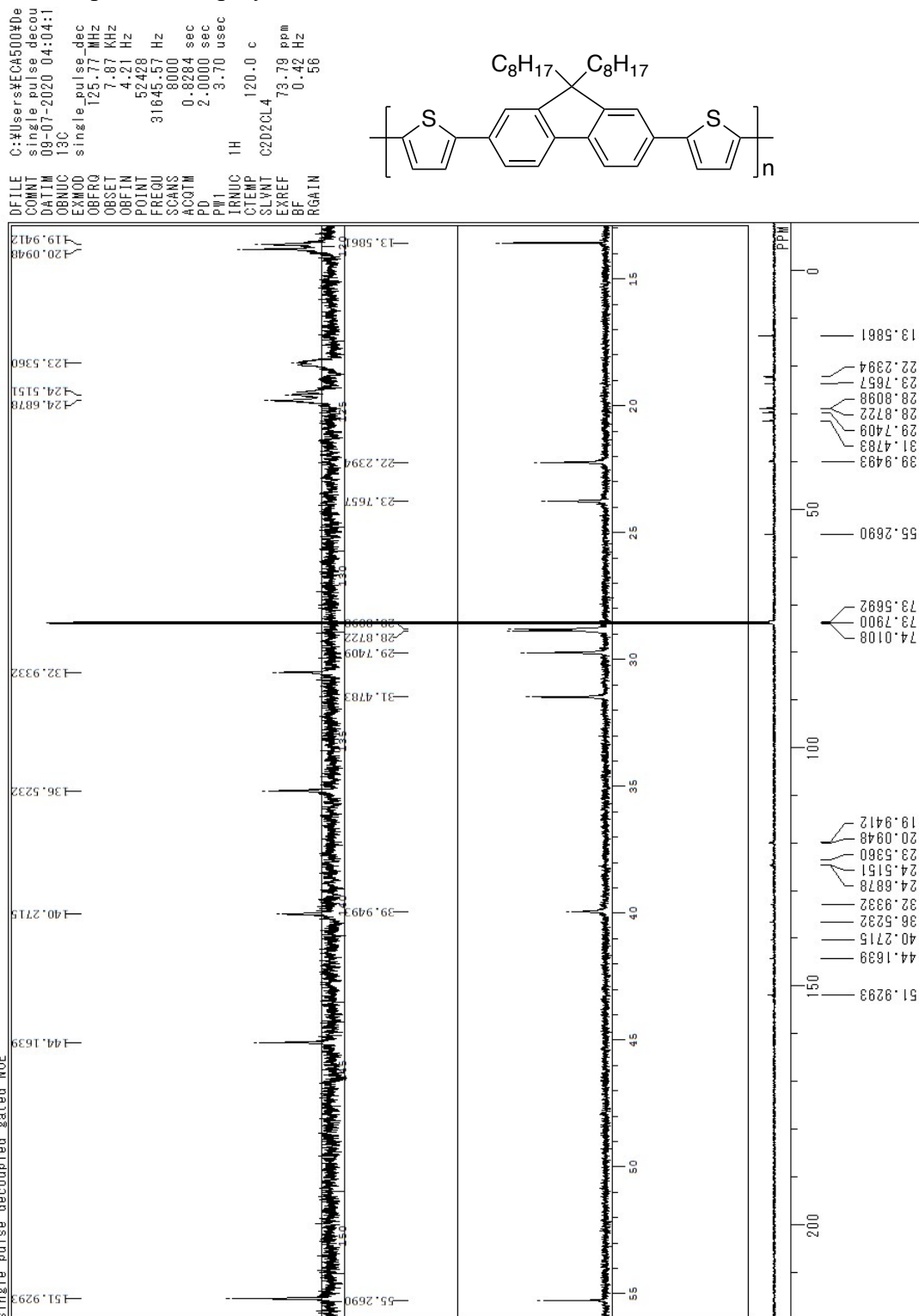
 ^1H NMR spectrum of polymer **2**

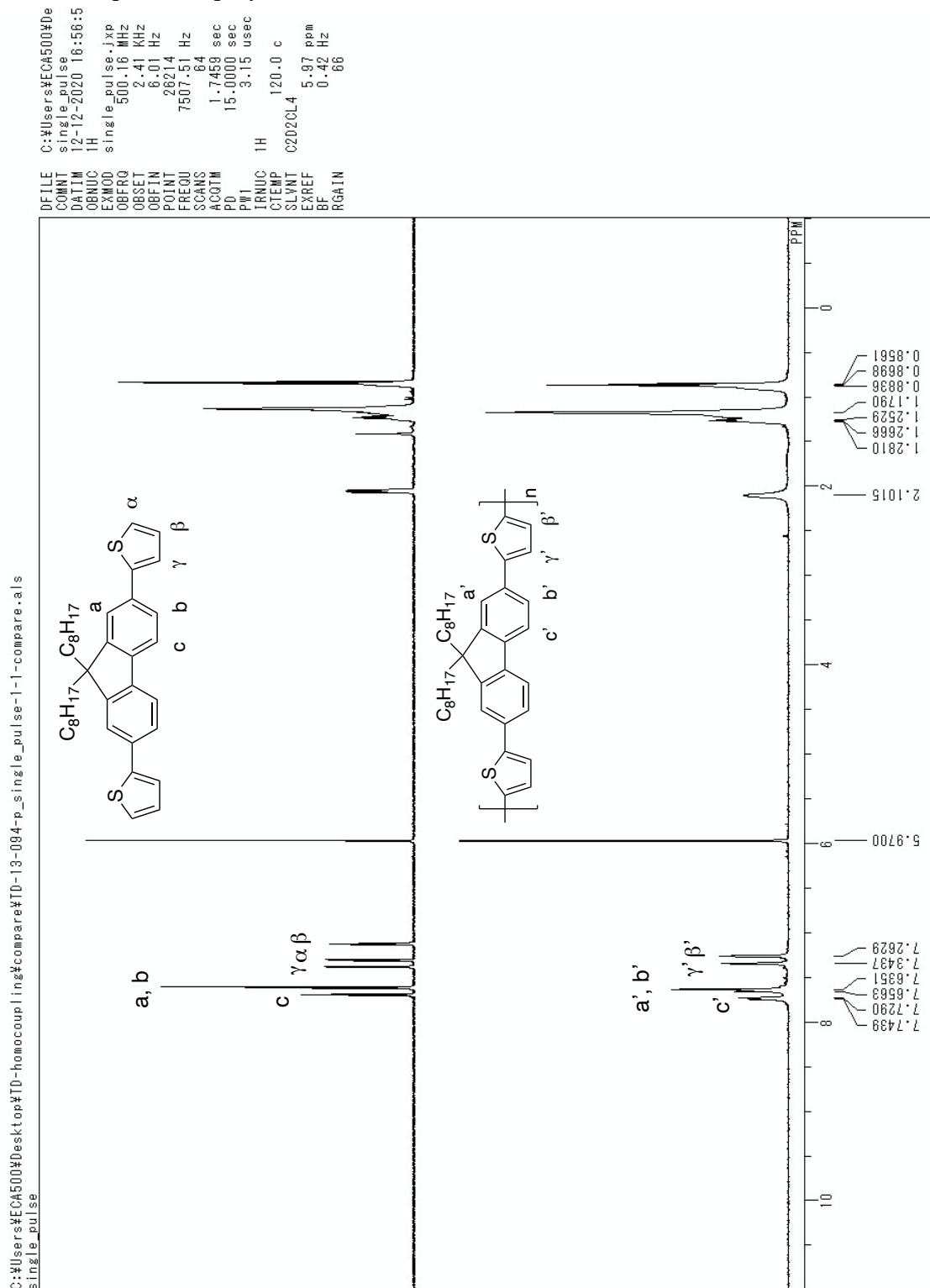
¹³C NMR spectrum of polymer 2

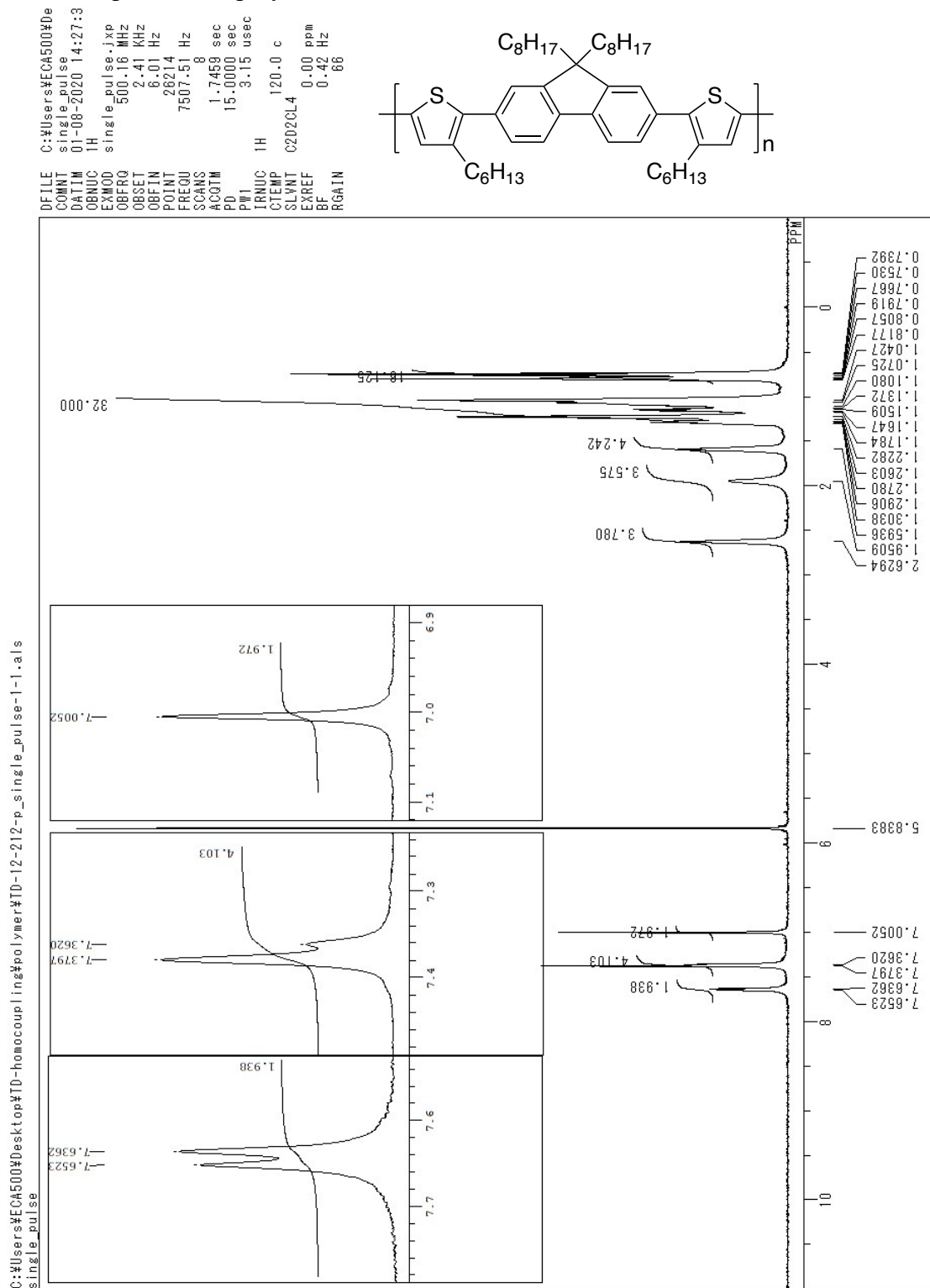
¹H NMR spectra of polymer **2** and its monomer

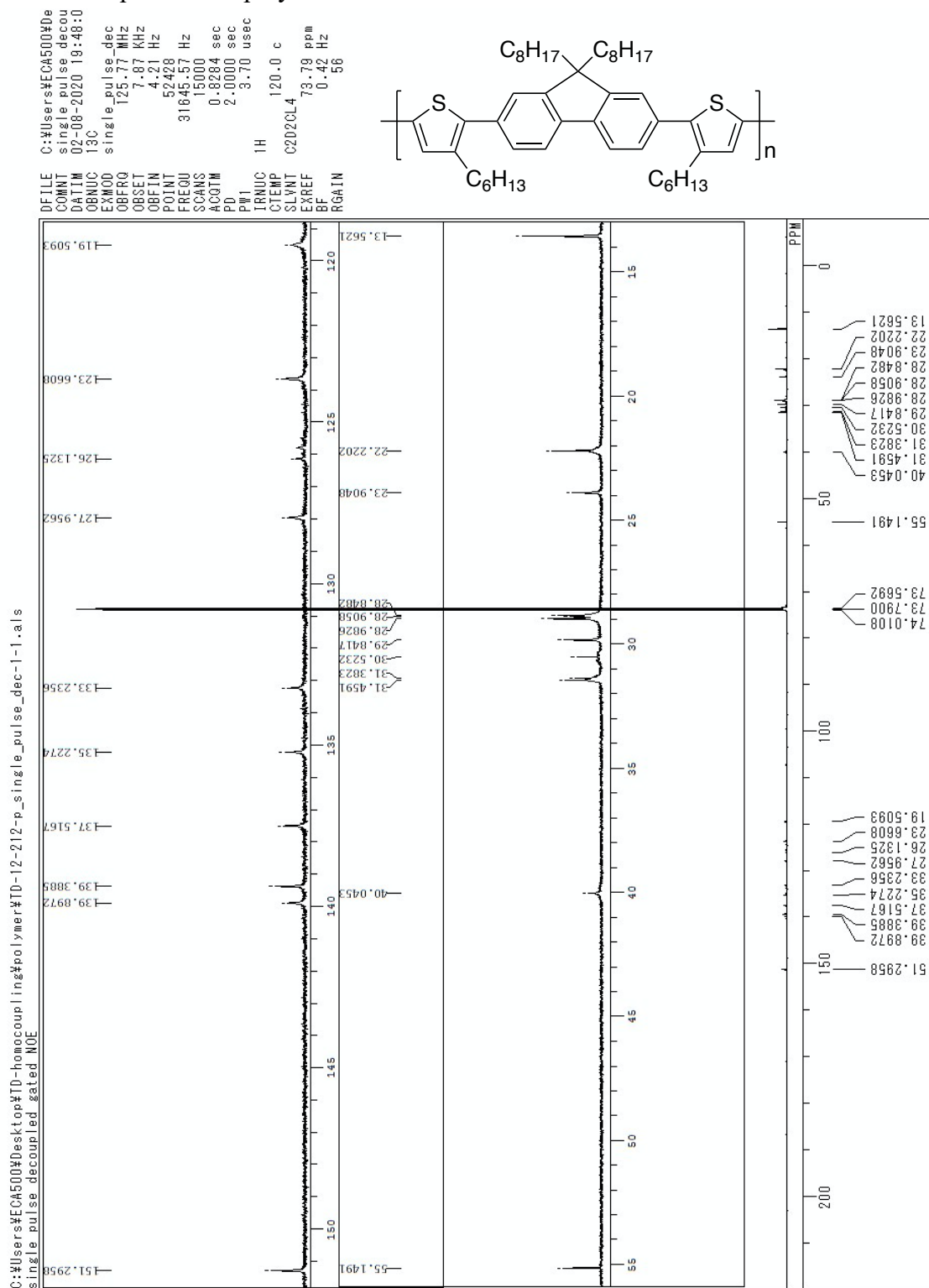
¹H NMR spectrum of polymer **3**

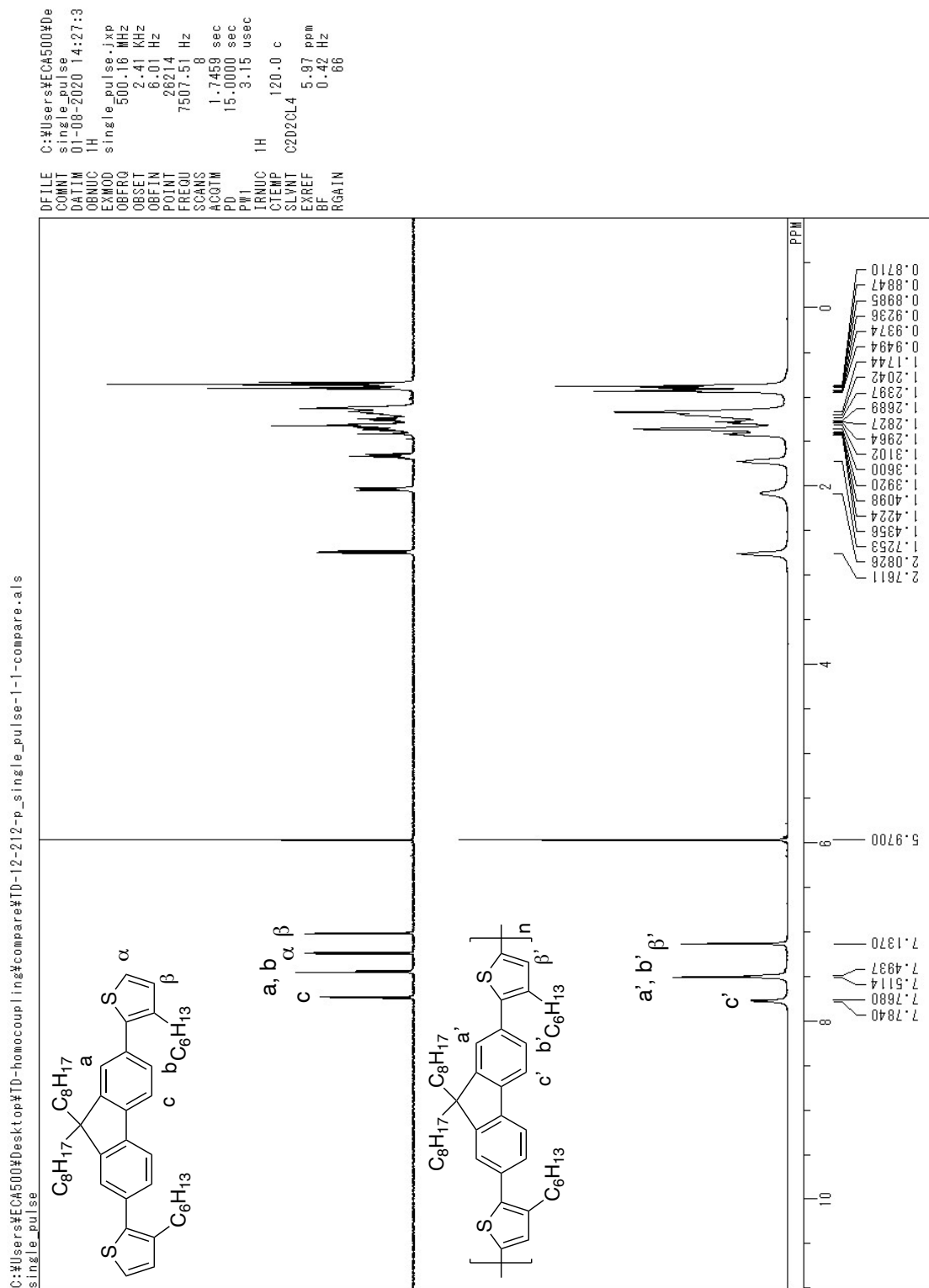
C:\Users\ECAS00\Desktop\TD-homocoupling\polymer\TD-12-144-p_single_pulse_dec-1-1.as

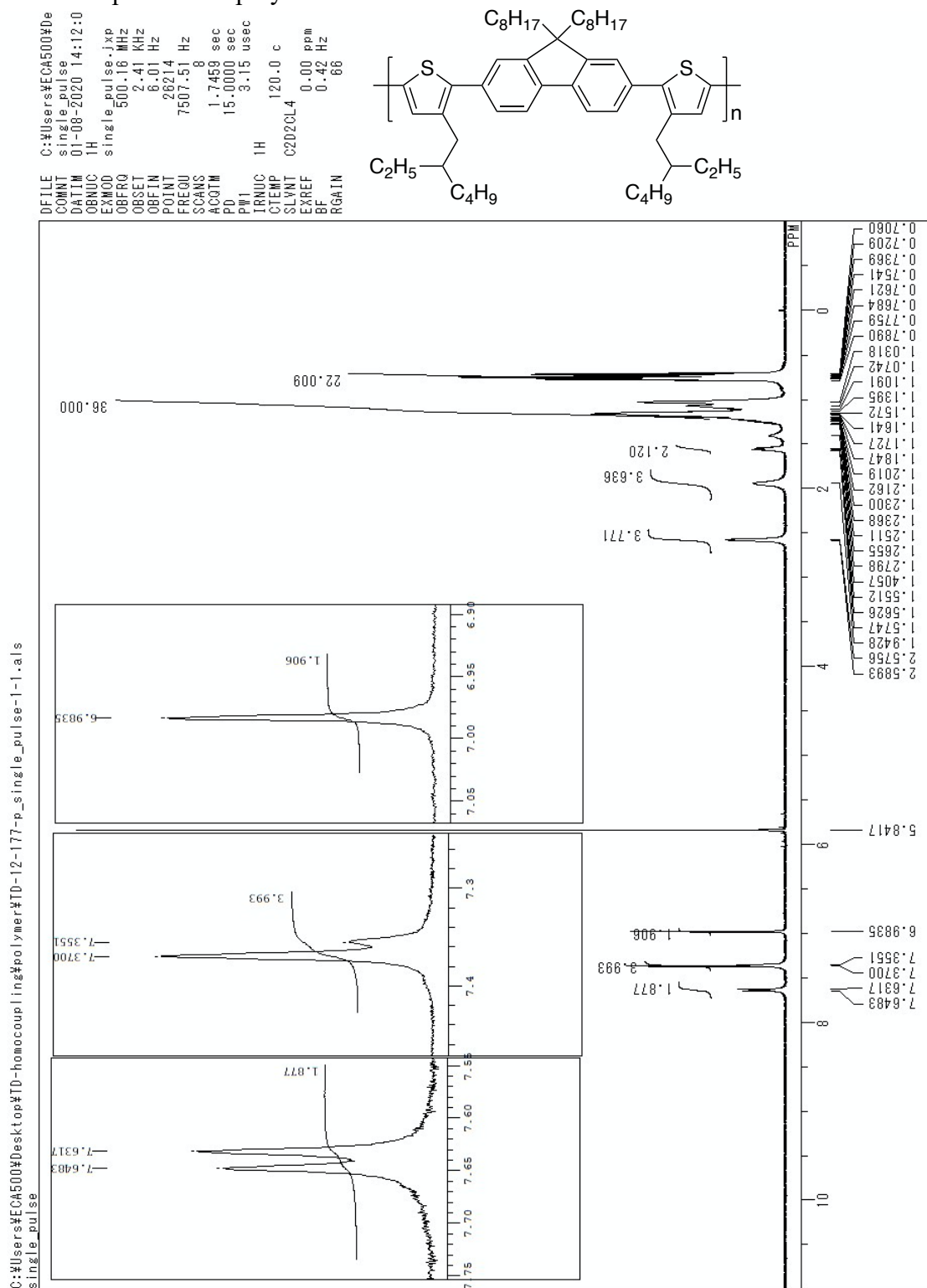


¹H NMR spectra of polymer **3** and its monomer

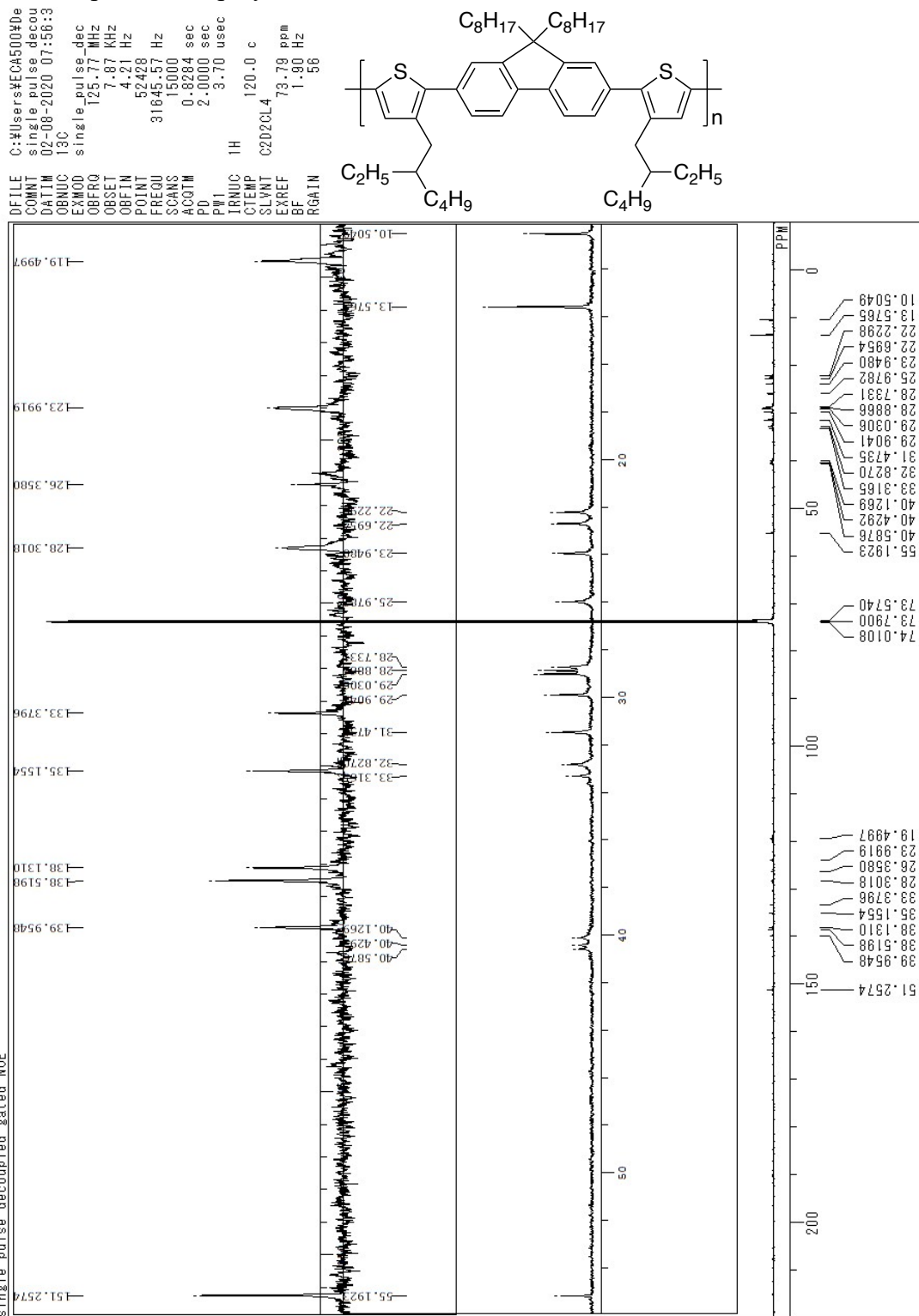
¹H NMR spectrum of polymer 4

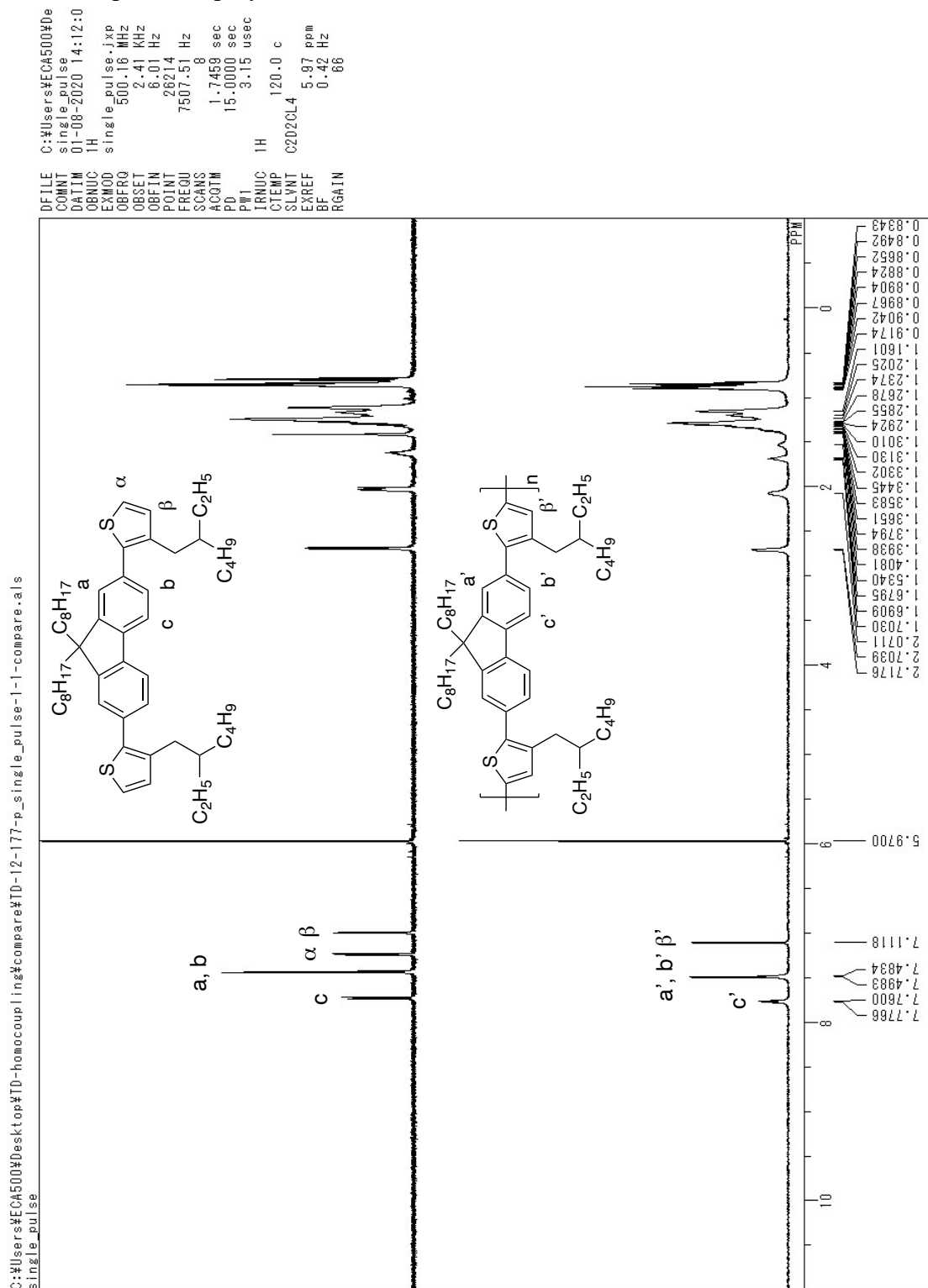
^{13}C NMR spectrum of polymer 4

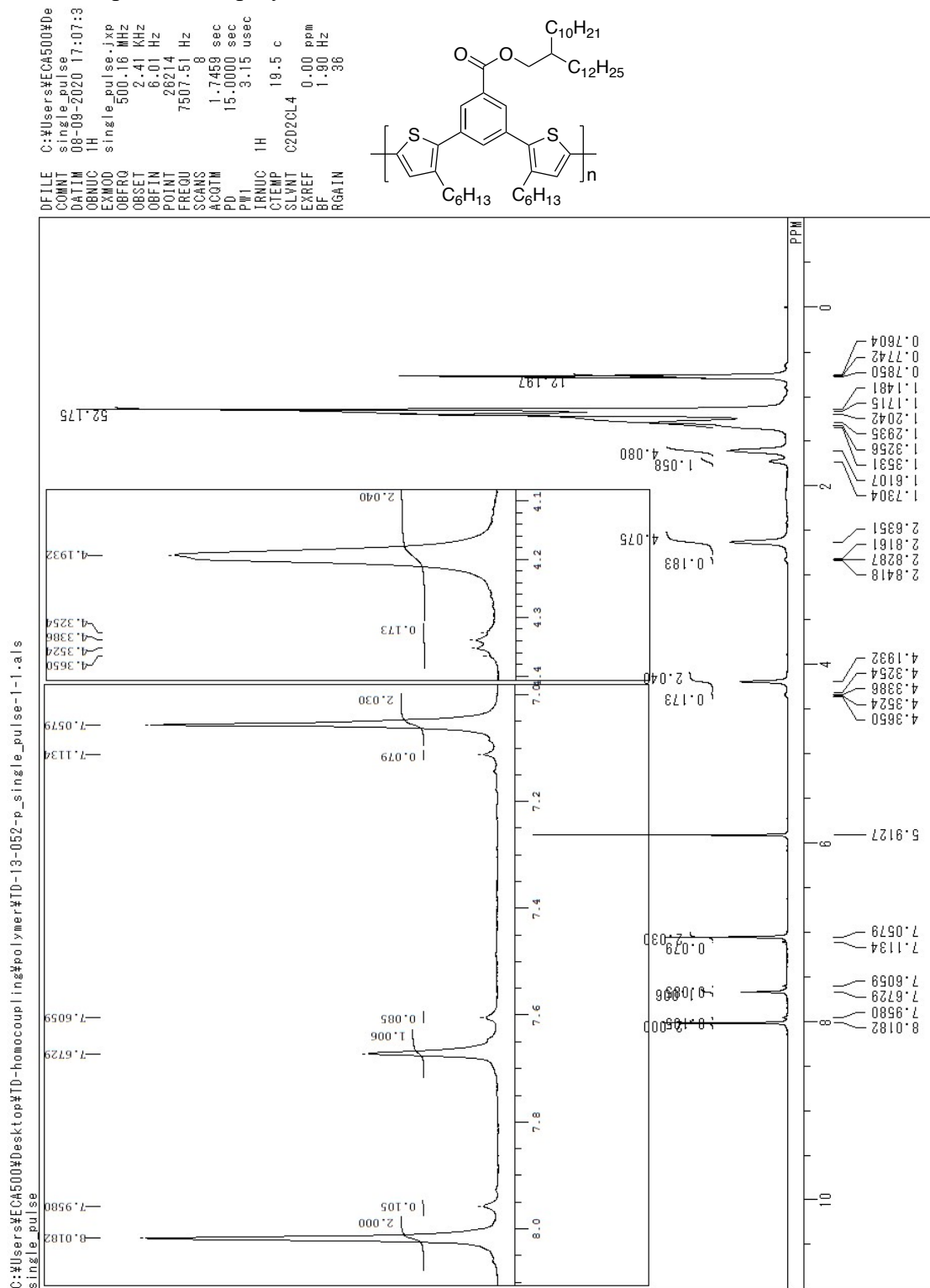
¹H NMR spectra of polymer **4** and its monomer

¹H NMR spectrum of polymer **5**

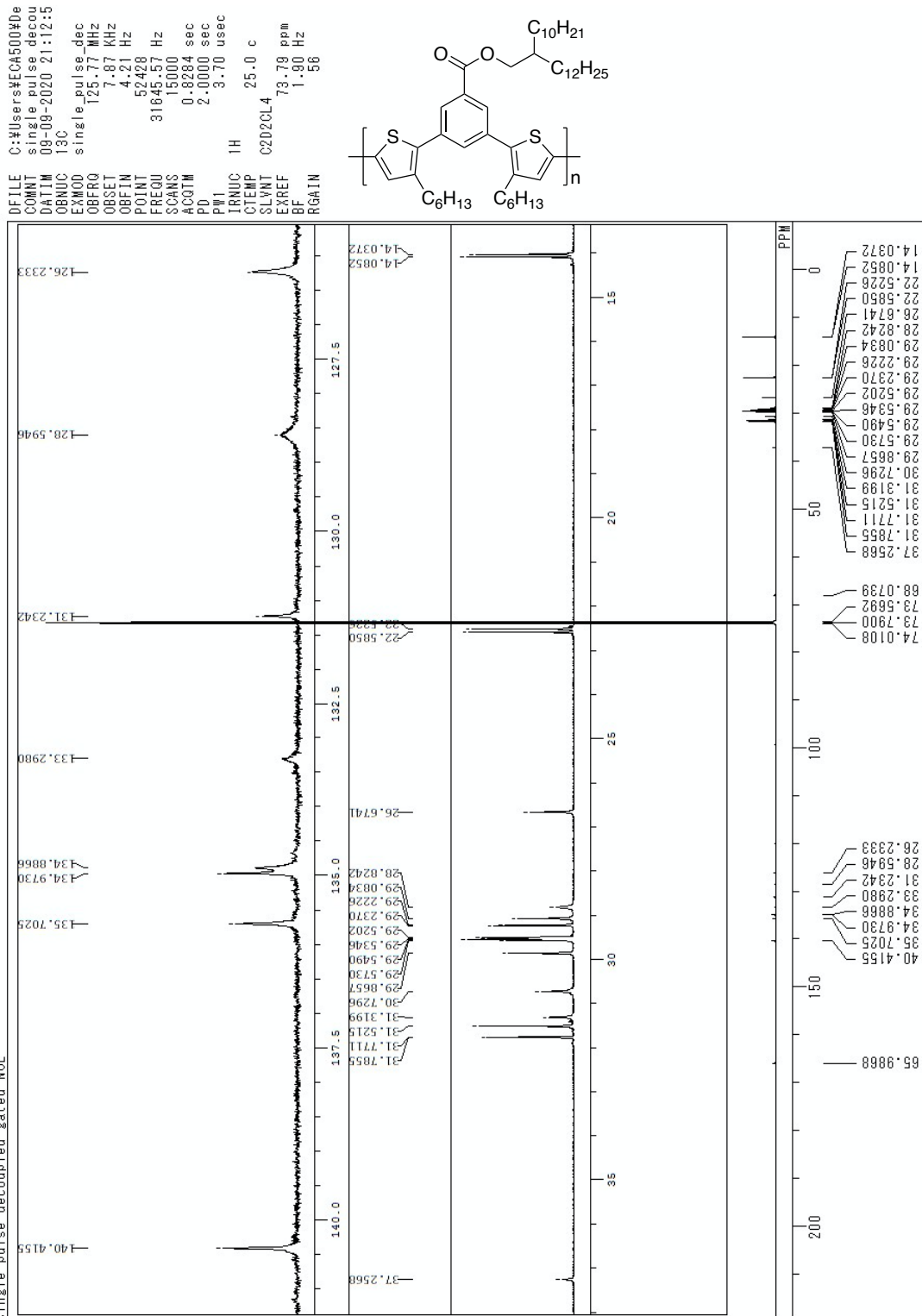
C:\Users\CA500\Documents\polymer\TD-12-177-p_single_pulse_dec-1-1.xls

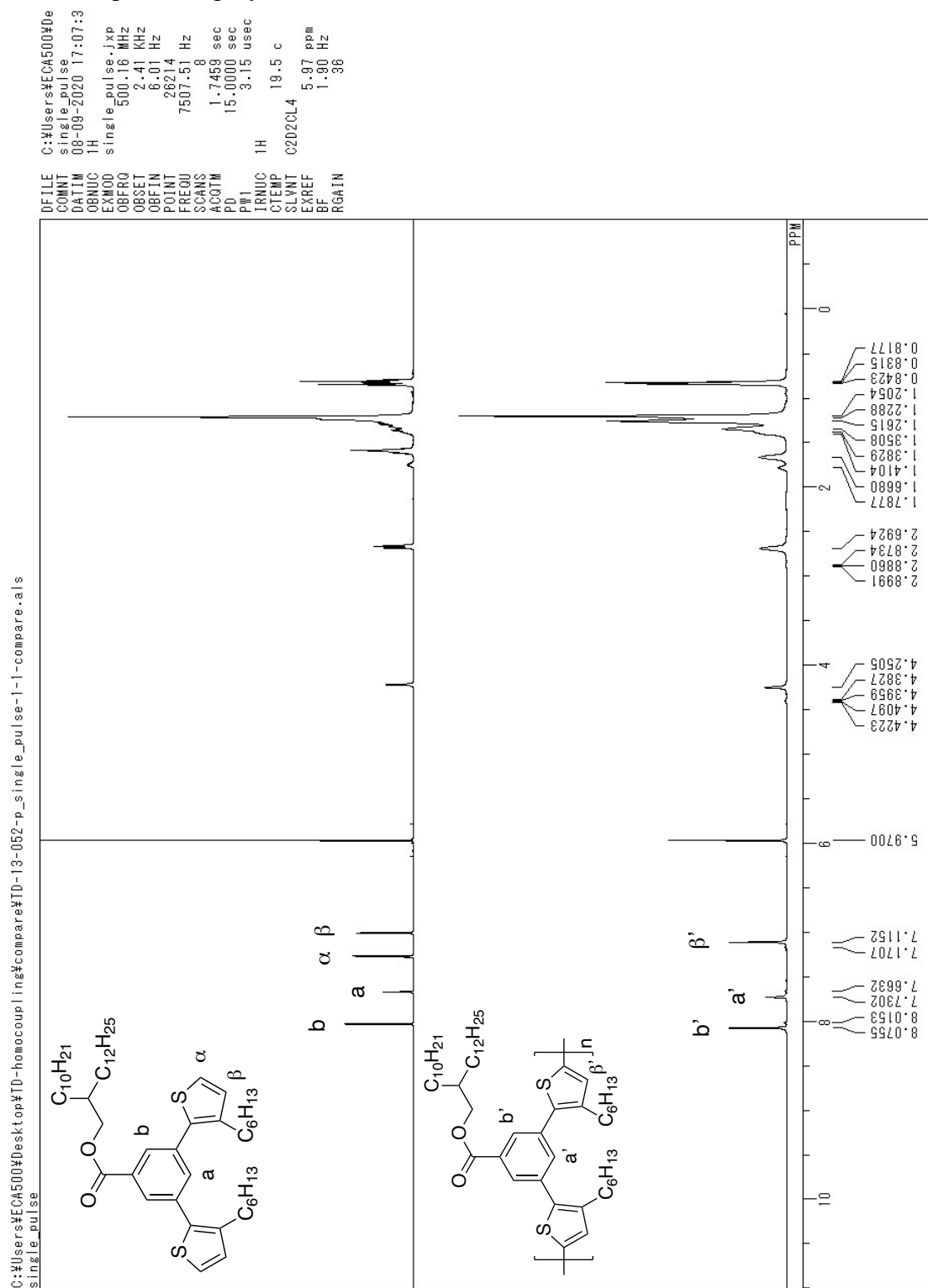


¹H NMR spectra of polymer **5** and its monomer

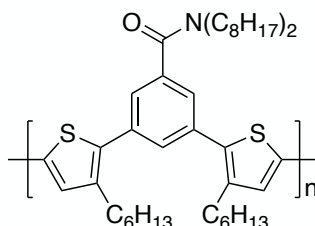
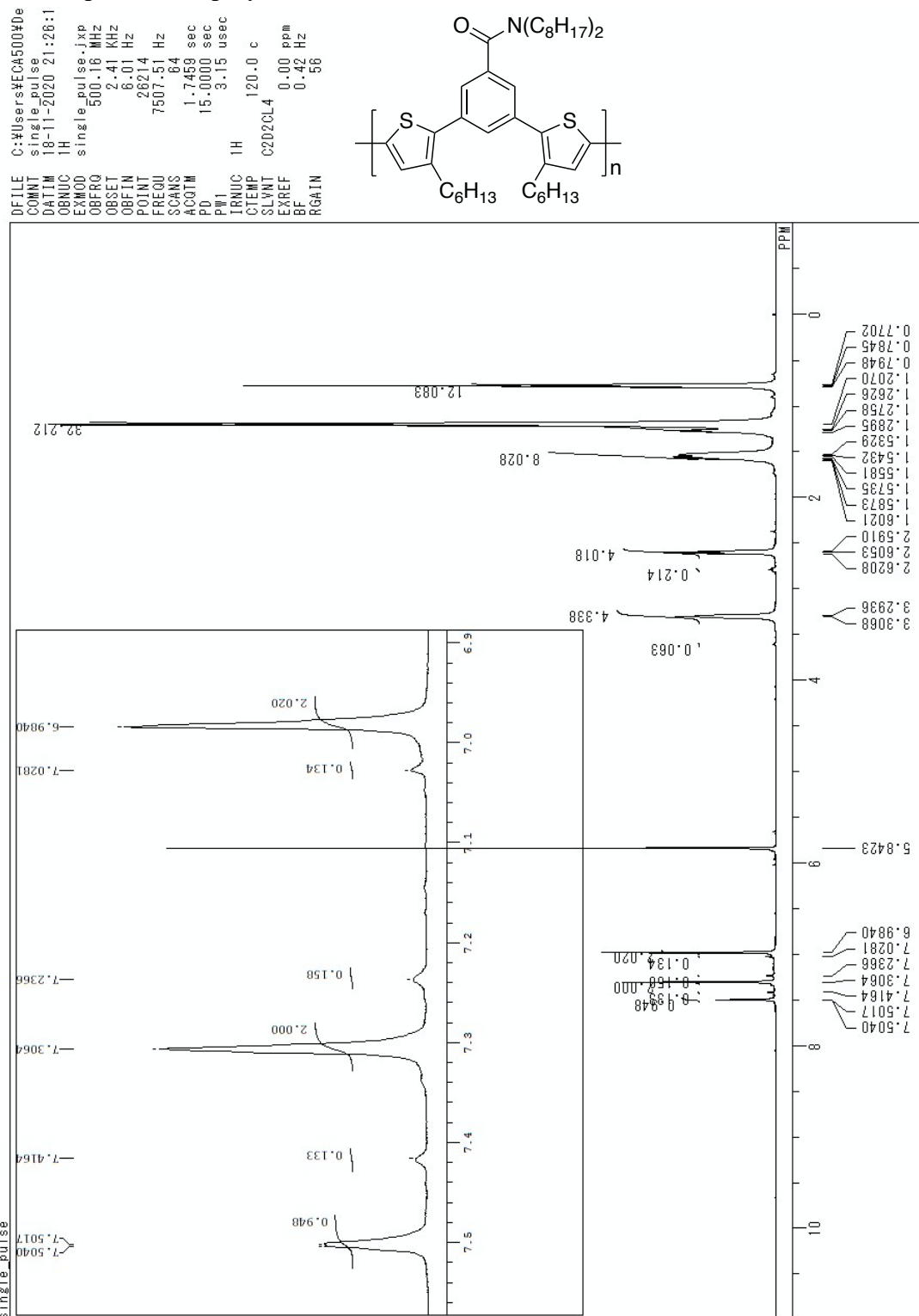
^1H NMR spectrum of polymer 6

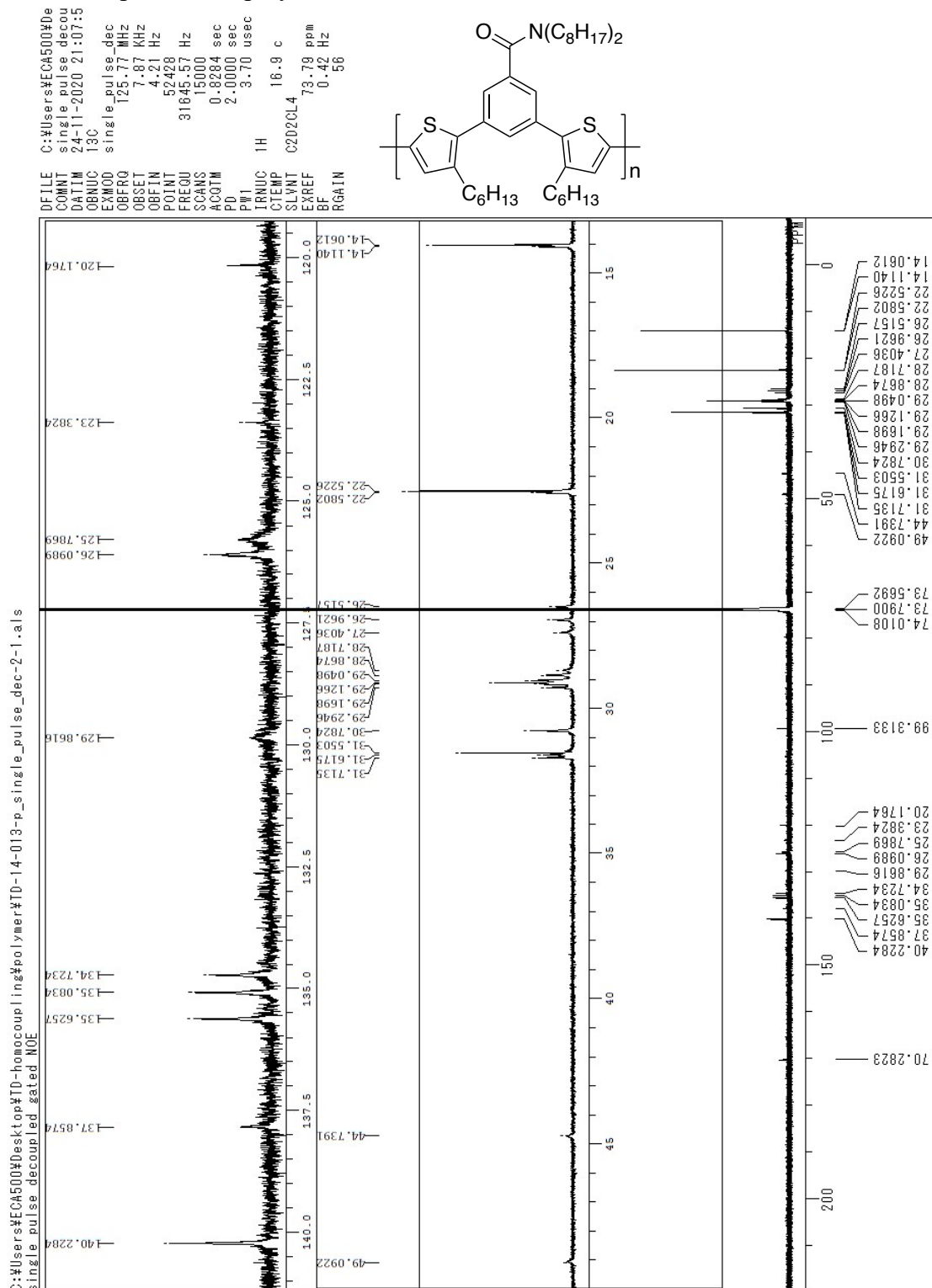
C:\Users\ECH500\Desktop\TD-13-052-polymer\TD-13-052-p_single_pulse_dec-1-1.a1.s
single pulse decoupled gated NOE

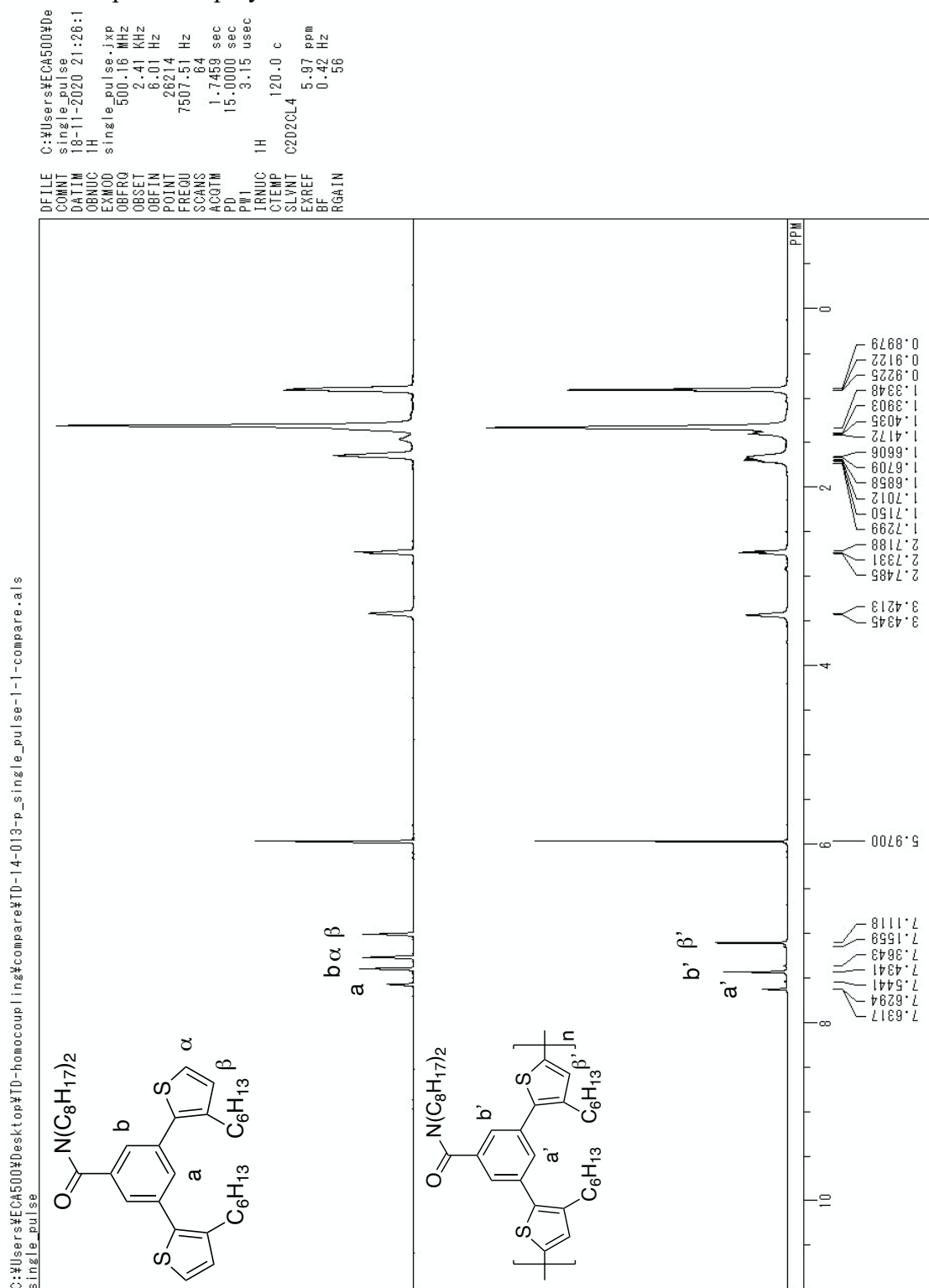


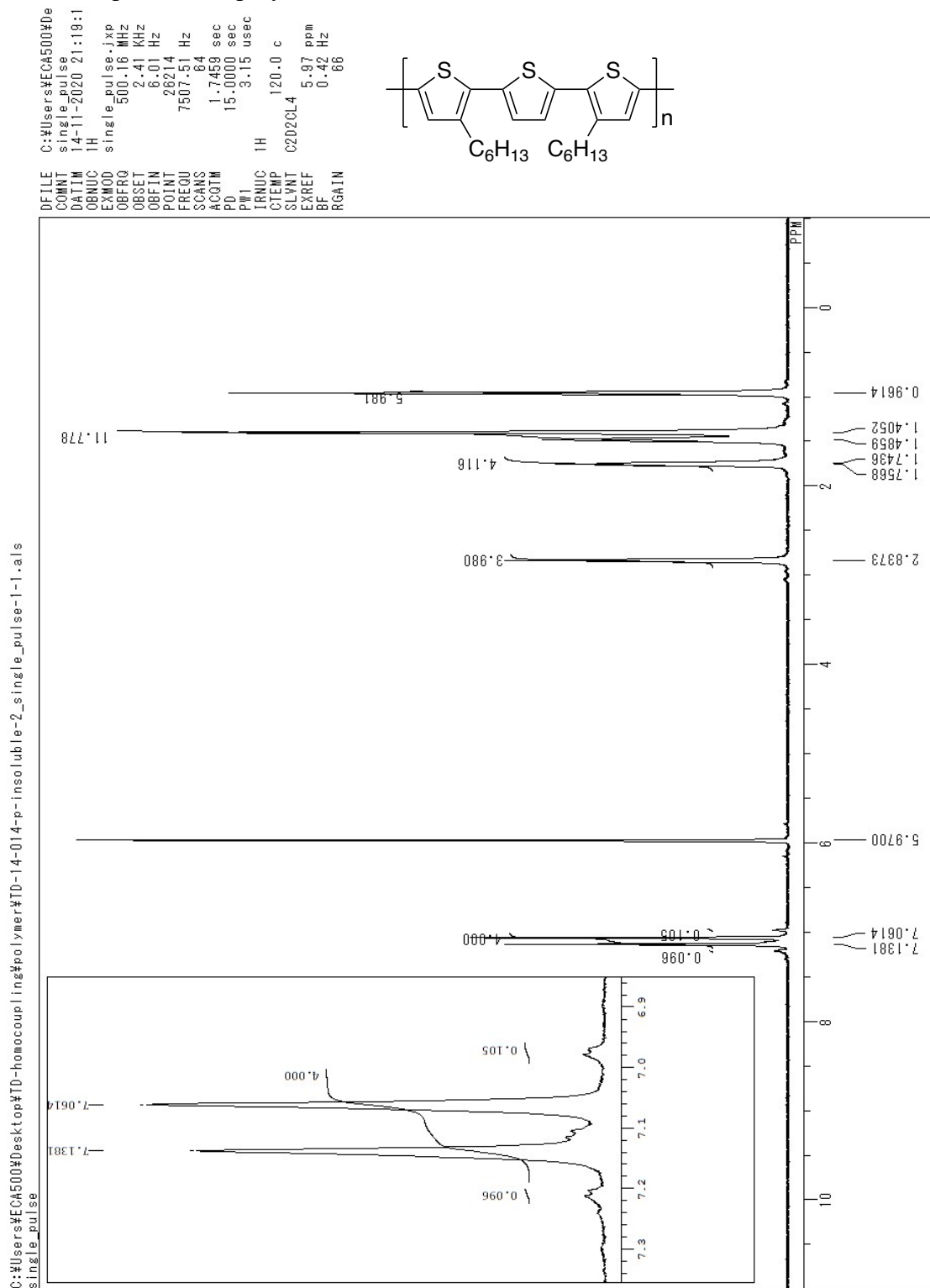
¹H NMR spectra of polymer 6 and its monomer

C:\Users\ECA500\Desktop\TD-homocoupling\polymer\TD-14-013-p_single_pulse-1-1.a.s



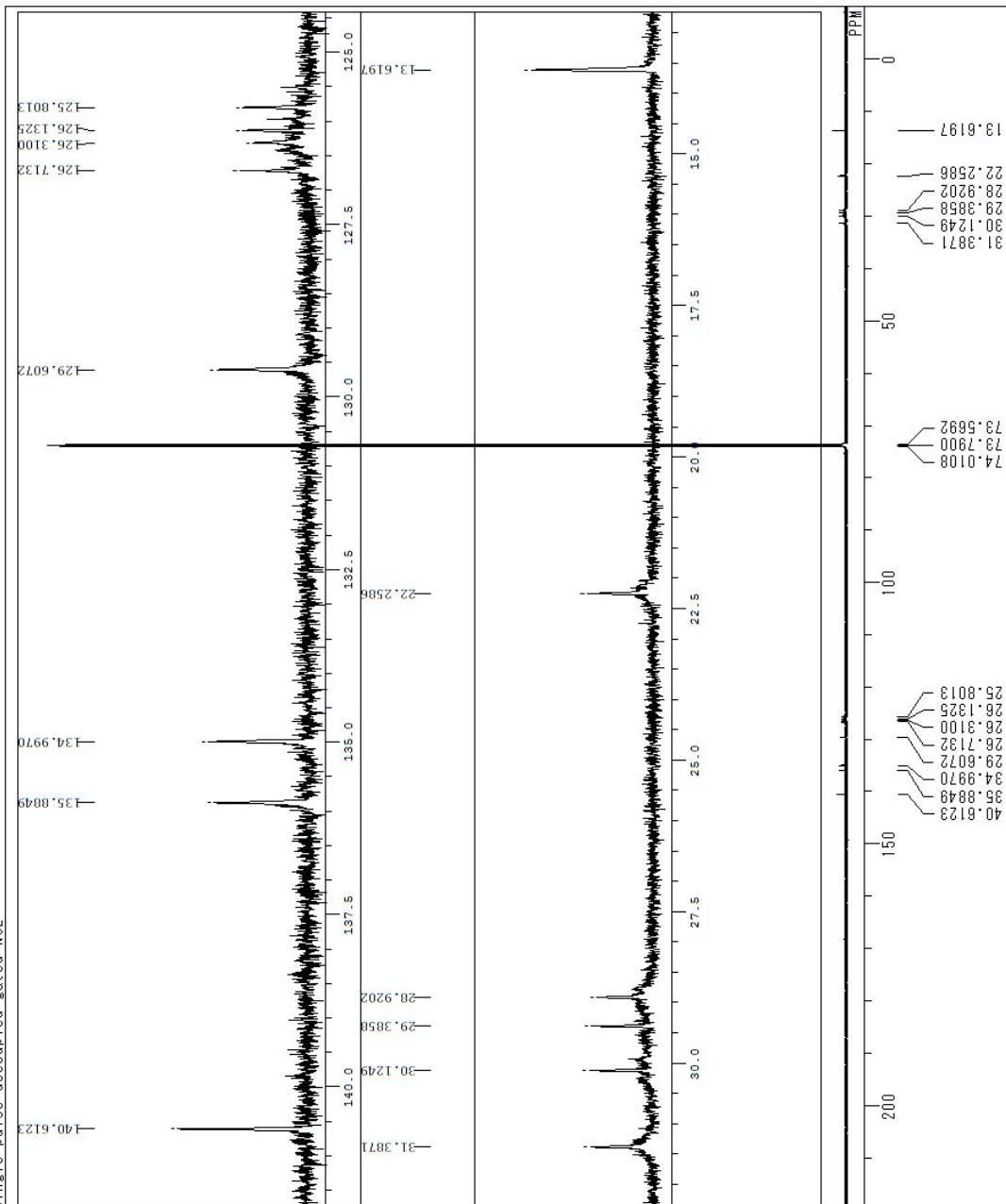
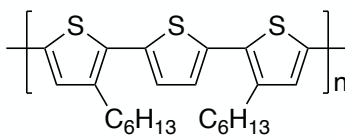
^{13}C NMR spectrum of polymer 7

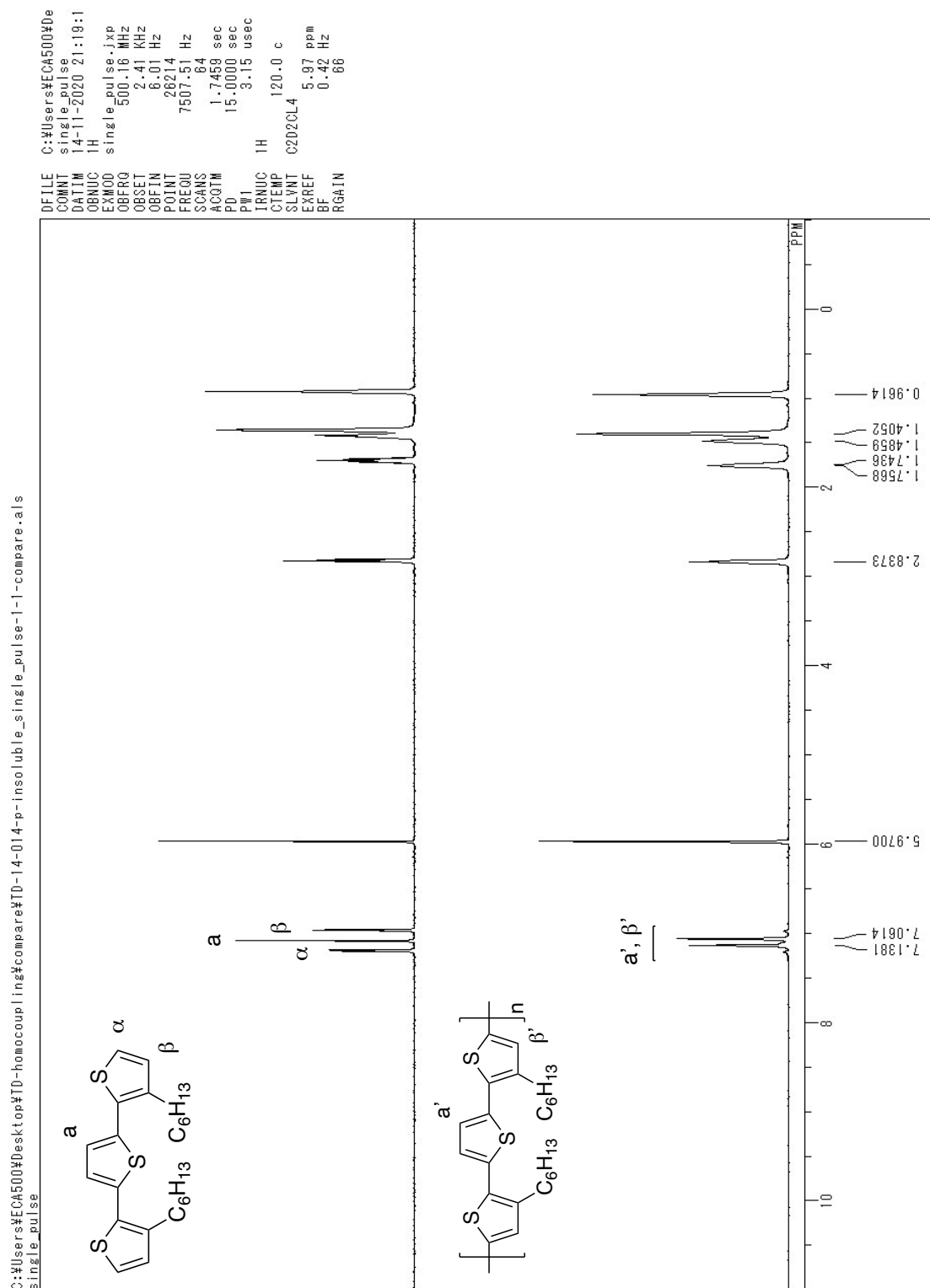
¹H NMR spectra of polymer **7** and its monomer

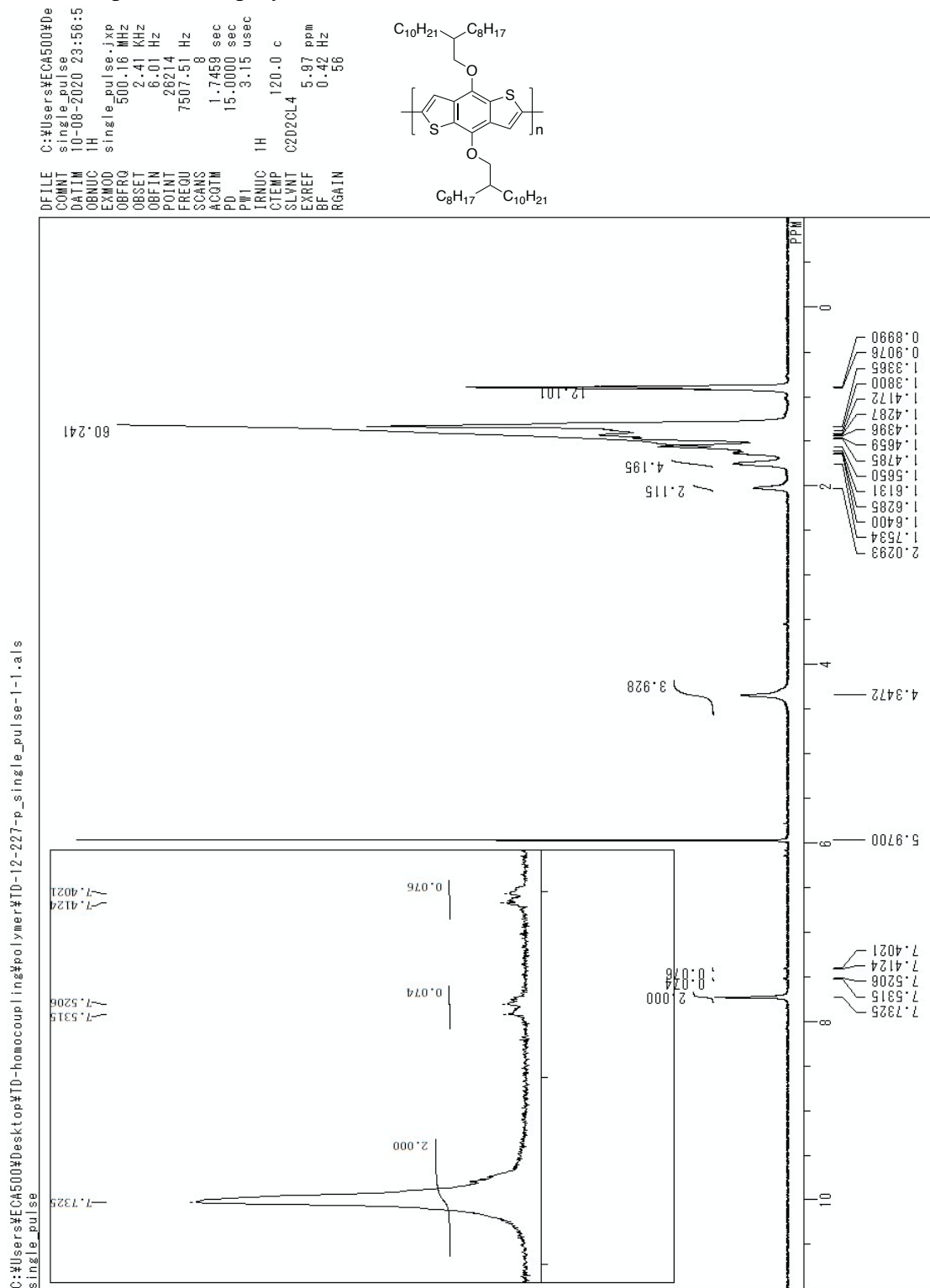
¹H NMR spectrum of polymer **8**

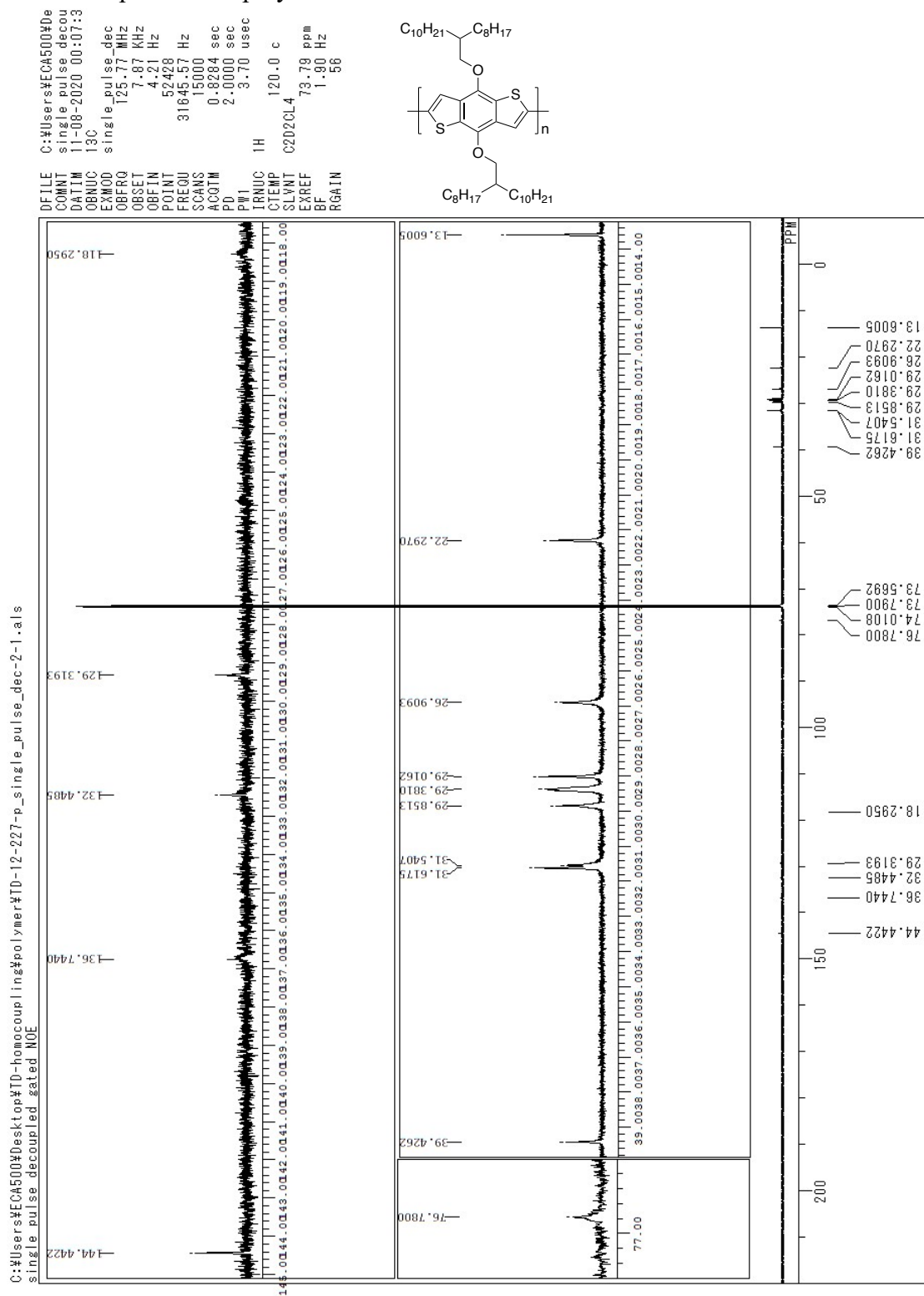
C:\User\5ECA500\Desktop\TD-4-014-p-insoluble_single_pulse_dec-1-1.xls

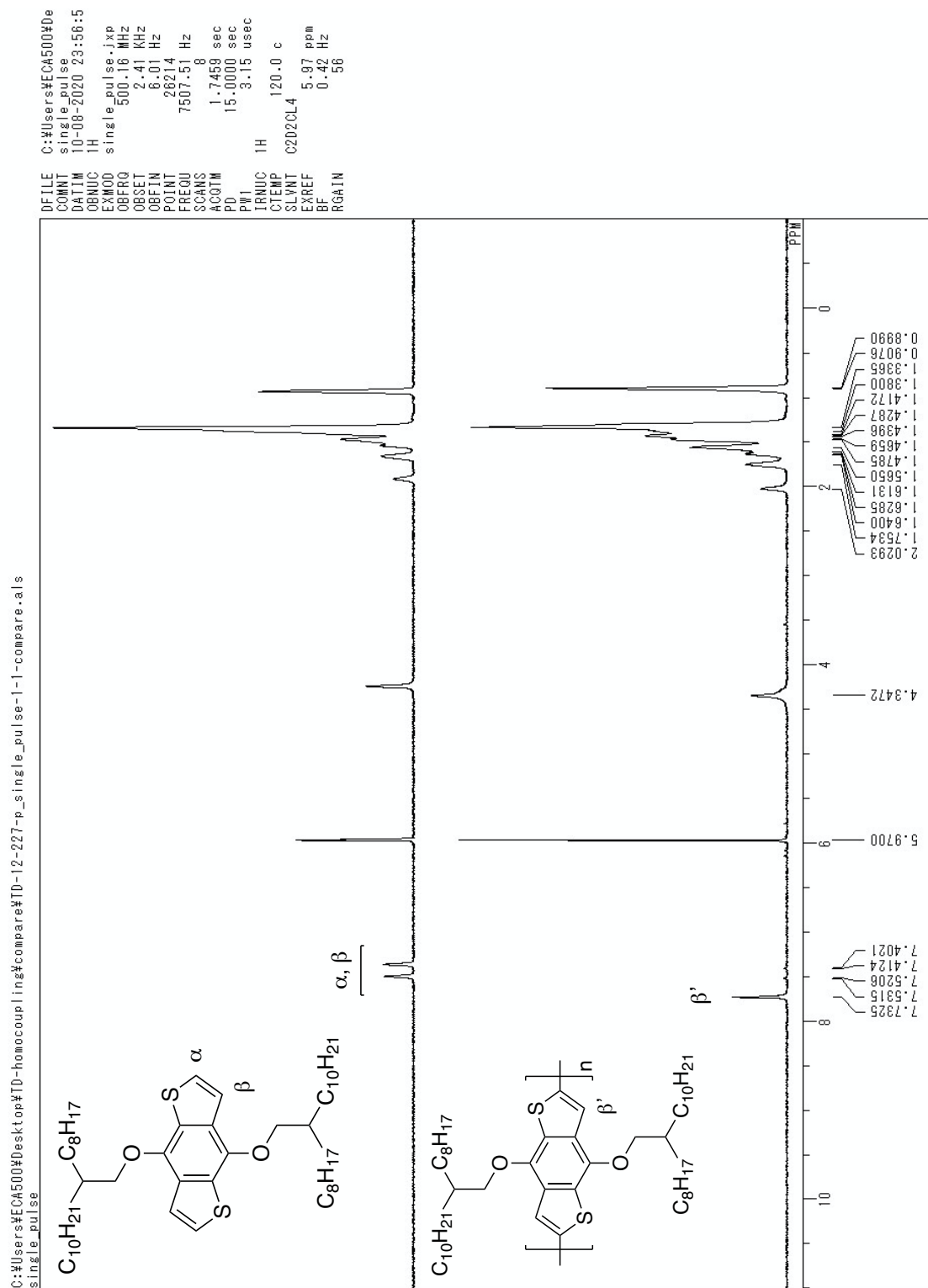
```
DFILE  COMNT  DATIM  OBNUC  EXMOD  OBFRQ  OBSET  OBFIN  POINT  FREQU  SCANS  ACQTM  PD  PW1  IRNUC  CTEMP  SLVNT  EXREF  BF  RGAIN
```

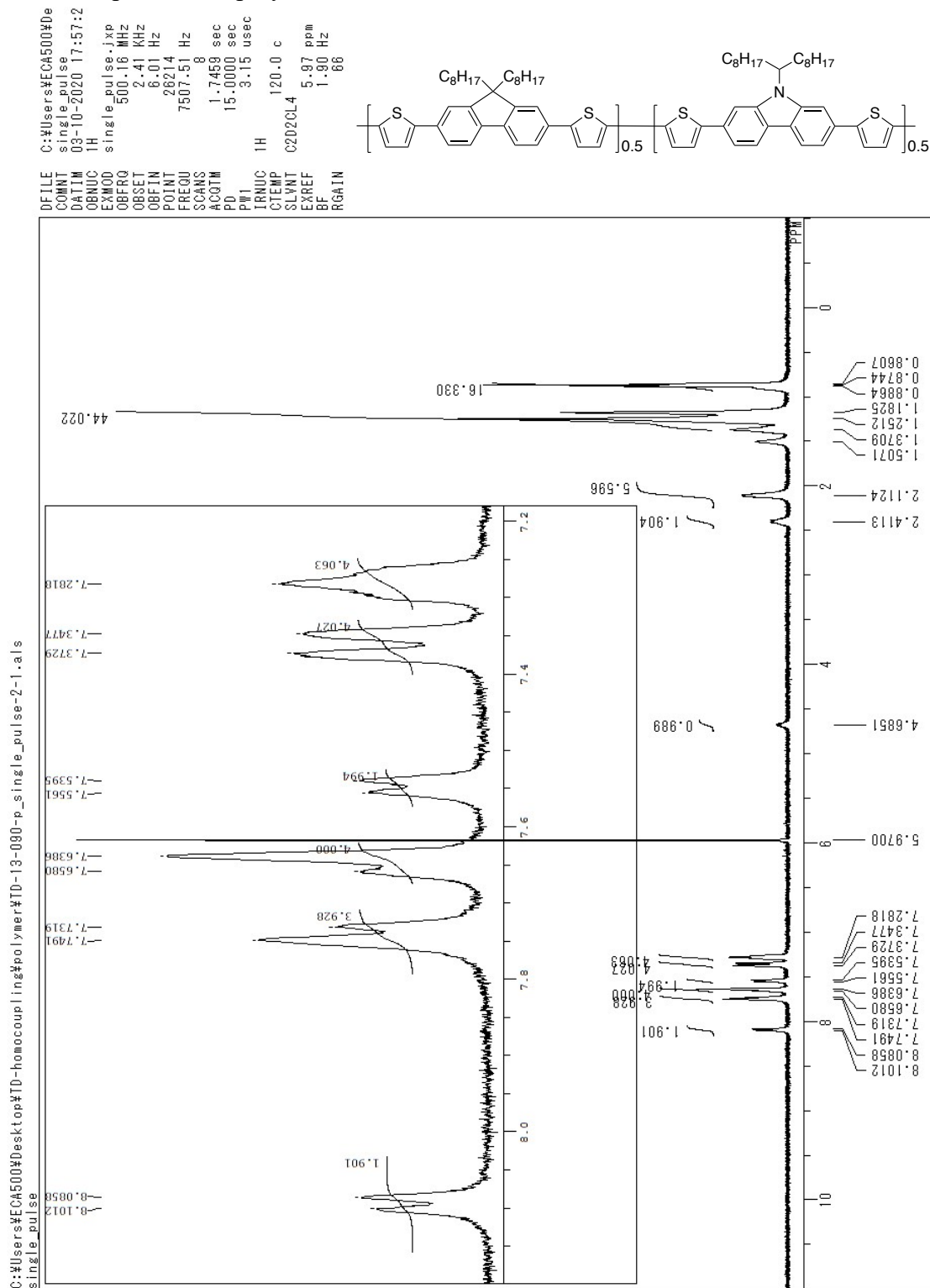


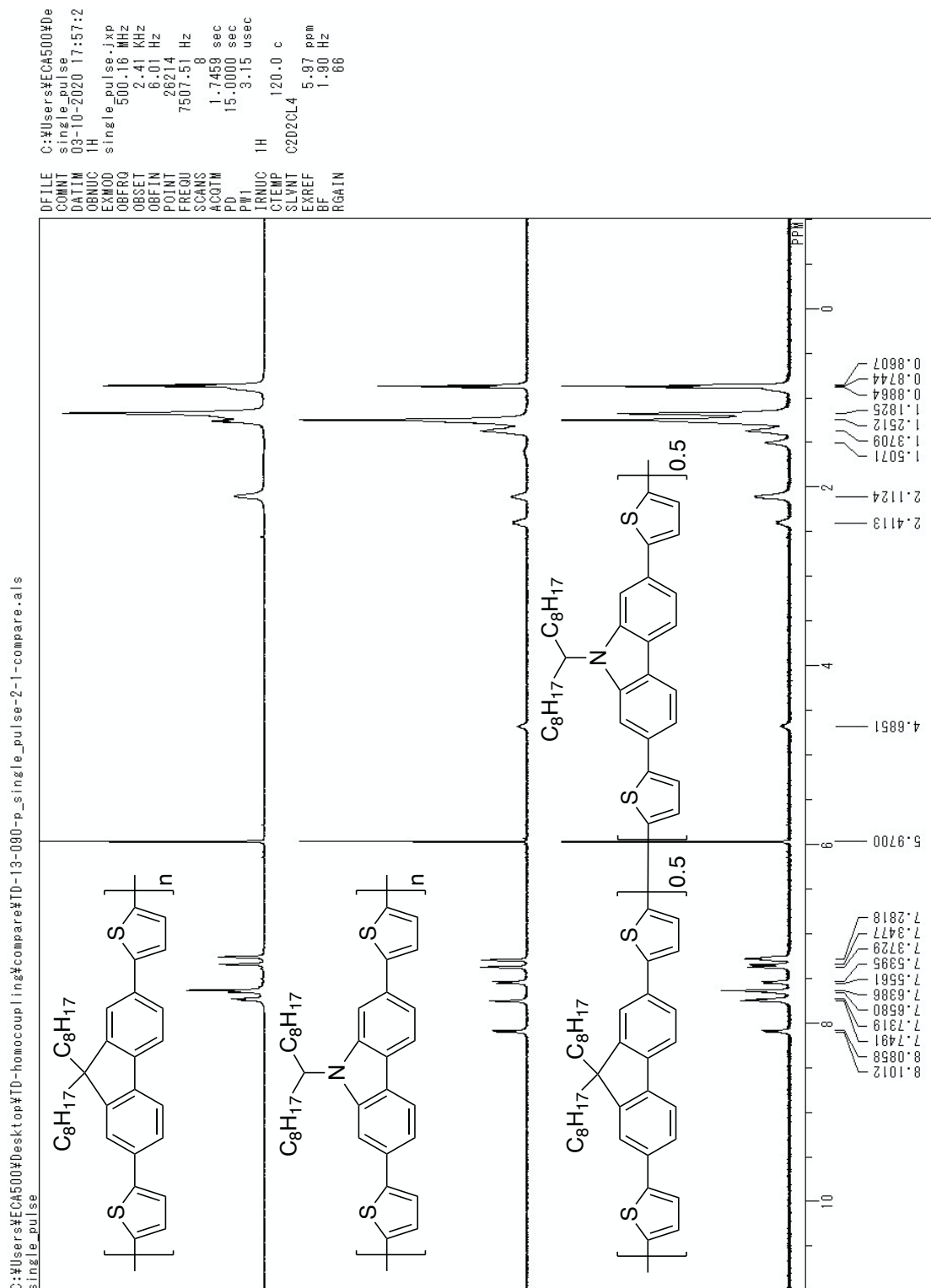
¹H NMR spectra of polymer **8** and its monomer

^1H NMR spectrum of polymer **9**

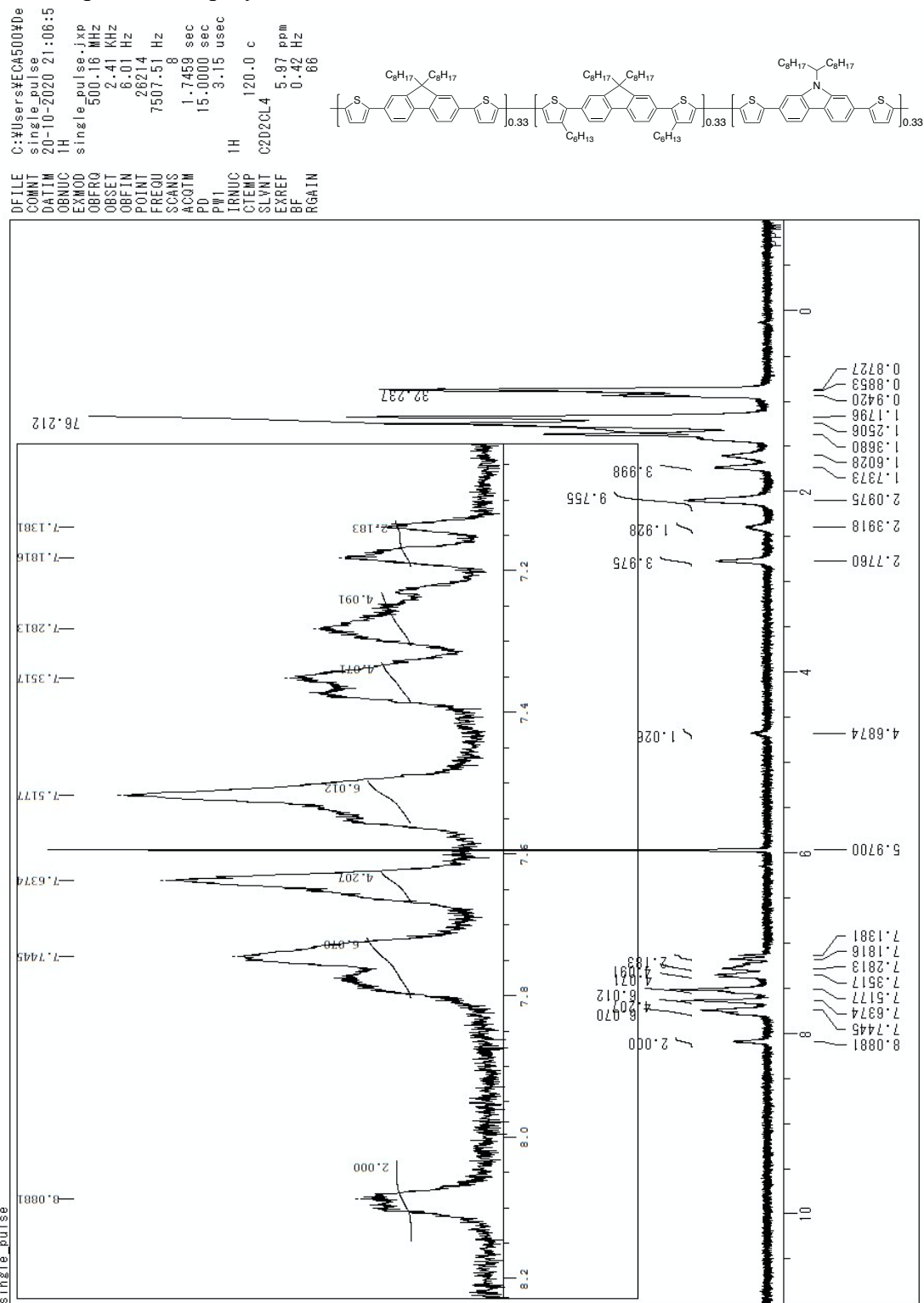
^{13}C NMR spectrum of polymer **9**

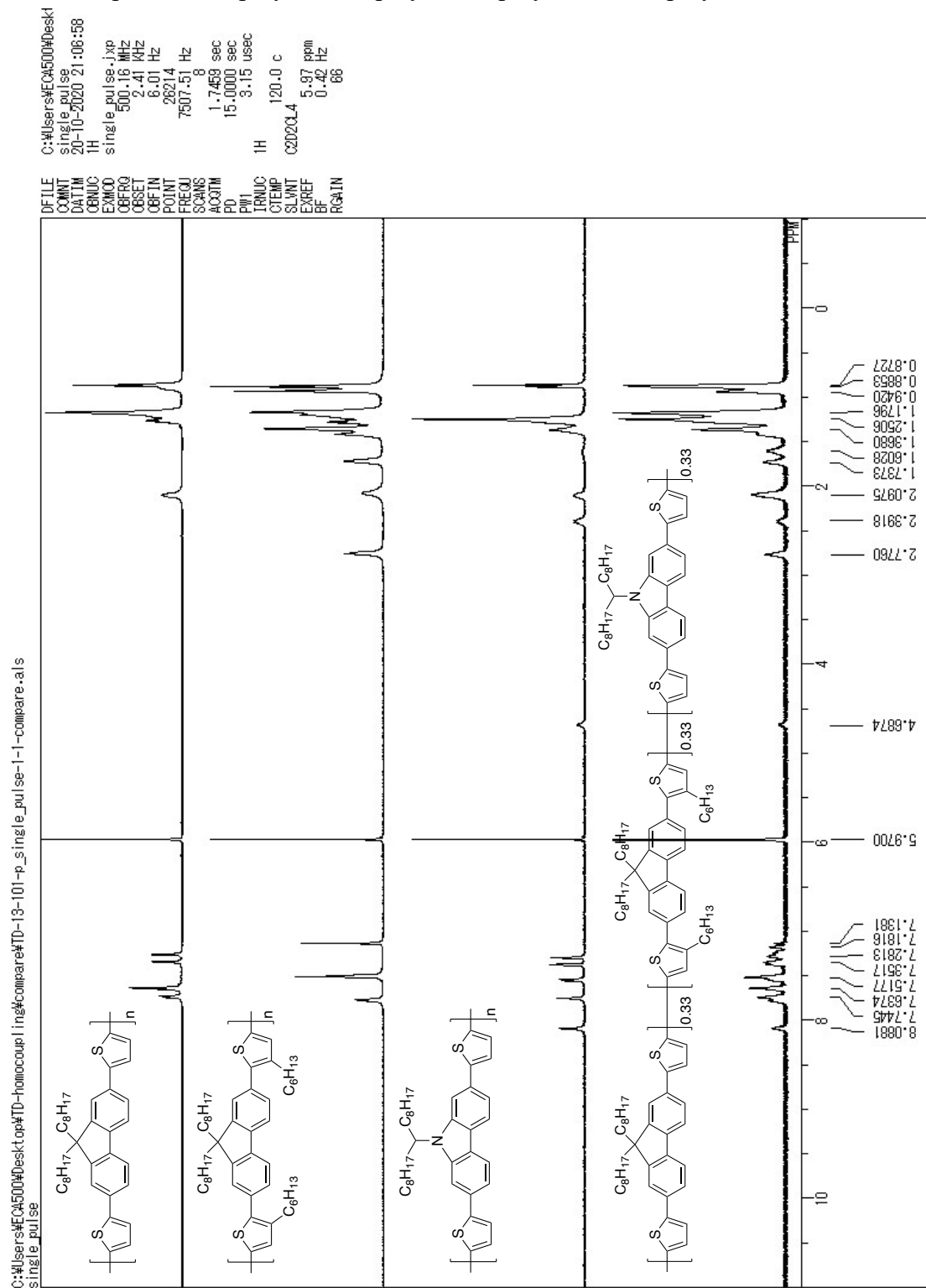
¹H NMR spectra of polymer **9** and its monomer

¹H NMR spectrum of polymer **10**

¹H NMR spectra of copolymer **10**, polymer **2**, and polymer **3**

C:\Users\ECA500\Desktop\TD-homocoupling\polymer\TD-13-101-p_single_pulse-1-1.a.s



¹H NMR spectra of copolymer **11**, polymer **2**, polymer **3**, and polymer **4**

(4-11. Application to perovskite solar cell については, 5 年以内に雑誌等で刊行予定のため, 非公開.)

4-14. References and notes

- ¹ (a) Meager, I.; Nikolka, M.; Schroeder, B. C.; Nielsen, C. B.; Planells, M.; Bronstein, H.; Rumer, J. W.; James, D. I.; Ashraf, R. S.; Sadhanala, A.; Hayoz, P.; Flores, J.-C.; Sirringhaus, H.; McCulloch, I. *Adv. Funct. Mater.* **2014**, *24*, 7109–7115. (b) Durban, M. M.; Kazarinoff, P. D.; Luscombe, C. K. *Macromolecules* **2010**, *43*, 6348–6352. (c) Usta, H.; Lu, G.; Facchetti, A.; Marks, T. J. *J. Am. Chem. Soc.* **2006**, *128*, 9034–9035. (d) Holliday, S.; Donaghey, J. E.; McCulloch, I. *Chem. Mater.* **2014**, *26*, 647–663. (e) Guo, X.; Baumgarten, M.; Müllen, K. *Progress in Polymer Science* **2013**, *38*, 1832–1908. (f) Huang, H.; Yang, L.; Facchetti, A.; Marks, T. J. *Chem. Rev.* **2017**, *117*, 10291–10318. (g) Zhao, X.; Zhan, X. *Chem. Soc. Rev.* **2011**, *40*, 3728–3743. (h) Wu, W.; Liu, Y.; Zhu, D. *Chem. Soc. Rev.* **2010**, *39*, 1489–1502. (i) Rasmussen, S. C.; Evenson, S. J.; McCausland, C. B. *Chem. Commun.* **2015**, *51*, 4528–4543. (j) Sirringhaus, H. *Adv. Mater.* **2014**, *26*, 1319–1335. (k) Sekine, C.; Tsubata, Y.; Yamada, T.; Kitano, M.; Doi, S. *Science and Technology of Advanced Materials* **2014**, *15*, 034203. (l) AlSalhi, M. S.; Alam, J.; Dass, L. A.; Raja, M. *Int. J. Mol. Sci.* **2011**, *12*, 2036–2054. (m) Boudreault, P.-L. T.; Najari, A.; Leclerc, M. *Chem. Mater.* **2011**, *23*, 456–469. (n) Arias, A. C.; MacKenzie, J. D.; McCulloch, I.; Rivnay, J.; Salleo, A. *Chem. Rev.* **2010**, *110*, 3–24. (o) Brabec, C. J.; Gowrisanker, S.; Halls, J. J. M.; Laird, D.; Jia, S.; Williams, S. P. *Adv. Mater.* **2010**, *22*, 3839–3856. (p) Helgesen, M.; Søndergaard, R.; Krebs, F. C. *J. Mater. Chem.* **2010**, *20*, 36–60. (q) Li, G.; Zhu, R.; Yang, Y. *Nature Photon* **2012**, *6*, 153–161. (r) Cheng, Y.-J.; Yang, S.-H.; Hsu, C.-S. *Chem. Rev.* **2009**, *109*, 5868–5923. (s) You, J.; Dou, L.; Hong, Z.; Li, G.; Yang, Y. *Progress in Polymer Science* **2013**, *38*, 1909–1928. (t) Ong, B. S.; Wu, Y.; Li, Y.; Liu, P.; Pan, H. *Chem. Eur. J.* **2008**, *14*, 4766–4778. (u) Zhang, Z.; Wang, J. *J. Mater. Chem.* **2012**, *22*, 4178.
- ² (a) Carsten, B.; He, F.; Son, H. J.; Xu, T.; Yu, L. *Chem. Rev.* **2011**, *111*, 1493–1528. (b) Sakamoto, J.; Rehahn, M.; Wegner, G.; Schlüter, A. D. *Macromol. Rapid Commun.* **2009**, *30*, 653–687. (c) Xu, S.; Kim, E. H.; Wei, A.; Negishi, E. *Science and Technology of Advanced Materials* **2014**, *15*, 044201.
- ³ (a) Wang, Q.; Zhang, B.; Liu, L.; Chen, Y.; Qu, Y.; Zhang, X.; Yang, J.; Xie, Z.; Geng, Y.; Wang, L.; Wang, F. *J. Phys. Chem. C* **2012**, *116*, 21727–21733. (b) Park, J. K.; Jo, J.; Seo, J. H.; Moon, J. S.; Park, Y. D.; Lee, K.; Heeger, A. J.; Bazan, G. C. *Adv. Mater.* **2011**, *23*, 2430–2435. (c) Kim, Y.; Cook, S.; Kirkpatrick, J.; Nelson, J.; Durrant, J. R.;

- Bradley, D. D. C.; Giles, M.; Heeney, M.; Hamilton, R.; McCulloch, I. *J. Phys. Chem. C* **2007**, *111*, 8137–8141. (d) Kim, J. S.; Lee, Y.; Lee, J. H.; Park, J. H.; Kim, J. K.; Cho, K. *Adv. Mater.* **2010**, *22*, 1355–1360. (e) Mao, Z.; Vakhshouri, K.; Jaye, C.; Fischer, D. A.; Fernando, R.; DeLongchamp, D. M.; Gomez, E. D.; Sauvé, G. *Macromolecules* **2013**, *46*, 103–112. (f) Koldemir, U.; Puniredd, S. R.; Wagner, M.; Tongay, S.; McCarley, T. D.; Kamenov, G. D.; Müllen, K.; Pisula, W.; Reynolds, J. R. *Macromolecules* **2015**, *48*, 6369–6377.
- ⁴ Yang, Y.; Nishiura, M.; Wang, H.; Hou, Z. *Coordination Chemistry Reviews* **2018**, *376*, 506–532.
- ⁵ (a) Pouliot, J.-R.; Grenier, F.; Blaskovits, J. T.; Beaupré, S.; Leclerc, M. *Chem. Rev.* **2016**, *116*, 14225–14274. (b) Bura, T.; Blaskovits, J. T.; Leclerc, M. *J. Am. Chem. Soc.* **2016**, *138*, 10056–10071. (c) Rudenko, A. E.; Thompson, B. C. *J. Polym. Sci. Part A: Polym. Chem.* **2015**, *53*, 135–147. (d) Dudnik, A. S.; Aldrich, T. J.; Eastham, N. D.; Chang, R. P. H.; Facchetti, A.; Marks, T. J. *J. Am. Chem. Soc.* **2016**, *138*, 15699–15709. (e) Bura, T.; Morin, P.-O.; Leclerc, M. *Macromolecules* **2015**, *48*, 5614–5620. (f) Mercier, L. G.; Leclerc, M. *Acc. Chem. Res.* **2013**, *46*, 1597–1605. (g) Matsidik, R.; Komber, H.; Luzio, A.; Caironi, M.; Sommer, M. *J. Am. Chem. Soc.* **2015**, *137*, 6705–6711. (h) Wakioka, M.; Ozawa, F. *Asian J. Org. Chem.* **2018**, *7*, 1206–1216. (i) Kuwabara, J.; Yasuda, T.; Choi, S. J.; Lu, W.; Yamazaki, K.; Kagaya, S.; Han, L.; Kanbara, T. *Adv. Funct. Mater.* **2014**, *24*, 3226–3233.
- ⁶ Tsuchiya, K.; Ogino, K. *Polym. J.* **2013**, *45*, 281–286.
- ⁷ (a) Gobalasingham, N. S.; Noh, S.; Thompson, B. C. *Polym. Chem.* **2016**, *7*, 1623–1631. (b) Zhang, Q.; Wan, X.; Lu, Y.; Li, Y.; Li, Y.; Li, C.; Wu, H.; Chen, Y. *Chem. Commun.* **2014**, *50*, 12497–12499. (c) Zhang, Q.; Li, Y.; Lu, Y.; Zhang, H.; Li, M.; Yang, Y.; Wang, J.; Chen, Y.; Li, C. *Polymer* **2015**, *68*, 227–233.
- ⁸ Huang, Q.; Qin, X.; Li, B.; Lan, J.; Guo, Q.; You, J. *Chem. Commun.* **2014**, *50*, 13739–13741.
- ⁹ Guo, Q.; Jiang, R.; Wu, D.; You, J. *Macromol. Rapid Commun.* **2016**, *37*, 794–798.
- ¹⁰ Wakim, S.; Blouin, N.; Gingras, E.; Tao, Y.; Leclerc, M. *Macromol. Rapid Commun.* **2007**, *28*, 1798–1803.
- ¹¹ Ziebart, C.; Federsel, C.; Anbarasan, P.; Jackstell, R.; Baumann, W.; Spannenberg, A.; Beller, M. *J. Am. Chem. Soc.* **2012**, *134*, 20701–20704.

- ¹² Ikariya, T.; Yamamoto, A. *J. Organometal. Chem.* **1976**, *118*, 65–77.
- ¹³ Donat-Bouillud, A.; Lévesque, I.; Tao, Y.; D'Iorio, M.; Beaupré, S.; Blondin, P.; Ranger, M.; Bouchard, J.; Leclerc, M. *Chem. Mater.* **2000**, *12*, 1931–1936.
- ¹⁴ Roncali, J. *Chem. Rev.* **1992**, *92*, 711–738.
- ¹⁵ (a) Carothers, W. H. *Chem. Rev.* **1931**, *8*, 353–426. (b) Flory, P. J. *Chem. Rev.* **1946**, *39*, 137–197.
- ¹⁶ (a) Sheina, E. E.; Liu, J.; Iovu, M. C.; Laird, D. W.; McCullough, R. D. *Macromolecules* **2004**, *37*, 3526–3528. (b) Yokoyama, A.; Miyakoshi, R.; Yokozawa, T. *Macromolecules* **2004**, *37*, 1169–1171. (c) Miyakoshi, R.; Yokoyama, A.; Yokozawa, T. *Macromol. Rapid Commun.* **2004**, *25*, 1663–1666. (d) Miyakoshi, R.; Yokoyama, A.; Yokozawa, T. *J. Am. Chem. Soc.* **2005**, *127*, 17542–17547. (e) Iovu, M. C.; Sheina, E. E.; Gil, R. R.; McCullough, R. D. *Macromolecules* **2005**, *38*, 8649–8656. (f) Yokoyama, A.; Suzuki, H.; Kubota, Y.; Ohuchi, K.; Higashimura, H.; Yokozawa, T. *J. Am. Chem. Soc.* **2007**, *129*, 7236–7237.
- ¹⁷ (a) Urien, M.; Wantz, G.; Cloutet, E.; Hirsch, L.; Tardy, P.; Vignau, L.; Cramail, H.; Parneix, J.-P. *Org. Electron.* **2007**, *8*, 727–734. (b) Camaioni, N.; Tinti, F.; Franco, L.; Fabris, M.; Toffoletti, A.; Ruzzi, M.; Montanari, L.; Bonoldi, L.; Pellegrino, A.; Calabrese, A.; Po, R. *Org. Electron.* **2012**, *13*, 550–559. (c) Cowan, S. R.; Leong, W. L.; Banerji, N.; Dennler, G.; Heeger, A. J. *Adv. Funct. Mater.* **2011**, *21*, 3083–3092. (d) Nikiforov, M. P.; Lai, B.; Chen, W.; Chen, S.; Schaller, R. D.; Strzalka, J.; Maser, J.; Darling, S. B. *Energy Environ. Sci.* **2013**, *6*, 1513–1520. (e) Ashraf, R. S.; Schroeder, B. C.; Bronstein, H. A.; Huang, Z.; Thomas, S.; Kline, R. J.; Brabec, C. J.; Rannou, P.; Anthopoulos, T. D.; Durrant, J. R.; McCulloch, I. *Adv. Mater.* **2013**, *25*, 2029–2034. (f) Estrada, L. A.; Deininger, J. J.; Kamenov, G. D.; Reynolds, J. R. *ACS Macro Lett.* **2013**, *2*, 869–873. (g) Usluer, Ö.; Abbas, M.; Wantz, G.; Vignau, L.; Hirsch, L.; Grana, E.; Brochon, C.; Cloutet, E.; Hadziioannou, G. *ACS Macro Lett.* **2014**, *3*, 1134–1138.
- ¹⁸ Still, W. C.; Kahn, M.; Mitra, A. *J. Org. Chem.* **1978**, *43*, 2923–2925.
- ¹⁹ Pangborn, A. B.; Giardello, M. A.; Grubbs, R. H.; Rosen, R. K.; Timmers, F. J. *Organometallics* **1996**, *15*, 1518–1520.
- ²⁰ Doba, T.; Ilies, L.; Sato, W.; Shang, R.; Nakamura, E. *Nat. Catal.* **2021**, *4*, 631–638.
- ²¹ Gallazzi, M. C.; Castellani, L.; Zerbi, G.; Sozzani, P. *Synthetic Metals* **1991**, *41*, 495–498.

Chapter 5.

本章については, 5 年以内に雑誌等で刊行予定のため, 非公開.

Chapter 6.

Conclusions and Perspectives

Transition-metal-catalyzed $C(sp^2)-H/C(sp^2)-H$ coupling has attracted much attention as one of the most straightforward methods to construct $C(sp^2)-C(sp^2)$ bonds. However, the application of this ideal transformation to the synthesis of redox-sensitive π -materials was hindered by the requirement of a strong oxidant for catalyst turnover. To overcome this problem, I focused on the low redox potential of $Fe(III)/Fe(I)$ to achieve iron-catalyzed $C-H/C-H$ coupling under mildly oxidative conditions.

Chapter 1 described that redox potential of catalyst is the limiting factor of the mildness of oxidant in transition-metal-catalyzed $C-H/C-H$ coupling and proposed that the low redox potential of $Fe(III)/Fe(I)$, which has been partially proved by the use of dihaloalkanes as a mild oxidant in iron-catalyzed $C-H$ activation reactions, would be a solution to solve the problem.

Chapter 2 described the development of iron-catalyzed regioselective thienyl $C-H/C-H$ homocoupling using tridentate phosphine as a ligand, $AlMe_3$ as a base, and oxalate as a mild oxidant. Tridentate phosphine ligand was uniquely effective for this transformation and oxalate served as an effective but mild oxidant to turnover the $Fe(III)/Fe(I)$ catalytic cycle taking advantage of the oxophilicity of $Al(III)$. The electronic bias created by a sulfur atom of thienyl groups helped to make the adjacent $C-H$ bond acidic enough for iron-catalyzed $C-H$ activation through a σ -bond metathesis mechanism. The reaction did not require a preinstalled directing group, giving direct access to useful π -conjugated dimeric and oligomeric thiophene compounds.

Chapter 3 described a modular method to synthesize conjugated tridentate phosphine ligands with different substituents. Sequential addition of two different organolithium reagents to $P(OPh)_3$ was the key to selectively obtain tridentate phosphine ligand out of bidentate or tetradentate ones. This method was applicable to the synthesis of aryl-TPs and heteroaryl-TPs and the pure products were obtained in high yields on a gram scale by recrystallization. This method accelerated the further exploration of iron-catalyzed regioselective thienyl $C-H/C-H$ coupling.

Chapter 4 described the development of iron-catalyzed regioselective thienyl $C-H/C-H$ polycondensation by improvement of iron-catalyzed regioselective thienyl $C-H/C-H$ homocoupling introduced in chapter 2. Heteroaryl-TP was designed to suppress catalyst deactivation by prevention of intramolecular $C-H$ activation of the ligand and effectively used as an optimal ligand for polycondensation. This reaction took place exclusively at the $C-H$ bond next to the sulfur atom of thienyl groups and no branching

of the polymer was observed. Monomers containing various kinds of redox-sensitive π -motifs were polymerized efficiently up to DP of 46, which demonstrated the effectiveness and mildness of the iron catalytic cycle. Because of the weak interaction of Fe(III) with the π -surface of the polymer chain, polycondensation proceeded through a step-growth mechanism and the residual iron was removed to less than 40 ppm by post treatment of a polymer with a thiol-functionalized silica scavenger. **(4-11. Application to perovskite solar cell** については, 5 年以内に雑誌等で刊行予定のため, 非公開.) This work highlighted the benefits of iron catalysis for the synthesis of π -conjugated polymeric compounds of importance in optoelectronic device applications.

(第 5 章については, 5 年以内に雑誌等で刊行予定のため, 非公開.)

In conclusion, iron-catalyzed C–H/C–H coupling reactions that proceed under mildly oxidative conditions were developed by utilizing the low redox potential of Fe(III)/Fe(I) cycle. Oxalate in combination with oxophilic Al(III) served as a mild oxidant to turn over the catalytic cycle and tridentate phosphine ligand was uniquely effective to control the reactivity of iron toward regioselective thienyl C–H activation. The reactions described herein highlighted the potential of iron, the most abundant transition-metal on earth, for the direct synthesis of functional small molecules and polymers of importance in materials science.

Finally, I would like to propose several directions for future research. First, the scope of this reaction system can be expanded to other (hetero)arenes by modulation of the ligand structure. Second, reactions of such (hetero)arenes with electrophiles are worth investigating. For example, carbonyl containing electrophiles such as redox-active esters and *N*-benzoyloxyamines may accept electron(s) and serve as a coupling partner after fragmentation. Third, application of iron-catalyzed C–H/C–H coupling to the synthesis of π -materials that cannot be synthesized by other transition-metal-catalyzed reactions should be considered. Polymers containing unstable bonds such as C–B and B–N bonds would be the candidates. In addition, development of iron-catalyzed C–H activation reactions utilizing other C–H activation modes such as concerted-metalation-deprotonation (CMD) or oxidative addition would draw out the potential of iron to its fullest. Furthermore, a series of tridentate phosphine ligands that can be synthesized by the method described in chapter 3 will give a great opportunity to investigate the catalysis of other transition metals. A compact tridentate coordination may be suitable for electron-deficient first-row transition metals with a small ionic radius.

List of Publications

Chapter 2–4.

1. "Iron-Catalysed Regioselective Thienyl C–H/C–H Coupling"

Takahiro Doba, Laurean Ilies, Wataru Sato, Rui Shang, Eiichi Nakamura

Nat. Catal. **2021**, 4, 631–638.

(Highlighted in Nature Portfolio Chemistry Community)

2. 「新規鉄触媒を用いた共役高分子合成方法および有機半導体デバイス」

中村栄一, Shang Rui, 道場貴大, 佐藤済

特願 2020-130678

Other publications not included in this thesis.

1. "Nakamura, E. Homocoupling-Free Iron-Catalysed Twofold C–H Activation/Cross-Couplings of Aromatics via Transient Connection of Reactants"

Takahiro Doba, Tatsuaki Matsubara, Laurean Ilies, Rui Shang, Eiichi Nakamura

Nat. Catal. **2019**, 2, 400–406.

(Highlighted in Nature Portfolio Chemistry Community, EurekaAlert, Alpha Galileo, and Chem-station, Press release)

2. "Chromium(III)-Catalyzed C(sp²)–H Alkynylation, Allylation, and Naphthalenation of Secondary Amides with Trimethylaluminum as Base"

Mengqing Chen, Takahiro Doba, Takenari Sato, Hlib Razumkov, Laurean Ilies, Rui Shang, Eiichi Nakamura

J. Am. Chem. Soc. **2020**, 142, 4883–4891.

3. 「第 6 章 Fe 触媒芳香族 C–H カップリング反応」

道場貴大, 中村栄一

直接的芳香族カップリング反応の設計と応用, シーエムシー出版, pp.63–73, 2019 年.

Acknowledgements

First, I wish to express my deepest gratitude to Professor, Dr. Eiichi Nakamura for his constructive advice, discussions, and constant encouragement throughout this work. I would like to express my deep appreciation to a former Associate Professor, Dr. Laurean Ilies (now in RIKEN) and a current Associate Professor, Dr. Rui Shang for their valuable advice, discussions, and encouragement.

I am particularly grateful to Professor, Dr. Shū Kobayashi, Professor, Dr. Hiroyuki Isobe, Professor, Dr. Shuichi Hiraoka, and Professor, Dr. Jun Terao for insightful comments and suggestions about this thesis.

I am also grateful to Associate Professor, Dr. Koji Harano and Associate Professor, Dr. Takayuki Nakamuro for their advice, encouragement, and support throughout this work. I was especially impressed by Associate Professor, Dr. Takayuki Nakamuro's vitality to change the research field.

I am grateful to Professor, Dr. Shū Kobayashi and Assistant Professor, Dr. Tomohiro Yasukawa for valuable comments and suggestions on the removal of residual catalyst from polymers. I am also grateful to Professor, Dr. Yutaka Matsuo and Assistant Professor, Dr. Hao-Sheng Lin for the application of polymers to perovskite solar cells.

I am grateful to Professor, Dr. Klaus Müllen (MPIP) and Associate Professor, Dr. Akimitsu Narita (OIST) for my research experience in Germany from August to October in 2019.

I would like to show my appreciation to Dr. Tatsuaki Matsubara for his valuable comments and suggestions on my master course studies, iron-catalyzed C–H/C–H cross-coupling of carboxamides with heteroarenes. I would also like to show my appreciation to Dr. Wataru Sato for his technical comments and suggestions regarding polymer chemistry. My appreciation also goes to Mr. Mengqing Chen for the collaboration with the chromium-catalyzed C–H functionalization project. I am also thankful to Br. Shota Fukuma for his technical comments and suggestions regarding X-ray crystal structure analysis.

I would like to show my appreciation to Dr. Takumi Yoshida, Dr. Yuki Itabashi, Dr. Takenari Sato, Mr. Yi Zhou, Mr. Toki Go, Mr. Haotian Yang, and Mr. Naoki Matsushita for their valuable comments and suggestions on iron chemistry in a former subgroup. I would also like to show my appreciation to Dr. Hiroki Nishioka, Dr. Hiyoroshi Hamada,

Mr. Takumi Sakamaki, Mr. Mengqing Chen, Mr. Olivier Chevalier, Mr. Mana Kawashima, Br. Shota Fukuma, Br. Akinori Takasugi, Br. Yosuke Miyazaki, and Shogo Aoki for their valuable comments and suggestions in a current subgroup. I am especially pleased to have a junior coworker, Br. Yosuke Miyazaki, who took over the iron project.

I am very happy to work with friendly colleagues, Dr. Hiroki Hanayama, Dr. Toshiki Shimizu, Dr. Ryosuke Sekine, Mr. Ko Kamei, and Mr. Takumi Sakamaki. They always motivated me and gave me enjoyable daily life in Nakamura Lab. I would also like to show my appreciation to all other members in Nakamura Lab.

I thank the Program of Leading Graduate Schools (MERIT) for financial support and giving various opportunities to learn from both academia and industry. All of my MERIT colleagues are appreciated, who are always inspiring me from other research fields of chemistry and physics. I also thank the Japan Society for Promotion of Science (JSPS) Research Fellowship for Young Scientists for financial support.

Finally, I would like to express my deep appreciation to my parents for their constant assistance and affectionate encouragement.

Takahiro Doba
February 2022